

INCREASING INCLUSION BODY EXTRACTABILITY AND  
RECOVERABILITY BY ALTERING FERMENTATION CONDITIONS IN  
HIGH CELL DENSITY ESCHERICHIA COLI CULTURES

A Dissertation

Presented to the Faculty of the Graduate School

of Cornell University

In Partial Fulfillment of the Requirements for the Degree of

Doctor of Philosophy

by

Rishard Hwa-Jye Chen

August 2009

© 2009 Rishard Hwa-Jye Chen

INCREASING INCLUSION BODY EXTRACTABILITY AND  
RECOVERABILITY BY ALTERING FERMENTATION CONDITIONS IN  
HIGH CELL DENSITY ESCHERICHIA COLI CULTURES

Rishard Hwa-Jye Chen, Ph. D.

Cornell University 2009

Volumetric protein production yields in *Escherichia coli* fermentations have improved with development of fed-batch high cell density cultures. The use of high cell densities has introduced need to obtain a better understanding of intercellular quorum sensing signals, glucose feeding strategies, and endotoxin removal during protein purification. The high purity of inclusion bodies (IBs) makes their extraction from host cell proteins in the cell lysate a standard procedure to simplify purification. The extraction is typically performed with centrifugation or tangential flow filtration, which are dependent on the IBs' size, density, and shape. The isolated IBs are then denatured, but the degree to which they are denatured can be dependent on their compactness. These qualities of IBs can all be influenced with fermentation growth conditions, but little research on this topic has been published.

A synthetic version of melanoma antigen A (Syn-Melan-A) was produced in high cell density *E. coli* cultures in complex medium under various temperatures, inducer concentrations, and feeding strategies. IBs produced at 30 °C, 37 °C, and 42 °C were 316, 215, and 231 nm in size and had densities of 1.26, 1.30, and 1.31 g/cm<sup>3</sup>, respectively. No significant changes in IB size or density were detected in fermentations using inducer in the range of 0.05 to 0.50 mM. Changing from a pH-stat feeding method that prevented glucose accumulation to an overfed culture could

increase IB size to 340 nm and IB density to 1.31 g/cm<sup>3</sup> at 37 °C. Similar results were obtained in a statistical design experiment in chemically defined medium.

Scanning electron microscopy was used to show that Syn-Melan-A IBs were amorphous when produced at 30 °C, granulated at 37 °C, and smooth at 42 °C.

Coomassie dye was used to show that these IBs had a 62%, 65%, and 68% accessibility, respectively, as determined by Bradford reaction.

Different fermentation temperatures were used also to determine their influence on the IB characteristics of Melan-A, SSX-2, NY-ESO-1, and enhanced green fluorescent protein (EGFP). Different temperatures were only effective in altering IB characteristics of Syn-Melan-A. This susceptibility is associated with slower production rate of Syn-Melan-A compared to natural Melan-A.



## BIOGRAPHICAL SKETCH

Rishard Chen was born in Santa Clara, California, on August 10, 1980 and completed most of his elementary and all of his high school education in the nearby town Saratoga. After high school, he moved to Cambridge, Massachusetts where he earned his undergraduate degree in chemical engineering from the Massachusetts Institute of Technology in 2002. In Branford, Connecticut, he worked at CuraGen Corporation where he met his wife Christy. They moved to Cornell together in 2004 with their two cats, Wormy and Rayman. The family of four will be leaving Cornell in 2009 and moving to San Francisco, California, for the next chapter of their lives. Rishard was able to find employment despite a world-wide economic recession.

Dedicated to  
my wife,  
our parents,  
and anyone else who cares about the work I am doing

## ACKNOWLEDGMENTS

I am very happy to be where I am today, and there are many people to thank that made this possible. Chronologically, I would like start by thanking Professor Pretindeer Virk, whose kind words and encouragement got me through my challenging time at MIT. I would also like to thank Professor Jean-François Hamel, who also showered me with vitalizing praise and brought me together with my first job at CuraGen. My final pillar of support from MIT has been my former lab TA José Manuel Otero, without whom I would never have discovered the GMP protein production facility at Cornell with which I am now so intimately involved.

At CuraGen, Dr. Gan Wei taught me everything I know about *E. coli* fermentation. He later sent me off to graduate school, knowing that he would lose one of his most favorite employees.

My special committee at Cornell is a triumvirate of power. Mike Shuler is one of the top chemical engineers in history that continues to amaze me with his unending wisdom. Matt DeLisa is the person I always felt best understood my research, and it was always a pleasure to discuss the science with him. Finally Carl Batt is the person I have had the most interaction with. The work I have done for the Ludwig Institute of Cancer Research has been a job, and he has been my boss.

Thanks must also go to my fellow classmates in the chemical engineering department as well as the entire Shuler and Batt labs.

## TABLE OF CONTENTS

Biographical Sketch.....	iii
Dedication.....	iv
Acknowledgments.....	v
Table of Contents.....	vi
List of Figures.....	xiv
List of Tables.....	xx
List of Abbreviations.....	xxi
List of Symbols.....	xxv

## CHAPTER 1. INCLUSION BODY FORMATION DURING RECOMBINANT PROTEIN PRODUCTION IN ESCHERICHIA COLI

1.1. Introduction.....	1
1.2. Protein expression in <i>Escherichia coli</i> .....	2
1.2.1. Recombinant DNA technology.....	2
1.2.2. The bacterium <i>E. coli</i> .....	3
1.2.3. Promoter selection.....	4
1.2.4. Co-expression.....	5
1.2.5. Strain selection.....	7
1.3. Bioprocess Development.....	9
1.3.1. Media selection.....	9
1.3.2. High cell density cultures.....	9
1.3.3. Purification schemes.....	11
1.4. Inclusion Bodies.....	12
1.4.1. IB formation.....	12

1.4.2.	Disadvantages.....	13
1.4.3.	Advantages.....	15
1.4.4.	Chaperone co-expression.....	17
1.4.5.	Chaperone deletion.....	18
1.4.6.	Process conditions.....	20
1.5.	Tailoring IB physical and chemical characteristics .....	21
1.5.1.	IB classes.....	21
1.5.2.	GFP studies.....	21
1.5.3.	IPTG concentrations.....	22
1.5.4.	Specific growth rates.....	22
1.5.5.	Fermentation Type.....	23
1.6.	Conclusions.....	23
	REFERENCES.....	25

## CHAPTER 2. FERMENTATION SETUP AND ASSAY DEVELOPMENT

2.1.	Background.....	36
2.2.	Proteins used.....	36
2.2.1.	EGFP.....	36
2.2.2.	SSX2.....	38
2.2.3.	NY-ESO-1.....	39
2.2.4.	Melan-A.....	40
2.3.	Creation of research cell banks.....	41
2.3.1.	Design of synthetic DNA sequence.....	41
2.3.2.	Plasmid production.....	44
2.3.3.	Plasmid construction.....	45
2.3.4.	Research cell bank transformation.....	46

2.3.5. Other plasmids.....	47
2.4. Fermentation conditions.....	48
2.4.1. Complex medium.....	48
2.4.2. Chemically defined medium.....	49
2.4.3. Fermentation conditions.....	51
2.4.4. Feeding strategies.....	53
2.4.5. Statistical design.....	54
2.5. Fermentation Measurements.....	55
2.5.1. Feeding Rate Calibration.....	55
2.5.2. Cell Density Measurements.....	56
2.5.3. Protein Production Measurements.....	57
2.6. Inclusion Body Isolation.....	59
2.7. Cesium chloride ultracentrifugation gradients.....	60
2.7.1. Ultracentrifugation introduction.....	60
2.7.2. Cesium chloride solutions.....	61
2.7.3. Ultracentrifugation experimental setup.....	62
2.7.4. Sedimentation equilibrium.....	64
2.8. Microscopy preparation and operation.....	64
2.8.1. Light microscopy.....	64
2.8.2. Cell and IB fixation and dehydration.....	65
2.8.3. Transmission electron microscopy of cells.....	66
2.8.4. Transmission electron microscopy of IBs.....	68
2.8.5. Scanning electron microscopy.....	69
2.8.6. Atomic force microscopy.....	70
2.9. Particle size distribution.....	72
2.9.1. Size estimation with tangential flow filtration.....	72

2.9.2. Size estimation with electron microscopy.....	73
2.9.3. Dynamic light scattering.....	73
2.10. Bradford total protein assay.....	74
2.11. Dry weights.....	75
2.12. IMAC chromatography.....	76
2.13 Conclusions.....	76
REFERENCES.....	78

## CHAPTER 3. THE DENSITY AND PARTICLE SIZE OF SYNTHETIC MELAN-A INCLUSION BODIES ARE DEPENDENT ON FERMENTATION CONDITIONS

3.1. Introduction.....	81
3.2. Inclusion body size and density trends from complex media studies.....	81
3.2.1. Feeding strategies.....	81
3.2.2. IPTG effects.....	84
3.2.3. Temperature effects.....	85
3.2.4. General trends.....	87
3.2.5. Size distribution analysis.....	90
3.3. Inclusion body size and density trends from chemically defined media studies..	92
3.3.1. DOE set-up.....	92
3.3.2. Growth rates.....	93
3.3.3. General trends.....	93
3.4. Summary.....	95
REFERENCES.....	97

## CHAPTER 4. ADDITIONAL INCLUSION BODY INFORMATION

4.1. Syn-Melan-A inclusion body structure.....	98
--	----

4.1.1. Syn-Melan-A inclusion body protein accessibility.....	98
4.1.2. Syn-Melan-A inclusion body morphology.....	100
4.2. Different proteins.....	101
4.2.1. Fermentation temperature effects on inclusion body density and size of various proteins.....	102
4.2.2. Fermentation Temperature and Inclusion Body Morphology.....	102
4.2.3. Production rates.....	104
REFERENCES.....	107

## CHAPTER 5. CONCLUSIONS AND RECOMMENDATIONS

5.1. Conclusions .....	108
5.2. Recommendations.....	110
5.3. Future work.....	111
5.3.1. Additional process parameters.....	111
5.3.2. Chaperone studies.....	112
5.3.3. Inclusion body formation .....	112
5.3.4. Protease monitoring.....	112
5.3.5. Inclusion body force measurements.....	114
REFERENCES.....	116

## APPENDIX 1. ADDITIONAL ASSAY METHODOLOGY AND DEVELOPMENT

A1.1. High performance liquid chromatography.....	118
A1.2. Limulus amebocyte lysate assay.....	121

## APPENDIX 2. FERMENTATION SETUP

A2.1. Feed volume calculations.....	122
-------------------------------------	-----



A2.2. Detailed fermentor vessel set-up.....	122
A2.3. Feeding method programs.....	125
A2.4. Chemically defined medium metals.....	129
A2.5. Temperature shift programs.....	130

### APPENDIX 3. SM14 PROCESS DEVELOPMENT

A3.1. Sm14 introduction.....	131
A3.2. Supernatant processing.....	131
A3.3. Direct hydrophobic interaction chromatography.....	131
A3.4. Direct anion exchange chromatography.....	132
REFERENCES.....	135

### APPENDIX 4. NY-ESO-1 PROCESS DEVELOPMENT

A4.1. NY-ESO-1 process development introduction.....	136
A4.2. NY-ESO-1 inclusion body wash.....	136
A4.3. NY-ESO-1 protein precipitation during ion exchange chromatography.....	139
A4.4. NY-ESO-1 protein precipitation during hydrophobic interaction chromatography.....	140
A4.5. NY-ESO-1 endotoxin removal.....	140
A4.5.1. NY-ESO-1 endotoxin removal during ion exchange chromatography...	140
A4.5.2. NY-ESO-1 endotoxin removal during nickel chromatography.....	141
A4.5.3. Additional NY-ESO-1 endotoxin removal attempts.....	144
A4.6. Purification of soluble NY-ESO-1.....	144
REFERENCES.....	146

### APPENDIX 5. NY-ESO-1 PROCESS FLOWCHARTS

.....	147
APPENDIX 6. MELAN-A EXPRESSION PROCESS DEVELOPMENT	
A6.1. Melan-A research cell bank screening.....	152
A6.2. Melan-A genetic stability study.....	153
A6.3. Melan-A production in BLR <i>E. coli</i> .....	154
A6.4. Synthetic Melan-A production.....	155
A6.5. GroEL coexpression in Syn-Melan-A production.....	156
A6.6. Harvesting conditions.....	156
A6.7. Melan-A secretion in <i>Pichia pastoris</i> .....	157
APPENDIX 7. MELAN-A PURIFICATION PROCESS DEVELOPMENT	
A7.1. Melan-A clarification and solubilization.....	160
A7.1.1. Homogenization.....	160
A7.1.2. Insoluble protein preparation 1: pellet wash.....	160
A7.1.3. Insoluble protein preparation 1: tangential flow filtration.....	161
A7.1.4. Insoluble protein preparation 1: denaturant lysis.....	162
A7.2. Melan-A immobilized metal affinity chromatography.....	162
A7.2.1. Introduction.....	162
A7.2.2. Soluble Melan-A capture attempts.....	163
A7.2.3. Insoluble Melan-A capture.....	164
A7.2.4. Melan-A refolding.....	167
A7.2.5. Cobalt column.....	168
A7.3. Melan-A ion exchange chromatography.....	169
A7.4. Melan-A hydrophobic interaction chromatography.....	171
A7.5. Melan-A size exclusion chromatography.....	172
A7.6. Identification of contaminating proteins.....	173

A7.7. Influence of reducing agent.....	175
A7.8. Additives to improve Melan-A purification.....	176
A7.9. Final Melan-A purification process.....	176
REFERENCES.....	178

## APPENDIX 8. MELAN-A SECONDARY STRUCTURE

A8.1. Predicted secondary structure.....	179
A8.2. Sample preparation.....	179
A8.3. Circular dichroism.....	180
A8.4. Fourier transform infrared spectroscopy.....	180

## APPENDIX 9. QUORUM SENSING STUDY

A9.1. Introduction to autoinducer 2.....	183
A9.2. Chemical synthesis attempt of autoinducer 2.....	186
A9.3. The <i>Vibrio harveyi</i> organism.....	187
A9.4. Autoinducer 2 detection assay.....	189
A9.5. Autoinducer 2 detection assay with glucose.....	190
A9.6. Intracellular autoinducer 2 measurements.....	194
A9.7. LuxS deletion mutants.....	195
A9.8. Lag phase studies.....	196
A9.9. Discussion.....	198
REFERENCES.....	200

## LIST OF FIGURES

Figure 1.1.	Simplified diagram of formation and degradation of soluble protein and inclusion bodies.....	14
Figure 2.1.	Hydropathicity plot of proteins used in this study. ....	37
Figure 2.2.	Plasmid maps of a) pET9a24a and b) Melan-A in vector pET9a24a .....	46
Figure 2.3.	Agarose gel of Melan-A plasmids extracted from transformed cells .....	51
Figure 2.4.	Fermentation profile during high cell density culture.....	53
Figure 2.5.	Simple experimental design using central composite design of experiment.....	55
Figure 2.6.	Feed rates at different feed pump settings.....	56
Figure 2.7.	Optical density and dry cell weight correlation.....	57
Figure 2.8.	Melan-A fractions after separation in sucrose ultracentrifugation.....	60
Figure 2.9.	Inclusion body bands in cesium chloride gradients.....	62
Figure 2.10.	Cesium chloride density in an ultracentrifugation gradient.....	63
Figure 2.11	Light microscopy image of fluorescently stained inclusion bodies....	65
Figure 2.12.	TEM image of <i>E. coli</i> sections producing Melan-A as inclusion bodies.....	67
Figure 2.13.	TEM image of washed inclusion bodies.....	68
Figure 2.14.	SEM image of <i>E. coli</i> cell and inclusion body bed.....	69
Figure 2.15.	AFM image of Melan-A inclusion bodies.....	70
Figure 2.16.	SEM images of AFM probes after exposure to inclusion bodies.....	71
Figure 2.17.	Example Bradford standard curve.....	75
Figure 3.1.	Feed rate data for different feeding types.....	82

Figure 3.2.	Gel densitometry of Melan-A production under different feeding strategies.....	83
Figure 3.3.	SDS-PAGE and Image J densitometry analysis of Melan-A fractions under different concentrations of IPTG.....	84
Figure 3.4.	SDS-PAGE and Image J densitometry analysis of Melan-A fractions under different fermentation temperatures.....	86
Figure 3.5.	Inclusion body density as a function of feed rate and growth temperature in complex media.....	88
Figure 3.6.	Inclusion body size as a function of feed rate and growth temperature in complex media.....	88
Figure 3.7.	Growth curves of Syn-Melan-A in complex media.....	89
Figure 3.8.	Inclusion body size distribution as determined by dynamic light scattering.....	91
Figure 3.9.	Linear feeding profiles for fermentations conducted in chemically defined media.....	92
Figure 3.10.	Growth curves of Syn-Melan-A in chemically defined media.....	94
Figure 3.11.	Inclusion body density as a function of feed rate and growth temperature in chemically defined media.....	96
Figure 3.12.	Inclusion body size as a function of feed rate and growth temperature in chemically defined media.....	96
Figure 4.1.	Protein accessibility in Syn-Melan-A inclusion bodies by Bradford .....	99
Figure 4.2.	Protein accessibility in Syn-Melan-A inclusion bodies by TEM.....	99
Figure 4.3.	SEM image of a Syn-Melan-A inclusion body at high magnification .....	100
Figure 4.4.	SEM images of Syn-Melan-A inclusion bodies.....	101

Figure 4.5.	Densities of inclusion bodies from multiple proteins produced at different temperatures.....	103
Figure 4.6.	Size of inclusion bodies from multiple proteins produced at different temperatures.....	103
Figure 4.7.	SEM images of SSX-2 inclusion bodies.....	104
Figure 4.8.	Protein production of Melan-A and Syn-Melan-A.....	105
Figure 5.1.	SEM image of AFM probe with inclusion bodies.....	114
Figure A1.1.	Absorbance of Melan-A protein at multiple wavelengths.....	119
Figure A1.2.	Chromatogram of bovine serum albumin on RP-HPLC.....	119
Figure A1.3.	Correlation of BSA concentration and peak area on the HPLC.....	120
Figure A1.4.	Chromatogram of Melan-A sample on RP-HPLC.....	120
Figure A2.1.	Biocommand program for glucose and base feed calculated values .....	123
Figure A2.2.	Biocommand program setup for feed addition.....	126
Figure A2.3.	Dissolved oxygen and pH profiles of fermentations in complex and chemically defined media.....	127
Figure A2.4.	Biocommand program for linear feed rate addition.....	128
Figure A2.5.	Biocommand program for temperature shift.....	130
Figure A3.1.	SDS-PAGE of Sm14 after TFF or HIC purification.....	132
Figure A3.2.	Silver stain of Sm14 after anion exchange purification.....	133
Figure A3.3.	SDS-PAGE of Sm14 produced at the manufacturing scale.....	134
Figure A4.1.	SDS-PAGE of NY-ESO-1 lysate fractions through a continuous centrifuge.....	137
Figure A4.2.	SDS-PAGE of tangential flow filtration fractions using a Tween-20 wash buffer.....	137
Figure A4.3.	IMAC chromatography profiles of NY-ESO-1.....	138

Figure A4.4. Endotoxin removal during IMAC under different protein load volumes and wash volumes of triton buffer.....	143
Figure A6.1. Western blot of Melan-A production in transformed cells.....	153
Figure A6.2. Western blot of Melan-A produced from different strains of <i>E. coli</i> .....	154
Figure A6.3. SDS-PAGE and western blot of Melan-A and Syn-Melan-A.....	155
Figure A6.4. Relative GroEL expression in Syn-Melan-A Gro7 cultures.....	156
Figure A6.5. SDS-PAGE of NY-ESO-1 and Syn-Melan-A under different harvesting conditions.....	157
Figure A6.6. Melan-A expression in <i>Pichia pastoris</i> .....	159
Figure A7.1. SDS-PAGE of Melan-A fractions during tangential flow filtration .....	161
Figure A7.2. SDS-PAGE of soluble Melan-A capture attempt on a nickel column .....	164
Figure A7.3. SDS-PAGE of insoluble Melan-A capture on a nickel column.....	165
Figure A7.4. Western blot of low imidazole washes of Melan-A on a nickel column .....	165
Figure A7.5. Chromatogram of Melan-A on a nickel column.....	166
Figure A7.6. Melan-A recovery on nickel column with different load preparations .....	167
Figure A7.7. SDS-PAGE of Melan-A capture on nickel column in 3 M urea.....	168
Figure A7.8. SDS-PAGE of Melan-A purified on a cobalt column.....	168
Figure A7.9. SDS-PAGE of Melan-A purified on ion exchange columns.....	170
Figure A7.10. Chromatogram of Melan-A on an ion exchange column.....	170
Figure A7.11. Ammonium sulfate dependence of Melan-A binding on a Phenyl column.....	171

Figure A7.12. SDS-PAGE of Melan-A purified on phenyl column.....	172
Figure A7.13. SDS-PAGE of Melan-A fractions through IMAC and SEC.....	173
Figure A7.14. SDS-PAGE of higher molecular contaminants in bulk Melan-A and NY-ESO-1 drug substance.....	174
Figure A7.15. SDS-PAGE of cancer antigens with and without reducing agent.....	175
Figure A7.16. SDS-PAGE and western blot of Syn-Melan-A during final purification process.....	177
Figure A8.1. Circular dichroism spectra of Syn-Melan-A inclusion bodies and refolded protein.....	180
Figure A8.2. FTIR spectra of Syn-Melan-A inclusion bodies and refolded protein .....	181
Figure A8.3. FTIR spectra of Syn-Melan-A inclusion bodies and refolded protein, enlarged.....	182
Figure A9.1. Agarose gel and sequence evaluation of <i>V. harveyi</i> 16s rRNA.....	188
Figure A9.2. Emission spectra of <i>V. harveyi</i> luminescence.....	190
Figure A9.3. Luminescence of <i>V. harveyi</i> culture with conditioned medium.....	190
Figure A9.4. Luminescence curves from diluted <i>V. harveyi</i> cultures with fermentation samples.....	191
Figure A9.5. Influence of glucose addition to autoinducer 2 bioassay.....	193
Figure A9.6. Effect of glucose on <i>V. harveyi</i> luminescence from conditioned medium.....	193
Figure A9.7. Autoinducer 2 levels during a high cell density fermentation.....	194
Figure A9.8. Agarose gel of FY-ygaG-RY and FYRY fragments.....	196
Figure A9.9. Growth curves of <i>E. coli</i> fermentations supplemented with conditioned medium.....	197



Figure A9.10. Autoinducer 2 levels in conditioned medium and their effect to decrease lag phase.....	198
---	-----

## LIST OF TABLES

Table 1.1.	Sample strains and vectors used to produce proteins for inclusion body studies.....	7
Table 2.1.	GCUA of natural Melan-A and Syn-Melan-A.....	41
Table 2.2.	Bradford standard preparation dilutions.....	75
Table 3.1.	Inclusion body density and size for synthetic Melan-A produced with different fermentation conditions in complex medium.....	87
Table A4.1.	Recovery of NY-ESO-1 through a Q XL column using different buffers .....	140
Table A4.2.	Endotoxin removal during IMAC under different triton concentrations, temperatures, and wash volumes.....	142
Table A9.1.	Summary of glucose effects on AI-2 bioassay from literature.....	192
Table A9.2.	Intracellular autoinducer 2 levels of a high cell density <i>E. coli</i> fermentation.....	195

## LIST OF ABBREVIATIONS

AFM	atomic force microscopy
AI-2	autoinducer 2
ANS	1-anilinonaphthalene 8-sulfonate
APS	alternative protein source
AXC	anion exchange
BMM	buffered minimal methanol
BMMH	buffered minimal methanol with histidine
BRC	Biotechnology Resource Center
BSA	bovine serum albumin
CD	circular dichroism
CFSE	6-carboxyfluorescein succinimidyl ester
cP	centipoise
.CV	calculated value
CV	column volume
CXC	cation exchange
DMSO	dimethyl sulfoxide
DNA	deoxyribonucleic acid
DO	dissolved oxygen
DOE	design of experiment
DTT	dithiothreitol
EDTA	ethylenediaminetetraacetic acid
EFT	elapsed fermentation time
EF-Tu	elongation factor thermo unstable
EGFP	enhanced green fluorescent protein

FF	fast flow
fmol	femtomole
FTIR	fourier transform infrared spectroscopy
g	gram
GCUA	graphical codan usage analysis
GFP	green fluorescent protein
GST	glutathione-S-transferase
HCDC	high cell density culture
HEPES	4-(2-hydroxyethyl)-1-piperazineethanesulfonic acid
HFBA	heptafluorobutyric acid
HIC	hydrophobic interaction chromatography
His	histidine
HPLC	high performance liquid chromatography
hr	hour
HSP	heat shock protein
IB	inclusion body
IDT	Integrated DNA Technologies
IEX	ion exchange
IMAC	immobilized metal affinity chromatography
IPTG	isopropyl-beta-D-thiogalactopyranoside
kg/m <sup>3</sup>	kilogram per cubic meter
kV	kilovolt
L	liter
LAL	limulus ameocyte lysate
LB	Luria broth
M	molar

MART-1	melanoma antigen recognized by T cells 1
Melan-A	melanoma antigen A
min	minute
mg	milligram
ml	milliliter
mM	millimolar
mRNA	messenger ribonucleic acid
N	normal
NBSC	New Brunswick Scientific
NEB	New England Biosciences
ng	nanogram
OD <sub>600</sub>	optical density measured at 600nm
PBS	phosphate buffered saline
PEP	phosphoenolpyruvate
perm, p	permeate
pI	isoelectric point
PID	proportional-integral-derivative
psi	pounds per square inch
PTFE	polytetrafluoroethylene
PW-USP	United States Pharmacopeia-grade purified water
rcf	relative centrifugal force
ret, r	retentate
RP-HPLC	reverse phase high performance liquid chromatography
rpm	rotations per minute
SDS	sodium dodecyl sulfate
SDS-PAGE	sodium dodecyl sulfate polyacrylamide gel electrophoresis

SEM	scanning electron microscopy
SP	set point
Syn-Melan-A	synthetic melanoma antigen A
TAE	tris-acetate-EDTA
TCA	trichloroacetic acid
TCA	tricarboxylic acid
TEM	transmission electron microscopy
TF	trigger factor
TFA	trifluoroacetic acid
TFF	tangential flow filtration
TRAIL	tumor necrosis factors related apoptosis inducing ligand 2
Tris	tromethamine
tRNA	transfer ribonucleic acid
UF	ultrafiltration
UFDF	ultrafiltration/diafiltration
v/v	volume to volume
VHb	<i>Vitreoscilla</i> hemoglobin-like molecule
YNB	yeast nitrogen base
YPD	yeast extract peptone dextrose

## LIST OF SYMBOLS

$\beta$	coefficient
$D_p$	particle diameter
$\Delta z$	probe deflection
$\varepsilon$	intercept
$F$	force
$g$	gravity
$k$	spring constant
$\mu$	fluid viscosity
$\mu\text{FD}$	microfaraday
$\mu\text{g}$	microgram
$\mu\text{l}$	microliter
$\mu\text{m}$	micrometer, or micron
$\rho_f$	fluid density
$\rho_p$	particle density
$U_o$	settling velocity
$X$	design parameter
$Y$	response parameter
$\Omega$	ohm
$^{\circ}\text{C}$	degrees Celsius





## CHAPTER 1

### INCLUSION BODY FORMATION DURING RECOMBINANT PROTEIN PRODUCTION IN *ESCHERICHIA COLI*

#### ***1.1 Introduction***

The biotechnology-based therapeutic market was \$9.2 billion in 2007 and is projected to continue its rapid growth to \$16.1 billion by 2011. Recombinant proteins account for 68% of this market share; the remainder is divided between monoclonal antibodies and vaccines [1]. The most commonly used expression system for marketed recombinant protein fermentations in 2009 is still the bacterium *Escherichia coli*, which is the system of choice for proteins that do not require eukaryotic-type processing, such as N-linked glycosylation [2]. Important therapeutics produced in *E. coli* include insulin, interferon alpha, interferon beta 1b, interferon gamma 1b, human growth hormone, bovine growth hormone, insulin growth factor-1 (IGF-1), keratinocyte growth factor, anti-VEGF (Fab), human granulocyte colony stimulating factor (G-CSF), and interleukin 2. Recombinant human insulin alone has a \$900 million market [1].

Bioprocess engineers have refined the processes designed to produce and purify these proteins to improve process yields. Yield improvements are important because they minimize the number of production campaigns needed to produce a required amount of protein which makes production more cost and time efficient and generally increases product consistency. There are still unexplored issues of *E. coli* protein production and purification that are in need of investigation that can likely result in further yield improvements throughout the industry.

Inclusion body (IB) extraction is a common purification procedure that has not been studied in detail. Even though equipment for such a procedure has been optimized, IB extraction can be facilitated and made more predictable by altering the physical characteristics of IBs. IBs also need to be solubilized to be purified and refolded, so their resistance to denaturant is also a relevant factor to consider for improving process yields. These IB qualities can be adjusted with changes to the *E. coli* fermentation during protein production.

Evaluation of IB characteristics has grown popularity in the last five years. The major findings are described in section 1.5. The findings, however, are anecdotal and have inconsistent design variables, such as different production strains and various culture conditions. Section 1.2 provides a review of different *E. coli* strains and promoters. Section 1.3 details relevant information in *E. coli* fermentations, and Section 1.4 summarizes general IB research over the last two decades.

## ***1.2. Protein expression in Escherichia coli***

### ***1.2.1. Recombinant DNA technology***

Extracting specific proteins of interest from natural sources or synthesizing them chemically typically generates low yields. Recombinant deoxyribonucleic acid (DNA) technology provides a more practical alternative for synthesizing these proteins. This technique was first demonstrated in *E. coli* over three decades ago [3] and is used commercially today for the production of a wide range of proteins.

Plasmids are extra-chromosomal DNA molecules that permit horizontal gene transfer amongst bacteria. With the advent of restriction enzymes [4], scientists have been able to splice foreign DNA into plasmids and insert them back into bacteria. A simple way to introduce plasmids into a bacterium is through chemical competence, a

treatment of highly-concentrated calcium ions and rapid temperature shifts. A selective marker on the plasmid, commonly antibiotic resistance, makes isolation of transformants possible. The plasmid is replicated as the cell replicates and uses the cell's machinery to overexpress its coded protein.

It should be noted that there are complications with producing a human antigen with a bacterial expression system. For example, a DNA sequence has to be modified by adding a ribosome binding site and removing any original intron sequences since prokaryotic cells lack the same messenger ribonucleic acid (mRNA) processing ability that eukaryotic cells have.

In addition to bacteria, certain yeast species, such as *Saccharomyces cerevisiae*, can also utilize plasmids. In other yeast species, such as *Pichia pastoris*, and in mammalian cell lines, such as Chinese Hamster Ovary (CHO) cells, a stable transfection is needed [5]. Foreign DNA must be introduced into the cell and then integrate into the host chromosome. Otherwise the foreign protein production will be transient and cease after the first cell division.

### **1.2.2. The bacterium *Escherichia coli***

For pharmaceutical production, fermentations with bacteria are often used instead of other general host systems because they are robust, relatively inexpensive to grow, and can produce large quantities of desired material in short periods of time. *E. coli* is frequently used as a host organism for these processes because it is humankind's most well-characterized organism, both in terms of physiology and genetics [6]. In 2003, 80% of the proteins submitted to the protein data bank to solve three-dimensional structures were prepared in *E. coli* [7].

A drawback of using a recombinant bacterial system is there are limitations to the complexity of bacterial products since *E. coli* will not perform any post-

translational processing that some proteins require to be functional. There are also many purification challenges because bacteria mainly overexpress target proteins intracellularly, which makes the protein's purification more troublesome compared to if the protein were secreted. These overexpressed proteins are often not folded properly and form IBs, insoluble protein aggregates, within the cell [8].

### ***1.2.3. Promoter selection***

Polypeptide synthesis requires that the DNA be used as a template to synthesize mRNA that is translated at a ribosome. To determine which specific section of DNA is expressed, promoters serve as non-coding regions of DNA that regulate the initiation of mRNA synthesis. Constitutive promoters are used for essential housekeeping genes and express their proteins at a constant rate. When selective markers include a code for antibiotic resistance, such a non-regulated promoter is standard. Overexpressed proteins instead utilize promoters that can be regulated. In addition to creating a metabolic burden, overexpressed proteins can also be toxic to the cell and their expression requires inducible activation.

Inducible promoters that are compatible with *E. coli* are plentiful, but few are suitable for industrial protein production. The promoters for *ara* and *tet* operons, for example, are not tightly regulated and will express basal levels of protein even in an uninduced state [9]. Promoters for *tac* and *trc* can only overexpress proteins to become 15-30% of the total cellular protein [10]. Even though the pH promoter can produce levels that are 40-50% of the total cellular protein, it is not well characterized [11]. The most commonly used promoter for industrial production is the bacteriophage T7 RNA polymerase expression system in pET vectors from Novagen (Darmstadt, Germany), making up 90% of the 2003 submissions to the protein data

bank [7]. Using this expression system, the protein of interest can account for 50% or more of the total cellular protein [12].

The T7 promoter comes from bacteriophage, a virus that infects bacteria. The promoter is tightly regulated because it is unrelated to other *E. coli* DNA sequences. This is a very strong promoter because T7 RNA polymerase is very specific to its own promoter and it elongates RNA chains over five times faster than *E. coli*'s native RNA polymerase [13]. When activated, so much of the cells resources become dedicated to the synthesis of the protein of interest that the expression of the target protein is typically much larger than the expression of any host proteins and cell growth commonly stops. Lysogens have been formed by infecting cells with a lambda phage and integrating its DNA into the *E. coli* chromosome as a prophage, a dormant form of the virus that will not kill its host cell. A lysogen, which is controlled by a *lacUV5* promoter that can be induced by lactose or the nonhydrolyzable lactose analog isopropyl-beta-D-thiogalactopyranoside (IPTG), is used to provide T7 RNA polymerase because it will only introduce one copy of the T7 polymerase gene into the bacteria. Otherwise there will be too much T7 polymerase in the cell during the un-induced state.

#### ***1.2.4. Co-expression***

Multiple proteins can be overexpressed in a single cell by introduction of multiple plasmids or by the inclusion of multiple protein codes on a single plasmid. For industrial applications, the goal is rarely to simultaneously produce multiple products, but co-expression is implemented to assist in the production of a single protein of interest. Common examples of this are plasmids that code for uncommon transfer ribonucleic acid (tRNA) molecules and plasmids that code for folding chaperones.

Codon biases need to be considered when producing large amount of heterologous protein. The DNA code is degenerate because different codons commonly code for the exact same amino acid. A unique tRNA molecule is needed to match codons with the proper amino acid. *E. coli* are prokaryotic organisms, but they are often used to produce eukaryotic proteins. The bacterium is populated with tRNA molecules that match up with codons proportionate to common bacterial proteins and may not be able to supply more eukaryotic-common codons needed for efficient heterologous protein translation. The lack of these uncommon tRNA forms is the main cause of a stringent response in *E. coli* fermentation [14]. This problem can be addressed by creating a synthetic code for the protein of interest, adjusting the DNA sequence for more efficient bacterial translation while leaving the final peptide sequence unchanged. Another approach is to co-express the uncommon tRNA molecules in a pRARE plasmid (see Rosetta “strain”) [15].

Besides draining cellular resources, protein overexpression also overloads the cell’s protein folding machinery. Molecular chaperones are also known as stress or heat shock proteins (HSP) because they are upregulated under such conditions to aid in proper protein folding. When a polypeptide that requires folding assistance is initially formed, it will commonly become associated with Trigger Factor (TF) or DnaK. DnaK binding and release are regulated by the DnaJ and GrpE co-chaperones, respectively. DnaK-DnaJ-GrpE together are known as the Hsp70 system. Although a protein folding intermediate can release and rebind to these initial chaperones, it may also be transferred to GroEL/GroES (Hsp60) for further folding assistance. Aside from these folding chaperones, the cell also utilizes holdases, particularly under stress conditions, to stabilize partially folded intermediates until folding chaperones become available. In cases where the foldases and holdases have both been saturated, protein aggregates can form. At this point, there are still deaggregating chaperones, such as

ClpB, that can reintroduce intermediate proteins back to DnaK. The co-expression of any one or more of these chaperones is discussed later in section 1.4.4.

### 1.2.5. Strain selection

The firm understanding of the *E. coli* genome and current molecular biology techniques allow for chromosomal changes that create custom strains. PEP carboxylase, for example, has been overexpressed in a specific *E. coli* mutant to convert PEP directly to oxaloacetate, ultimately preventing acetate accumulation [16]. The thioredoxin pathway can be altered to permit disulfide formation in the cytoplasm (see Origami and AD494 strains) [11]. Modifications have even allowed N-linked glycosylation to occur in *E. coli* [17]. More general strains include *E. coli* O157:H7, a pathogenic strain that can result in lethal food poisoning, and *E. coli* K-12, commonly used in basic laboratory studies. Among each major strain, there are also additional variations. Some variants of the K-12 strain are C600 and MC4100 [18], which have been used in IB studies (see Table 1.1).

**Table 1.1. Sample strains and vectors used to produce proteins for inclusion body studies.** Inclusion body data has been generated from different *E. coli* strains and vectors. Le Thanh, used a *tac* promoter.

source	strain	vector	protein
Hoffman	BL26	pNF	$\beta$ -galactosidase
Kang	C600	pBV	TRAIL
Le Thanh	MC4100	<i>tac</i>	$\alpha$ -glucosidase
Margreiter	K12 HMS174	pET30a	$\beta$ -lactamase
Vera	BL21(DE3)	pET21b(+)	GFP

The most common production strains of *E. coli*, however, do not have so much variation. After a collective analysis of 10,000 proteins, several groups came to a consensus that recombinant protein expression should be attempted using a T7 promoter in a derivative of BL21(DE3) *E. coli* by default [19]. This strain is useful because it does not code for the Lon and OmpT proteases which ultimately increases protein expression yields. BLR strains are derived from BL21 strains and also lack RecA. RecA is a protein that repairs DNA, and its absence is helpful for plasmid stability. Its recombinase properties can alter plasmids, or even insert antibiotic resistance into the bacterial chromosome. BL26 is a derivative of BL21 that lacks LacZ which will prevent natural  $\beta$ -galactosidase activity.

Another BL21 derivative is the C41 strain (see Walker strain). The C41(DE3) strain continues to grow and does not experience a stress response after induction. This strain functions by limiting the accumulation of mRNA of the overexpressed protein, decreasing an mRNA overload [20]. The entire genetic difference is two mutations in the *lacUV5* promoter, dampening T7 polymerase production [21]. These strains are advertised as optimized for making soluble proteins from IB-prone proteins and membrane proteins [7]. Since C41 *E. coli* are derived from BL21, they also lack the ability to produce the Lon and OmpT proteases. It has also been shown that such strains of bacteria will ultimately produce less sigma-32, DnaK, and ClpB in response to stress conditions when compared to HB101, TOP10, or JM105 strains [22]. These proteins aid in protein folding and de-aggregation.



### ***1.3. Bioprocess Development***

#### ***1.3.1. Medium Selection***

The two major categories of fermentation medium are complex media, which are made up of natural compounds such as yeast extract, and chemically defined media, which are completely made up from a known chemical composition. Although complex media often offer a surplus of needed growth and protein production components, cultures grown in defined media are better controlled and exhibit reproducible behavior.

Defined media are typically made up a pH buffer, carbon source, nitrogen source, and trace metals. The trace metals must be dissolved in a highly acidic solution to stay in solution. Chemically defined medium permits higher cell densities and reduces the formation of acetate, a toxic by-product of metabolism [23]. On the manufacturing scale, there has also been concern with products that originate from animal sources, making chemically defined media a more attractive choice than most complex media.

#### ***1.3.2. High cell density cultures***

High cell density cultures (HCDC) are roughly defined as 50 g of dry cell weight per liter or above, some reaching as high as 115 g/L [24]. This can be compared to *E. coli* grown in Luria broth (LB) which reach a peak dry cell weight of about 1 g/L. Even though the protein titer is not directly proportional to the cell density [25], the volumetric productivity is still much higher in HCDC. In one typical example, increasing a non-HCDC culture's cell density by 60% resulted in an approximate 12% drop in cellular specific productivity. The result was still an

increase of the volumetric productivity by 40% [26]. To maximize productivity, industrial processes that grow *E. coli* are regularly performed with HCDC.

To achieve a HCDC, enough resources (i.e. carbon, nitrogen, oxygen) must be provided to the cells. The controlled introduction of these nutrients to the culture is also critical. High levels of metals can be toxic, and high levels of oxygen can lead to unwanted oxidation. A common carbon source in *E. coli* fermentation is glucose, and even high levels of it will indirectly harm the growth of a HCDC. High levels of glucose accumulate as pyruvate and saturate the cell's tricarboxylic acid (TCA) cycle. When this happens, the remaining pyruvate is converted to acetate. Acetate accumulation, which is very common in production fermentations [27], ultimately becomes toxic to the cells because undissociated forms of acetate can diffuse into the cells and lower internal pH [28].

For controlled introduction of nutrients, a fed-batch type of fermentation is the most practical [29]. Feedback control feeding strategies, which adjust feed rates based on available online measurements, are common because of their ease of use. A pH-stat control increases the feeding rate of a glucose-saturated medium to the bioreactor in response to rises in pH [30]; a dissolved oxygen (DO) -stat control calculates feed rates based on oxygen consumption responses to pauses of feed [31]. Both feedback control methods indirectly detect cell lysis that occurs upon complete glucose starvation. Upon the initiation of cell death, the medium pH increases since alkaline intracellular space is released, and dissolved oxygen rises because there are fewer cells left to use the supplied oxygen. Thus these strategies keep the cells in a constant near-death state. More complicated DO-stat controls have evolved by determining feed rates based on oxygen consumption during glucose pulses [32].

Other feeding protocols based on specific growth rate or maintenance of glucose levels are more gentle on the cells, but they often cannot keep glucose levels

at an absolute minimum. Feeding at the industrial scale may sometimes even just be a constant feed rate for ease of operation. These feeding profiles result in acetate accumulation early in the fermentation and cell starvation at the end. A linear feed rate or a step feed try to maintain the operational simplicity of a constant feed while alleviating the major stresses a constant feed rate creates.

### **1.3.3. Purification schemes**

Cell isolation is a typical first step after a fermentation has reached completion. The bacteria are separated from their growth medium via centrifugation. Intracellular protein is released by breaking open the cells. Although this can be performed chemically or with sonication, the most practical method for large culture volumes is performed with high pressure homogenization.

After cell lysis, soluble and insoluble protein fractions can be separated. Insoluble protein in *E. coli* forms aggregates known as IBs which are discussed in section 1.4. These aggregates are large enough to be separated by tangential flow filtration (TFF) [33] or centrifugation [34]. A more recently studied technique is sedimentation flow-field fractionation [35], but it is difficult to scale-up and the separation principle is the same as centrifugation. Isolated IBs must then be solubilized in chaotropic agents, such as urea or guanidine [36], before further processing.

Once in a solubilized state, protein can be purified using column chromatography. Protein solution is passed through functionalized resin beads that have specific affinities. For example, an anion exchange column has positively charge beads and will only bind negative proteins. Different concentrations of salt solution, a salt gradient, or even changes in buffer pH can be used to elute the bound protein. Some proteins may be produced with a gene modified to encode for an amino acid tag

to facilitate such purification. A His tag is commonly an additional six histidine residues synthesized at either terminus of a protein. It specifically binds to nickel in immobilized metal affinity chromatography (IMAC) and can be eluted with imidazole.

Solubilized protein must be refolded during the course of the purification process by the removal of the introduced chaotropic agent. Precautions are taken to prevent protein aggregation during refolding [37]. Refolding can be done as a final step through dilution, followed by concentration. The chaotropic agent can also be washed out while the protein is bound on a chromatography column.

#### ***1.4. Inclusion bodies***

##### ***1.4.1. IB formation***

Inclusion bodies (IBs) are insoluble protein aggregates that routinely form during heterologous protein overexpression. There are two explanations, possibly synergistic, for why IBs are formed. First, recombinant proteins that serve as human therapeutics are naturally made in mammalian cells. This eukaryotic environment is non-reducing and allows for disulfide bonds to form. The intracellular space of *E. coli* is reducing and will not allow any disulfides to form. If a disulfide bond is necessary for the structure of a given protein, then it will not be able to fold properly in the *E. coli* cytosol. Second, protein production aims to overexpress target proteins within the cell. These levels can reach an unnatural 50% of the total cellular protein [38]. This product overwhelms the cell's ability to fold it properly. It should be noted that there is still some mystery in IB formation – some mammalian proteins have no thiol groups and still form IBs in low concentrations; some recombinant proteins can be expressed in a soluble form [39].

More specifically, IBs are dynamic structures whose size is dependent on protein production rates, chaperone folding, and protease degradation rates. A nascent protein may also have the fate to be transported out of the cell, but this would require a proper secretory sequence. Based on this simplified model (see Figure 1.1), IBs will only form when protein production exceeds the rate that the *E. coli* cell can properly fold the protein into a stable, soluble form or degrade it. This frequently happens with the overexpression of recombinant proteins [38]. So even native *E. coli* proteins, such as  $\beta$ -galactosidase can form IBs.

#### ***1.4.2. Disadvantages***

IB formation has been criticized as the main bottleneck in protein production [40], and many therapeutics have not been marketed as a result of them [41]. Proteins become insoluble and aggregate because they are not folded properly. Aside from making much of the protein inaccessible because it is aggregated, misfolded protein loses functionality and would then be considered of no therapeutic or enzymatic use. Although misfolded protein can be denatured with chaotropic agents and refolded, this process can be inefficient and costly [42].

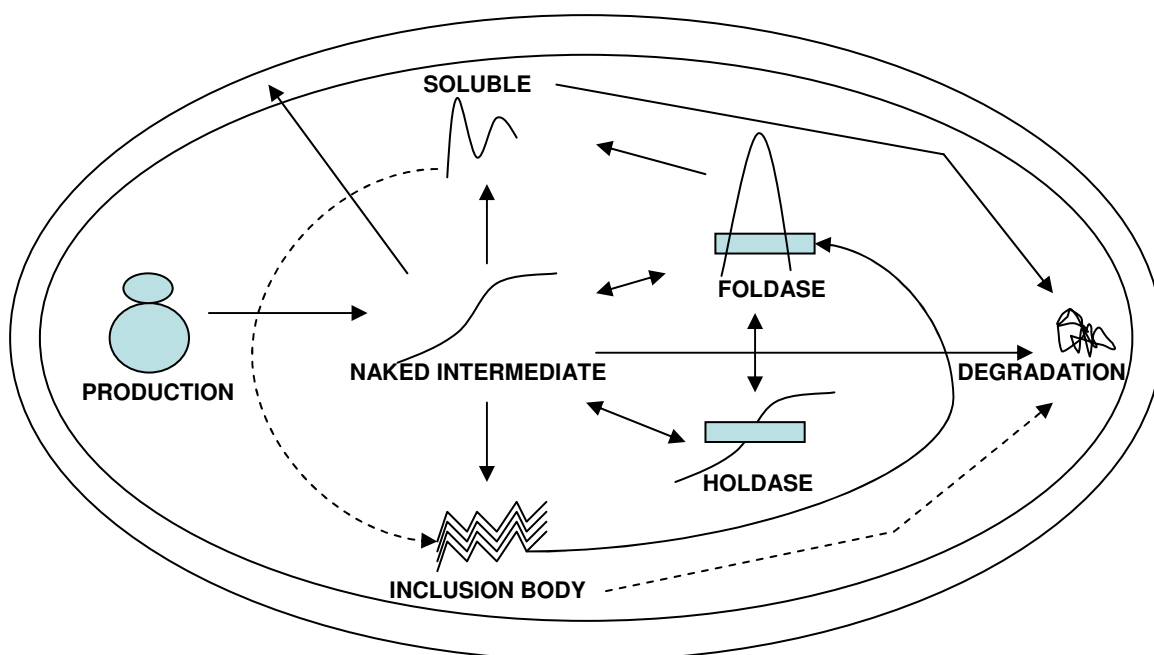


**Figure 1.1. Simplified diagram of formation and degradation of soluble protein and inclusion bodies.**

Nascent polypeptides are produced at the bacteria's ribosome. The protein intermediate then has several fates, depending on if it encounters a chaperone, protease, or neither. Double arrows indicate iterative steps. Dotted arrows represent unconfirmed steps.

More recent findings have suggested that there is some organized protein folding in IBs. There have been several reports of IBs that have been found to be a collection of  $\beta$ -sheets connected by hydrogen bonds, not dissimilar to amyloid aggregates. Although these  $\beta$ -sheets typically replace  $\alpha$ -helices found in the soluble structure, such as in  $\beta$ -lactamase [43], the protein in IBs does have activity, particularly the embedded regions in the core of the aggregate [44]. Because IBs are very porous, this trend suggests that some IBs can at least be used as catalysts [41]. It is unknown whether this feature applies to all IBs. Regardless of their activity, however, proteins must be solubilized to be subjected to conventional chromatographic techniques necessary for purification. A biochemical and

biophysical characterization of the protein cannot be performed until the protein is isolated in a soluble and monodispersed form [45].

To compound matters, IB formation is the norm in recombinant production processes [39]. Insulin-like growth factor-I [46] and leptin [47] are two of the very limited number of cases where protein has been produced in large soluble quantities within *E. coli*. In these cases, the protein was transported to the periplasmic space of the cell.

### ***1.4.3. Advantages***

There are actually key positive qualities of IBs that make them helpful in protein production. Because IB formation is typically unavoidable, it stands to reason that processes should take advantage of these positive qualities. As aggregates, the protein will be less accessible. This isolation of recombinant proteins is useful when manufacturing unstable proteins because they are protected from proteases [48]. In the case of producing proteins that may be toxic to the cell, the cell is then protected since these proteins are not functional [49]. Another very attractive feature of IBs is their ability to aid in purification processes.

IBs themselves are comprised almost exclusively of recombinant protein, with purities that can reach over 90% [42]. The remainder of the protein is largely chaperones and proteases that were associated with these recombinant proteins as they aggregated [50]. It has been shown, in fact, that mixtures of two different protein folding intermediates, P22 tail spikes and coat proteins, will not randomly aggregate, but they will instead selectively form pure aggregates [51]. Thus if the IBs of an *E. coli* fermentation can be isolated, much of the purification work has already been completed. IB isolation is a relatively simple process because IBs are much larger than all other cellular contaminants.

The general form for particle settling velocity in a centrifuge is analogous to the well-established equation for solid particle settling:

$$U_o = \frac{gD_p^2(\rho_p - \rho_f)}{18\mu} \quad (1)$$

where  $U_o$  is the settling velocity,  $g$  is the gravitational force,  $D_p$  is the particle diameter,  $\rho_p$  and  $\rho_f$  are the densities of the particles and fluid, and  $\mu$  is the viscosity of the fluid. In the case of centrifugation, the  $g$  value can be substituted with an applied gravity force, which is 5,000-12,000 $g$  for IBs [39]. Unfortunately, the density of IBs (~1.3 g/ml) is only slightly higher than water [52] and the viscosity of cell lysate can be rather high. Fortunately, there is an exponential dependence on particle size that dictates that larger particles are easier to separate than smaller particles.

There are several different types of filters used for IB isolation. These ultrafiltration processes are all strongly dependent on particle size. IB structures have been determined to be very porous and in cylindrical and ovoid shapes [53]. Because protein is typically pushed through filters at high pressures, the compressibility and shape of IBs become an issue. One type of filter is a depth filter. Like a centrifuge, depth filters that act as a molecular sieve have a strong dependence on particle size and some influence from particle density and fluid viscosity. The other common type of filter, anisotropic membranes, has a thin porous layer on top that ideally has fixed pore sizes that particles must be smaller than to pass through. If large IBs are obtained, the pore sizes can be correspondingly large, which will permit the removal of more contaminants. In addition, a cake layer forms to inhibit flux through the membrane, and the resistance of this cake is decreased when particle size is larger. Just as in the case of centrifugation, filtration is also made more efficient when IB particles are larger.



#### ***1.4.4. Chaperone co-expression***

Some of the main evidence that IBs form from protein folding intermediates is the identity of the impurities found in IBs. Some of these proteins are the elongation factor EF-Tu and the large ribosomal subunits L7, L12, and L13, suggesting IB formation is associated with protein synthesis [50]. Furthermore, research has shown that manipulating the levels of folding chaperones in the cell can affect IB formation.

The most dramatic and extensive results using chaperones for IB manipulation has been performed with DnaK and GroEL. It has been suggested that the effects caused by other chaperones in IB formation have limited effect in comparison to these two chaperones [54]. *In vitro* experiments have shown that high DnaK concentrations can decrease insoluble protein levels by 90%. GroEL, HtpG, IbpB, and BSA could not decrease insoluble protein by more than 25% in these same experiments [55]. When immunolabeling was performed for these main chaperones in *E. coli* sections, it was found that DnaK is localized at the periphery of IBs and GroEL is located throughout the cell, including inside the protein aggregate [56]. A conclusion that could be made is that folding intermediates in contact with DnaK do not simultaneously aggregate. Instead, DnaK becomes associated with aggregated protein, which is understandable because it works in combination with the deaggregation role of ClpB [55]. Meanwhile, GroEL can be trapped within IBs, and it may even possibly play a role in their formation and structure.

It has been shown that coexpressing DnaJK or GroESL can increase yields of active protein. Nishihara used *E. coli* strain MG1655 to produce Cryj2, an allergen of Japanese cedar pollen [57]. Thomas used *E. coli* strain JM105 to produce preS2-S'-B-galactosidase and got identical results [58]. Both groups found that coexpressing DnaJK or GroESL could increase soluble levels of their target protein 3-6 fold and 4 fold, respectively. These experiments were all done at 30°C. Thomas also showed

that DnaK coexpression maintained its effect at 37°C and 42°C, but GroEL had no effect at these elevated temperatures. It was also shown that coexpressing  $\sigma^{32}$ , a transcription factor that promotes the synthesis of DnaK, DnaJ, GrpE, GroEL, and GroES, could cause a 2-3 fold increase in soluble protein.

It has been noted, however, that these chaperone coexpressions are not able to increase the solubility for many specific proteins. Coexpressing chaperones to increase soluble protein levels appear to succeed on a “trial-and-error” basis [59]. Also, less aggregated protein does not mean that there will be more soluble protein available. One group found that GroEL would break apart human basic fibroblast growth factor IBs but that this protein is proteolysed instead of being introduced into the soluble fraction [60]. In other cases where more soluble protein was made, GroESL caused severe proteolysis [61].

#### ***1.4.5. Chaperone deletion***

Knocking out *dnaJ* and *dnaK* resulted in higher total expression of recombinant protein and much higher aggregation of Cryj2. *GroEL* and *groES* mutants produced slightly lower amounts of total protein and produced more unstable Cryj2, but there was no noticeable difference in aggregation percentages [57]. In another study that used the protein VP1LAC as a model, it was agreed that knocking out *dnaK* results in larger IBs, but *groEL* removal resulted in numerous small protein aggregates with a much higher soluble protein fraction. *GroES* knockouts did not show these phenomena [54].

These results can be explained by additional findings about the roles of these chaperones. When protein production is stopped, which can be done with the proper antibiotic, cytoplasmic IBs can be degraded in a matter of hours [62]. As such, even if net production is slow, there is always a rapid rate of protein synthesis and degradation

at play within the cell. If DnaK is not present to assist in IB deaggregation, then IB formation will be effectively irreversible and the total amount of recombinant protein and its percentage in IBs will increase appreciably, as observed. Meanwhile, the complete absence of GroEL has been shown to increase IB instability [54]. This may seem contradictory since both the overexpression and deletion of GroEL both cause decreased aggregation. A possible explanation is that GroEL is an integral part of the natural IB structure, and its overabundance aids in disaggregation. This may explain the dual roles of GroEL in supporting IB formation in the wildtype and increasing solubility at higher concentrations when it is coexpressed.

The *rpoH* gene encodes for the  $\sigma^{32}$  factor. Levels of this transcription factor are directly proportional to levels of DnaK, DnaJ, GrpE, GroEL, and GroES. A  $\Delta rpoH$  mutant produced several fold more protein, all in the insoluble fraction [57]. It should be noted, however, that there are consequences for using such knockout mutants. Particularly, removing *rpoH* causes severe growth defects and such cells can only be grown at 20°C [63]. Even operating at low levels of DnaK or GroEL has been shown to have cytotoxic effects that may influence IB kinetics indirectly [64].

Further caution should be taken when interpreting data from these studies because chaperone levels are interconnected. For example, *clpA* mutants have higher levels of DnaK and GroEL. When DnaK accumulates in the cell, sigma-32 production is inhibited; GroEL accumulation does not have this effect [65]. It has also been shown that when GroE levels are reduced in the cell,  $\sigma^{32}$  expression increases to compensate [66]. This may simply be a response to accumulated unfolded protein within the cell.

#### ***1.4.6. Process conditions***

There have been numerous strategies developed to minimize IB formation on the fermentation scale. Lowering temperature is the most common method to increase the percentage of soluble protein [67]. These low growth temperatures have also been shown to improve the solubility of the protein in IBs [68]. Similarly, better protein folding has been shown to be a result of slower feeding [69] and decreased promoter induction [70]. These methods likely decrease the rate of protein synthesis so that the available folding chaperones are not titrated. Increasing medium osmolarity with certain salts, such as betaine and proline, also aid in folding [71]. Salts have been shown to complement the folding ability of GroEL [72]. For some proteins, site directed mutagenesis has been able to greatly enhance the amount of properly folded protein produced in the cell [73].

IB formation can be increased by increasing temperature, which has been demonstrated for temperatures up to 44°C, or by decreasing the pH of growth medium, as low as 5.5. [74]. The amount of acetate accumulation permitted during fermentation is relevant since it will influence the pH.

Different types of medium will also influence IB formation. An enriched medium has been shown to increase soluble protein [75]. It has also been observed for  $\beta$ -galactosidase that IB formation can be avoided by growth in a complex medium [76]. Complex media avoid a stringent response commonly caused by using defined media [77]. On the other hand, it has also been shown with microarray analysis that the metabolic burden caused by growing cells at high cell densities is decreased in a chemically defined medium [78].

Other growth conditions have given inconsistent results in terms of IB formation. Low dissolved oxygen levels, for example, can cause more or less IB formation depending on the promoter and vector used [79]. Adding ethanol (3% v/v)

to cultures increases IB formation for some proteins but has the opposite effects for others [80].

There has been some work connecting fermentation conditions with levels of sigma-32 expression. Production of this factor is induced by high temperatures, starvation conditions [81], and damaged protein [82]. Damaged protein can be induced by alcohol (ethanol), heavy metals ( $\text{CdCl}_2$ ), antibiotics (novobiocin), and hydrogen peroxide. Adding dithiothreitol (DTT) to cause a reducing stress increases DnaK levels and decreases that of GroEL [83].

### ***1.5. Tailoring IB physical and chemical characteristics***

#### ***1.5.1. IB classes***

At any given time, there is a distribution of IBs within a cell [84]. Using differential centrifugation, two groups of *Vitreoscilla* hemoglobin-like molecule (VHb) IBs were obtained from *E. coli* lysate. One-dimensional and two-dimensional gel electrophoresis data suggested that the composition of these IB populations may be different [85]. A separate study of GFP-GST IBs suggested that there could be four different aggregation classes of those IBs, mainly inferred from different densities [86].

#### ***1.5.2. GFP studies***

When induced in LB medium at an optical density of 0.5, insoluble GFP from cultures with plasmid pET21-b in BL21(DE3) *E. coli* was shown to have more fluorescent activity at lower production temperatures. This IB activity phenomenon was also observed in a fusion of GFP and a point mutant of A $\beta$ 42 Alzheimer peptide [87]. Additionally, it was found that GFP-A $\beta$ 42 IBs produced at higher temperatures

were more stable with respect to chemical denaturation when using proteinase K or guanidine hydrochloride. It was also found, using phase contrast microscopy, that IBs produced at 18 °C were 0.9  $\mu\text{m}$  in size while IBs produced from 25 °C to 42 °C were 1.1 to 1.2  $\mu\text{m}$  in size.

Using a light scattering method, the size of GFP IBs was analyzed for cultures where different IPTG concentrations, temperatures, and time post-induction were used [88]. IBs produced at 37 °C were in the size of 550-690 nm in 0.1 mM IPTG and 645-715 nm in 2 mM IPTG. IBs produced at 30 °C spanned the range of 500-950 nm regardless of IPTG concentration.

### ***1.5.3. IPTG concentrations***

Unlike GFP (Section 1.5.2), a study of a  $\beta$ -lactamase variant showed that increasing IPTG concentrations from 1 to 20  $\mu\text{mol}$  per g dry cell weight decreased the diameter of inclusion bodies from  $446 \pm 50$  to  $371 \pm 52$  nm. Size measurements were conducted using sedimentation field-flow fractionation [89].

### ***1.5.4. Specific growth rates***

Different-sized IBs were formed when apoptosis-inducing ligand 2 (Apo2L) was produced in *E. coli* with different specific growth rates immediately prior to induction in a complex medium [90]. Growing at 0.05  $\text{hr}^{-1}$ , Apo2L IBs were 0.28  $\mu\text{m}$  in size and had a trypsin digest half-time of 26 min. The Apo2L IBs made when growing at 0.15  $\text{hr}^{-1}$  at preinduction were 0.34  $\mu\text{m}$  in size, had a trypsin digest half-time of 55 min, and were described as being more spherical. The circular dichroism spectra of the first group of IBs more closely resembled the native spectra of soluble protein.

Growth rates were limited during the production of  $\alpha$ -galactosidase in a fed-batch *E. coli* fermentation. IBs formed and  $\alpha$ -galactosidase activity was low when the growth rate at induction was  $0.2 \text{ hr}^{-1}$ . No IBs were formed and activity was high at an induction growth rate of  $0.06 \text{ hr}^{-1}$ . At an induction growth rate of  $0.12 \text{ hr}^{-1}$ , IBs did form and protein activity was not compromised, reinforcing the concept of different IB classes [91].

#### ***1.5.5. Fermentation Type***

IB formation has already been shown to be different in shake flasks instead of bioreactors. Shake flask cultures tend to have more IB formation due to the lack of pH control [92].

Protein aggregation produced during fed-batch fermentations is different than batch fermentations. The fibroblast growth factor hFGF-2, for example, forms IBs when grown in batch mode ( $\text{OD}_{600} = 0.4\text{-}0.6$ ), but much of the protein becomes soluble when grown in a fed-batch fermentation ( $\text{OD}_{600} = 100$ ) [76].

When switching from a complex medium in shake flasks to a defined medium in a fed-batch bioreactor, protein activity was found to be much higher for the production of  $\alpha$ -galactosidase [91]. Although defined media typically favor IB formation, the use of a fed-batch fermentation outweighed this contribution.

#### ***1.6. Conclusions***

IB formation is common in the production of recombinant proteins. Most previous data has focused on decreasing the amount of insoluble protein in such productions. The methods to do this, typically by adjusting chaperone levels, are complicated to practically implement and often partially effective at best. These studies have also mostly been performed in shake flasks, but results will change if

protein is produced in a HCDC. Previous studies also ignore the physical and chemical characteristic of IBs, although these qualities may affect final protein yields. This study aims to determine the effects of HCDC conditions on IB quality to suggest fermentation improvements to increase industrial process yields.

As illustrated in Table 1.1, IB studies have been inconsistent at the cellular level with regards to the protein, plasmid, and *E. coli* strain studied. These studies have also been inconsistent on the manufacturing level with regards to media composition, cell densities, and feeding strategies. It is one of this study's goals to summarize and discover new data on IB-dependence of fermentation conditions using a single, representative system of recombinant protein production.



## REFERENCES

- 1) G. Tamburini, The World (Biotech) API's Market, Chemical Pharmaceutical Generic Association (Milan, Italy, 2008).
- 2) E. Langer, Capitalizing on novel expression systems, Genet. Eng. Biotechnol. News 29 [2009] 12.
- 3) S. Cohen, A. Chang, H. Boyer, R. Helling, Contruction of biologically functional bacterial plasmids *in vitro*, Proc. Nat. Acad. Sci. USA 70 [1973] 3240-3244.
- 4) D. Nathans, H. Smith, Restriction endonucleases in the analysis and restructuring of DNA molecules, Annu. Rev. Biochem. 44 [1975] 273-293.
- 5) C. Chen, H. Okayama, High-efficiency transformation of mammalian cells by plasmid DNA, Mol. Cell Biol. 7 [1987] 2745-2752.
- 6) G. Georgiou, Optimizing the Production of Recombinant Proteins in Microorganisms, AIChE J. 34 [1988] 1233-1248.
- 7) H. Sørensen, K. Mortensen, Advanced genetic strategies for recombinant protein expression in *Escherichia coli*, J. Biotechnol. 115 [2005] 113-128.
- 8) D. Williams, R. Van Frank, W. Muth, J. Burnett, Cytoplasmic inclusion bodies in *Escherichia coli* producing biosynthetic human insulin proteins, Science 215 [1982] 687-689.
- 9) R. Lutz, H. Bujard, Independent and tight regulation of transcriptional units in *Escherichia coli* via the LacR/O, the TetR/O and AraC/I<sub>1</sub>-I<sub>2</sub> regulatory elements, Nucleic Acids Res. 25 [1997] 1203-1210.
- 10) F. Baneyx, Recombinant protein expression in *Escherichia coli*, Curr. Opin. Biotechnol. 10 [1999] 411-421.
- 11) S. Jana, J. Deb, Strategies for efficient production of heterologous proteins in *Escherichia coli*, Appl. Microbiol. Biotechnol. 67 [2005] 289-298.

- 12) F. Studier, B. Moffatt, Use of bacteriophage T7 RNA polymerase to direct selective high-level expression of cloned genes, *J. Mol. Biol.* 189 [1986] 113-130.
- 13) M. Chamberlin, J. McGrath, L. Waskell, New RNA polymerase from *Escherichia coli* infected with bacteriophage T7, *Nature* 228 [1970] 227-231.
- 14) J. Kane, Effects of rare codon clusters on high-level expression of heterologous proteins in *Escherichia coli*, *Curr. Opin. Biotechnol.* 6 [1995] 494-500.
- 15) G. Dieci, L. Bottarelli, A. Ballabeni, S. Ottonello, tRNA-assisted overproduction of eukaryotic ribosomal proteins, *Prot. Expr. Pur.* 18 [2000] 346-354.
- 16) W. Farmer, J. Liao, Reduction of aerobic acetate production by *Escherichia coli*, *Appl. Environ. Microbiol.* 63 [1997] 3205-3210.
- 17) M. Wacker, D. Linton, P. Hitchen, M. Nita-Lazar, S. Haslam, S. North, M. Panico, H. Morris, A. Dell, B. Wren, M. Aebi, N-Linked Glycosylation in *Campylobacter jejuni* and its functional transfer into *E. coli*, *Science* 298 [2002] 1790-1793.
- 18) J. Peters, T. Thate, N. Craig, Definition of *Escherichia coli* MC4100 genome by use of a DNA array, *J. Bacteriol.* 185 [2003] 2017-2021.
- 19) S. Graslund, P. Nordlund, J. Weigelt, J. Bray, B. Hallberg, O. Gileadi, S. Knapp, U. Oppermann, C. Arrowsmith, R. Hui, J. Ming, S. Dhe-Paganon, H. Park, A. Savchenko, A. Yee, A. Edwards, R. Vincentelli, C. Cambillau, R. Kim, S. Kim, Z. Rao, Y. Shi, T. Terwilliger, C. Kim, L. Hung, G. Waldo, Y. Peleg, S. Abeck, T. Unger, O. Dym, J. Prilusky, J. Sussman, R. Stevens, S. Lesley, I. Wilson, A. Joachimiak, F. Collart, I. Dementieva, M. Donnelly, W. Eschenfeldt, Y. Kim, L. Stols, R. Wu, M. Zhou, S. Burley, J. Emtage, J. Sauder, D. Thompson, K. Bain, J. Luz, T. Gheyi, F. Zhang, S. Atwell, S. Almo, J. Bonanno, A. Fiser, S. Swaminathan, F. Studier, M. Chance, A. Sali, T. Acton, R. Xiao, L. Zhao, L.

- Ma, J. Hunt, L. Tong, K. Cunningham, M. Inouye, S. Anderson, H. Janjua, R. Shastry, C. Ho, D. Wang, H. Wang, M. Jiang, G. Montelione, D. Stuart, R. Owens, S. Daenke, A. Schutz, U. Heinemann, S. Yokoyama, K. Bussow, K. Gunsalus, Protein production and purification, *Nat. Methods* 5 [2008] 135-146.
- 20) B. Miroux, J. Walker, Over-production of proteins in *Escherichia coli*: mutant hosts that allow synthesis of some membrane proteins and globular proteins at high levels, *J. Mol. Biol.* 260 [1996] 289-298.
- 21) S. Wagner, M. Klepsch, S. Schlegel, A. Appel, R. Draheim, M. Tarry, M. Hogbom, K. Wijk, D. Slotboom, J. Persson, J. Gier, Tuning *Escherichia coli* for membrane protein overexpression, *Proc. Natl. Acad. Sci. USA* 105 [2008] 14371-14376.
- 22) J. Seo, D. Kang, H. Cha, Comparison of cellular stress levels and green-fluorescent-protein expression in several *Escherichia coli* strains, *Biotechnol. Appl. Biochem.* 37 [2003] 103-107.
- 23) H. Meyer, C. Leist, A. Fiechter, Acetate formation in continuous culture of *Escherichia coli* K12 D1 on defined and complex media, *J. Biotechnol.* 1 [1984] 355-358.
- 24) V. Babaeipour, S. Shojaosadati, S. Robatjazi, R. Khalizadeh, N. Magsoudi, Over-production of human interferon- $\gamma$  by HCDC of recombinant *Escherichia coli*, *Process Biochem.* 42 [2007] 112-117.
- 25) G. Kleman, W. Strohl, Developments in high cell density and high productivity microbial fermentation, *Curr. Opin. Biotechnol.* 5 [1994] 180-186.
- 26) S. Yim, K. Jeong, S. Lee, High-level secretory production of human granulocyte-colony stimulating factor by fed-batch culture of recombinant *Escherichia coli*, *Bioprocess Biosyst. Eng.* 24 [2001] 249-254.

- 27) G. Luli, W. Strohl, Comparison of growth, acetate production, and acetate inhibition of *Escherichia coli* strains in batch and fed-batch fermentations, Appl. Environ. Microbiol. 56 [1990] 1004-1011.
- 28) D. Repaske, J. Adler, Change in intracellular pH of *Escherichia coli* mediates the chemotactic response to certain attractants and repellents, J. Bacteriol. 145 [1981] 1196-1208.
- 29) L. Yee, H. Blanch, Recombinant protein expression in high cell-density fed-batch cultures of *Escherichia coli*, Biotechnology 10 [1992] 1550-1556.
- 30) J. Robbins, K. Taylor, Optimization of *Escherichia coli* growth by controlled addition of glucose, Biotechnol. Bioeng. 34 [1989] 1289-1294.
- 31) M. Åkesson, E. Karlsson, P. Hagander, J. Axelsson, A. Tocaj, On-line detection of acetate formation in *Escherichia coli* cultures using dissolved oxygen responses to feed transients, Biotechnol. Bioeng. 64 [1999] 590-597.
- 32) J. Zawada, J. Swartz, Maintaining rapid growth in moderate-density *Escherichia coli* fermentations, Biotechnol. Bioeng. 89 [2005] 407-415.
- 33) S. Forman, E. DeBernardez, R. Feldberg, R. Swartz, Crossflow filtration for the separation of inclusion bodies from soluble proteins in recombinant *Escherichia coli* cell lysate, J. Membr. Sci. 48 [1990] 263-279.
- 34) B. Batas, C. Schiraldi, J. Chaudhuri, Inclusion body purification and protein refolding using microfiltration and size exclusion chromatography, J. Biotechnol. 68 [1999] 149-158.
- 35) S. Williams, G. Raner, W. Ellis, J. Giddings, Separation of protein inclusion bodies from *Escherichia coli* lysates using sedimentation field-flow fractionation, J. Microcolumn Sep. 9 [1997] 233-239.

- 36) W. Lim, J. Rösger, S. Englander, Urea, but not guanidinium, destabilizes proteins by forming hydrogen bonds to the peptide group, *Proc. Natl. Acad. Sci. USA* 106 [2009] 2595-2600.
- 37) A. Jungbauer, W. Kaar, Current status of technical protein refolding, *J. Biotechnol.* 128 [2007] 587-596.
- 38) F. Baneyx, M. Mujacic, Recombinant protein folding and misfolding in *Escherichia coli*, *Nat. Biotechnol.* 22 [2004] 1399-1408.
- 39) F. Marston, The purification of eukaryotic polypeptides synthesized in *Escherichia coli*, *Biochem. J* 240 [1986] 1-12.
- 40) S. Ventura, Sequence determinants of protein aggregation: tools to increase protein solubility, *Microb. Cell Fact.* 4 [2005].
- 41) E. García-Fruitós, N. González-Montalbán, M. Morell, A. Vera, R. Ferraz, A. Arís, S. Ventura, A. Villaverde, Aggregation as bacterial inclusion bodies does not imply inactivation of enzymes and fluorescent proteins, *Microb. Cell Fact.* 4 [2005].
- 42) E. Clark, Protein refolding for industrial processes, *Curr. Opin. Biotechnol.* 12 [2001] 202-207.
- 43) T. Przybycien, J. Dunn, P. Valax, G. Georgiou, Secondary structure characterization of beta-lactamase inclusion bodies, *Protein Eng.* 7 [1994] 131-136.
- 44) N. González-Montalbán, E. García-Fruitós, A. Villaverde, Recombinant protein solubility--- does more mean better? *Nat. Biotechnol.* 25 [2007] 718-720.
- 45) J. Stegemann, R. Ventzki, A. Schrödel, A. de Marco, Comparative analysis of protein aggregates by blue native electrophoresis and subsequent sodium dodecyl sulfate-polyacrylamide gel electrophoresis in a three-dimensional geometry gel, *Proteomics* 5 [2005] 2002-2009.

- 46) J. Joly, W. Leung, J. Swartz, Overexpression of *Escherichia coli* oxidoreductase increases recombinant insulin-like growth factor-I accumulation, Proc. Natl. Acad. Sci. USA 95 [1998] 2773-2777.
- 47) K. Jeong, S. Lee, Secretory production of human leptin in *Escherichia coli*, Biotechnol. Bioeng. 67 [2000] 398-407.
- 48) H. Hellebust, M. Murby, L. Abrahmsen, M. Uhlen, S. Enfors, Different approaches to stabilize a recombinant fusion protein, Bio/Technology 7 [1989] 165-168.
- 49) M. Howell, K. Blumenthal, Cloning and expression of a synthetic gene for *Cerebratulus lacteus* neurotoxin B-IV, J. Biol. Chem. 264 [1989] 15268-15273.
- 50) U. Rinas, J. Bailey, Protein compositional analysis of inclusion bodies produced in recombinant *Escherichia coli*. Appl. Microbiol. Biotechnol. 37 [1992] 609-614.
- 51) M. Speed, D. Wang, J King, Specific aggregation of partially folded polypeptide chains: the molecular basis of inclusion body composition. Nat. Biotechnol. 14 [1996] 1283-1287.
- 52) G. Taylor, M. Hoare, D. Gray, F. Marston, Size and density of protein inclusion bodies, Biotechnology 4 [1986] 553-557.
- 53) G. Bowden, G. Georgiou, Folding and aggregation of  $\beta$ -lactamase in the periplasmic space of *Escherichia coli*, J. Biol. Chem. 265 [1990] 16760-16766.
- 54) M. Carrió, A. Villaverde, Role of molecular chaperones in inclusion body formation, FEBS Lett. 537 [2003] 215-221.
- 55) A. Mogk, T. Tomoyasu, P. Goloubinoff, S. Rudiger, D. Roder, H. Langen, B. Bukau, Identification of thermolabile *Escherichia coli* proteins: prevention and reversion of aggregation by DnaK and ClpB, EMBO J 18 [1999] 6934-6949.

- 56) M. Carrió, A. Villaverde, Localization of chaperones DnaK and GroEL in bacterial inclusion bodies, *J. Bacteriol.* 187 [2005] 3599-3601.
- 57) K. Nishihara, M. Kanemori, M. Kitagawa, H. Yanagi, T. Yura, Chaperone coexpression plasmids: differential and synergistic roles of DnaK-DnaJ-GrpE and GroEL-GroES in assisting folding of an allergen of Japanese cedar pollen, *Appl. Environ. Microbiol.* 64 [1998] 1694-1699.
- 58) J. Thomas, F. Baneyx, Protein misfolding and inclusion body formation in recombinant *Escherichia coli* cells overexpressing heat-shock proteins, *J. Biol. Chem.* 271 [1996] 11141-11147.
- 59) M. Weickert, D. Doherty, E. Best, P. Olins, Optimization of heterologous protein production in *Escherichia coli*, *Curr. Opin. Biotechnol.* 7 [1996] 494-499.
- 60) U. Rinas, F. Hoffman, E. Betiku, D. Estapé, S. Marten, Inclusion body anatomy and functioning of chaperone-mediated *in vivo* inclusion body disassembly during high-level recombinant protein production in *Escherichia coli*, *J. Biotechnol.* 127 [2007] 244-257.
- 61) L. Roman, E. Sheta, P. Martasek, S. Gross, Q. Liu, B. Masters, High-level expression of functional rat neuronal nitric oxide synthase in *Escherichia coli*, *Proc. Natl. Acad. Sci. USA* 92 [1995] 8428-8432.
- 62) M. Carrió, A. Villaverde, Protein aggregation as bacterial inclusion bodies is reversible, *FEBS Lett.* 489 [2001] 29-33.
- 63) Y. Zhou, N. Kusukawa, J. Erickson, C. Gross, T. Yura, Isolation and characterization of *Escherichia coli* mutants that lack the heat shock sigma factor  $\sigma^{32}$ , *J. Bacteriol.* 170 [1988] 3640-3649.
- 64) N. González-Montalbán, M. Carrió, S. Cuatrecasas, A. Arís, A. Villaverde, Bacterial inclusion bodies are cytotoxic *in vivo* in absence of functional chaperones DnaK or GroEL, *J. Biotechnol.* 118 [2005] 406-412.

- 65) A. da Silva, R. Simão, M. Susin, R. Baldini, M. Avedissian, S. Gomes, Downregulation of the heat shock response is independent of DnaK and  $\sigma^{32}$  levels in *Caulobacter crescentus*, Mol. Microbiol. 49 [2003] 541-553.
- 66) M. Kanemori, H. Mori, T. Yura, Effects of reduced levels of GroE chaperones on protein metabolism: enhanced synthesis of heat shock proteins during steady-state growth of *Escherichia coli*. J. Bacteriol. 176 [1994] 4235-4242.
- 67) Y. Shirano, D. Shibata, Low temperature cultivation of *Escherichia coli* carrying a rice lipoxygenase L-2 cDNA produces a soluble and active enzyme at a high level. FEBS Lett. 271 [1990] 128-130.
- 68) A. Vera, N. González-Montalbán, A. Arís, A. Villaverde, The conformational quality of insoluble recombinant proteins is enhanced at low growth temperature, Biotechnol. Bioeng. 96 [2007] 1101-1106.
- 69) B. Hoffman, J. Broadwater, P. Johnson, J. Harper, B. Fox, W. Kenealy, Lactose fed-batch overexpression of recombinant metalloproteins in *Escherichia coli* BL21(DE3): process control yielding high levels of metal-incorporated, soluble protein, Protein Expr. Purif. 6 [1995] 646-654.
- 70) M. Weickert, M. Pagratis, S. Curry, R. Blackmore, Stabilization of apoglobin by low temperature increases yield of soluble recombinant hemoglobin in *Escherichia coli*, Appl. Environ. Microbiol. 63 [1997] 4313-4320.
- 71) S. Diamant, N. Eliahu, D. Rosenthal, P. Goloubinoff, Chemical chaperones regulate molecular chaperones *in vitro* and in cells under combined salt and heat stresses, J. Biol. Chem. 276 [2001] 39586-39591.
- 72) P. Voziyan, M. Fisher, Chaperonin-assisted folding of glutamine synthetase under nonpermissive conditions: Off-pathway aggregation propensity does not determine the co-chaperonin requirement, Protein Sci. 9 [2000] 2405-2412.



- 73) M. Murby, E. Samuelsson, T. Nguyen, L. Mignard, U. Power, H. Binz, M. Uhlen, S. Stahl, Hydrophobicity engineering to increase solubility and stability of a recombinant protein from respiratory syncytial virus, *Eur. J. Biochem.* 230 [1995] 38-44.
- 74) L. Strandberg, S. Enfors, Factors influencing inclusion body formation in the production of a fused protein in *Escherichia coli*, *Appl. Environ. Microbiol.* 57 [1991] 1669-1674.
- 75) J. Moore, A. Uppal, F. Maley, G. Maley, Overcoming inclusion body formation in a high-level expression system, *Protein Expr. Purif.* 4 [1993] 160-163.
- 76) F. Hoffman, J. Heuvel, N. Zidek, U. Rinas, Minimizing inclusion body formation during recombinant protein production in *Escherichia coli* at bench and pilot plant scale, *Enzyme Microb. Technol.* 34 [2004] 235-241.
- 77) A. Panda, R. Khan, S. Mishra, R. Appa, & S. Totey, Influences of yeast extract on the specific cellular yield of ovine growth hormone in *E. coli*, *Bioprocess Eng.* 22 [2000] 379-383.
- 78) Y. Wei, J. Lee, C. Richmond, F. Blattner, J. Rafalski, R. LaRossa, High-density microarray-mediated gene expression profiling of *Escherichia coli*, *J. Bacteriol.* 183 [2001] 545-556.
- 79) G. Georgiou, P. Valax, Isolating inclusion bodies from bacteria, *Method Enzymol.* 309 [1999] 48-58.
- 80) J. Thomas, F. Baneyx, Divergent effects of chaperone overexpression and ethanol supplementation on inclusion body formation in recombinant *Escherichia coli*, *Protein Expr. Purif.* 11 [1997] 289-296.
- 81) Y. Wang, P. deHaseth, Sigma 32-dependent promoter activity *in vivo*: sequence determinants of the *groE* promoter, *J. Bacteriol.* 185 [2003] 5800-5806.

- 82) R. Rosen, E. Ron, Proteome analysis in the study of the bacterial heat-shock response, *Mass Spectrometry Rev.* 21 [2002] 244-265.
- 83) R. Gill, H. Cha, A. Jain, G. Rao, W. Bentley, Generating controlled reducing environments in aerobic recombinant *Escherichia coli* fermentations: effects on cell growth, oxygen uptake, heat shock protein expression, and *in vivo* CAT activity, *Biotechnol. Bioeng.* 59 [1998] 248-259.
- 84) M. Carrió, J. Cochero, A. Villaverde, Dynamics of *in vivo* protein aggregation: building inclusion bodies in recombinant bacteria. *FEMS Microbiol. Lett.* 169 [1998] 9-15.
- 85) R. Hart, U. Rinas, J. Bailey, Protein composition of *Vitreoscilla* hemoglobin inclusion bodies produced in *Escherichia coli*, *J. Biol. Chem.* 265 [1990] 12728-12733.
- 86) A. Schrödel, A. de Marco, Characterization of the aggregates formed during recombinant protein expression in bacteria, *BMC Biochem.* 6 [2005].
- 87) N. Sánchez de Groot, S. Ventura, Effect of temperature on protein quality in bacterial inclusion bodies, *FEBS Lett.* 580 [2006] 6471-6476.
- 88) J. Luo, M. Leeman, A. Ballagi, A. Elfving, Z. Su, J. Janson, K. Wahlund, Size characterization of green fluorescent protein inclusion bodies in *E. coli* using asymmetrical flow field-flow fractionation--- multi-angle light scattering, *J. Chromat. A* 1120 [2006] 158-164.
- 89) G. Margreiter, P. Messner, K. Caldwell, K. Bayer, Size characterization of inclusion bodies by sedimentation field-flow fractionation, *J. Biotechnol.* 138 [2008] 67-73.
- 90) H. Kang, A. Sun, Y. Shen, D. Wei, Refolding and structural characteristics of TRAIL/Apo2L inclusion bodies from different specific growth rates of recombinant *Escherichia coli*, *Biotechnol. Prog.* 23 [2007] 286-292.

- 91) H. Le Thanh, F. Hoffmann, Optimized production of active  $\alpha$ -glucosidase by recombinant *Escherichia coli*. Evaluation of processes using *in vivo* reactivation from inclusion bodies, *Biotechnol. Prog.* 21 [2005] 1053-1061.
- 92) L. Strandberg, A. Veide, S. Enfors, Production of the hybrid protein staphylococcal protein A/*Escherichia coli*  $\beta$ -galactosidase with *E. coli*, *J. Biotechnol.* 6 [1987] 225-238.

## CHAPTER 2

### FERMENTATION SETUP AND ASSAY DEVELOPMENT

#### **2.1. Background**

The goal of this project was to determine how fermentation conditions influenced the physical and chemical properties of IB formation during industrial-like protein production in *E. coli*. Several enabling steps were necessary to gather this data. First, cell banks had to be created with various IB-forming proteins. Second, set of HCDC fermentation process had to be created that demonstrated standard variations in fermentation processes. Third, techniques to measure the IB density, size, morphology, and chemical resistance had to be developed.

#### **2.2. Proteins used**

Multiple proteins were used in this study to determine the generality of any phenomena observed. A range of proteins were selected based on their likelihood to form IBs. These were EGFP, SSX2, NY-ESO-1, and Melan-A.

##### **2.2.1. EGFP**

Enhanced Green Fluorescent Protein (EGFP) is a 29 kDa recombinant protein made of 265 amino acids. There are His tags on both the N- and C- terminus. It was selected as an ideal protein that exists as a soluble cytosolic protein when produced in *E. coli*. EGFP differs from Green Fluorescent Protein (GFP) by a single point mutation. Even though it has been demonstrated to have improved fluorescent properties [93], the excitation and emission spectra for EGFP are identical to GFP [94]. GFP has been used in the past in IB studies, particularly because its fluorescence

can be quantified to estimate proper protein folding [95]. According to a hydropathicity chart created by Vector NTI software (see Figure 2.1), EGFP is a very hydrophilic protein.

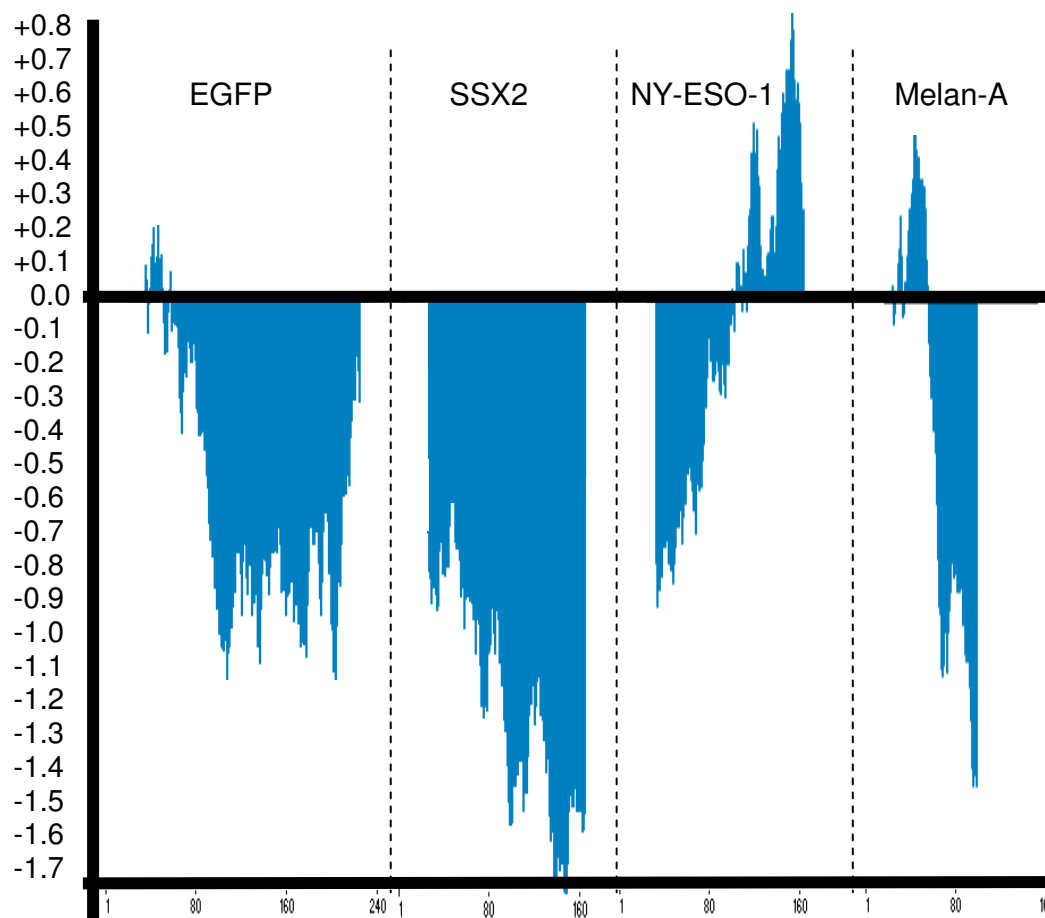


**Figure 2.1. Hydropathicity plot of proteins used in this study.** Values shown are calculated estimates from Vector NTI software based on protein sequence. Positive values represent hydrophobic regions. Negative values represent hydrophilic regions.

EGFP DNA sequence:

```
atggtgagcaaggcgaggagctgtcaccggggtggtgccatcctggtcgagctggacggcgacgtaaacggc
cacaagttcagcgtgtccggcgagggcgaggcgatgccacctacggcaagctgacctgaagttcatctgcacca
ccggcaagctgcccgtgccctggcccaccctcgtgaccacctgacctacggcgtgcagtgttcagccgctacccc
gaccacatgaagcagcagcaacttcttcaagtccgccatgcccggaaggctacgtccaggagcgcaccatcttcttcaag
```

gacgacggcaactacaagacccgcgccgaggtgaagttcgagggcgacaccctggtgaaccgcatcgagctgaa  
 gggcatcgacttcaaggaggacggcaacatcctggggcacaagctggagtacaactacaacagccacaacgtctat  
 atcatggccgacaagcagaagaacggcatcaaggtgaacttcaagatccgccacaacatcgaggacggcagcgtg  
 cagctcgccgaccactaccagcagaacacccccatcgggcgacggccccgtgctgctgcccgacaaccactacctg  
 agcaccagtcggccctgagcaaagacccaacgagaagcgcgatcacatggtcctgctggagttcgtgaccgccg  
 ccgggatcactctcgcatggacgagctgtacaagtag

EGFP amino acid sequence:

mvskgeelftgvvpilveldgdvnghkfsvsgegedatygkltlkficttgklpvpwptlvtlttygvqcsrypd  
 hmkqhdfksampegyvqertiffkddgnyktraevkfegdtlvnrielkgidfkdgnilghkleynynshnv  
 yimadkqkngikvnfkirhniedgsvqladhyqqntpigdgpvllpdnhylstqsalskdpnekrdhmvllfvt  
 aagitlgmdelyk

### 2.2.2. SSX2

SSX2 is a cancer testis antigen that has been shown to activate both CD4 and CD8 T cells of the adaptive immune system against several different types of cancer, such as synovial sarcoma [96]. It is classified as a nuclear protein and is even more hydrophilic than EGFP (see Figure 2.1).

SSX2 DNA sequence:

atgaacggagacgacgcctttgcaaggagaccacggttggtgctcaaataccagagaagatccaaaaggccttcg  
 atgatattgccaataacttcttaaggaagagtgggaaaagatgaaagcctcggagaaaatcttctatgtgtatatgaag  
 agaaagtatgaggctatgactaaactaggttcaaggccaccctcccaccttcatgtgtaataaacgggccgaagact  
 tccaggggaatgatttgataatgaccctaaccgtgggaatcaggttgaacgtcctcagatgactttcggcaggctcca  
 gggaatctccccgaagatcatgcccaagaagccagcagaggaaggaaatgattcggaggaagtgccagaagcatc  
 tggcccacaaaatgatgggaaagagctgtgcccccgggaaaaccaactacctctgagaagattcacgagagatct

ggacccaaaaggggggaacatgcctggaccacagactgcgtgagagaaaacagctggtgatttatgaagagatca  
gcgaccctgaggaagatgacgagtaa

SSX2 amino acid sequence:

mngddafarrptvgaqipekiqkafddiakyskeewekmkasekifyvymkrkyeamtklgfkatlppfmc  
nkraedfqgndldndpnrgnqverpqmtfgrlqgispkimpkpkpaegndseevpeasgpqndgkelcppgk  
pttsekihersgpkrgehawthrlrerqqlviyeedispeedde

### 2.2.3. NY-ESO-1

NY-ESO-1 is a cancer testis antigen expressed on over 50% of all cancer tumors, including esophageal cancer where it was initially isolated [97]. It also has been shown to activate both CD4 and CD8 T cells and is currently being tested in Phase I clinical trials. NY-ESO-1 has a large hydrophobic region (see Figure 2.1).

NY-ESO-1 DNA sequence:

atgcaggccgaaggccggggcacagggggttcgacgggcgatgctgatggcccaggaggccctggcattcctgat  
ggcccaggggggaatgctggcggcccaggagaggcgggtgccacgggcggcagaggtccccggggcgagg  
ggcagcaagggcctcggggccgggaggaggcggcccgcggggtccgatggcggcgcggttcagggtgaat  
ggatgctgcagatgcggggccagggggccggagagccgcctgcttgagttctacctgccatgcctttcgcgacac  
ccatggaagcagagctggcccgcaggagcctggcccaggatggcccaccgcttcccgtgccaggggtgcttctga  
aggagttcactgtgtccggcaacatactgactatccgactgactgctgcagaccaccgccaactgcagcttccatca  
gtcctgtctccagcagctttccctgttgatgtggatcacgcagtgtttctgccgtgttttggtcagcctccctcagg  
gcagaggcgctaa

NY-ESO-1 amino acid sequence:

mrgshhhhhhghsmqae grtggtgdadgpggpgipdgpggnaggpggeagatggrgprgagaarasgpggg  
aprgphggaasglngccrcgargpesrllefylampfatpmeaelarrslaqdapplvpvgvllkeftvsgniltirt  
aadhrqlqlsissclqqlslm witqcflpvflaqqpsgqrr

#### 2.2.4. *Melan-A*

Melanoma antigen A (Melan-A), also known as melanoma antigen recognized by T-cells 1 (MART-1), is a membrane protein that serves as a differentiation antigen [98]. The sequence was extracted from tumor-infiltrating lymphocytes in T-cells that act in cancer regression. Able to stimulate CD4 and CD8 T cell responses, it is also hypothesized to function as a possible melanoma cancer vaccine. There is evidence that this antigen is expressed in 80-90% of primary tumors [99]. Aside from a direct treatment, this antigen can also be used to assay antibodies that are being developed to target cancer cells directly. It has a major hydrophobic domain (see Figure 2.1).

Melan-A DNA sequence:

atgccgcgcgaagatgcgcacttcatttatggttacccgaaaaaggggcatggccacagctacaccacggctgaaga  
ggccgcgggtatcggcattctgaccgtgacacctgggagtgcttactgctcattggctgttggtattgccgtcgccgtaacg  
gttaccgcgcattgatggataaaagtcttcattgttgccactcagtgctgccttaacacgtcgctgcccgaagaagggtt  
gatcatcgggacagcaaagtatctctgcaggagaaaaactgcgaacctgtggttccaatgccaccacggcttatga  
gaaactgtccgcagaacagtcgccgccacctattcaccgtga

Melan-A amino acid sequence:

mpredahfiygyppkkghghsyttaeaaagiltvilgvliligwycrrrngyralmdkslhvgtqcaltrrcpqe  
gfdhrdskvslqekncepvvpnappayeklsaeqspppysp



## 2.3. Creation of research cell banks

### 2.3.1. Design of synthetic DNA sequence

The primary protein used in this study was Melan-A. A His-tag was added to this protein to aid in purification. A synthetic version of this plasmid was designed to avoid stringent responses based on codon bias. Graphical Codon Usage Analyzer ([www.gcua.de](http://www.gcua.de)) was used to determine the frequency of codons used in K-12 *Escherichia coli*. The data for this strain was readily available, and it was assumed that this strain would have a very similar codon usage compared to a C41 strain. The genetic code of Melan-A was altered manually to match this codon bias as closely as possible. The original DNA sequence and new DNA sequence listed in Table 2.1.

**Table 2.1. GCUA of natural Melan-A and Syn-Melan-A.** Codons and their frequency in K-12 *E. coli* are shown. The frequency of each codon in the natural Melan-A DNA sequence is also shown with frequencies in an adjusted synthetic sequence.

Amino Acid	Codon	K12	Melan-A	Syn-Melan-A
Alanine	GCT	16.1%	41.7%	16.7%
	GCC	27.0%	33.3%	25.0%
	GCA	21.3%	16.7%	25.0%
	GCG	35.6%	8.3%	33.3%
Arginine	AGA	3.6%	62.5%	0.0%
	AGG	2.0%	0.0%	0.0%
	CGT	38.2%	0.0%	37.5%
	CGC	40.0%	12.5%	50.0%
	CGA	6.4%	12.5%	0.0%
	CGG	9.8%	12.5%	12.5%
Asparagine	AAT	44.9%	66.7%	33.3%
	AAC	55.1%	33.3%	66.7%
Aspartic Acid	GAT	62.6%	50.0%	75.0%
	GAC	37.4%	50.0%	25.0%
Cysteine	TGT	44.3%	80.0%	40.0%
	TGC	55.7%	20.0%	60.0%

**Table 2.1. (Continued)**

(Stop)	TAA	64.5%	0.0%	0.0%
	TAG	6.5%	0.0%	0.0%
	TGA	29.0%	100.0%	100.0%
Glutamine	CAA	34.6%	75.0%	25.0%
	CAG	65.4%	25.0%	75.0%
Glutamic Acid	GAA	69.0%	44.4%	66.7%
	GAG	31.0%	55.6%	33.3%
Glycine	GGT	33.8%	10.0%	30.0%
	GGC	40.5%	40.0%	40.0%
	GGA	10.7%	20.0%	10.0%
	GGG	14.9%	30.0%	20.0%
Histidine	CAT	57.1%	18.2%	54.5%
	CAC	42.9%	81.8%	45.5%
Isoleucine	ATT	50.8%	0.0%	60.0%
	ATC	42.1%	100.0%	40.0%
	ATA	7.2%	0.0%	0.0%
Leucine	CTT	10.3%	18.2%	9.1%
	CTC	10.4%	27.3%	9.1%
	CTA	3.7%	0.0%	0.0%
	CTG	49.8%	27.3%	54.5%
	TTA	13.0%	18.2%	18.2%
	TTG	12.8%	9.1%	9.1%
Lysine	AAA	76.6%	66.7%	83.3%
	AAG	23.4%	33.3%	16.7%
Methionine (Start)	ATG	100.0%	100.0%	100.0%
Phenylalanine	TTT	57.2%	50.0%	50.0%
	TTC	42.8%	50.0%	50.0%
Proline	CCT	15.9%	36.4%	18.2%
	CCC	12.2%	18.2%	9.1%
	CCA	19.0%	45.5%	18.2%
	CCG	52.8%	0.0%	54.5%
Serine	AGT	15.1%	14.3%	8.3%
	AGC	27.9%	14.3%	58.3%
	TCT	14.5%	42.9%	8.3%

**Table 2.1. (Continued)**

	TCC	14.9%	0.0%	8.3%
	TCA	12.3%	28.6%	8.3%
	TCG	15.4%	0.0%	8.3%
Threonine	ACT	16.5%	20.0%	0.0%
	ACC	43.7%	20.0%	60.0%
	ACA	13.0%	40.0%	0.0%
	ACG	26.8%	20.0%	40.0%
Tryptophan	TGG	100.0%	100.0%	100.0%
Tyrosine	TAT	56.9%	57.1%	57.1%
	TAC	43.1%	42.9%	42.9%
Valine	GTT	25.8%	33.3%	33.3%
	GTC	21.6%	16.7%	16.7%
	GTA	15.4%	0.0%	0.0%
	GTG	37.1%	50.0%	50.0%

Codons that were changed are shown in bold. Added nucleotides are italicized.

old sequence:

atg cca cgc gag gac gct cac ttc atc tat ggt tac ccc aag aag ggg cac ggc cac tct  
 tac acc acg gct gaa gag gcc gct ggg atc ggc atc ctg aca gtg atc ctg gga gtc tta ctg  
 ctc atc ggc tgt tgg tat tgt aga aga cga aat gga tac aga gcc ttg atg gat aaa agt ctt cat  
 gtt ggc act caa tgt gcc tta aca aga aga tgc cca caa gaa ggg ttt gat cat cgg gac agc  
 aaa gtg tct ctt caa gag aaa aac tgt gaa cct gtg gtt ccc aat gct cca cct gct tat gag  
 aaa ctc tct gca gaa cag tca cca cca cct tat tca cct gcg gcc gca ctc gag cac cac cac  
 cac cac cac tga

new sequence:

cat atg **ccg** cgc **gaa gat gcg** cac ttc **att** tat ggt tac **ccg aaa** aag ggg **cat** ggc cac **agc**  
 tac acc acg gct gaa gag gcc **gcg ggt** atc ggc **att** ctg **acc** gtg atc ctg gga gtc tta ctg  
 ctc **att** ggc tgt tgg tat **tgc cgt cgc cgt aac ggt** tac **cgc gca** ttg atg gat aaa agt ctt cat

gtt ggc act **cag** tgt gcc tta aca **cgt cgc** tgc **ccg** caa gaa ggg ttt gat cat cgg gac agc  
aaa **gta** tct **ctg cag** gag aaa aac **tgc** gaa cct gtg gtt ccc aat **gcg** cca **ccg** gct tat gag  
aaa **ctg tcc** gca gaa cag **tgc cgc** cca cct tat tca **ccg** gcg gcc gca **ctg gaa** cac **cat** cac  
**cat** cac **cat** tga gga tcc

In addition to the codon changes, the new sequence also contains additional nucleotides at both ends. These sequences coded for restriction sites so that restriction enzymes could be used to create sticky ends on the sequence. Specifically, the *CATATG* sequence codes for NdeI and the *GGATCC* sequence codes for BamHI.

The synthetic Melan-A (Syn-Melan-A) sequence with the improved codon bias for *E. coli* was synthesized by Integrated DNA Technologies (IDT, Coralville, IA). The DNA sequence was synthesized in a pZER0-2 vector. The synthesized plasmid was resuspended to 124 ng/μl in DNase free water to create a working plasmid solution.

### **2.3.2. Plasmid production**

The pZER0-2 vectors were produced in Top10 *E. coli* cells. A heat shock transformation was performed by adding 1 μl of the working plasmid solution to 50 μl of One Shot Top10 competent cells (Invitrogen, Carlsbad, California). This solution was left on ice for 30 min. The solution was then placed at 42°C for 35 seconds before being returned to ice for another 2 min. The transformed cells were then diluted with 250 μl SOC medium (0.5 % (w/v) yeast extract, 2 % (w/v) tryptone, 8.6 mM NaCl, 2.5 mM KCl, 20 mM MgSO<sub>4</sub>, 20 mM glucose) and put in a 37°C shaker for 1 hr. 50 μl of these cells were then spread on LB plates containing 100 μg/ml kanamycin and left in a 37°C incubator overnight.

One of the colonies that formed was grown in 20 ml of LB medium supplemented with kanamycin overnight at 37°C. Plasmid extraction was performed on these cultures with a Miniprep Kit (Qiagen, Valencia, CA) following the instructions in the kit without modification. Using kit solutions, the cells were pelleted, resuspended, and lysed. The lysis was neutralized with another solution and the precipitated protein was removed by centrifugation. Supernatant containing the plasmids was run through the kit's miniprep column, which was subsequently rinsed with kit wash buffer and eluted with DNase free water.

### ***2.3.3. Plasmid construction***

Steps were taken to transfer the Syn-Melan-A sequence from its pZErO-2 vector to a pET9a24a vector. This plasmid, pET9a24a, was a combination of two commercially available plasmids (Novagen, Darmstadt, Germany). The promoter and kanamycin resistance from the pET9a plasmid was conserved, and the multiple cloning site of pET24a was added (see Figure 2.2a). The creation of this vector was performed by Dr. Todd Vannelli (Cornell University, Ithaca, NY).

NdeI and BamHI restriction enzymes were obtained from New England Biosciences (NEB, Beverly, MA). According to the manufacturer, these enzymes function with optimal activity in NEB Buffer 2 with added bovine serum albumin (BSA). 2 µg of the pZErO-2 plasmid was added to 5 µl of 10x NEB Buffer 2 and 0.5 µl of 100x BSA. Water was added to bring this volume up to 46 µl before 1 µl of NdeI and BamHI enzymes were each added. The digest was incubated at 37°C for 4 hr. The digestion was then set at 65°C for 10 min to deactivate the enzymes. An identical digestion was also performed with the pET9a24a vector.

Digested pZErO-2 with Syn-Melan-A insert and pET9a24a vector were run on a 1% agarose gel in Tris-Acetate-EDTA (TAE) buffer. Bands of the Syn-Melan-A

DNA insert and pET9a24a vector were cut out and purified using a Plasmid Maxi Kit (Qiagen, Valencia, CA). Aliquots of 30 fmol of the purified digested vector and 90 fmol of the insert were mixed together and diluted to 17  $\mu$ l. 2  $\mu$ l of ligation buffer and 1  $\mu$ l of ligase were added to this solution, and the solution was incubated at 16°C overnight. The solution was then left at room temperature for 1 hr and then put on ice. Another transformation into One Shot Top10 cells was performed, and kanamycin resistant colonies were grown up overnight. The Syn-Melan-A pET9a24a plasmid was extracted with a Miniprep. The plasmid map, as displayed by Vector NTI software, is shown in Figure 2.2b.

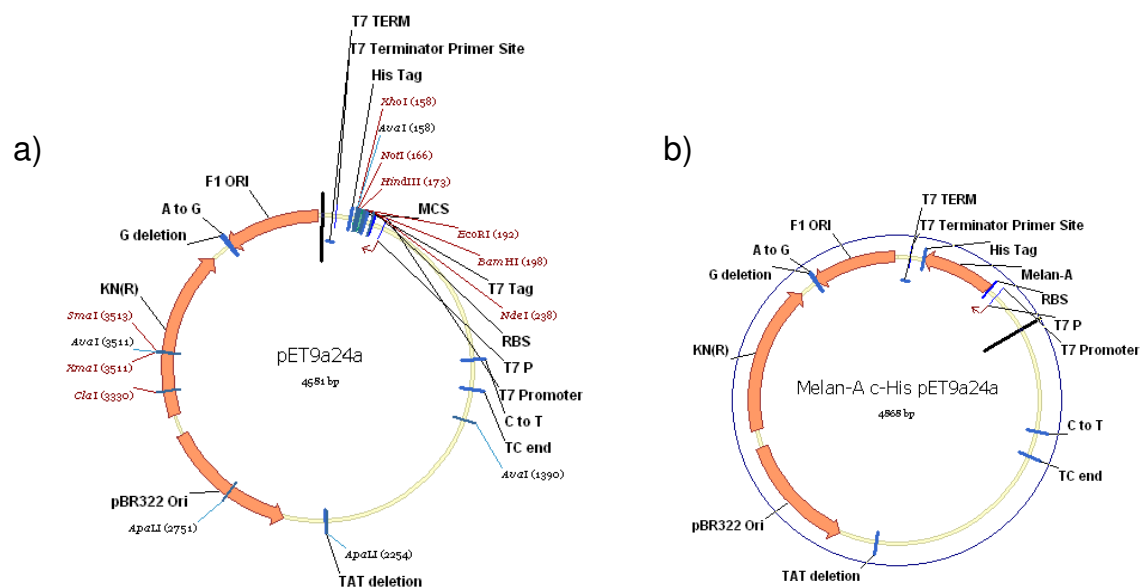


**Figure 2.2. Plasmid maps of a) pET9a24a and b) Syn-Melan-A in vector pET9a24a.**

#### 2.3.4. Research cell bank transformation

C41(DE3) *E. coli* cells (Lucigen, Middleton, WI) were made chemically competent in the following way. An aliquot of 250  $\mu$ l of an overnight culture of C41

cells were used to inoculate 25 ml of APS Luria Broth (LB) glycine medium (20 g/L APS LB, 1.1% glycine, 5 g/L NaCl) in a 125 ml baffled shake flask. These cells were grown at 25°C until the optical density measured at 600 nm ( $OD_{600}$ ) reached 0.5. This culture was then put on ice for 10 min. The cells were pelleted in a HERMLE Z400\_K refrigerated centrifuge (Labnet, Edison, NJ) at 4°C at 5,000g for 10 min and resuspended in 5 ml of ice cold transformation buffer (4 g/L HEPES, 15 ml 1 M  $CaCl_2$ , 18.64 g/L KCl, 10.88 g/L  $MnCl_2 \cdot 4H_2O$ , 25  $\mu$ l/ml 1 M DTT). The cell suspension was incubated on ice for another ten min before being pelleted again. This pellet was resuspended in 0.93 ml of ice cold transformation buffer and 70  $\mu$ L of DMSO. The cell suspension was left on ice for an additional 10 min and then frozen in 100 ml aliquots at -80°C.

A heat shock transformation with the Syn-Melan-A plasmid into the competent C41 cells was performed using the same protocol used for the Top10 cells and previous plasmid constructs. The cells were grown in LB medium until they reached an  $OD_{600}$  of 1.5, which was representative of early exponential growth. At this point, sterilized glycerol was added to a final concentration of 15% (v/v). 1 ml aliquots were frozen at -80°C. This concluded the construction of the Syn-Melan-A research cell bank.

### **2.3.5. Other plasmids**

Like Syn-Melan-A, all proteins used in this study were present in pET9a24a plasmids in C41(DE3) *E. coli*. The SSX2, EGFP, and NY-ESO-1 research cell banks were constructed, with analogous techniques as the Syn-Melan-A plasmid, by Chung-Jr Huang, Dr. Nuttawee Niamsiri, and Dr. Todd Vannelli, respectively (Cornell University, Ithaca, NY). The SSX2 and EGFP genes were not synthetic. The NY-ESO-1 DNA sequence was synthetic, but it was designed by only changing the rarely

used *E. coli* codons in the sequence to frequently used *E. coli* codons. In Leucine, for example, the *CTA* codons (4% natural frequency) were changed to *CTG* (50% natural frequency), but the *TTA* codons (11% natural frequency) were unchanged regardless of frequency present in the protein code.

In the case of SSX2 and NY-ESO-1, a second transformation was performed. These transformed cell banks were individually made chemically competent, and a pRARE plasmid (Novagen, Darmstadt, Germany) was inserted into each using a heat shock transformation. Preparing chemically competent cells and heat shock transformation procedures were identical to those described above. Properly transformed cells were selected from plates of LB medium and agar that ultimately contained both 100 µg/ml kanamycin and 34 µg/ml chloramphenicol.

## ***2.4. Fermentation conditions***

### ***2.4.1. Complex medium***

Two types of complex media were used for each fermentation. A complex batch medium was used for the inoculum and initial bioreactor growth. Once the dextrose in the complex batch medium was depleted, a complex feed medium was added to the fermentor at a controlled rate.

The recipe for the complex batch medium used in this study was 3 g/L  $[\text{NaPO}_3]_6$ , 1.6 ml/L 2 M  $\text{MgSO}_4 \cdot 7\text{H}_2\text{O}$ , 1.9 g/L Citrate·H<sub>2</sub>O, 2.1 g/L  $\text{NH}_4\text{Cl}$ , 0.1 g/L  $\text{FeSO}_4 \cdot 7\text{H}_2\text{O}$ , 15 g/L yeast extract, 20 g/L dextrose, 0.2 µg/L  $\text{MnCl}_2 \cdot 4\text{H}_2\text{O}$ , pH 7.0. When grown in a bioreactor, 0.4 ml/L of Antifoam 204 was added. The complex feed medium used was 3 g/L  $[\text{NaPO}_3]_6$ , 10.5 g/L  $\text{MgSO}_4 \cdot 7\text{H}_2\text{O}$ , 2.6 g/L  $\text{Na}_3\text{Citrate} \cdot 2\text{H}_2\text{O}$ , 3 g/L  $(\text{NH}_4)_2\text{CO}_3$ , 0.1 g/L  $\text{FeSO}_4 \cdot 7\text{H}_2\text{O}$ , 210 g/L yeast extract, 275 g/L dextrose, 2.4



$\mu\text{g/L}$   $\text{MnCl}_2 \cdot 4\text{H}_2\text{O}$ . Isopropyl- $\beta$ -D-thiogalactopyranoside (IPTG) was also added to the feed medium, to a final fermentation concentration of 2.25 mM.

The same complex medium was used for all proteins used in this study. All media contained 100  $\mu\text{g/ml}$  kanamycin for sterility and genetic stability. 34  $\mu\text{g/ml}$  chloramphenicol was added to all SSX2 and NY-ESO-1 media. Even though contamination in the feeding phase could not outgrow the HCDC culture, it was added with the intention to prevent any cells lacking plasmid to overtake the culture. In BL21(DE3), plasmids can be stable throughout logarithmic phase but unstable during stationary phase [100].

Ferrous sulfate, ammonium hydroxide, manganese chloride, ammonium carbonate, kanamycin, chloramphenicol, and Antifoam 204 were obtained from Sigma-Aldrich (St. Louis, MO). Dextrose and ammonium chloride were obtained from Thermo Fisher Scientific. Sodium hexametaphosphate, citric acid, magnesium sulfate, and sodium citrate were obtained from Mallincrodt Baker (Phillipsburg, NJ). Yeast extract and IPTG was obtained from EMD Biosciences (San Diego, CA).

#### ***2.4.2. Chemically defined medium***

The transformed cells were adapted to a chemically defined medium recipe taken from the literature [101]. Modifications were made to the medium composition to better accommodate a high cell density process. The final chemically defined batch medium composition was 14.6 g/L  $\text{K}_2\text{HPO}_4$ , 4.1 g/L  $\text{NaH}_2\text{PO}_4 \cdot \text{H}_2\text{O}$ , 8.0 g/L  $(\text{NH}_4)_2\text{SO}_4$ , 40.0 g/L dextrose, 20.0 ml/L 1 M  $\text{MgSO}_4$ , 4.75 ml/L trace metals, 0.05 g/L  $\text{CaCl}_2$ . When grown in a bioreactor, 1.0 ml/L of Antifoam 204 was added to the chemically defined batch medium. Chemically defined feed medium was 500 g/L dextrose, 10 g/L  $(\text{NH}_4)_2\text{SO}_4$ , 50 ml/L 1 M  $\text{MgSO}_4$ , and 10 ml/L trace metals. The trace metal recipe was 260.0 g/L  $\text{FeSO}_4 \cdot n\text{H}_2\text{O}$ , 15.5 g/L  $\text{CuSO}_4 \cdot 5\text{H}_2\text{O}$ , 21.1 g/L

$\text{CoCl}_2 \cdot 6\text{H}_2\text{O}$ , 45.0 g/L  $\text{MnSO}_4 \cdot \text{H}_2\text{O}$ , 21.1 g/L  $\text{Na}_2\text{MoO}_4 \cdot 2\text{H}_2\text{O}$ , 29.2 g/L  $\text{ZnSO}_4 \cdot 7\text{H}_2\text{O}$ , 5.26 g/L  $\text{H}_3\text{BO}_3$ , 26.3 ml/L  $\text{H}_2\text{SO}_4$ . Dextrose was obtained from Thermo Fisher Scientific. Curpic sulfate, cobalt chloride, and dibasic potassium phosphate were obtained from Sigma-Aldrich (St. Louis, MO). All other chemicals were from Mallincrodt Baker (Phillipsburg, NJ).

Transformed cells from a glycerol stock of complex medium were used to inoculate a 250 ml unbaffled shake flask of chemically defined medium. Once the cells reached an optical density of 1.0, indicating entry into early exponential growth two days post-inoculation, they were also banked. This process was repeated once more with the new bank to fully adapt the cells, minimizing the observed initial lag in growth. To confirm the adaptation, the plasmids from the cells were extracted with a MiniPrep. The restriction enzymes used to construct the original plasmids were used and the DNA fragments were run on an agarose gel; the respective restriction fragments matched (Figure 2.3). These cells have also been grown in 2.5 L HCDC and shown to express Melan-A.

An attempt to adapt these cells to a chemically defined medium containing  $[\text{NaPO}_3]_6$  as the sole phosphate source failed. Also known as phosphate glass, this hexametaphosphate is a polymeric chain that prevents precipitation with metals in media. Unfortunately cells were not able to grow on it, suggesting that the usable phosphate source in the complex medium came solely from the yeast extract. Cells could be grown in complex medium lacking the  $[\text{NaPO}_3]_6$ , but the original recipe was not changed to maintain consistency amongst all fermentations conducted.

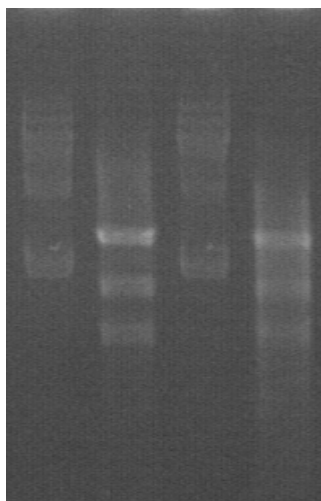


**Figure 2.3. Agarose gel of Melan-A plasmids extracted from transformed cells.** Lanes 1 and 2 show uncut and cut plasmids extracted from transformed cells, respectively. Lanes 3 and 4 show uncut and cut plasmids extracted from chemically defined medium adapted cells.

#### ***2.4.3. Fermentation conditions***

Fermentations were conducted in a 2.5 L Bioflo 3000 fermentor (New Brunswick Scientific, Edison, NJ). AFS-Biocommand Bioprocessing software version 2.6 (New Brunswick Scientific) was used for data acquisition and parameter control. The pH of the medium was adjusted with the addition of 5 N sodium hydroxide. The dissolved oxygen was maintained above 40 % air saturation with oxygen-enriched air. Temperature was maintained with a jacketed base.

One liter of batch medium was autoclaved per fermentation. Two fermentor units were sterilized for 45 min at 121°C. Calibration of the pH probe was performed prior to sterilization with individually packed pH 4 and 7 standards (VWR, West Chester, PA). A solution of 5 N sodium hydroxide was added to the fermentator to bring the pH to 7.0. This operating pH was confirmed on an external pH meter. Filtered air entered the fermentor through a ring sparger located directly below the impeller at 2 L/min, 1 vvm of the final volume. The two data points for dissolved

oxygen (DO) calibration were created by unplugging the probe and by allowing the medium to reach 100% air saturation. DO started at 100% air saturation, and oxygen-enriched air was added to keep the DO level at 40% air saturation in the latter stages of the fermentation. Temperature of batch cultures were all 37°C, and agitation was 1,000 rpm. pH was maintained at 7.0. An example profile is shown in Figure 2.4.

Some of the medium components were not autoclaved and instead filter sterilized through a 0.22 µm pore size vacuum filter (Nalgene Labware, Rochester, NY). For the complex batch medium, dextrose, magnesium sulfate, manganese chloride, and antibiotics were added to the fermentor after reactor sterilization. For the complex feed medium, yeast extract, sodium hexametaphosphate, ammonium carbonate, and IPTG were added after the other components were autoclaved. For the chemically defined batch medium, only the potassium phosphate and sodium phosphate were autoclaved with the reactor. All other components were added from filter-sterilized stocks. The entire chemically defined feed medium was filter sterilized, and the filtered trace metals were added post-sterilization.

A 45 ml inoculum was grown for each fermentation in a 250 ml unbaffled shake flask. Complex batch medium was used and inoculated with 45 µl of thawed research cell bank and grown at 37°C in a MaxQ 5000 shaker (Barnstead, Dubuque, Iowa). After 7-9 hr, the OD<sub>600</sub> was 2.5, suggesting cells were in mid-exponential growth phase, and 40 ml (4% v/v) of the inoculum was added to the fermentor. After 6 hr, the dextrose in the medium would be depleted, as indicated by a rise in pH. Feeding was initiated until the feed medium was depleted, typically 20-40 hr elapsed fermentation time. Cell broth was collected in 500 ml centrifuge bottles (Corning, Corning, NY) and pelleted by centrifugation in a Sorvall RC-5B centrifuge using a SH-3000 rotor (Thermo Fisher Scientific, Waltham, MA) at 4°C for 40 min at 4,000 rcf. Supernatant was discarded and cell pellets were stored at -20°C.

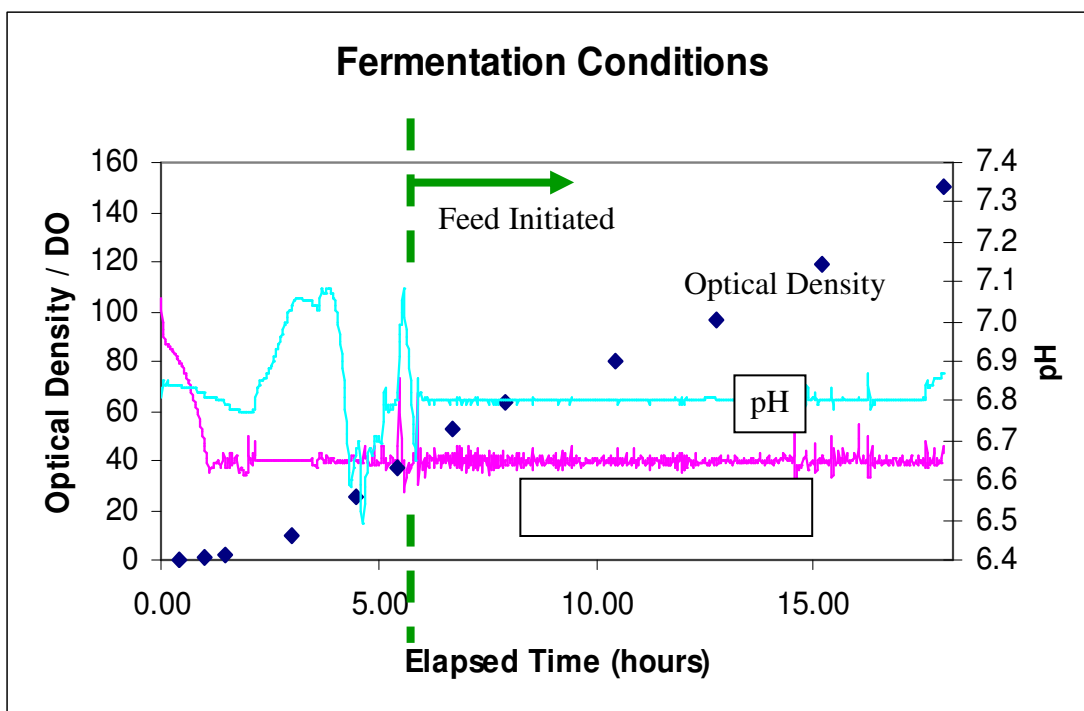


**Figure 2.4. Melan-A Fermentation profile during high cell density culture.** Dissolved oxygen and pH were continuously monitored. A pH spike at 6 hr elapsed fermentation time indicated that feeding needed to be initiated. Optical density was measured from reactor samples.

#### 2.4.4. Feeding strategies

Various feeding strategies were used in this study's fermentations. The default feeding method performed was a pH-stat technique. In this technique, feed medium was added to the fermentor in response to pH increases, which are a response to limited carbon. Decreases in pH are created by acetic acid production as a subsequent result of feeding. As a result, base addition is terminated once feeding begins.

Constant feeding techniques added feed medium to the reactor at a constant rate. Values of 25, 45, and 80 ml/hr were used. pH was maintained with 1 M phosphoric acid at the slowest feed rate and with 5 M sodium hydroxide at the higher two constant feed rates. A step feed method started feeding 25 ml/hr, and this feed rate would increase by 10 ml/hr at every pH spike. Base control with sodium

hydroxide was needed. A linear feed also started at 25 ml/min and increased linearly at different rates.

It was also during feeding that protein production started because IPTG was included in the feed medium. Therefore, any variables to be changed in the fermentation, such as temperature, were initiated when feeding started.

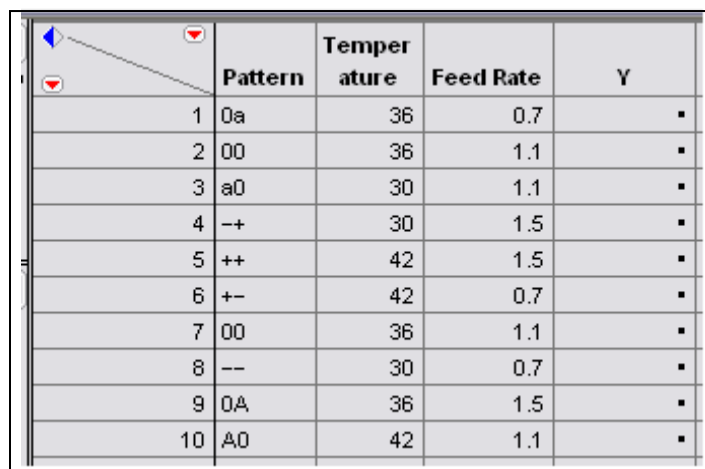
#### **2.4.5. Statistical Design**

Multiple fermentation parameters have been shown to influence IB formation. Statistical design of experiments allow us to evaluate factors independently while varying several factors simultaneously, ultimately reducing the number of experiments necessary to get accurate estimates. These studies typical look at two-factor interactions which result in an equation for a response variable as shown [102].

$$Y = \beta_o + \sum_{i=1}^k \beta_i X_i + \sum_{i=1}^k \beta_{ii} X_i^2 + \sum_{j=1}^k \sum_{i < j=1}^k \beta_{ij} X_i X_j + \epsilon \quad (2)$$

Here,  $Y$  is the response parameter, such as inclusion body size or density.  $X_i$  are the design parameters, such as fermentation temperature, that influence the response parameter. All other variables are coefficients or intercepts. A factorial design explores the main effects of each factor ( $X_i$ ) on two levels (-1, +1). The number of experiments needed are  $2^X$ . When the factors are too numerous, then a fractional factorial design is used that reduces the total number of experiments, while still generating enough data to get estimates of main effects. A central composite design uses three (-1, 0, +1) or more levels to see generate response surface designs.

SAS-JMP software was used to design a central composite design of experiment (DOE) to analyze various fermentation parameters on IB formation. Relevant parameters were temperature, feeding rate, growth rate, IPTG concentration,



	Pattern	Temperature	Feed Rate	Y
1	0a	36	0.7	▪
2	00	36	1.1	▪
3	a0	30	1.1	▪
4	—+	30	1.5	▪
5	++	42	1.5	▪
6	+—	42	0.7	▪
7	00	36	1.1	▪
8	--	30	0.7	▪
9	0A	36	1.5	▪
10	A0	42	1.1	▪

**Figure 2.5. Simple experimental design using central composite design of experiment.** Two factors, temperature and feed rate, are tested over three levels each. One experiment is performed in duplicate to determine the error variation. Experiments designed for 36°C were performed at 37°C.

and pH. Because growth rate could be considered a dependent variable, it was observed, but it was not included in the experimental design. Various linear feed rates were used in this experimental design, but the design does not accommodate different feeding strategies, so these set of experiments were conducted outside the statistical experimental set. IPTG concentration and pH were not included in the experimental design to keep a manageable number of necessary experiments. The final design, after randomization, is shown in Figure 2.5.

## ***2.5. Fermentation Measurements***

### ***2.5.1. Feeding Rate Calibration***

The Biocommand Software constantly monitored a unitless pump rate (0-125) for the addition of feed medium to the bioreactor. This pump rate had to be calibrated to determine the actual amount of feed added to the fermentor at any given time. This was done by manually weighing feed medium reservoir and calculating the amount of

feed removed at various time points. For simplicity, these measurements were done during constant feeding pump rates. Results are summarized in Figure 2.6.

At a constant feeding rate of 8.0, 55.5 g of complex feed medium was added per hr. This rate was 109.0 g/hr for a constant feeding rate of 16.0. For a single pump rate unit, the constant feed rates of 8.0 and 16.0 added 6.812 and 6.813 g/hr, respectively. The complex feed medium density of 1.176 g/ml was determined by measuring the mass of a 50 ml sample. Each pump unit was therefore equivalent to 5.793 ml/hr.

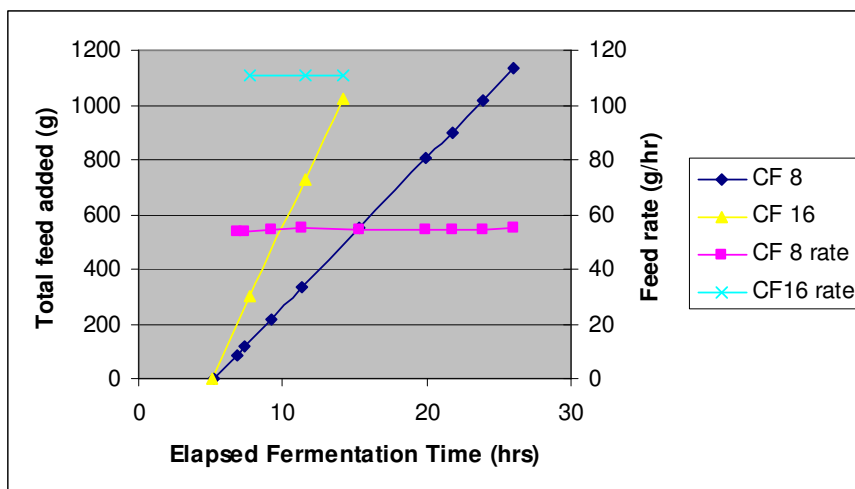


**Figure 2.6. Feed rates at different feed pump settings.** The amount of feed added at pump setting 8 and 16 are shown. Also indicated on the secondary axis the actual feed rate at various timepoints.

### 2.5.2. Cell Density Measurements

Optical density was the primary value measured to determine the cell density at any given time throughout the fermentation. Measurements were performed on an Ultrospec 2000 spectrophotometer (General Electric Healthcare, Piscataway, NJ). Measurements were performed at a wavelength of 600 nm. The spectrophotometer was blanked with 800 ml of phosphate buffered saline (PBS) in a 1.5 ml polymethyl



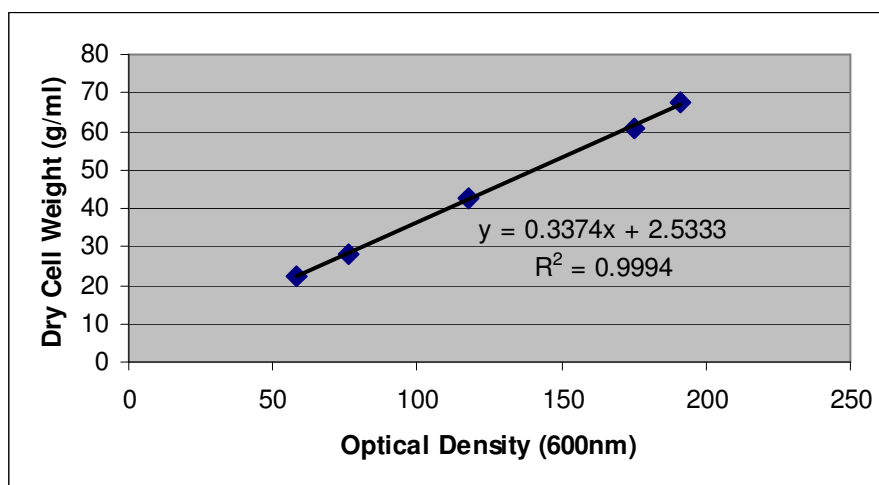


**Figure 2.7. Optical density and dry cell weight correlation.** Fermentation broth samples were taken throughout a fermentation. Optical density samples were measured using a spectrophotometer and dry cell weights were measured from cell pellets from 1 ml broth.

methacrylate semi-micro disposable cuvette (Brand, Wertheim, Germany). A five hundred-fold serial dilution was performed in PBS. A 100  $\mu$ l aliquot of fermentation broth was mixed with 900  $\mu$ l of PBS, and 100  $\mu$ l of this mixture was mixed with another 900  $\mu$ l aliquot of PBS. Finally, 200  $\mu$ l of this mixture was added and mixed with the PBS in the cuvette, and a measurement was taken.

A method for measuring dry cell weights is described in Section 2.11. Values for optical density and dry cell weight were compared to determine a correlation (Figure 2.7). For the spectrophotometer and cells used in this study, this correlation value was approximately 0.34 g/ml per optical density unit. An absorbance of 1.0 at 600 nm is roughly equivalent to  $5 \times 10^8$  to  $10^9$  cells/ml [100].

### 2.5.3. Protein Production Measurements

Samples were taken at various timepoints throughout all fermentation runs performed in this study. Cells were pelleted in a HERMLE Z200\_M/U non-

refrigerated centrifuge (Labnet, Edison, NJ) for 3 min at 12,000 rcf in 1 ml aliquots. The supernatant was removed and the cell pellet was stored at -20°C.

Cell pellets were lysed using a chemical lysis buffer (100 µl/ml bugbuster (Novagen, Darmstadt, Germany), 1 µl/ml lysozyme, 50 mM Tris, 1 mM EDTA, 1 mM β-mercaptoethanol). The cell pellets were thawed and suspended in this buffer. For the cell masses used in this study, it was necessary to leave the suspensions shaking overnight. Soluble and insoluble fractions were separated using centrifugation for 10 min at 12,000 rcf.

The samples were subjected to sodium dodecyl sulphate polyacrylamide gel electrophoresis (SDS-PAGE). All gels and reagents were purchased from Invitrogen (Carlsbad, CA). An aliquot of 10 µl of each protein fraction was added to 60 µl 8 M urea, 25 µl NuPAGE 4x lithium dodecyl sulphate (LDS) buffer, and 5 µl β-mercaptoethanol. This sample was heated at 65°C for 10 min, cooled to room temperature, and centrifuged at 1,000 rcf briefly. Samples were then loaded onto NuPAGE 10% Bis-Tris gels. For 10, 12, and 15 well gels, 10, 7.5, and 5 ml of sample was loaded into each well. Gels were run in a Novex Mini Cell box at 200 V for 38 min. After rinsing the gel for 5 min in deionized water three times, it was stained in SimplyBlue Safestain overnight. The stained gel was destained in deionized water for at least 2 hr. Western blots were performed using reagents from a WesternBreeze kit (Invitrogen, Carlsbad, CA). The transfer was performed at 30 V for 90 min.

Gels were scanned on a Stylus CX4200 scanner (Epson, Long Beach, CA). Images were subjected to analysis using Image J densitometry software (National Institutes of Health, Bethesda, MD). Without a standard, Image J software can be used to compare pixel counts of protein bands on the same gel based on area and color density. The software is primarily used for rough estimates only. Protein fractions can be compared to determine percentages of protein in the soluble or insoluble

fractions. Protein bands from different fermentations can also be compared to determine relative increases or decreases in production.

## ***2.6. Inclusion body isolation***

Frozen cell pellets were restored to their original 450 ml broth volumes in 20 mM Tris buffer, pH 8.0. The cell pellets were permitted to thaw in a 37°C water bath for 10-20 min. Cell pellets were then resuspended and blended before being introduced to an Emulsiflex-C3 microfluidizer (Avestin, Ontario, Canada). Resuspended cell pellets were sent through the homogenizer three times at 12,000 peak psi.

To obtain optimal separation, IBs were separated by centrifugation in the same centrifuge used in Section 2.5.3 for 10 min at 12,000 rcf in 1.5 ml aliquots. Supernatant was removed as the soluble protein fraction. The pellet was resuspended in IB wash buffer (50 mM Tris, 1% Tween-20, 1 mM EDTA, 200 mM NaCl, 1 mM  $\beta$ -mercaptoethanol, pH 8.0). The resuspension was allowed to rock at room temperature for 10 min. The wash, resuspension, and incubation with IB wash buffer was repeated once, and the IBs were then washed twice in 20 mM Tris.

It has been found that a significant amount of membrane proteins co-precipitates with IBs during cell lysis [103]. These detergent washes are necessary to remove the membrane proteins. In an ultracentrifugation sucrose gradient, it was found that if inclusion bodies were not washed, contaminating proteins would drag them into heavy fractions (see Figure 2.8).

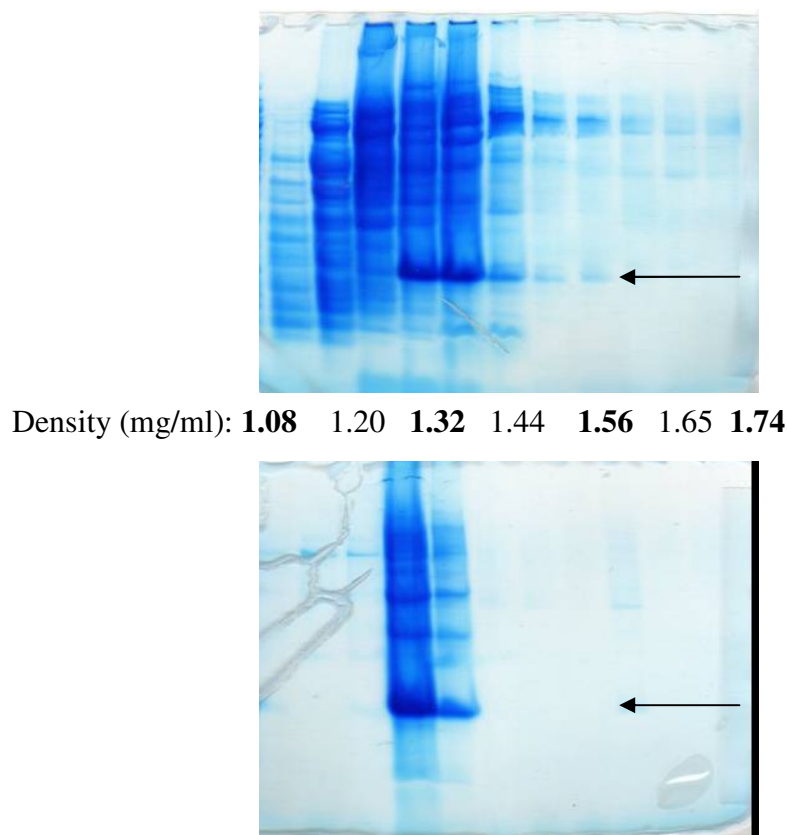


**Figure 2.8. Melan-A fractions after separation in sucrose ultracentrifugation.** Cell lysate (top) and washed inclusion bodies (bottom) of Melan-A were separated in a continuous gradient of sucrose. The Melan-A monomer is indicated by the arrows. Unwashed inclusion bodies in the cell lysate were pulled into heavier fractions by their contaminating proteins.

## ***2.7. Cesium chloride ultracentrifugation gradients***

### ***2.7.1. Ultracentrifugation introduction***

IBs have been shown to be separable by ultracentrifugation. Preparative ultracentrifugation is performed in a centrifuge that runs under vacuum to minimize friction and reach very high rotational speeds. It is typically coupled with a sucrose gradient to separate cell organelles. Cesium chloride gradients have also been used to separate nucleic acids [104]. There is also precedence of using ultracentrifugation to

determine the density of IBs. The most recent work has gathered IBs between sucrose layers [105, 106].

### ***2.7.2. Cesium chloride solutions***

An improved chemical gradient to use for IB ultracentrifugation instead of sucrose is cesium chloride; the range of densities is more appropriate. Published IB densities are 1,340 and 1,240 kg/m<sup>3</sup> for IFN-gamma and prochymosin, respectively [107]. A separate study of 24 different proteins, not in IB form, resulted in densities ranging from 1.25 to 1.37 kg/m<sup>3</sup> [108]. As a reference, 40% and 65% sucrose solutions have densities of 1,176 kg/m<sup>3</sup> and 1,316 kg/m<sup>3</sup>, respectively. Meanwhile 34% and 70% solutions of cesium chloride have densities of 1,250 kg/m<sup>3</sup> and 1520 kg/m<sup>3</sup>, respectively. Sucrose gradients are not in the proper range to measure the density of heavier IBs.

Solution manageability, which improves assay consistency, is another advantage of cesium chloride. Previous IB ultracentrifugation utilized a step gradient, so IBs settled at the interfaces of steps to suggest a density range. For improved resolution, a continuous gradient can be poured, which would provide more precise densities, but sucrose viscosity makes this difficult. A 40% solution of sucrose has a viscosity of 5.187 [109]. A digital paddle SV-10 sine-wave Vibro viscometer (KSV Instruments, Helsinki, Finland) was used to measure a 1.34 cP viscosity for a 34% solution of cesium chloride. In addition to being relative dense, easily prepared, and having a low viscosity, homogeneous cesium chloride solutions will form a gradient during centrifugation. Therefore pouring a step or continuous gradient is not necessary.

### ***2.7.3. Ultracentrifugation experimental setup***

The ultracentrifuge, rotor, and tubes used were from Beckman Coulter (Fullerton, CA). A 34% cesium chloride solution ( $1.25 \text{ kg/m}^3$ ) was used in all IB ultracentrifugation. Beckman Coulter 14 x 89 mm polyallomer centrifuge tubes were used. An aliquot of 11.4 ml of the homogeneous solution was added to each tube. 100  $\mu\text{l}$  of washed inclusion bodies solution was added to the top of each solution. This was less than 1% of the total volume, and small amounts of solutes do not disrupt the gradient formation [110]. The tubes were then centrifuged at  $180,000g$  ( $38,000 \text{ rpm}$ ) for 15 hr at  $4^\circ\text{C}$  on an SW 41 Ti rotor. Since the IBs were clearly visible within the gradient (see Figure 2.9), the depth of the IBs could be directly measured.

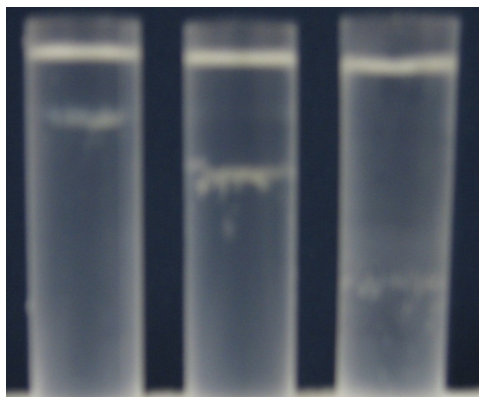


**Figure 2.9. Inclusion body bands in cesium chloride gradients.** From left to right, inclusion body samples were cultured at  $30^\circ\text{C}$ ,  $37^\circ\text{C}$ , and  $42^\circ\text{C}$ . Bands that are denser travel farther down the cesium chloride gradient.

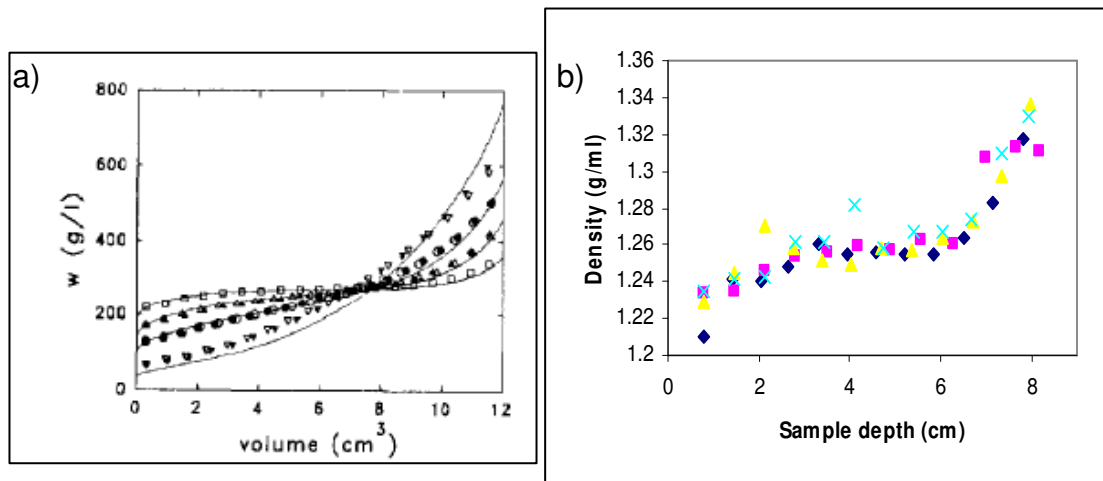


**Figure 2.10. Cesium chloride density in an ultracentrifugation gradient.** a) Cesium chloride gradient density as a function of sample volume. The variable  $w$  is the solute concentration and volume is measured from the top of the tube. Centrifugation durations were 2 (■), 5 (▲), 10 (●), and 71 (▼) hr. Solid lines represent simulation values [110]. b) This study's measurements of density versus sample depth, also measured from top of the tube. Centrifugation was performed for 15 hr.

Fractions were removed by pumping a 50% cesium chloride solution, colored with bromophenol blue, into the bottom of the tube via a syringe. These fractions were collected in pre-weighed eppendorf tubes. Volumes collected in these tubes were measured using pipetmen. The density of each fraction could then be determined. Known volumes of water were added into an empty ultracentrifugation tube, and their depth from the rim of the tube was measured. It was then possible to construct a correlation between sample depth and density (see Figure 2.10b). The data comes from one run with 20 mM Tris buffer added and three runs with different batches of washed IBs.

A similar density graph was created by Minton under different conditions [110]. In this case, the initial density of the cesium chloride gradient was 1.5 kg/m<sup>3</sup> and the centrifugation was performed at 40,000 rpm at 25°C. The general trend of these graphs are similar (see Figure 2.10a). It makes sense that as a gradient forms,

fractions at the top of the tube will get lighter, fractions at the bottom will get heavier, and middle fractions will be in steady-state flux with unchanged density values.

#### **2.7.4. Sedimentation equilibrium**

Sedimentation equilibrium experiments allow particles to travel through a gradient until they reach a point in the gradient that has an identical density. This is different than sedimentation velocity experiments that measure the distance a particle travels in a viscous solution over time. Sedimentation equilibration experiments were conducted so that IB density could be determined independent of IB size or shape. It can be calculated that IBs reached equilibrium based on the sedimentation equation (Eq. 1).

$$\Delta\rho = \frac{18\mu U_o t}{g D_p^2} = \frac{18 \times 0.00134 \frac{\text{kg}}{\text{m} \cdot \text{s}} \times 0.085 \text{m}}{180,000 \times 9.8 \frac{\text{m}}{\text{s}^2} \times (2 \times 10^{-7} \text{m})^2 \times 54,000 \text{s}} = 1 \times 10^{-7} \frac{\text{kg}}{\text{m}^3} \quad (3)$$

This calculation means that for an inclusion body the size of 200  $\mu\text{m}$  to travel the entire 8.5 cm length of the ultracentrifugation tube, it would have to have a density difference greater than the final value shown in Equation 3.

### **2.8. Microscopy preparation and operation**

#### **2.8.1. Light microscopy**

A washed IB solution could be viewed under a light microscope only after the IBs were fluorescently stained. Two different stains were used, 6-carboxyfluorescein succinimidyl ester (CFSE) and 1-anilinonaphthalene 8-sulfonate (ANS). Both stains were obtained from Invitrogen (Carlsbad, CA) The CFSE stain, advertised as an amine binder, was self-fluorescent and had to be washed out of IB solutions with repeated



pelleting and resuspension in 20 mM Tris buffer. The ANS stain, advertised as a lipid binder, only fluoresced after binding, so solutions were immediately usable under the microscope. Images from both stains were visually identical. Samples were filtered through a 0.8  $\mu\text{m}$  filter. Filtering through a 0.45  $\mu\text{m}$  filter seemed to remove most of the particles.

The microscope used had a 10x magnification on the eyepiece and a 100x magnification on the objective lens, providing a 1,000x magnified image. The sample was 10  $\mu\text{l}$  of IB solution after the addition 1  $\mu\text{l}$  ANS stain. The image was viewed through a film of oil over the cover slip. Images of the ANS stain are shown in Figure 2.11.

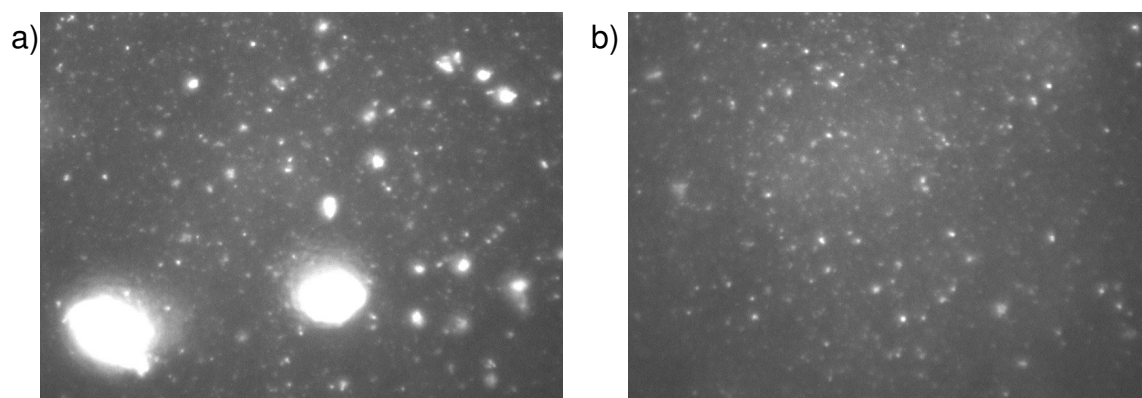


**Figure 2.11. Light microscopy image of fluorescently stained inclusion bodies.** Images are at 1000x magnification after ANS stain a) without filtration and b) with filtration.

### **2.8.2. Cell and IB fixation and dehydration**

To prepare *E. coli* cells and IBs for electron microscopy, a fixation step was needed. All fixation solutions were in 0.1 M sodium cacodylate buffer, pH 7.2. Cells and IBs were pelleted using 12,000 rcf centrifugation for 3 and 10 min, respectively, using the centrifuge described in Section 2.5.3. A 0.5 ml aliquot of fermentation harvest was pelleted and resuspended in 4% formaldehyde and 0.5% glutaraldehyde.

Washed IBs, as detailed in Section 2.6, were resuspended in 2.0% glutaraldehyde. Incubation in the fixatives was performed at 4°C overnight. Glutaraldehyde has terminal aldehyde groups that are able to cross-link the lysine groups in adjacent proteins.

Fixative was removed by pelleting and resuspending the IBs three times in buffer. Each resuspension was incubated on ice for 10 min. After washes, pellets were further fixed and stained with 0.1% osmium tetroxide. Osmium tetroxide acts as a secondary fixative that reacts with lipid moieties. Fixative was removed again with three 10 min washes with incubations on ice with 0.1 M sodium cacodylate.

The *E. coli* cells had an additional embedding step. The fixed cell pellet was resuspended in a hot 1% agarose solution at approximately 50°C. Before the agarose solidified, cells were pelleted. The cell pellet was extracted into 1 mm cubes with a razor blade.

Cell-enriched agarose cubes were incubated in 25% ethanol and rocked for 10 min. Fixed IB pellets were resuspended in 25% ethanol and rocked for 10 min. These dehydration incubations were repeated for 50%, 75%, 95%, and 100% ethanol.

### ***2.8.3. Transmission electron microscopy of cells***

Transmission electron microscopy (TEM) works by shooting electrons at a sample. These electrons undergo diffraction when they collide with the sample and are then focused through electromagnetic lenses to create an image. Because of the short wavelengths of the X-rays generated from the impaction, very high magnifications and resolutions can be reached, which make TEM ideal for imaging microstructures. Inclusion bodies have been visualized by TEM in the past [111, 112].

Cells were fixed with formaldehyde, glutaraldehyde, and osmium tetroxide, as described in Section 2.8.2. They were then embedded in agarose and gradually

dehydrated in 100% ethanol, also described in Section 2.8.2. The cells cubes were then incubated in a 2:1 ethanol:unicryl solution for 30 min. The infiltration solution was then changed to 1:2 ethanol:unicryl and then unicryl only.

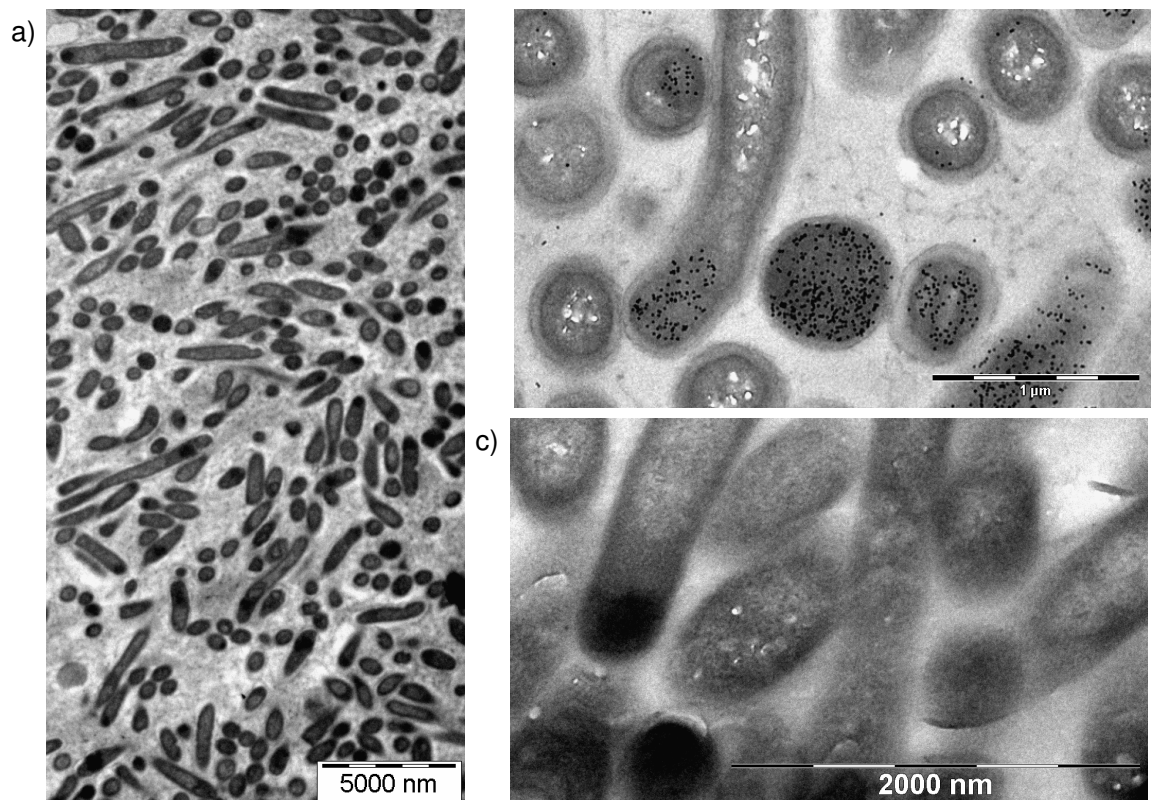


**Figure 2.12. TEM image of *E. coli* sections producing Melan-A as inclusion bodies.** a) Low magnification view of *E. coli* cells in TEM. b) Inclusion bodies are labeled with gold nanoparticles. c) Inclusion bodies are stained with osmium tetroxide.

Single cell cubes were transferred to embedding capsules (BEEM, West Chester, PA) and then submerged in fresh unicryl. The capsules were then incubated at 65°C for two days to polymerize the unicryl. The cells could then be sectioned using a diamond knife in an ultramicrotome. The thin slices (50 – 100 nm) were placed on nickel-gilded 300 mesh hex microscopy grids (Electron Microscopy Sciences, Hatfield, PA).

These sections were viewed in Tecnai T-12 TEM (FEI, Hillsboro, OR). Note that the some of the cells are elongated (see Figure 2.10a). This is commonly seen in bacteria that overproduce protein [113].

#### **2.8.4. Transmission electron microscopy of IBs**

Instead of sectioning, washed IBs could be diluted to a concentration of 0.03 mg/ml and directly placed on gold gilded nickel grids (Electron Microscopy Sciences) coated with formvar. To confirm the presence of Melan-A in these bodies, 10 nm goat-anti-mouse IgG gold (Electron Microscopy Sciences) were used to label them. These gold nanoparticles were applied as a secondary antibody, much like how a western blot is performed. Based on images obtained, IB sizes ranged from 0.1  $\mu\text{m}$  to 0.6  $\mu\text{m}$  in diameter (see Figure 2.13).

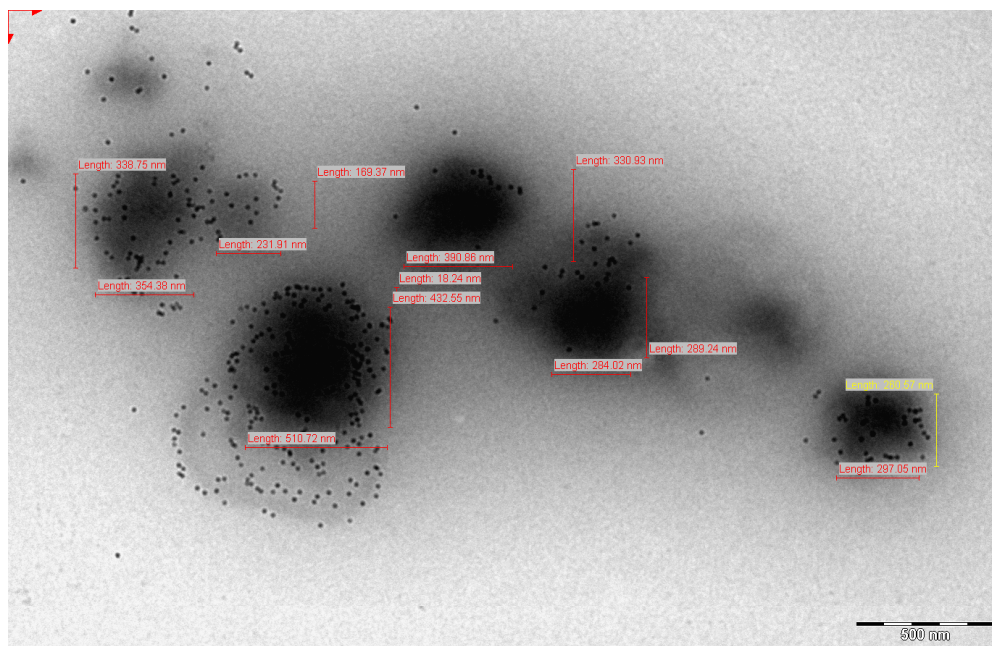


**Figure 2.13. TEM image of washed inclusion bodies.** Inclusion bodies have been labeled with antibody-conjugated gold nanoparticles. Image is taken at 26,000x magnification.

### 2.8.5. Scanning electron microscopy

Although IBs have been visualized with scanning electron microscopy in the past [105, 114], none of these images have gone beyond 20,000x magnification [115]. This study examined IBs at up to 50,000x magnification to visualize finer details.

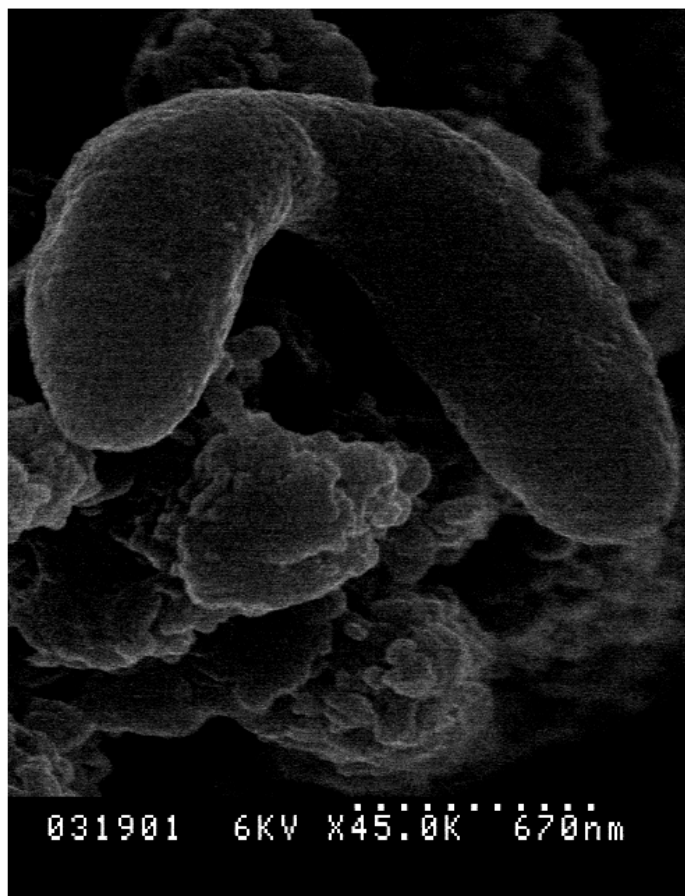


**Figure 2.14. SEM image of *E. coli* cell and inclusion body bed.** A suspected *E. coli* bacterium is shown (top) that survived homogenization, detergent washing, and IB SEM preparation. In the background (bottom) are 300  $\mu\text{m}$  inclusion bodies. Dotted white line is the scale bar.

As described in Section 2.8.2, washed IBs were dehydrated to 100% ethanol after being fixed with glutaraldehyde and osmium tetroxide. Each IB suspension was then syringed through a 0.2  $\mu\text{m}$  nylon syringe filter (Thermo Fisher Scientific,

Waltham, MA). A razor blade was used to slice open the filter casing and extract the filter paper that collected the IBs. This filter was placed in 100% ethanol.

The IBs were then dried using a Balzers Union CPD 020 critical point dryer (BAL-TEC, Balzers, Liechtenstein). The 100% ethanol was washed out with liquid carbon dioxide. The carbon dioxide was then sublimed at 31°C at 73.8 bar. Dried samples were then given a 10 nm coat of gold palladium using a sputter coater (Technics Hummer V). The IB samples were then viewed in a Hitachi 5900 SEM (Maidenhead, Berkshire, UK). An example image is shown in Figure 2.14.

#### ***2.8.6. Atomic Force Microscopy***

Atomic Force Microscopy (AFM) brushes a probe along the surface of a sample. The probe rests on the tip of a cantilever which is mounted on a piezo. A laser is used to detect deflections as the probe responds to changes in surface topography.

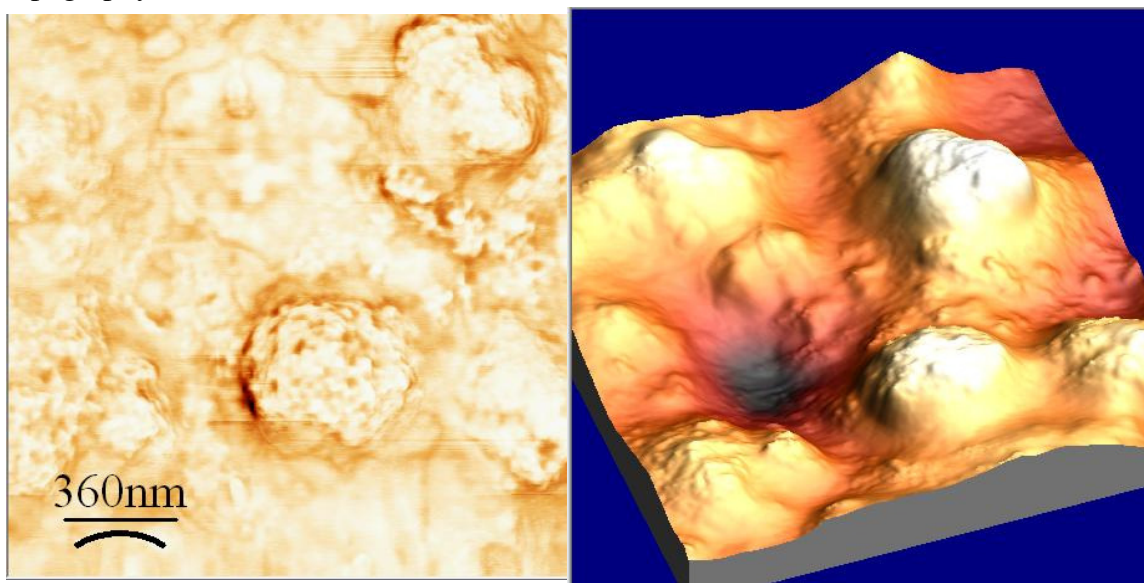


**Figure 2.15. AFM image of Melan-A inclusion bodies.** Images of inclusion bodies obtained from dry samples in tapping mode on the Dimension 3100 AFM (left) and a software generated 3-D representation (right).

Washed IB solution was filtered through a 0.8  $\mu\text{m}$  filter and 10  $\mu\text{l}$  was placed on a poly-d-lysine coated 35 mm glass bottom culture dish (MatTek, Ashland, MA). This solution was allowed to dry and analyzed on an Dimension 3100 AFM (Veeco, Plainview, NY). Figure 2.15. shows an example image obtained in tapping mode using a silicon probe.

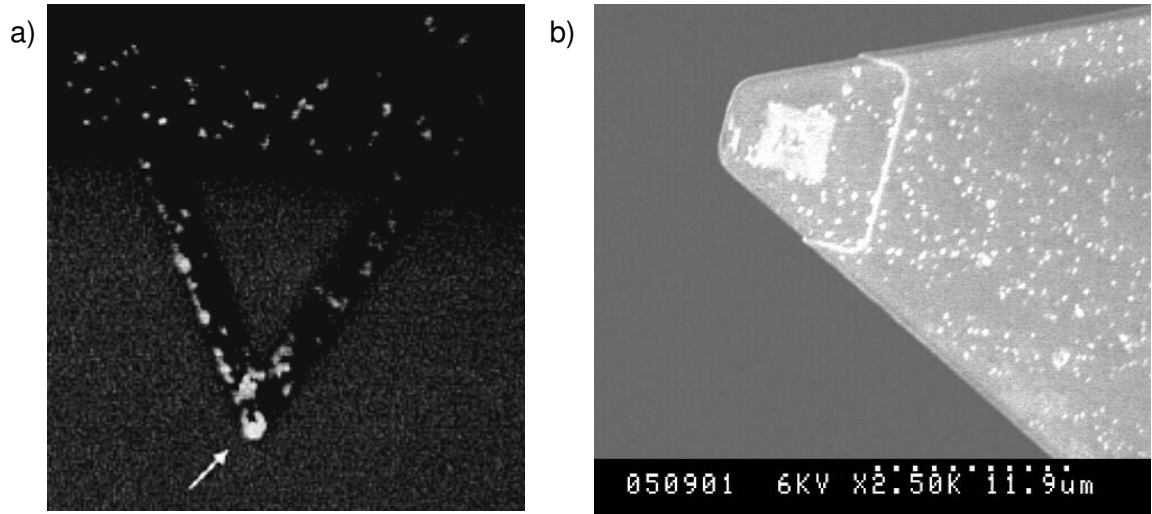


**Figure 2.16. SEM images of AFM probes after exposure to inclusion bodies.** a) Wangsa's image and b) this study's image of an AFM probe after attempting to perform force measurements on inclusion bodies in solution.

AFM imaging was also attempted on a Picoplus AFM (Agilent, Santa Clara, CA) with wet samples diluted into PBS. A silicon nitride probe was used. The probe analyzed these samples in contact mode. Force measurements could be conducted on these particles based on Hooke's Law:

$$F = -k\Delta z \quad (4)$$

$k$  is the cantilever spring constant, and  $\Delta z$  is the deflection in the probe at the force  $F$ . Corrections must be made for piezo sensitivity. Unfortunately force measurements continued to increase over time because the probe would get fouled. This was confirmed by taking an SEM image of a used probe (see Figure 2.16b). Interestingly,

this same type of image was obtained from a group that used AFM to measure IB force in the past [116] (see Figure 2.16a).

## ***2.9. Particle size distribution***

For centrifugation, a particle size distribution is necessary to calculate accurate collection efficiencies. When collection efficiencies are calculated based off average particle size alone, values are inflated. For example, if 100% collection can be accomplished at the average particle size, this would not be true if there were a distribution of sizes. Particles that were larger would still be collected, but particles that were smaller would not. For filtration, pore sizes cannot simply match the average particle size because any smaller particles in the distribution will not be retained. These are the very practical reasons for why it is necessary to know the particle size distribution.

### ***2.9.1. Size estimation with tangential flow filtration***

Cell lysate has been routinely washed via tangential flow filtration (TFF). During a TFF process, a protein solution is re-circulated back into a reservoir while being pumped parallel to a filter membrane. A portion of the solution passes through the membrane due to a pressure difference; particulates larger than the membrane's pore size are retained. IBs are washed using TFF using a detergent solution to remove bacterial membrane proteins because the tangential flow prevents IBs from fouling the filter membrane.

In the instances when TFF was used to wash Melan-A IBs, no back pressure was applied and a membrane cassette (Pall, East Hills, NY) with 0.45  $\mu\text{m}$  pores was used to retain the IBs. If 10-20 psi transmembrane pressure was applied, there is some



Melan-A loss in the permeate. These data suggest that there is a distribution of Melan-A IBs that span below and above 0.45  $\mu\text{m}$  in diameter.

When NY-ESO-1 IBs were washed using the TFF unit, a 0.45  $\mu\text{m}$  filter was not able to retain the inclusion bodies. This problem was solved by using a 0.22  $\mu\text{m}$  filter.

### ***2.9.2. Size estimation from electron microscopy***

Although TEM is normally a very appropriate tool for measuring particle size, it was not applicable to IB measurements. If IBs were measured from cell sections, there was no indication which plane of the IB was being measured. The measurement would not be accurate unless the sectioning was done to obtain the widest cross-section of the IB. Measuring washed IBs in TEM was also unreliable since the objects were three-dimensional and difficult to focus as a result. Inconsistencies in focusing would compromise the accuracy of the measurement. The same issue applied to SEM imaging. These techniques were all very good, however, at providing a size estimate for the IBs in this study. For example, the IBs shown in Figure 2.10, 2.11, and 2.12 were from Melan-A produced at 42°C using a pH stat feeding method. The IBs produced under these conditions are about 300  $\mu\text{m}$ .

### ***2.9.3. Dynamic light scattering***

The size distribution of IBs was ultimately determined via measurements of their zeta potential. Dynamic light scattering techniques have been shown to accurately measure particle sizes that span from nanometers to several microns in diameter [117]. A zetasizer instrument (Malvern, Worcestershire, UK) measures the fluctuations in light scattering. Smaller particles are more susceptible to Brownian motion and give larger fluctuations.

Washed IBs were filtered through a 0.8  $\mu\text{m}$  filter and 10  $\mu\text{l}$  was diluted into 0.5 ml of Milli-Q water. The filtration was necessary to remove IB aggregates as earlier demonstrated in Figure 2.9. The ultrapure diluent was necessary because other buffers would give false particle measurements. Samples were transferred to a 1.5 ml polystyrene semi-micro disposable cuvette (Perfector Scientific, Atascadero, CA) and measured in triplicate. The refractive indices of water and protein were used to calculate particles sizes and assumed to be 1.33 and 1.45, respectively. Calculated particle sizes of IBs ranged from 20 – 400 nm. These measurements agreed with estimates obtained from TFF, SEM, TEM, and AFM.

#### ***2.10. Bradford total protein assay***

Coomassie dye reacts with all proteins, particularly lysine and arginine residues. This change is colorimetric and can be quantified using spectroscopy at 595 nm. A 2 mg/ml BSA stock was diluted into standards with concentrations of 0.025, 0.125, 0.25, 0.50, 0.75, 1.00, 1.25, and 1.50 mg/ml. The dilutions used to make these standards is shown in Table 2.2. A 10  $\mu\text{l}$  aliquot of each standard was added in triplicate to wells in a 96-well plate. A 10  $\mu\text{l}$  aliquot of cell lysate, soluble protein, or IBs were also added in triplicate to the plate. An additional 295  $\mu\text{l}$  of refrigerated Pierce Coomassie dye (Thermo Fisher Scientific, Waltham, MA) was added to each well, and the samples were incubated at room temperature for 10 minutes. A GENios plate reader (Tecan, Männedorf, Switzerland) was then used to measure the absorbance of each well at 595 nm. The BSA samples were used as a standard curve, which is the most commonly used standard for the Bradford assay. An example standard curve is shown in Figure 2.17.

**Table 2.2. Bradford standard preparation dilutions.** Bovine serum albumin was diluted to various concentrations at regular intervals from 0 to 1.5 mg/ml. The dilution order for how these standards were prepared is shown.

Vial	Water (ul)	BSA (ul)	Conc. mg/ml
A	125	375 of Stock	1.500
B	105	175 of Stock	1.250
C	400	400 of Stock	1.000
D	175	175 of A	0.750
E	325	325 of C	0.500
F	325	325 of E	0.250
G	325	325 of F	0.125
H	400	100 of G	0.025
I	400	0	0.000

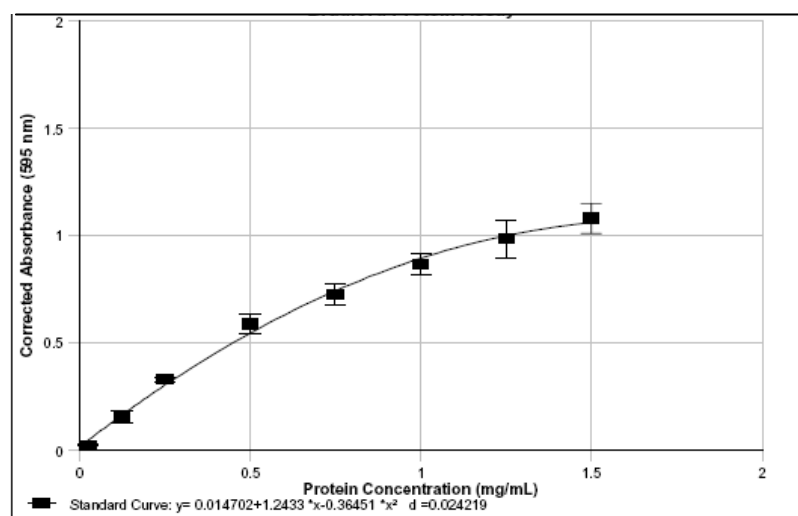


**Figure 2.17. Example Bradford standard curve.** The standard curve is made of freshly made dilutions of BSA in water. All measurements are taken in triplicate.

## 2.11 Dry weights

The dry weight of cells or IBs could be measured with the following procedure. Eppendorf tubes were pre-weighed using an analytical balance. A 1 ml aliquot of cell broth or washed IB solution were added to a tube and centrifuged at 12,000 rcf in the same centrifuge described in Section 2.5.3. Cells were pelleted for 3

min; IBs were pelleted for 10 min. A pipetteman was used to remove the supernatant without disturbing the pellet. Cells grown in a chemically defined medium pelleted with salts, so these pellets were resuspended in 20 mM Tris buffer and pelleted again three times. The wet cell pellet was then placed on a 95°C heating block overnight. Dried pellets were re-weighed, correcting for the weight of the empty tube.

### **2.12. IMAC chromatography**

An IMAC column was used to capture selected batches of Melan-A protein. Two 1 ml solutions of washed Melan-A IBs for each selected condition were pelleted and resuspended in either 2, 4, or 8 M urea buffers containing 100 mM sodium phosphate, pH 7.5. The solubilized inclusion bodies were added to a new 1 ml HisTrap column (General Electric Healthcare, Piscataway, NJ) that had been equilibrated with 3 column volumes (CV) of the respective urea buffer. After the protein was loaded on the column, 3 CV this same urea buffer was used to chase the unbound protein off the column. Another urea buffer with 85 mM imidazole was then loaded on the column for 3 CV to remove any non-specific binding protein. 3 CV of a third urea buffer with 500 mM imidazole was used to elute the protein. This protein was quantified using a Bradford assay, as described in Section 2.10.

### **2.13. Conclusion**

Fermentation procedures were set up that varied temperature, IPTG concentration, oxygen levels, and feeding profiles for Melan-A producing *E. coli*. Runs with varying temperatures were also performed with HCDCs producing EGFP, SSX2, and NY-ESO-1. IBs from all of these runs were collected. IB density was determined using cesium chloride gradients, IB sizes were estimated using dynamic light scattering, and IB protein accessibility was determined by

comparing Bradford protein values with dry weights. The chemical stability of the IBs was tested with various levels of urea, and protein accessibility and IMAC recovery were measured.

## REFERENCES

- 93) O. Thastrup, S. Tullin, L. Poulsen, S. Bjørn, S. Petersen, Fluorescent proteins, [1995] US patent.
- 94) M. Chalfie, Y. Tu, G. Euskirchen, W. Ward, D. Prasher, Green fluorescent protein as a marker for gene expression, *Science* 263 [2004] 802-805.
- 95) E. García-Fruitós, A. Arís, A. Villaverde, Localization of functional polypeptides in bacterial inclusion bodies, *Appl. Environ. Microbiol.* 73 [2007] 289-294.
- 96) U. Sahin, O. Türeci, H. Schmitt, B. Cochlovius, T. Johannes, R. Schmits, F. Stenner, G. Luo, I. Schobert, M. Pfreundschuh, Human neoplasms elicit multiple specific immune-responses in the autologous host, *Proc. Natl. Acad. Sci. USA* 92 [1995] 11810-11813.
- 97) S. Gnjatic, H. Nishikawa, A. Jungbluth, A. Güre, G. Ritter, E. Jäger, A. Knuth, Y. Chen, L. Old, NY-ESO-1: review of an immunogenic tumor antigen, *Advances in Cancer Research* 95 [2006] 1-30.
- 98) P. Romero, D. Valmori, M. Pittet, A. Zippelius, D. Rimoldi, F. Levy, V. Dutoit, M. Ayyoub, V. Rubio-Godoy, O. Michielin, P. Guillaume, P. Batard, I. Luescher, F. Lejeune, D. Lienard, N. Rufer, P. Dietrich, D. Speiser, J. Cerottini, Antigenicity and immunogenicity of Melan-A/MART-1 derived peptides as targets for tumor reactive CTL in human melanoma, *Immunological Reviews* 188 [2002] 81-96.
- 99) Y. Kawakami, S. Eliyahu, C. Delgado, P. Robbins, L. Rivoltini, S. Topalian, T. Miki, S. Rosenberg, Cloning of the gene coding for a shared human melanoma antigen recognized by autologous T-cells infiltrating into tumor, *Proc. Natl. Acad. Sci. USA* 91 [1994] 3515-3519.

- 100) F. Studier, B. Moffatt, Use of bacteriophage T7 RNA polymerase to direct selective high-level expression of cloned genes, *J. Mol. Biol.* 189 [1986] 113-130.
- 101) M. Åkesson, Probing control of glucose feeding in *Escherichia coli* cultivations, PhD Thesis ISRN LUTFD2/TFRT 1057 SE, Department of Automatic Control, Lund Institute of Technology, Sweden [1999].
- 102) W. Zhi, J. Song, F. Ouyang, J. Bi, Application of response surface methodology to the modeling of  $\alpha$ -amylase purification by aqueous two-phase systems, *J. Biotechnol.* 118 [2005] 157-165.
- 103) R. Hart, U. Rinas, J. Bailey, Protein composition of *Vitreoscilla* hemoglobin inclusion bodies produced in *Escherichia coli*, *J. Biol. Chem.* 265 [1990] 12728-12733.
- 104) M. Meselson, F. Stahl, The replication of DNA in *Escherichia coli*, *Proc. Natl. Acad. Sci. USA* 44 [1958], 671-682.
- 105) G. Georgiou, P. Valax, Isolating inclusion bodies from bacteria, *Method Enzymol.* 309 [1999] 48-58.
- 106) A. Schrödel, A. de Marco, Characterization of the aggregates formed during recombinant protein expression in bacteria, *BMC Biochem.* 6 [2005].
- 107) G. Taylor, M. Hoare, D. Gray, F. Marston, Size and density of protein inclusion bodies, *Biotechnology* 4 [1986] 553-557.
- 108) J. Ifft, Sedimentation equilibrium of proteins in density gradients, *Biophys. Chem.* 5 [1976] 137-157.
- 109) C. James, D. Mulcahy, B. Steel, Viscometer calibration standards: viscosities of water between 0 and 60°C and of selected aqueous sucrose solutions at 25°C from measurements with a flared capillary viscometer, *J. Phys. D: Appl. Phys.* 17 [1984] 225-230.

- 110) A. Minton, Simulation of the time course of macromolecular separations in an ultracentrifuge. I. Formation of a cesium chloride density gradient at 25°C, *Biophys. Chem.* 42 [1992] 13-21.
- 111) P. Petrov, E. Jay, I. Ivanov, Inclusion bodies in recombinant *E. coli* producing human calcitonin tetramer, as visualized by immuno-gold electron microscopy, *Biol. Cell* 61 [1987] 1-4.
- 112) M. Carrió, A. Villaverde, Localization of chaperones DnaK and GroEL in bacterial inclusion bodies, *J. Bacteriol.* 187 [2005] 3599-3601.
- 113) G. Georgiou, J. Telford, M. Shuler, D. Wilson, Localization of inclusion bodies in *Escherichia coli* overproducing  $\beta$ -lactamase or alkaline phosphatase, *Appl. Environ. Microbiol.* 52 [1986] 1157-1161.
- 114) G. Bowden, Structure and morphology of protein inclusion bodies in *Escherichia coli*, *Nat. Biotechnol.* 9 [1991] 725-730.
- 115) H. Kang, A. Sun, Y. Shen, D. Wei, Refolding and structural characteristics of TRAIL/Apo2L inclusion bodies from different specific growth rates of recombinant *Escherichia coli*, *Biotechnol. Prog.* 23 [2007] 286-292.
- 116) N. Wangsa-Wirawan, A. Ikai, B. O'Neill, A. Middelberg, Measuring the interaction forces between protein inclusion bodies and an air bubble using an atomic force microscope, *Biotechnol. Prog.* 17 [2001] 963-969.
- 117) D. Black, M. McQuay, M. Bonin, Laser-based techniques for particle-size measurements: a review of sizing methods and their industrial applications, *Prog. Energ. Combust.* 22 [1996] 267-306.



## CHAPTER 3

### THE DENSITY AND PARTICLE SIZE OF SYNTHETIC MELAN-A INCLUSION BODIES ARE DEPENDENT ON FERMENTATION CONDITIONS

#### ***3.1. Introduction***

High cell density cultures (HCDC) of *E. coli* were used to produce protein from a synthetic Melan-A plasmid. Syn-Melan-A protein readily formed inclusion bodies (IBs) which could be extracted and measured for density and particle size using the techniques described in Chapter 2. These IBs were produced in both complex and chemically defined media.

In complex medium experiments, the variables changed in the fermentations were feeding strategies, IPTG concentrations, and culture temperature. In chemically defined medium experiments, a statistical design of experiment was used to examine the effects of feeding rate and temperature only.

#### ***3.2. Inclusion body size and density trends from complex medium studies***

##### ***3.2.1. Feeding strategies***

As detailed in Chapter 2, initial cell growth was done in a batch medium and feed medium was gradually added to the reactor upon glucose depletion. One set of media contained yeast extract; the other set was completely chemically defined. Both types of fermentations were confirmed to be glucose-limiting because the addition of only a glucose solution was able to reverse any rises in pH and dissolved oxygen (DO).

Various feeding strategies were used to grow synthetic Melan-A in complex medium. These runs were all performed at 37°C and pH 7.0. A pH-stat feeding method added feed medium in constant responses to rises in pH. Since the pH-stat feeding profile was regularly reproducible, it was possible to calculate a linear feed rate to feed approximately at the same rate as the pH-stat feeding method. It was also possible to create a step feed, which mimicked pH-stat feeding profile with five distinct feed rates. Constant feed strategies were also employed with a different constant feed rate per run. The total fermentation time of the constant feed fermentations varied, but the total amount of feed added was the same in all runs. The feeding profiles are shown in Figure 3.1.

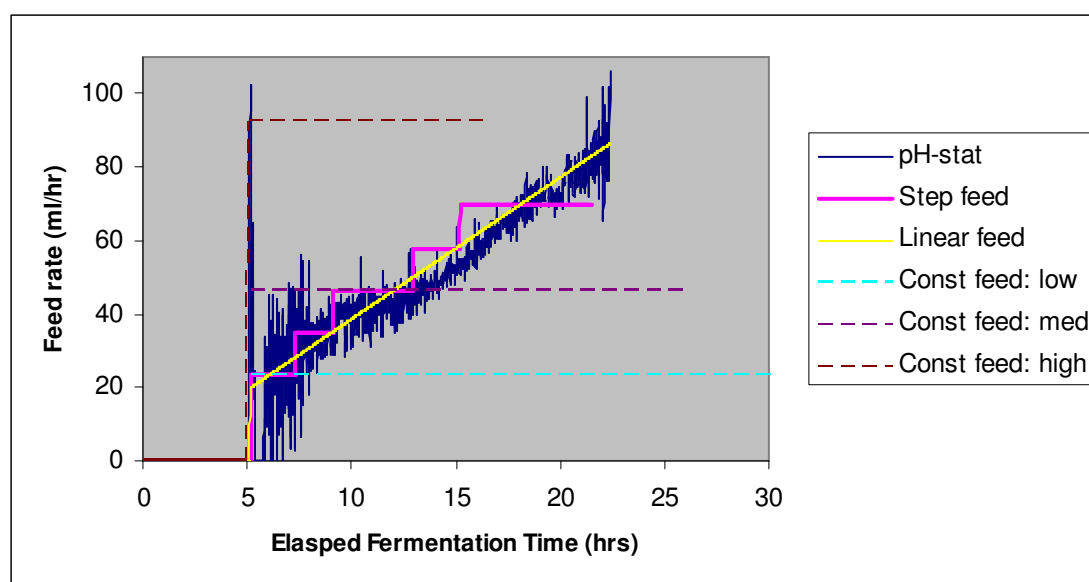


**Figure 3.1. Feed rate data for different feeding types.** Linear and step feeding profiles attempted to reproduce the pH-stat feeding profile. Dotted lines represent constant feeding rates. The low constant feed rate fermentation continued until 46 hr of elapsed fermentation time.

Almost identical cell growth was observed between pH-stat, step, linear, and medium constant feeding rates (Figure 3.7). Lower densities were reached with low

and high constant feed rates. Despite the difference in cell density, volumetric productivity of protein was roughly equivalent in these fermentations (Figure 3.2).

The density of IBs produced using different feeding methods varied (Table 3.1). The major trend for density was that higher feeding rates led to denser IBs. Even in the case of pH-stat versus linear and step feeds, IBs produced using a pH-stat feeding method had lower densities. This agrees with the trend that limited

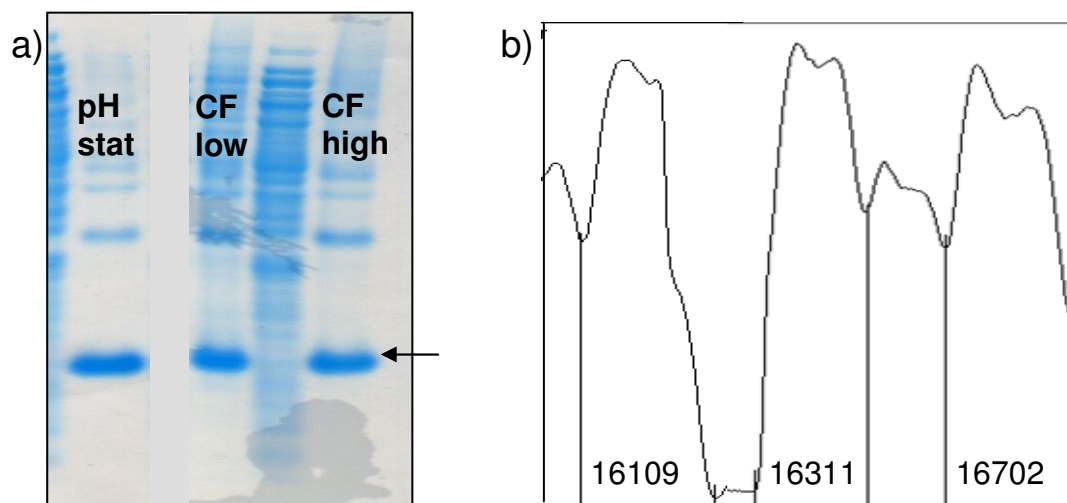


**Figure 3.2. Gel densitometry of Melan-A production under different feeding strategies.** a) SDS-PAGE of synthetic Melan-A insoluble fractions produced under fermentations using pH-stat, low constant feed, and high constant feed. Melan-A protein is indicated by the arrow. b) Image J gel densitometry analysis of gel shown.

feed creates less dense IBs because pH-stat feeding feeds just under the amount the nutrients need to prevent starvation. So although the feeding profiles of pH-stat, step, and linear feed seem very similar, the borderline starvation response allowed in pH-stat feeding affects the IB density.

A trend in IB size based on feeding condition (Table 3.1) was also observed. Although not as obvious as the density trend, it appears that the size of IBs produced under pH-stat conditions at 37°C are  $220 \pm 16$  nm, while IBs produced at 37°C with other feeding strategies are  $299 \pm 32$  nm. Again, this can be attributed to the

starvation response triggered throughout a pH-stat fermentation. If cell starvation is the cause, it is not immediately obvious why the lowest constant feeding rate fermentation did not also elicit a similar response as the pH-stat fermentations. This may be attributed to the excess glucose present in the bioreactor at the start of all constant feed strategies. It may also be possible that the lowered feed was able to slow down the bacterial growth rate, thus decreasing glucose demand.

### 3.2.2. IPTG Effects

Four different concentrations of IPTG were used. These concentrations in the complex feed medium were 0.1, 0.5, 1.0, and 4.5 mM. The feed medium was gradually added to the fermentor, increasing the IPTG concentrations in the reactor to final values of 0.05, 0.25, 0.50, and 2.25 mM. Although the latter values may seem high compared to the typical micromolar concentrations in *E. coli* studies [118],

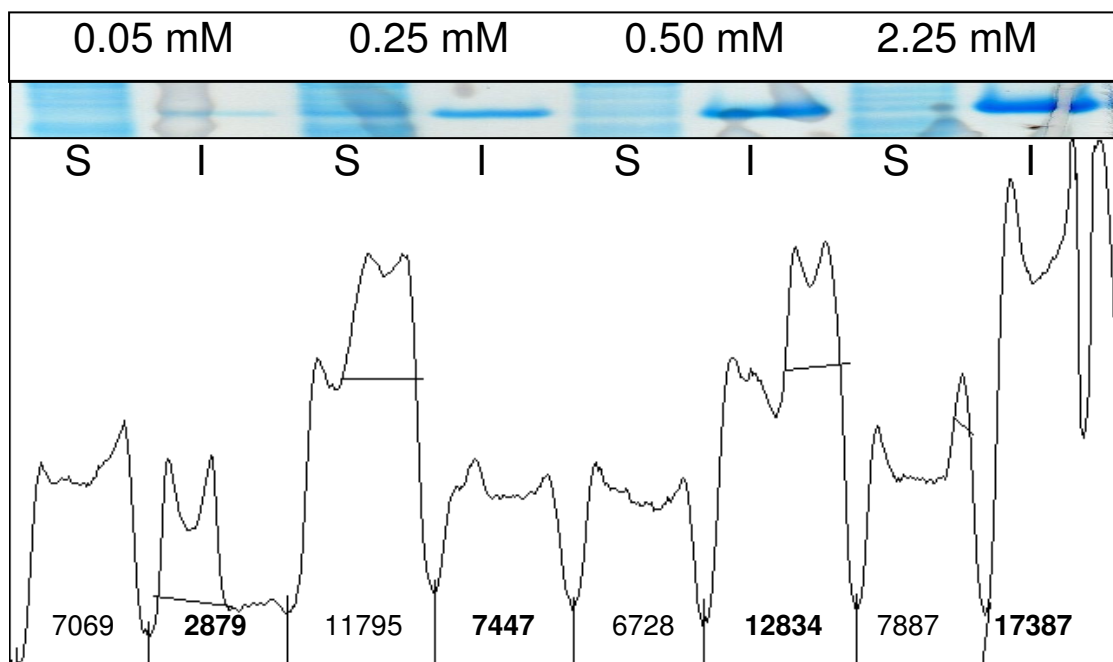


**Figure 3.3. SDS-PAGE and Image J densitometry analysis of Melan-A fractions under different concentrations of IPTG.** Soluble (S) and insoluble (I) fractions of each sample are shown.

IPTG concentrations up to 3 mM are common in HCDC [119]. Indeed, as seen in Figure 3.3, a higher level of IPTG increases final Melan-A production. Focusing on only the insoluble protein fraction, which is primarily where Melan-A is located, 0.05, 0.25, and 0.50 mM IPTG respectively generate 17%, 43%, and 74% of the Melan-A generated with 2.25 mM IPTG.

Another condition studied was the method of IPTG addition. Instead of gradually adding IPTG to the culture with the feed medium, IPTG was added directly to the fermentor upon initiation of the feeding phase. An amount of 4.5 ml 1 M IPTG solution was added to the vessel, creating an initial concentration of 4.5 mM in the reactor that was gradually diluted to a final concentration of 2.25 mM as feed was added to the vessel.

The density of Syn-Melan-A IBs produced from any of the four concentrations of IPTG tested in this study was  $1.294 \pm 0.004$  g/ml. The particle sizes of these IBs were  $221 \pm 16$  nm. Even though using different IPTG concentrations did alter the amount of Melan-A produced in the fermentor, there was no noticeable difference in the density or particle size of the resultant IBs. Even when IPTG was added directly to the fermentor, there was no effect on IB density, and IBs were only slightly larger at 248 nm. These observations suggest that the rate of Syn-Melan-A production does not alter IB properties. Further discussion is provided in Section 5.1.

The growth curves of the cultures were identical regardless of the amount or method of IPTG added. Therefore the IPTG concentrations did not need to be normalized per cell.

### ***3.2.3. Temperature Effects***

Syn-Melan-A was grown at three different temperatures in complex medium using a pH-stat feeding method to a final concentration of 2.25 mM IPTG. These

temperatures were 30°C, 37°C, and 42°C. All fermentations were maintained at 37°C during the inoculum and batch phase. When feeding was initiated, temperature was changed to 30°C or 42°C for the duration of the fermentation.

Although it is expected that more Syn-Melan-A would be produced in the soluble fraction at 30°C, this was not the case. As seen in Figure 3.4, there is very little difference in Syn-Melan-A production when cultures were grown at 30°C or 37°C. There is less Syn-Melan-A produced at 42°C in the insoluble fraction. This response was expected since proteases are very active during the heat shock response.

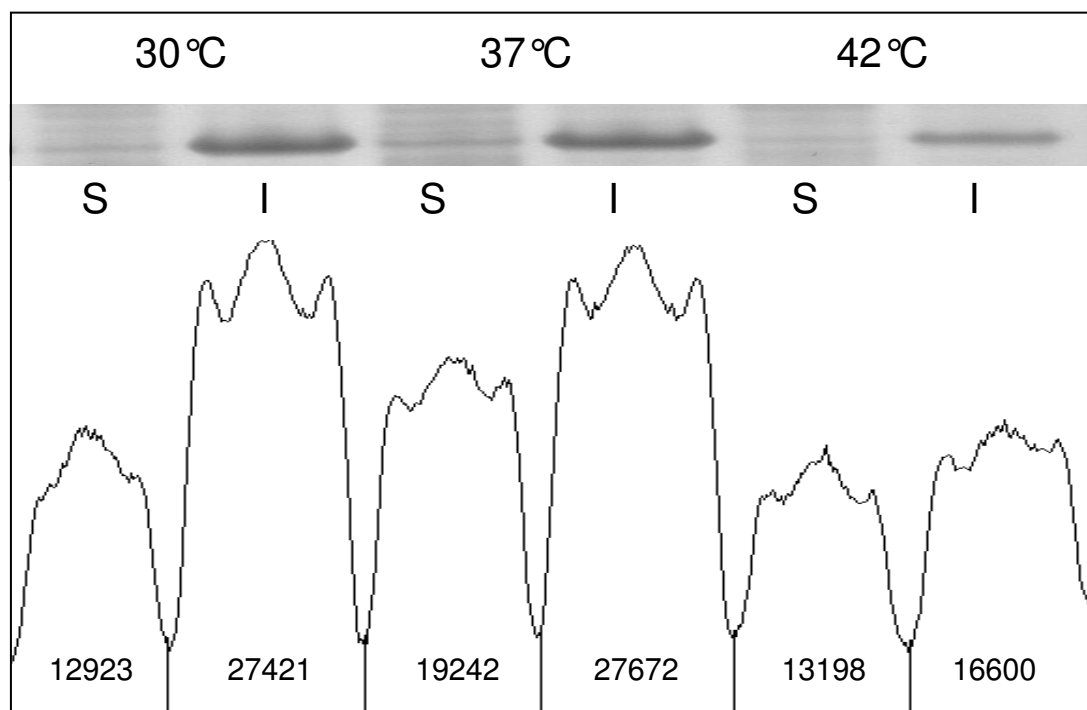


**Figure 3.4. SDS-PAGE and Image J densitometry analysis of Melan-A fractions under different fermentation temperatures.** Soluble (S) and insoluble (I) fractions of each sample are shown.

There is the largest disparity in IB density when producing cultures were grown at different temperatures. The densities spanned from 1.258 to 1.308 g/ml. Particle sizes of IBs produced at 37°C and 42°C were about  $223 \pm 8$  nm, and IBs

produced at 30°C were  $316 \pm 17$ . IBs produced at 30°C were larger than those produced at 37°C, but they were also less dense. IBs produced at 42°C were denser than their 37°C counterparts, but cultures at 42°C ultimately produced less.

### 3.2.4. General trends

IB density and size data based on the fermentations performed in complex medium are summarized in Table 3.1.

**Table 3.1. Inclusion body density and size for synthetic Melan-A produced with different fermentation conditions in complex medium.**

Temp	Feed Style	IPTG conc	IB density	IB size
°C		mM	(g/ml)	(nm)
37	pH-stat	0.05	1.294	$217 \pm 9$
37	pH-stat	0.25	1.299	$211 \pm 1$
37	pH-stat	0.50	1.292	$209 \pm 9$
37	pH-stat	2.25*	1.294	$248 \pm 9$
37	pH-stat	2.25	1.296	$215 \pm 5$
30	pH-stat	2.25	1.258	$316 \pm 17$
42	pH-stat	2.25	1.308	$231 \pm 6$
37	const: low	2.25	1.276	$296 \pm 29$
37	const: med	2.25	1.296	$273 \pm 9$
37	const: high	2.25	1.310	$340 \pm 21$
37	linear	2.25	1.303	$267 \pm 9$
37	step	2.25	1.303	$287 \pm 31$

\* In one set of conditions, IPTG was added directly to the fermentor

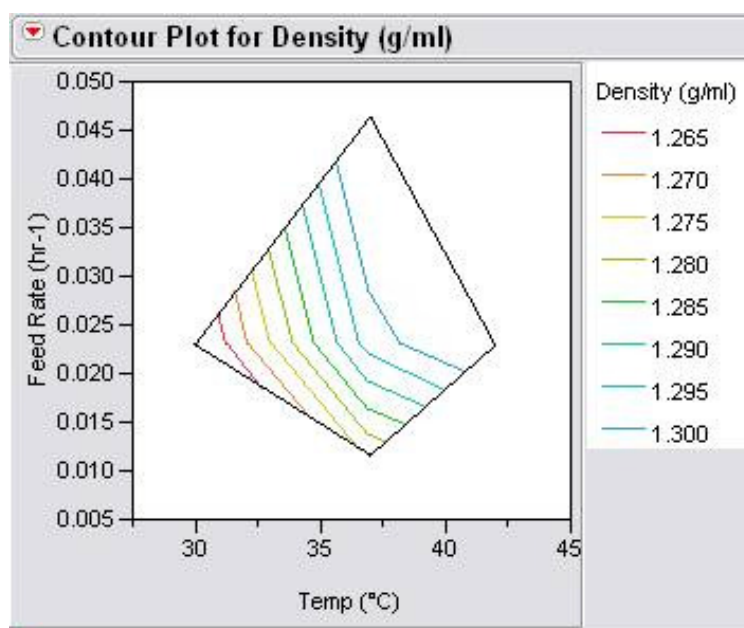


**Figure 3.5. Inclusion body density as a function of feed rate and growth temperature in complex medium.** Vertical lines in the contour plot indicate that inclusion body density had a stronger dependence on temperature than feeding rate. The pH-stat, step, and linear feeding rates were inputted as medium feeding rate on this plot.

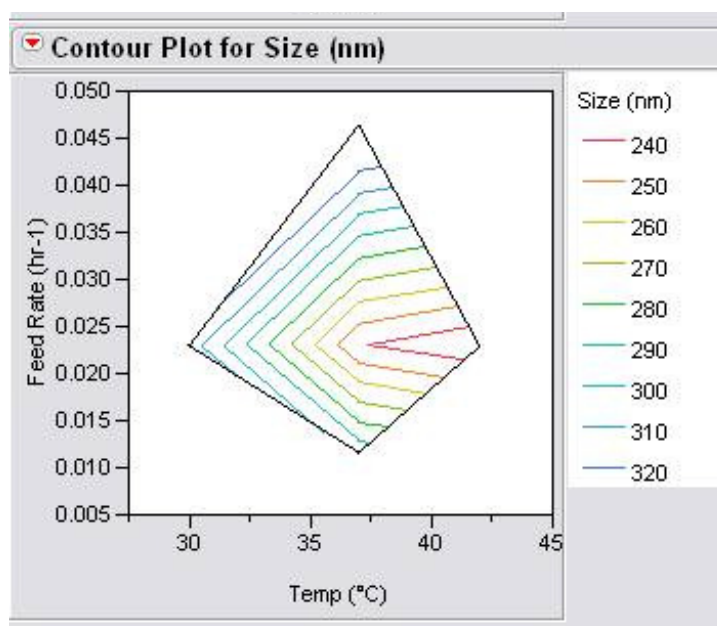


**Figure 3.6. Inclusion body size as a function of feed rate and growth temperature in complex medium.** Diagonal lines indicate that both feed rate and growth temperature contributed equally to the inclusion body size. The pH-stat, step, and linear feeding rates were inputted as medium feeding rate on this plot.



The quantity and rate of IPTG addition did not affect IB density, but feed rates and growth temperatures did have an effect. Feeding strategies that limited glucose levels during the fermentations resulted in less dense IBs. Meanwhile, the feed rates that supplied more levels of glucose in excess of the cells' needs produced denser IBs. Even more dramatic was the effect different growth temperatures had on IB density, as illustrated in Figure 3.5. IB density increased proportionately with growth temperature.

In terms of IB size, feeding profiles and growth temperatures, again, both had an influence, whereas IPTG concentration did not. Larger IBs were produced when IPTG was added directly to the fermentor instead of being gradually added with the

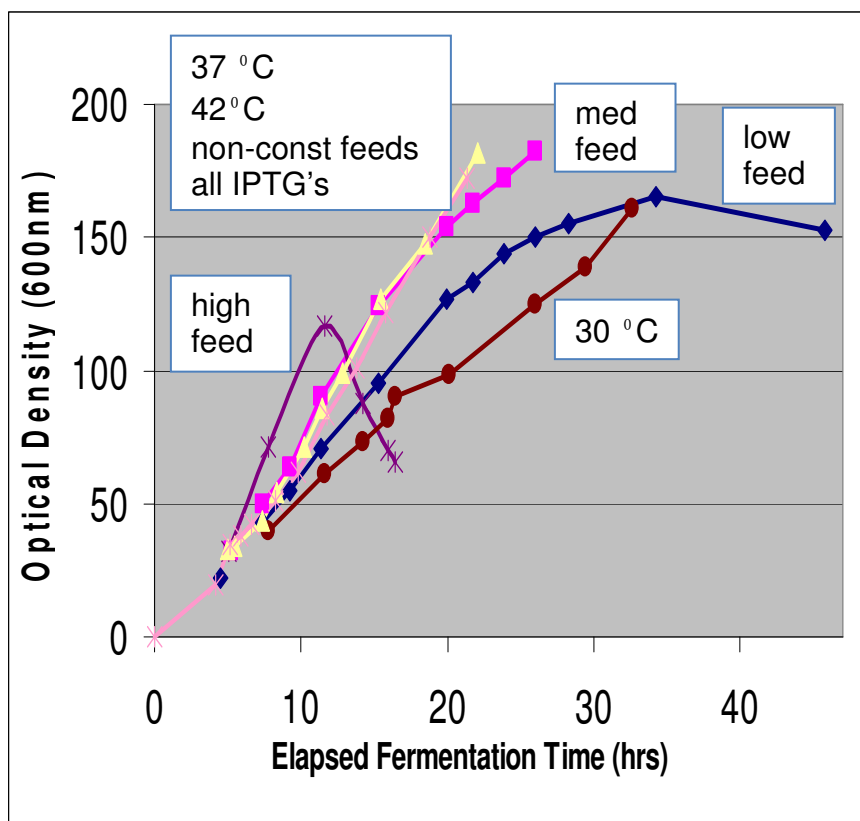


**Figure 3.7. Growth curves of Syn-Melan-A in complex medium.** Cell density is measured by optical density at 600 nm. Non-constant feed rates consist of pH-stat, linear, and step feeds. All IPTG runs and runs with different temperatures were conducted using the pH-stat feeding method.

feed medium. Aside from the direct addition of IPTG and the run at 30°C, all fermentations using a pH-stat feeding profile resulted in smaller inclusion bodies. As a higher excess of glucose was inputted into the fermentor, IB size increased.

An excess of IPTG is toxic to cells, and high levels of glucose in the fermentor lead to an accumulation of inhibitory levels of acetate. Although it could be suspected that conditions with the direct addition of IPTG or with the highest constant feed rate could be responsible for larger IB size due to toxicity, a decrease in cell growth was only found in the fermentation with the highest constant feed rate (Figure 3.7). The other factor that these two runs have in common is faster production rates. On the other hand, the largest IBs were produced at 30°C and when the lowest constant feed rate was used. As seen in Figure 3.7, both of these conditions retarded growth rates. Although it seems contradictory, this data suggests that larger IBs were created both when protein production speed was increased and decreased from the runs with standard growth temperature and feeding rate.

### ***3.2.5. Size distribution analysis***

The size distributions of the complex medium studies are shown in Figure 3.8. When IBs were produced using a pH-stat feeding method at 37 °C or 42 °C, the calculated diameters of IBs were Gaussian distributions. At 30 °C, the IBs formed two populations, which were smaller and larger than the IBs produced at 37 °C or 42 °C. A similar distribution occurred when IBs were produced using a step feed or low constant feed protocol. When the constant feed rate was increased, the smaller population was reduced, creating a shoulder. When the highest constant feed rate was used, this smaller population was no longer detected.

Size distributions had previously been examined using sedimentation fast-flow fractionation [120]. In these studies, Gaussian distributions of IB size were

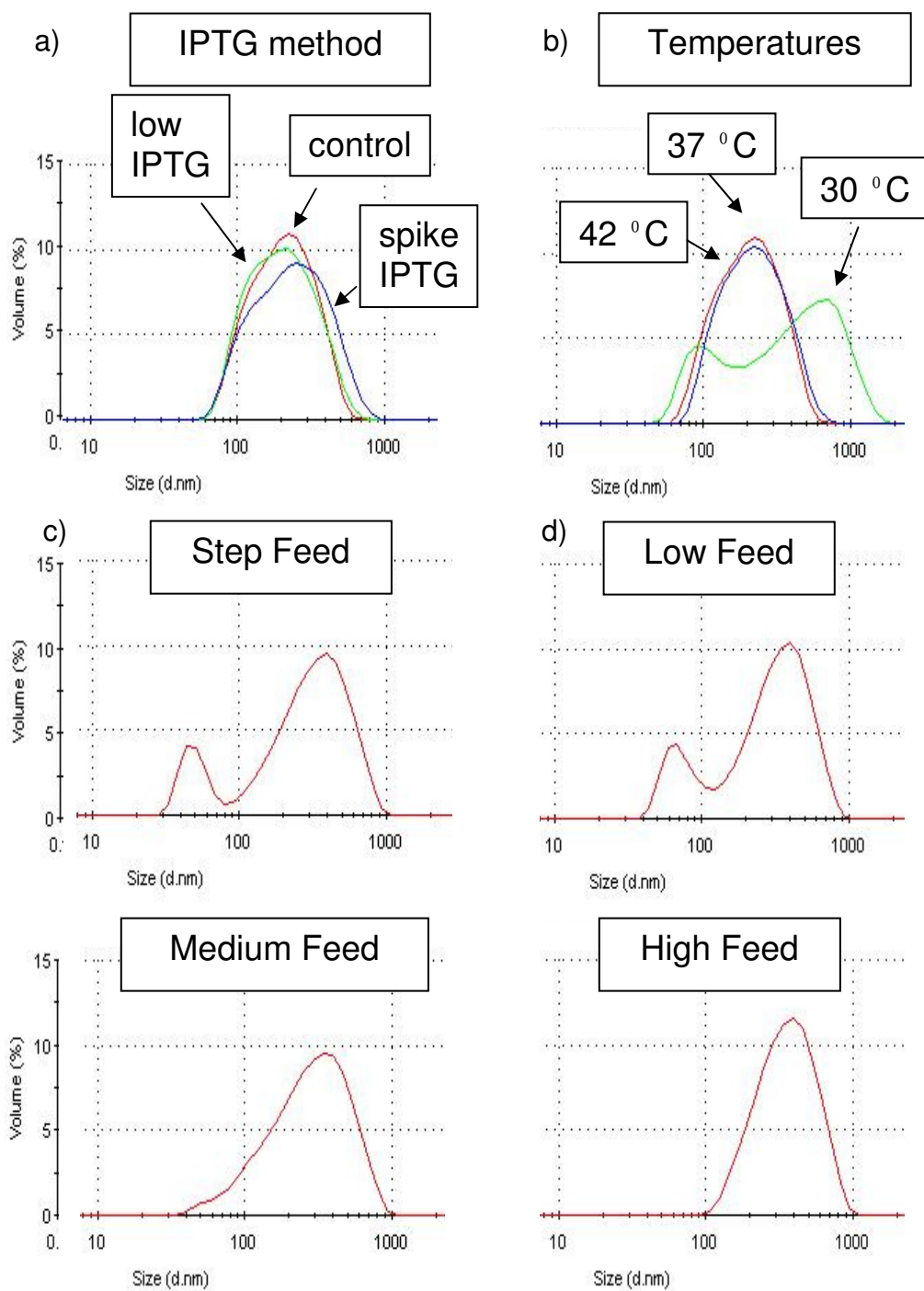


**Figure 3.8. Inclusion body size distribution as determined by dynamic light scattering.**

found at 37 °C cultures and two distinct populations were generated during 30 °C cultures. A shoulder of smaller sized particles was detected when IPTG concentrations were reduced twenty-fold.

### ***3.3. Inclusion body size and density trends from chemically defined medium studies***

#### ***3.3.1. DOE set-up***

A statistical experimental design was created to evaluate the effects of temperature and feeding rate on IB size and density. IPTG was not listed as a factor because it did not have influence on IB size and density in complex medium studies. Constant, pH-stat, step, and linear feeding strategies were also used in complex medium studies. Although these conditions were relevant, they were qualitative and could not be subjected to a quantitative statistical design. As such, only a series of linear feed rates were used. These feeding profiles are shown in Figure 3.9.

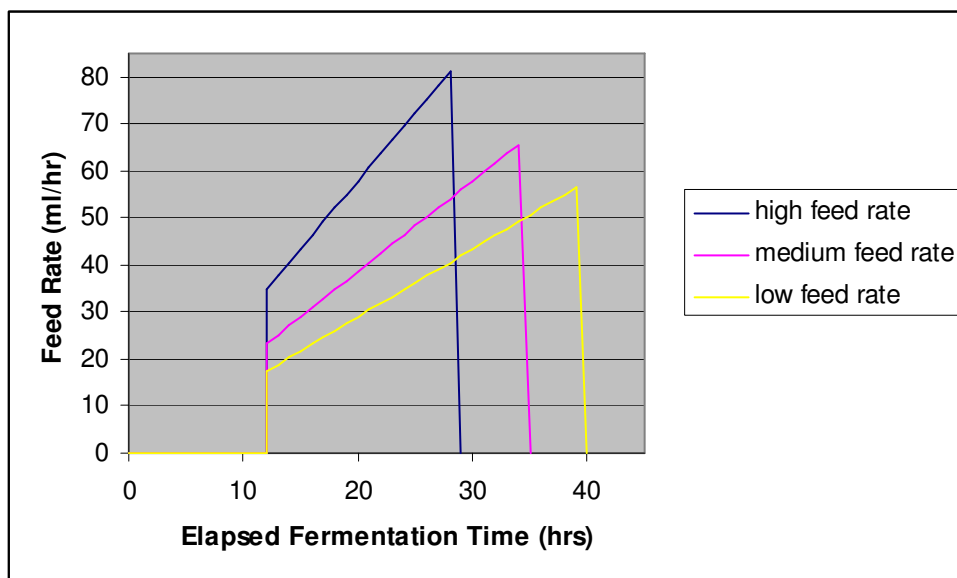


**Figure 3.9. Linear feeding profiles for fermentations conducted in chemically defined medium.** Three different linear feeding rates were used in the chemically defined medium fermentations. In all instances, 1 L of chemically defined feed medium was added to 1 L of chemically defined batch medium in the bioreactor.

### **3.3.2. Growth rates**

The optical densities of the chemically defined medium fermentations are plotted in Figure 3.10. The batch growth ended 12 hr after reactor inoculation. Regardless of fermentation condition, growth rates were identical up to 15 hr. At this point, the fermentations began to diverge into different growth rates. The fermentation with the high feed rate grew the fastest, followed by the fermentation grown at 30°C. This is somewhat expected since glucose was the limiting reagent in these fermentations, and an excess of glucose should therefore lead to faster growth rates. A similar phenomenon is observed with the 30°C fermentation since the cells at this temperature would have a slower metabolism and therefore would consume glucose at a slower rate than cells grown at warmer temperatures. The fermentations at 37°C under low and medium feed rates had identical growth profiles. The fermentation conducted at 42°C showed a decrease in cell growth rate beyond 19 hr. This decrease in growth rate could be explained by increased glucose consumption during the heat shock response.

### **3.3.3. General trends**

The results of the statistical design using chemically defined medium are shown in Figures 3.11 and 3.12. The feed rates shown in the axis are average feed rates per ml of final fermentation volume.

The density profile of Syn-Melan-A IBs in chemically defined medium (Figure 3.11) is very similar to that produced in complex medium (Figure 3.5). There is a weak dependence on feed rate, where higher feeding rate results in denser IBs. A much stronger dependence on growth temperature is also apparent, where lower temperatures result in less dense IBs and higher temperatures result in denser IBs.

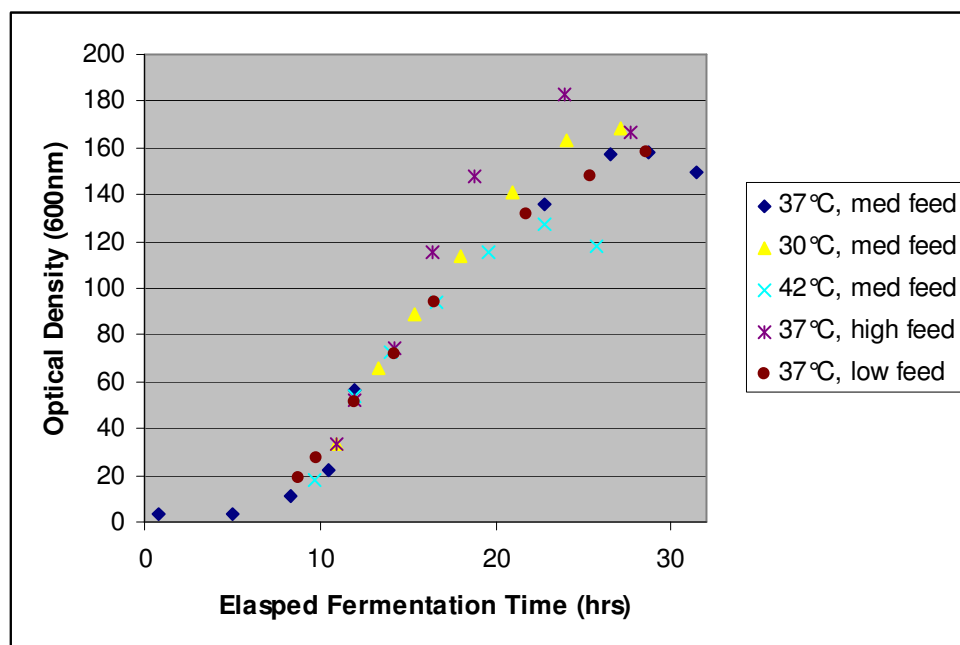


**Figure 3.10. Growth curves of Syn-Melan-A in chemically defined medium.** Feeding began at 12 hr elapsed fermentation time. All growth curves were identical until 15 hr. Growth rates were dependent on the excess glucose in the bioreactor.

The particle size influence has some commonalities with the analogous results from complex medium (Table 3.1). Again, IB size increases both when temperatures from 37°C are decreased to 30°C or increased to 42°C. The difference between the chemically defined medium results (Figure 3.11) and the complex medium results (Figure 3.6) is only that there is less dependence on feeding rate in the chemically defined medium results than in complex medium. This discrepancy may be explained by the fact that the range of feeding rates used in the chemically defined medium experiments were not as extreme those used with complex medium or that linear feeding rates were less harsh than constant feeding rates. The different extremities of feeding methods can be seen in the respective growth profiles (Figures 3.10 and 3.7). The high feed rate in the complex medium experiments was high enough to suspect toxic acetate accumulation, as would be indicated by the rapid drop in cell growth

approximately 5 hr after feeding was initiated. No such phenomenon was observed with the chemically defined medium. The low feed rate in complex medium was limiting enough to reduce growth rate, whereas no change in growth rate was detected in the low feed with chemically defined medium.

### ***3.4. Summary***

Syn-Melan-A IB size and density could be altered changing culture temperatures, feeding methods, and feeding rates. The concentration of IPTG and the rate of IPTG introduction were not crucial parameters. Similar results were obtained regardless if a complex medium or chemically defined medium was used.

The Syn-Melan-A IB density increased proportionately with culture temperature. Density also increased slightly with an increase in constant feeding rates. The smallest IBs were formed when a pH-stat feeding method was used. Larger IBs formed when feeding methods that did not have feedback-control were used. When the growth rate of the cells was slowed down by temperature, limited feed, or acetate toxicity, larger IBs were formed.

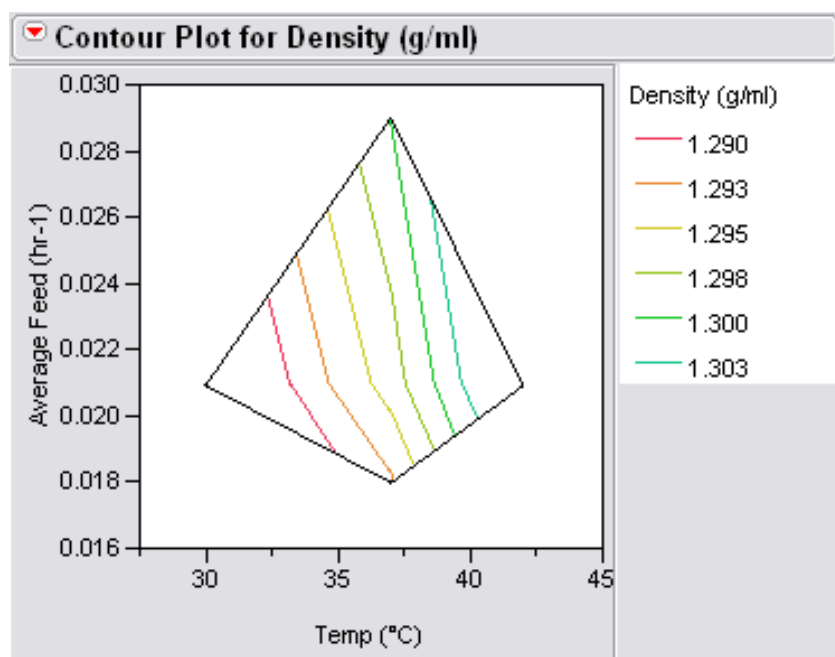


**Figure 3.11. Inclusion body density as a function of feed rate and growth temperature in chemically defined medium.** Vertical lines in the contour plot indicate that inclusion body density had a stronger dependence on temperature than feeding rate.

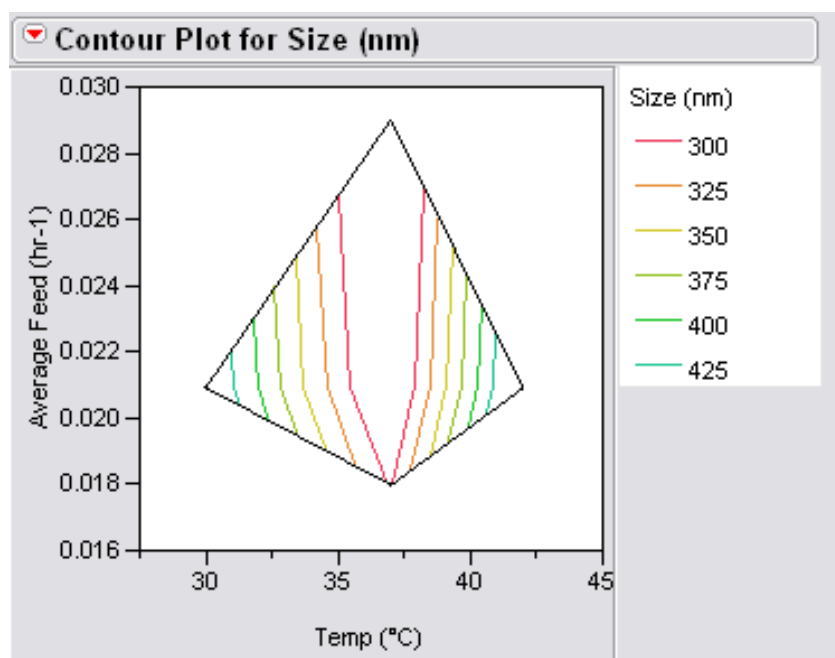


**Figure 3.12. Inclusion body size as a function of feed rate and growth temperature in chemically defined medium.** Vertical lines again indicate that the feeding rate was not important in determining the size of inclusion bodies produced in chemically defined medium. Inclusion bodies got larger when grown temperature was not 37°C.



## REFERENCES

- 118) C. Austin, J. Mizdrak, A. Matin, N. Sirijovski, P. Kosim-Satyaputra, R. Willows, T. Roberts, R. Truscott, G. Polekhina, M. Parker, J. Jaime, Optimised expression and purification of recombinant human indoleamine 2,3-dioxygenase, *Prot. Expr. Purif.* 37 [2004] 392-398.
- 119) V. Babaeipour, S. Shojaosadati, S. Robatjazi, R. Khalizadeh, N. Magsoudi, Overproduction of human interferon- $\gamma$  by HCDC of recombinant *Escherichia coli*, *Process Biochem.* 42 [2007] 112-117.
- 120) G. Margreiter, P. Messner, K. Caldwell, K. Bayer, Size characterization of inclusion bodies by sedimentation field-flow fractionation, *J. Biotechnol.* 138 [2008] 67-73.

## CHAPTER 4

### ADDITIONAL INCLUSION BODY INFORMATION

#### ***4.1. Syn-Melan-A inclusion body structure***

Chapter 3 detailed the influence of fermentation conditions on the density and size of Syn-Melan-A IBs. Although these are the most important factors involved in IB extraction, the shape and structure of IBs should also be considered. All of these factors will influence IB separation with both centrifugation and tangential flow filtration.

##### ***4.1.1. Syn-Melan-A inclusion body protein accessibility***

Dry protein weights (Section 2.11) of IBs were measured to determine the amount of protein present. Protein concentration estimates were also determined using a Bradford total protein assay. Whereas the dry protein weight measured all of the protein present, the Bradford assay could only measure the protein exposed that could react with the Coomassie dye used in the assay. These values could be compared to determine the percentage of protein accessible. Results are shown in Figure 4.1.

The graph shows that protein accessibility changes depending on fermentation conditions. General trends show that protein accessibility drops slightly as the fermentation temperature goes up and when feed rates go down

Accessibility was also observed using immunochemistry on TEM samples. IBs produced at 30°C and 42°C were subjected to TEM analysis as described in Section 2.8.4. Anti-mouse gold nanoparticles bound to a monoclonal Melan-A antibody. Almost none of this antibody was able to bind to the Syn-Melan-A IB

produced at 42°C. Meanwhile, the 30°C Syn-Melan-A IB was heavily labeled (Figure 4.2). This agrees with previous data that suggested inclusion bodies produced at 42 °C were more chemically stable than the 37 °C counterparts [121].

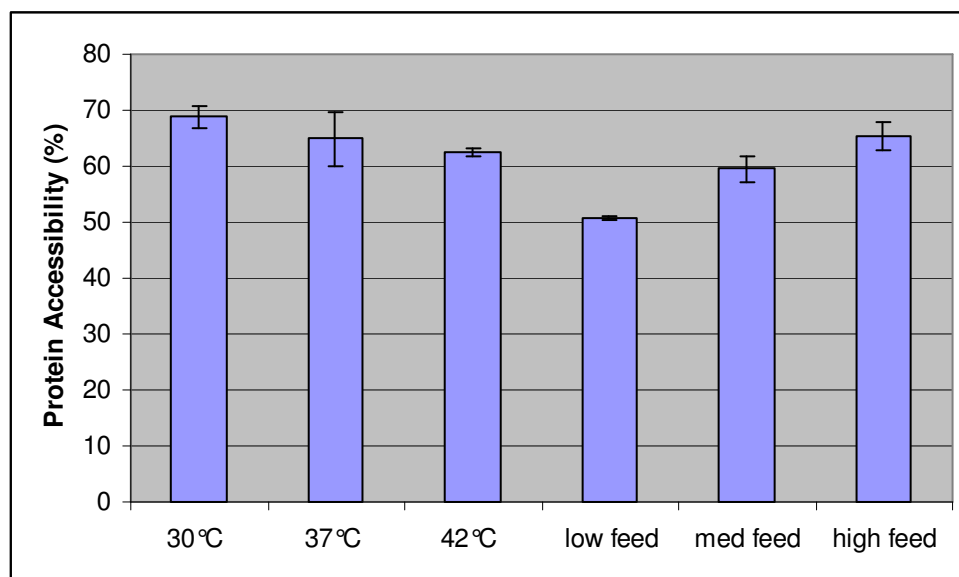


**Figure 4.1. Protein accessibility in Syn-Melan-A inclusion bodies by Bradford.** Accessibility was determined using a ratio of total protein determined by Bradford assay with the protein determined using dry weight. Each of these assays was run in triplicate.

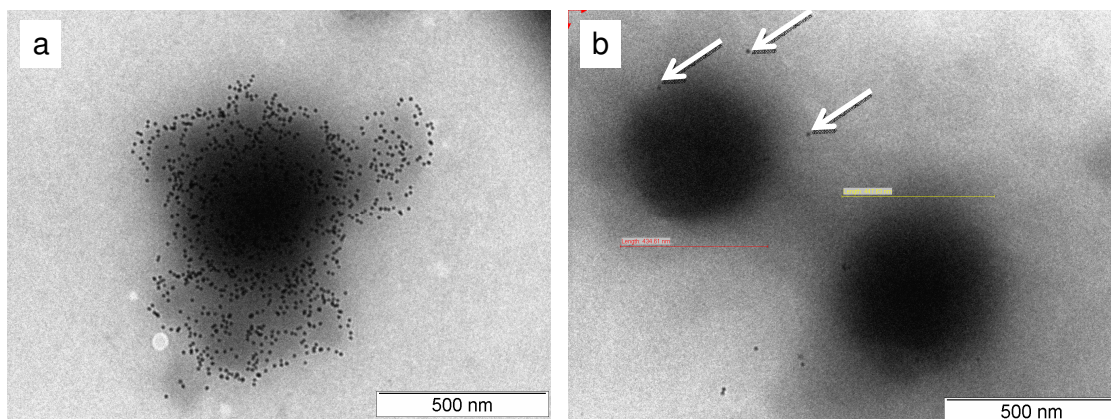


**Figure 4.2. Protein accessibility in Syn-Melan-A inclusion bodies by TEM.** Inclusion bodies were labeled with 10 nm gold nanoparticles. a) Syn-Melan-A inclusion body produced at 30°C. b) Syn-Melan-A inclusion bodies produced at 42°C.

#### ***4.1.2. Syn-Melan-A inclusion body morphology***

When Syn-Melan-A IBs were observed on an SEM, it was found that there was clearly a different morphology for the IBs produced at different temperatures (Figure 4.4). Syn-Melan-A IBs produced at 30°C were almost amorphous in shape, while the individual IBs particles produced at 37°C were much more discrete. The individual 37°C IBs appear to be a cluster of smaller particles (Figure 4.3). As an aside, there are typically only 1 or 2 IBs detected in a single bacterium, and this cluster composition makes sense since there would be initially multiple nucleation sites for aggregation. The 42°C IBs were very discrete and spherical.

These images agree with the results that suggest Syn-Melan-A IBs produced at lower temperatures are less dense and that Syn-Melan-A IBs produced at higher temperature are more dense. These data also agree with the protein accessibility data, which suggests that protein in denser IBs was less accessible.

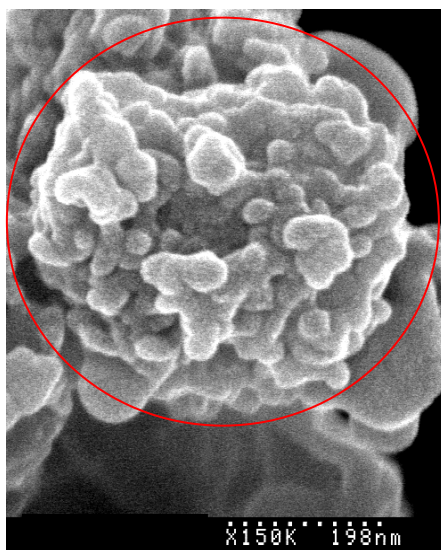


**Figure 4.3. SEM image of a Syn-Melan-A inclusion body at high magnification.** Inclusion bodies were produced at 37°C using a pH-stat feeding method in complex medium. The magnification was 150,000x. Scale bar is the white dotted line. A single inclusion body is circled in red.

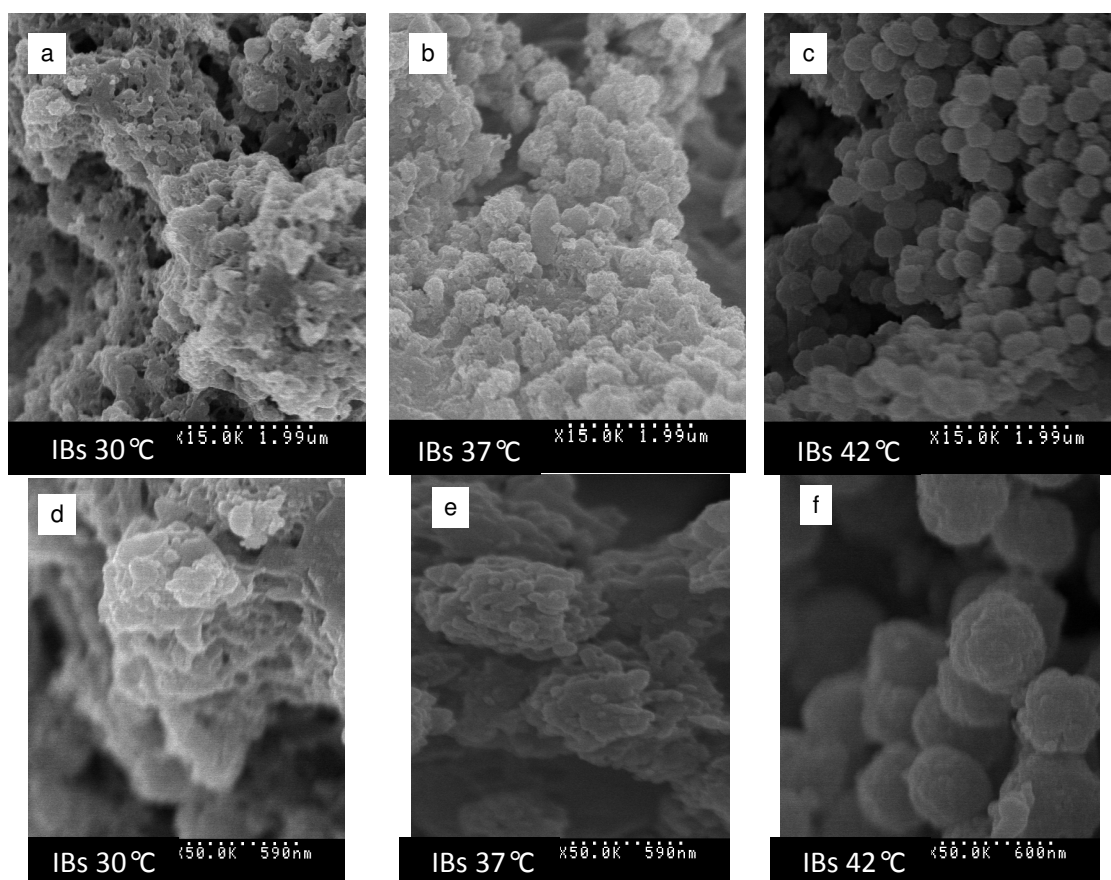


**Figure 4.4. SEM images of Syn-Melan-A inclusion bodies.** Scale bar is the white dotted line. a) Syn-Melan-A inclusion bodies produced at 30°C viewed at 15,000x magnification, b) 37°C, 15,000x, c) 42°C, 15,000x, d) 30°C, 50,000x, e) 37°C, 50,000x, f) 42°C, 50,000x

#### **4.2. Different proteins**

As detailed in Section 1.5.2, many of the most recent IB studies have used GFP as a model protein. GFP is convenient because it is a well-studied protein in biotechnology and its activity can be quantified using fluorescence. It has not been shown, however, how IB formation mechanisms compare amongst different proteins. For example, the many phenomena detailed in Chapter 3 and Section 4.1 for Syn-Melan-A may not be applicable to GFP. Section 4.2 analyzes IBs produced at different temperatures for several different proteins.

#### ***4.2.1. Fermentation temperature effects on inclusion body density and size of various proteins***

The IB density determination by cesium chloride ultracentrifugation, as described in Section 2.7, was highly reproducible. When comparing IBs of Syn-Melan-A, it was found that cultures grown at different temperatures showed the largest disparity in IB density. In particular, low temperatures resulted in less dense IBs, and high temperatures resulted in more dense IBs. Additional proteins were tested to determine if this trend was universal.

EGFP and SSX2 were each produced at 30°C and 42°C. Although the density difference in Syn-Melan-A IBs produced at these two temperatures was 50 mg/ml, it was only 2 mg/ml for both of these two hydrophilic proteins. NY-ESO-1, a hydrophobic protein, was also subjected to this same analysis, but temperature also showed minimal effect on NY-ESO-1 IB density with a difference of 5 mg/ml for IBs produced at 30°C and 42°C. The non-synthetic version of Melan-A was also investigated, and IBs produced at 30°C and 42°C also had a 5 mg/ml density difference. It should be noted that in all cases, IBs produced at 42°C were denser than those produced at 30°C, but these density differences were trivial compared to that of Syn-Melan-A IBs. These results are illustrated in Figure 4.5.

#### ***4.2.2. Fermentation temperature and inclusion body morphology***

The visual morphology phenomenon observed with Syn-Melan-A (Figure 4.4) was not observed in the IBs of other proteins analyzed in this study (Figure 4.7). For the most part, IBs produced from other proteins were all identical in morphology. These IBs were not as spherical as the Melan-A IBs produced at 42°C, but they were similar. All of these IBs had similar densities (Figure 4.5).

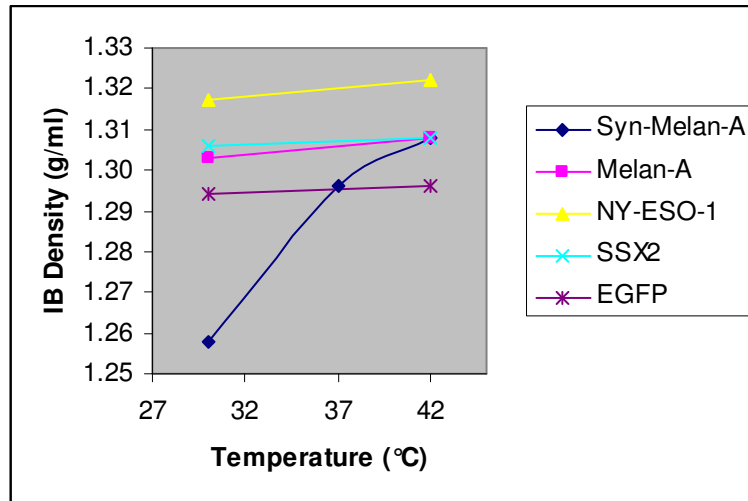


**Figure 4.5. Densities of inclusion bodies from multiple proteins produced at different temperatures.** Fermentations were conducted in complex medium using a pH-stat feeding method. Densities were determined using cesium chloride ultracentrifugation gradients. Syn-Melan-A inclusion bodies have a much more noticeable dependence on temperature than other proteins in this study.

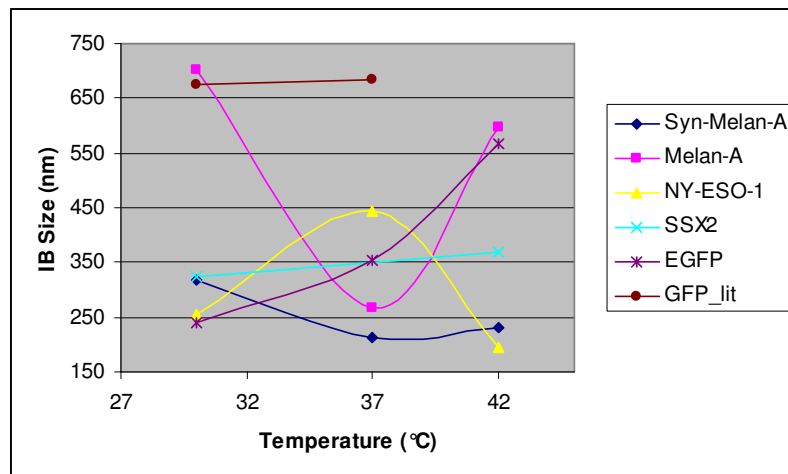


**Figure 4.6. Size of inclusion bodies from multiple proteins produced at different temperatures.** Fermentations were conducted in complex medium using a pH-stat feeding method except for the GFP data, which was taken from literature [122].

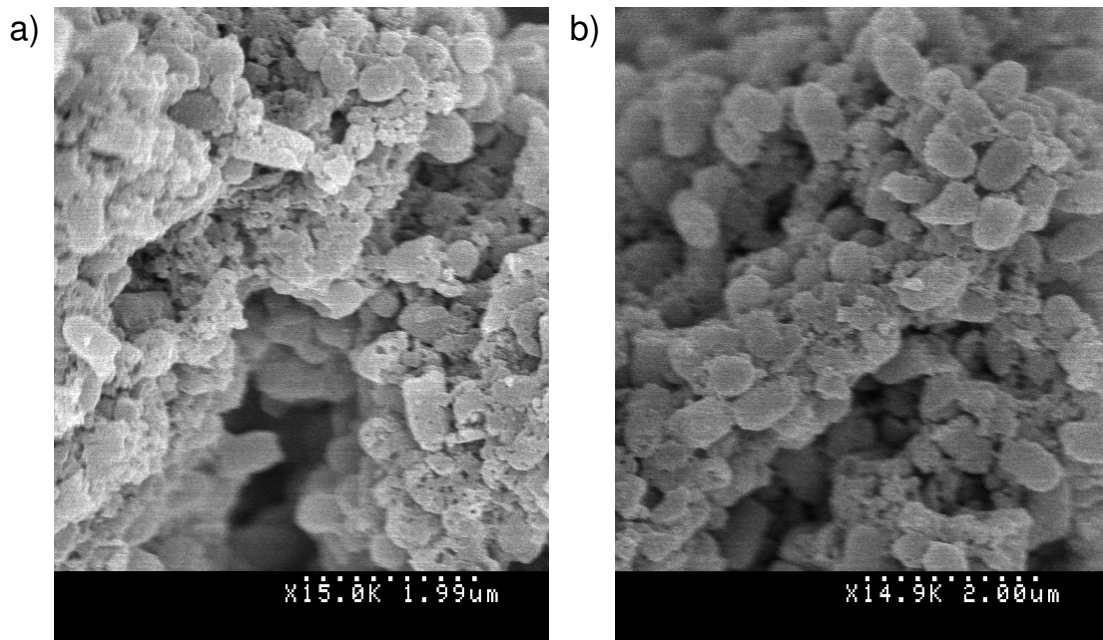


**Figure 4.7. SEM images of SSX-2 inclusion bodies.** Scale bar is the white dotted line. a) SSX2 inclusion bodies produced at 30°C viewed at 15,000x magnification, b) 42°C, 15,000x. These inclusion bodies have very similar morphologies, that are most similar to Syn-Melan-A inclusion bodies produced at 42°C.

#### 4.2.3. Production rates

In terms of the density and morphology of IBs, only Syn-Melan-A seemed to have a dependence on fermentation temperature. This temperature dependence was not a result of general hydrophobicity because NY-ESO-1 IBs did not have this temperature dependence. The Syn-Melan-A results were not a result of a unique protein sequence because the non-synthetic version of the protein also did not exhibit any temperature dependence. The primary difference between Syn-Melan-A and Melan-A was that the Syn-Melan-A plasmid had been altered so that more common *E. coli* DNA codons would be used to produce the exact same amino acid sequence. Also different is that fact that the Syn-Melan-A *E. coli* did not include a pRARE plasmid. The presense of the pRARE plasmid alone did not account for the IB



temperature dependence since it was present in SSX2, NY-ESO-1, and Melan-A, but not EGFP or Syn-Melan-A.

The different DNA sequence of Syn-Melan-A and Melan-A with pRARE plasmid did have an influence on protein production rates. This is an important factor, as IBs tend to form when protein production exceeds the capacity of the protein folding machinery in the cell.

Figure 4.8 shows data from Melan-A and Syn-Melan-A fermentations. Even though the growth rates and feed consumed for both runs overlap, the relative protein productions, as determined by gel densitometry, are quite different. The Melan-A fermentation produced about 30% more protein than the Syn-Melan-A fermentation. Although the synthetic version of the gene is designed for faster translation, the non-synthetic version of the gene was complemented with a pRARE plasmid, which made this increased production possible.

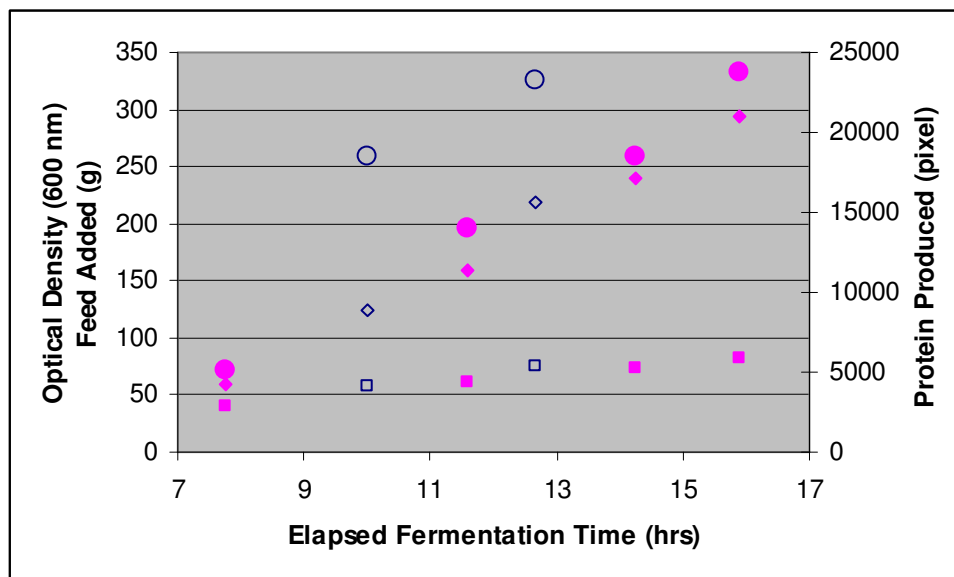


**Figure 4.8. Protein production of Melan-A and Syn-Melan-A.** Data from two fermentations are provided. Fermentations were conducted at 30°C using pH-stat feeding with complex medium. Open symbols are for Melan-A, and closed symbols are for Syn-Melan-A. Optical density (□, ■), feed consumed (◇, ◆), and protein produced (○, ●) are shown.

There are studies that examine the IB-characteristics of single point mutations. For human interleukin-1 $\beta$ , single point mutations could noticeably alter the amount of IB formation [123]. It has also been shown single point mutations in the fusion of Alzheimer-rated peptide A $\beta$ 42 to GFP can alter the protein activity found in IBs [124]. These studies, however, focus on the effects of slightly altering a protein sequence. Melan-A and Syn-Melan-A are the first proteins where observing IB characteristics in the same proteins with different production rates via codon biases has been performed. It is also possible that the increase in production rate is a function of plasmid copy numbers in the cell, which were not determined in this study.

## REFERENCES

- 121) N. Sánchez de Groot, S. Ventura, Effect of temperature on protein quality in bacterial inclusion bodies, *FEBS Lett.* 580 [2006] 6471-6476.
- 122) J. Luo, M. Leeman, A. Ballagi, A. Elfving, Z. Su, J. Janson, K. Wahlund, Size characterization of green fluorescent protein inclusion bodies in *E. coli* using asymmetrical flow field-flow fractionation--- multi-angle light scattering, *J. Chromat. A* 1120 [2006] 158-164.
- 123) B. Chrnyk, J. Evans, J. Lillquist, P. Young, R. Wetzel, Inclusion body formation and protein stability in sequence variants of Interleukin-1 $\beta$ , *J. Biol. Chem.* 268 [1993] 18053-18061.
- 124) N. Sánchez de Groot, S. Ventura, Protein activity in bacterial inclusion bodies correlates with predicted aggregation rates, *J. Biotechnol.* 125 [2006] 110-113.

## CHAPTER 5

### CONCLUSIONS AND RECOMMENDATIONS

#### ***5.1. Conclusions***

Industrial protein manufacturing process development is made up of expression, fermentation, purification, analytical, and formulation groups. Whereas the goals of a purification group are clearly to produce >99% pure protein without contamination of endotoxin or viral particles, the goal of the fermentation group is less clear. Beyond exceeding a reasonable protein titer in the fermentation broth, skilled fermentation scientists should be able to manipulate the characteristics of the intracellular protein to aid in the downstream development. An understanding of how fermentation conditions influence IBs is a step towards this goal.

In summary, this study has shown that IB characteristics are subject to fermentation conditions. Syn-Melan-A IBs became denser when their respective production fermentations were operated at elevated temperatures or overfed glucose. Feeding methods that minimized glucose to starvation levels, such as the popular pH-stat feeding method, did not have any effect on growth rate or protein production, but they decreased IB density. IPTG concentrations, on the other hand, did not have an influence on the density of IBs produced.

IB sizes increased whenever the culture temperature or feed rate deviated from an ideal pH-stat configuration operating at 37 °C. Larger IBs had been obtained for cultures lowered to 30 °C in previous studies [125]. IB size has also been found to increase for cultures when growth temperatures were increased to 42 °C [126]. These separate studies initially appeared conflicting, but this study shows that the same results are obtained given otherwise identical culture conditions. Likewise, the same

concept applied to feeding rates. With constant feeding rates, IB size increased when feed rates were both increased and decreased. In both cases, growth became inhibited, implying that IB size was smallest when an ideal pH-stat configuration operating at 37 °C is used. The pH-stat feeding method, which constantly starves the cells of glucose, actually created smaller sized IBs than all of the constant feeding rates tested. The fact that a severe glucose limitation created smaller inclusion bodies agrees with studies of TRAIL protein [127].

Therefore to improve extraction of Syn-Melan-A IBs from cell lysate with centrifugation or tangential flow filtration, an excess of glucose in the reactor culture is recommended. In terms of temperature, 42 °C cultures resulted in a decrease of protein production, possibly through increased degradation, and 30 °C cultures created the largest IBs. Therefore, these low temperatures are also recommended for enhanced IB extraction. It should be noted, however, that 30 °C cultures seem to produce two populations of IB sizes. These results were independently obtained from this study's dynamic light scattering as well as previous studies [128].

It was also important to find that this dependence on fermentation conditions was not applicable to all recombinant proteins. This is in agreement with a study that showed the choice of the target protein would alter IB formation [129]. In fact, Syn-Melan-A had a crucial low protein production rate that made fermentation conditions relevant. For proteins produced fast enough, no extraction improvement is made by changing temperature. Temperature influence on IBs is so great, that it is likely feeding rates would also have no influence.

It was expected that IPTG concentration would make a large difference because the IB formation is ultimately determined by production rate. Previous studies have suggested that decreasing IPTG creates both smaller IBs [125] and larger IBs [128]. A possible explanation for this is the protein dependence because each

protein is innately produced at a different rate. In this study, Melan-A with a pRARE plasmid seemed to be produced so quickly that not even producing the protein at 30 °C influenced the IB characteristics. Syn-Melan-A was produced slowly enough that decreasing IPTG further did not influence the characteristics of its IBs at 37 °C. IPTG may actually have an effect on proteins that are produced faster than Syn-Melan-A.

Slowing down production seems to create less compact aggregates that are composed of more active protein. Soluble protein yields also improve for certain proteins under slow production rates. Therefore if the goal of a process is to create more active protein, low temperatures and limiting feed rates should be employed.

## **5.2. Recommendations**

An attempt was made in this study to mimic industrial *E. coli* fermentation conditions as closely as possible. As such, the choice of *E. coli* strain used, as well as the custom-created plasmid vector could have been improved. C41 is a direct derivative of BL21 and therefore still contains RecA. A BLR strain is much more commonly used in industry. Also, an unmodified commercial vector is also recommended. Also, even though EGFP and GFP are very similar, an unmodified GFP protein should have been used for better direct comparison with literature data. These slight deviations were all done in this study as a matter of convenience.

The dynamic light scattering assay can also be improved. Data from the zetasizer regularly gave numbers that were beyond the estimated range of IB size based on microscopy. Either through altered sample preparations or run conditions, it should be possible to find conditions yielding consistent results between these two methods.

### **5.3. Future work**

Aside from the recommendations listed above, this study has established many steps that make it worthwhile to continue this research. Most IB studies do not use IBs produced under industrial conditions, particularly using HCDC. This is an important factor because industrial protein production is when IB quality is the most significant. Also, this study has created, to the author's knowledge, the best protocol for determining IB density as well as the most detailed IB SEM images ever taken. The following areas can be explored using the established fermentation platform and assays.

#### **5.3.1. Additional process parameters**

This study focused on feeding rates and temperatures. The study of IPTG was not complete because reduced levels of IPTG needed to be tested on proteins other than Syn-Melan-A which already had a reduced production rate.

In addition, other parameters that are normally controlled in an industrial fermentation are pH and dissolved oxygen. Previous literature has described pH conditions lower than 5.5 [130]. This is very different than 7.0, but large extracellular pH changes are necessary since *E. coli* regulate their internal acidity tightly. Some industrial processes are also producing proteins at minimal oxygen levels. That is not to say that the fermentations are anaerobic or oxygen-limited, but oxygen levels are still undetectable. A glucose spike can be used to determine adequate oxygen levels in these cases [131].

Ultimately there are also many less conventional methods to alter cell metabolism. Acetic acid, ethanol, heavy metals, antibiotics, hydrogen peroxide, and DTT can all be added in various levels, and their effects on IBs could be studied.

### **5.3.2. Chaperone studies**

One of the major rules in IB formation is that IBs will form when protein production exceeds the cell's folding capacity. Folding is performed largely by DnaK and GroEL. If these chaperones are coexpressed, proteins produced at relatively fast rates may become susceptible to changes in fermentation temperature and feeding rate. Commercial plasmids are available from Takara Bio (Madison, WI): pKJE7 for dnaK-dnaJ-grpE and pGro7 for groES-groEL. These plasmids carry an ampicillin resistance and are induced with arabinose. They can be introduced into Syn-Melan-A *E. coli* with a heat shock transformation as described in Section 2.3.4. Antibodies for these chaperones for western blot quantification are also commercially available.

### **5.3.3. Inclusion body formation**

For the sheer excessive number of samples to process, the only IB samples studied in detail were at the end of fermentation. Instead of exploring many different fermentation conditions, it may be worthwhile to examine the IBs formed throughout the course of a fermentation. A particular useful tool would be immunochemistry performed on cell sections in TEM. This would allow us to visualize how IBs are formed.

There may also be a protein-dependence on IB formation. For example, Syn-Melan-A begins forming IBs before any soluble protein is produced. This is different than fusion growth hormone. That protein was initially produced in the soluble form and then formed IBs as the expression level increased.

### **5.3.4. Protease monitoring**

In order to determine the amount of actual protein production the folding machinery of a cell can handle, it is necessary to be able to monitor protease activity.



Net protein production is the difference of protein produced and the protein that is degraded. SDS-PAGE analysis only provides data about net protein production, so the reason for reduced protein present at 42°C is not certain. It was assumed that this lower protein was the result of increased protease activity at this higher temperature, but it is possible that protein production itself was somehow reduced.

Although the strains of *E. coli* used in this study lack the Lon and OmpT proteases, there are still 22 other known *E. coli* proteases. In addition to Lon, there are at least eleven more proteases located in the cytoplasm, the rest being periplasmic or membrane proteases [132]. In particular it has been shown that ClpP, a subunit of the Clp protease, can influence inclusion body degradation [133]. In addition to Clp protease subunits, it is possible that FtsH, although associated with the inner membrane, also plays a significant role in cytoplasmic protein degradation [134].

There are a couple of established methods for measuring protease activity. There is a fluorescent protease assay kit (Pierce), which is based on casein digestion. Specifically, casein is labeled with fluorescein isothiocyanate, and the fluorescence properties of this substrate will change as it is digested by proteases. There are also zymogram gels (Invitrogen) that are based on the proteases ability to digest a casein or gelatin substrate. These show up as clear bands on a stained gel and have the advantage of estimating the molecular weights of the active proteases [135]. Artifacts commonly caused by the gelatin can be avoided using an electroblotting procedure [136].

A good preliminary experiment to perform may be to measure the rate of protease activity in *E. coli* C41(DE3) on Melan-A. Although fast rates have been reported in other strains, the lack of Lon may make the remaining protease activity negligible. After taking a zero timepoint sample during an active fermentation, protein production can be arrested *in vivo* using chloramphenicol [137]. In our case,

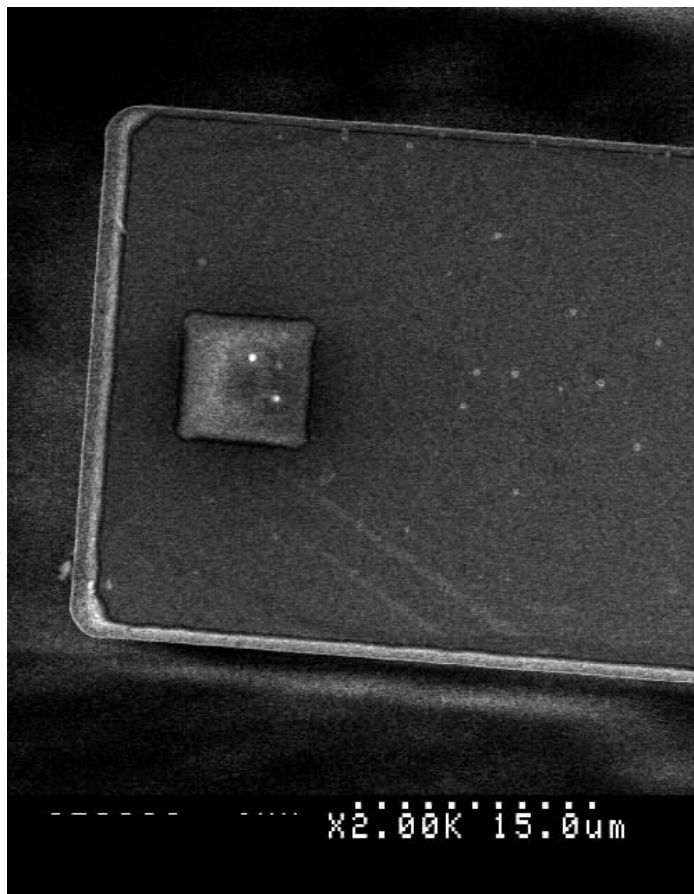


**Figure 5.1. SEM image of AFM probe with inclusion bodies.** An AFM probe was submerged in an inclusion body solution and washed. A resulting finite number of inclusion bodies were present on the probe.

we would have to operate without the pRARE plasmid or use another antibiotic, such as any in the macrolide class. It should be possible to determine degradation rates by performing assays to detect Melan-A levels in samples at timepoints after protein arrest has been initiated.

#### **5.3.5. Inclusion body force measurements**

An assay to measure inclusion body stiffness using atomic force microscopy was developed. The plan was to use a custom probe that had a blunt platform, as shown in Figure 5.1. This platform would be pressed against a mica surface and the

force would be measured. The force would then be divided by the number of IBs on the platform, as can be determined with SEM.

## REFERENCES

- 1) J. Luo, M. Leeman, A. Ballagi, A. Elfving, Z. Su, J. Janson, K. Wahlund, Size characterization of green fluorescent protein inclusion bodies in *E. coli* using asymmetrical flow field-flow fractionation--- multi-angle light scattering, *J. Chromat. A* 1120 [2006] 158-164.
- 2) N. Sánchez de Groot, S. Ventura, Effect of temperature on protein quality in bacterial inclusion bodies, *FEBS Lett.* 580 [2006] 6471-6476.
- 3) H. Kang, A. Sun, Y. Shen, D. Wei, Refolding and structural characteristics of TRAIL/Apo2L inclusion bodies from different specific growth rates of recombinant *Escherichia coli*, *Biotechnol. Prog.* 23 [2007] 286-292.
- 4) G. Margreiter, P. Messner, K. Caldwell, K. Bayer, Size characterization of inclusion bodies by sedimentation field-flow fractionation, *J. Biotechnol.* 138 [2008] 67-73.
- 5) S. Peternel, J. Grdadolnik, V. Gaberc-Porekar, R. Komel, Engineering inclusion bodies for non denaturing extraction of functional proteins, *Microb. Cell Fact.* 7 [2008] 1-9.
- 6) L. Strandberg, S. Enfors, Factors influencing inclusion body formation in the production of fused protein in *Escherichia coli*, *Appl. Environ. Microbiol.* 57 [1991] 1669-1674.
- 7) J. Zawada, J. Swartz, Maintaining rapid growth in moderate-density *Escherichia coli* fermentations, *Biotechnol. Bioeng.* 89 [2005] 407-415.
- 8) S. Harcum, W. Bentley, Response dynamics of 26-, 34-, 39-, 54-, and 80-kDa proteases in induced cultures of recombinant *Escherichia coli*, *Biotechnol. Bioeng.* 42 [1993] 675-685.

- 9) A. Vera, A. Arís, M. Carrió, N. González-Montalbán, A. Villaverde, Lon and ClpP proteases participate in the physiological disintegration of bacterial inclusion bodies, *J. Biotechnol.* 119 [2005] 163-171.
- 10) F. Baneyx, M. Mujacic, Recombinant protein folding and misfolding in *Escherichia coli*, *Nat. Biotechnol.* 22 [2004] 1399-1408.
- 11) D. Michaud, Gel electrophoresis of proteolytic enzymes, *Anal. Chim. Acta* 372 [1998] 173-185.
- 12) S. Visal-Shah, T. Vrain, S. Yelle, B. Nguyen-Quoc, D. Michaud, An electroblotting, two-step procedure for the detection of proteinases and the study of proteinase/inhibitor complexes in gelatin-containing polyacrylamide gels, *Electrophoresis* 22 [2001] 2646-2652.
- 13) A. Rozkov, T. Schweder, A. Veide, S. Enfors, Dynamics of proteolysis and its influence on the accumulation of intracellular recombinant proteins, *Enzyme Microb. Technol.* 27 [2000] 743-748.

## APPENDIX 1

### ADDITIONAL ASSAY METHODOLOGY AND DEVELOPMENT

#### ***A1.1. High performance liquid chromatography***

A reverse phase high performance liquid chromatography (RP-HPLC) method was created. The goal of this method was to characterize and quantify protein samples. A Waters (Milford, MA) 1525 Binary HPLC Pump was used to load samples and run a gradient of mobile phase A [0.1% trifluoroacetic acid (TFA) in HPLC-grade water] and mobile phase B [0.09% TFA in acetonitrile] through a Poros® R2 10 mm 4.6mmD/50mmL stainless steel column (Applied Biosystems, Foster City, CA). The column was storage in a 50:50 solution of HPLC-grade water and acetonitrile. HPLC-grade water was created by filtering deionized water through a 0.22 µm vacuum filter (Nalgene Labware, Rochester, NY) to remove gases and particulates. Samples and buffers were sent through a Waters In-Line Degasser AF and guard column prior to entering the column. Protein was detected coming off the column in a Waters 2996 Photodiode Array Detector. Waters Empower Pro software was used to run the system.

A spectrophotometer, described in 2.5.2, was used to determine the optimal wavelength for detecting protein on the HPLC. A purified sample of Melan-A was used. The wavelength that provided the greatest absorbance value was 277 nm (Figure A1.1).

The column flowrate and pressure limit was 2.0 ml/min and 2500 psi. After the column was equilibrated with mobile phase A, 200 µl of protein sample was loaded on the column and chased with a gradient from 0% to 100% mobile phase B over 10 min. Peak areas could be quantified using the Empower Pro software (Figure

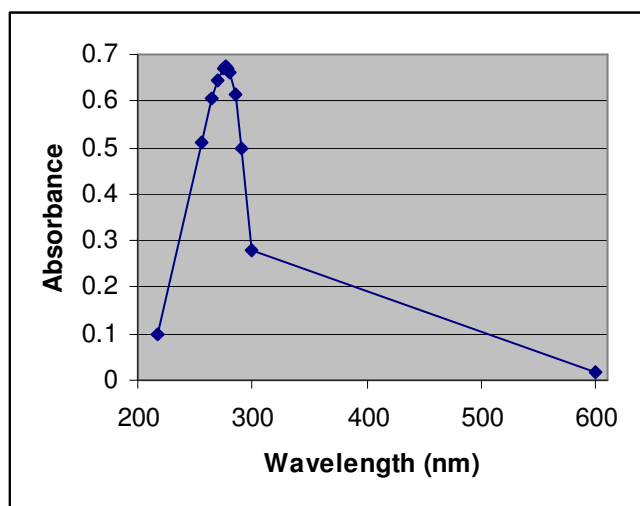


**Figure A1.1. Absorbance of Melan-A protein at multiple wavelengths.** The absorbance of a post-HIC Melan-A sample was measured at multiple wavelengths in a spectrophotometer. The optimal wavelength was 277 nm.

A1.2). Bovine serum albumin (BSA) was used to calibrate the peak area. Solutions of 0.05, 0.10, 0.40, and 0.70 mg/ml BSA were run through the HPLC. The load concentration and quantified peak area had a very linear relationship (Figure A1.3). Melan-A samples did not show a good resolution when run through the HPLC column. In attempts to improve this, various changes to the experimental set-

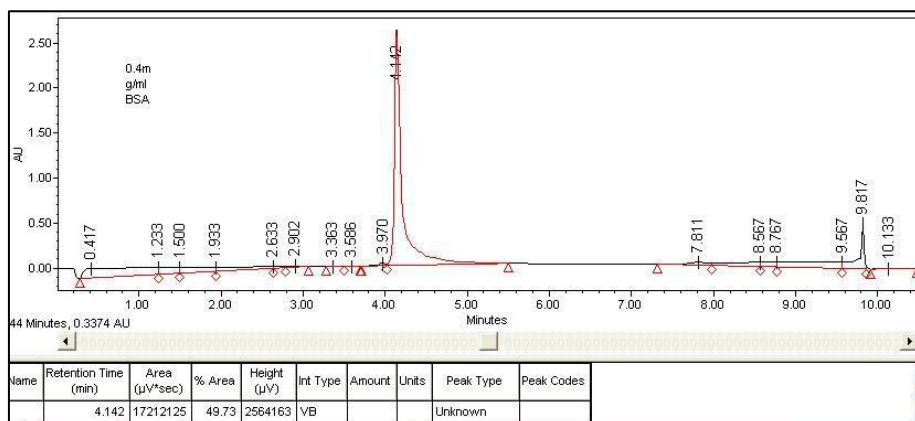


**Figure A1.2. Chromatogram of bovine serum albumin on RP-HPLC.** BSA was loaded onto a reverse phase HPLC column and eluted with an increasing gradient of acetonitrile. Peak area was quantified using Empower Pro software.

up were made. In one case, the TFA in the mobile phases was substituted with heptafluorobutyric acid (HFBA). In another case, 1% sodium dodecyl sulfate (SDS) was added to mobile phase A; SDS did not dissolve in mobile phase B. A Poros® R1 column was also used because it had different hydrophobic binding qualities as the R2 column. In all cases, HPLC chromatograms of Melan-A were single broad peaks despite having many protein impurities (Figure A1.4).

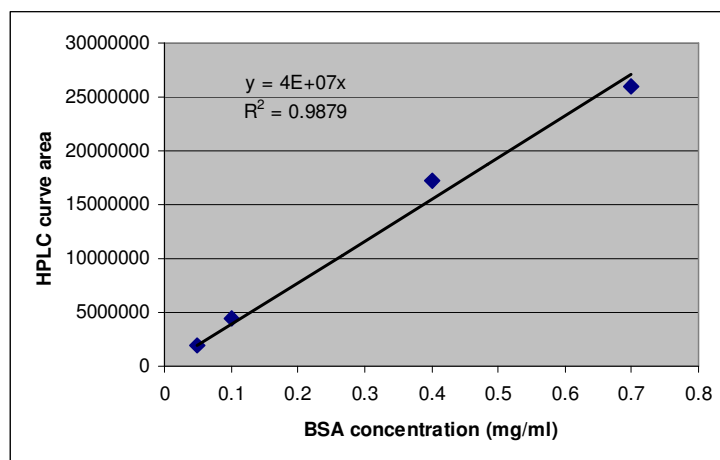


**Figure A1.3. Correlation of BSA concentration and peak area on the HPLC.** Known protein concentrations of BSA samples were plotted against the resulting peak area. Results were very linear.

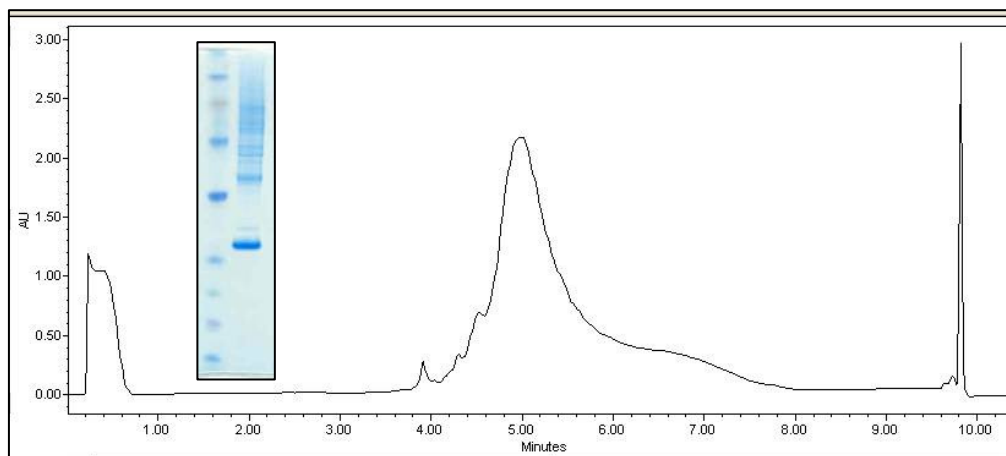


**Figure A1.4. Chromatogram of Melan-A sample on RP-HPLC.** SDS-PAGE of Melan-A load (inset) show multiple impurities in the sample. The impurities are indistinguishable from Melan-A on the HPLC chromatogram.



### ***A1.2. Limulus ameobocyte lysate Assay***

Bacterial endotoxin has been found to react with the limulus ameobocyte lysate (LAL) obtained from horseshoe crabs. An Endosafe Endochrome-K kit (Charles River, Wilmington, MA) was used to measure the level of LAL-reactive material in purified protein samples. All samples were run in triplicate on a 96-well plate. The standard curve was produced with 10 ng of *E. coli* O55:B5 control standard endotoxin (Charles River). The endotoxin was reconstituted in LAL-free water to a concentration of 50 EU/ml and diluted to 0.05, 0.5, and 5 EU/ml standards.

Depending on expected endotoxin concentration, samples were diluted  $5 \times 10^3$ ,  $2 \times 10^4$ ,  $5 \times 10^5$ , or  $2 \times 10^6$  fold. Dilutions were performed in two steps in pyrogen-free tubes (Charles River). A volume of 2 ml was appropriate for adequate vortexing of the samples. The first step was a dilution performed in 4 M urea. The second step was a 100-fold dilution into LAL-free water. This resulted in a sample with a final concentration of 40 mM urea. Removing all of the urea caused the protein to precipitate and created false-negative results.

The diluted samples were pipetted into a 96-well plate in triplicate in 100  $\mu$ l aliquots. Each vial of LAL (Charles River) was reconstituted in 3.5 ml of water and 100  $\mu$ l was added to each sample. The plate was read using a kinetic measurement over the course of five hr. The assay provided volumetric endotoxin concentrations of the diluted samples. These values were corrected for dilutions made and protein concentration.

## APPENDIX 2

### FERMENTATION SETUP

#### *A2.1. Feed volume calculations*

All fermentations were conducted in BioFlo units (NBSC, New Brunswick, NJ) controlled using Biocommand Plus software (NBSC). The BioFlo unit had internal PID controllers to maintain a set agitation, temperature, and dissolved oxygen level. When feed medium or base was added, arbitrary pump units were used. The actual flow rates these pump rates generate depended on the type of tubing used. Tygon® 3350 silicone tubing (Saint-Goblain, Valley Forge, PA) was used for sodium hydroxide and both complex and chemically defined feed media addition. The tubing dimensions were 3/32 x 7/32 for sodium hydroxide and 1/8 x 1/4 for feed medium. Ammonium hydroxide was added with Masterflex C-Flex® 1/8 x 1/4 tubing (Cole-Parmer, Vernon Hills, IL) to prevent air accumulation in the tubing. In addition to calculating feed rates by measuring the mass of feed reservoirs (Section 2.5.1), total addition volumes were also calculated in real-time by the software. An example program is shown in Figure A2.1. These programs provided a Calculated Value (.CV) for the base and glucose feeds.

#### *A2.2. Detailed fermentor vessel set-up*

Incomplete complex feed medium was made in several steps. First, 210 g of granulated yeast extract was dissolved into a 500 ml solution in a 1 L bottle. Meanwhile hot water was used to dissolve 0.1 g ferrous sulfate heptahydrate, 10.5 g magnesium sulfate heptahydrate, sodium citrate dihydrate, 0.6 mg manganese chloride tetrahydrate, and 275 ml dextrose into a separate 500 ml solution. The second solution

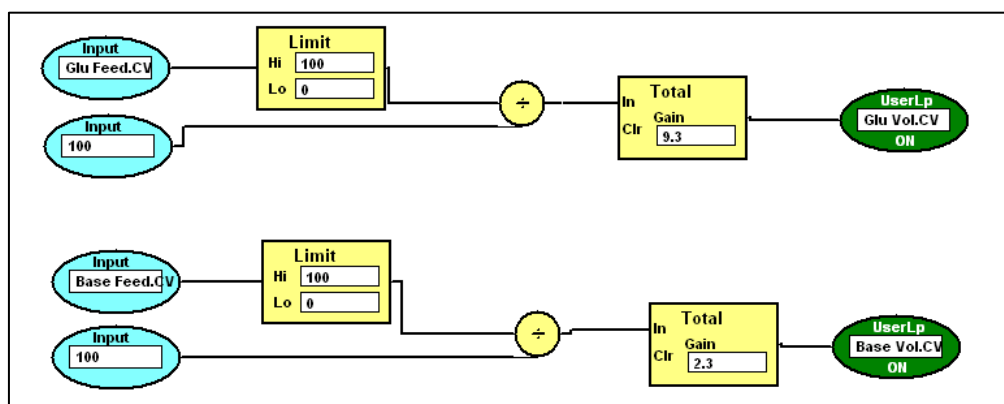


**Figure A2.1. Biocommand program for glucose and base feed calculated values.** Based on the tubing used, a program was created to determine the cumulative addition of glucose and base feeds. The program shown determines base volumes of sodium hydroxide.

was put in a 1 L bottle with a stir bar and feeding tubing. The feeding tubing reached the bottom of the bottle and led to additional tubing to a male quick connect (Cole-Parmer, Vernon Hills, IL). When both solutions were completely dissolved, they were autoclaved together for 30 min. Should 1 L of each solution be made, they were autoclaved together for 45 min.

The sources of medium components are provided in Section 2.4.1. Incomplete complex batch medium was made by dissolving 0.1 g ferrous sulfate heptahydrate, 3.0 g sodium hexametaphosphate, 2.1 g ammonium chloride, 1.9 g citric acid monohydrate, 2.0 ml 30% ammonium hydroxide, and 15 g granulated yeast extract into a 1 L solution. This inoculum medium was poured into a 2.5 L fermentation vessel, and 0.4 ml Antifoam 204 was added to the fermentor directly.

The pH probe was calibrated by putting the probe into fresh pH 7.0 and 4.0 standards. After at least 10 min of equilibration in each buffer, the BioFlo unit was calibrated under the Calibration screen. The Zero was set to 7.0 and the Span was set to 4.0 when the probe had equilibrated in the respective buffers.

The reactor was prepared by first fully inserting the baffles into the fermentor. A headplate was then evenly sealed on top of the fermentor with four bolts. The headplate was positioned so that the inserted probes would fit in the gap in the baffles. O-rings were used to snugly insert the pH and dissolved oxygen probes into the headplate. Acro polytetrafluoroethylene (PTFE) 0.2  $\mu\text{m}$  air filters (Pall, East Hills, NY) were placed on the sample port and ring sparger. The sample port was closed, and the lines for the ring sparger and harvest were clamped. Female quick connects (Cole-Parmer) were placed on the addition ports. Aluminum foil was used to wrap the impeller, probe electrodes, air filters, quick connects, and the condenser port. The condenser base and exhaust were individually wrapped in aluminum foil. Before autoclaving, a coolant exhaust was placed on the fermentor's water jacket. The reactor and condenser were autoclaved for 30 min. If two reactors were autoclaved, the cycle would be set for 45 min.

While the fermentor was still hot after being removed from the autoclave, the aluminum foil over the condenser base and condenser port were removed. The condenser was then inserted into the headplate. The fermentor was placed on the BioFlo unit and coolant return and supply lines were attached to the condenser and reactor water jacket. The chiller was turned on and the Temperature was set to Prime mode. After at least 1 min, the Temperature mode was set to PID with a setpoint of 37°C. The temperature probe was inserted into the headplate, and the probe casing was filled with water. The motor was mounted on top of the impeller, and the Agitation was set to PID mode at a setpoint of 1,000 rpm. Under Calibration, the dissolved oxygen Zero was set to 0% prior to attaching the probe. The pH and dissolved oxygen probe cables were then attached. The dissolved oxygen cable was allowed to polarize the dissolved oxygen probe for a minimum of 6 hrs before Span calibration.

A complex batch medium supplement was prepared by adding 40 ml 50% glucose, 1 ml 100 mg/ml kanamycin sulfate, 1 ml 34 mg/ml chloramphenicol, 1.6 ml 2 M magnesium sulfate heptahydrate, and 0.1 ml 2 g/L manganese chloride tetrahydrate to a sterile 50 ml conical. When the reactor temperature had cooled, the Gas setting was set at Manual, and the air flow rate was set at 2-2.5 L/min and attached to the vessel. The medium supplement was then added to the fermentor.

When the feed medium components had cooled, 20 ml 150 g/L hexametaphosphate, 20 ml 150 g/L ammonium carbonate, 1 ml 100 mg/ml kanamycin sulfate, 1 ml 34 mg/ml chloramphenicol, and 4.5 ml of 1 M IPTG were added to the yeast solution. The yeast solution was then added to the dextrose solution. After the complex feed medium was mixed, the feed tubing was primed and attached to the bioreactor through Pump 1. Feed 1 was set to Acid mode with a setpoint of 0.0.

Within a few hours of inoculation, a 5 M sodium hydroxide solution was attached to the bioreactor through Pump 3. The line was primed, pH was set to PID mode, and the pH setpoint was slowly increased to 7.0. Feed 3 was set to Base mode with a setpoint of 15.0. The pH of a medium sample could be measured externally, and the pH setpoint could be readjusted accordingly.

The dissolved oxygen calibration Span was set to 100%. The dissolved oxygen mode was set to O<sub>2</sub>, and the setpoint was set to 40%. An oxygen tank was attached to the BioFlo unit that supplied pure oxygen at approximately 10 psi.

At inoculation, the appropriate Biocommand program was initiated.

### ***A2.3. Feeding method programs***

Most fermentations were performed using a pH-stat feeding method. In such a feeding strategy, the feed medium was added as an “Acid” using the BioFlo unit’s internal software. Unfortunately the C41 cells caused a pH rise prior to glucose

depletion in the early stage of each fermentation (see Figure 2.4). Therefore the Set Point (SP) of the maximum feeding rate value of the Acid was set at 0.0 at the start of the run and later changed to 30.0. The pH-stat feeding was used to control culture pH, and thus the base addition had to be shut off when feeding was initiated. These changes were automated with the Biocommand program setup shown in Figure A2.2.

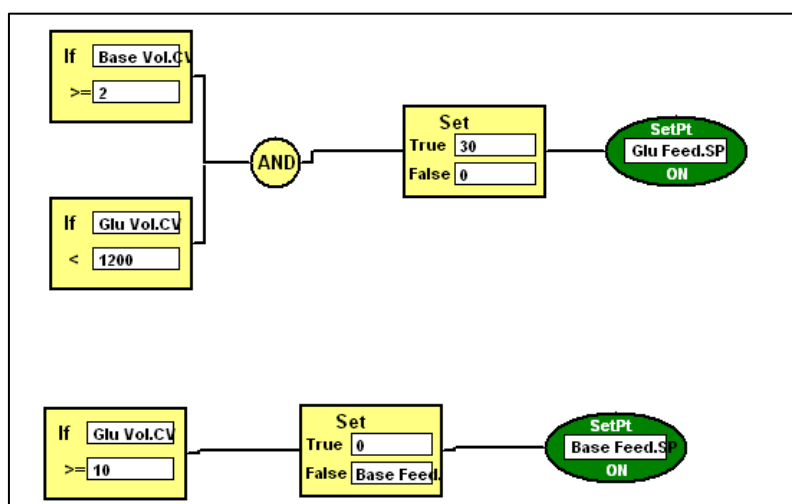


**Figure A2.2. Biocommand program setup for feed addition.** After a known amount of base was added to the fermentor, the maximum feeding rate was given a value. After feed had been added to the fermentor, base addition was turned off.

The premature pH spike only occurred when C41 *E. coli* cells were grown in the complex batch medium. The actual pH spike caused by glucose depletion occurs at 6 hr elapsed fermentation time. As shown in Figure A2.3, this pH spike did not occur during the early growth phase in the chemically defined batch medium. This spike was also not present when BL21 and BLR strains of *E. coli* were used. In these cases, a program, such as the one shown in Figure A2.2, was not used.

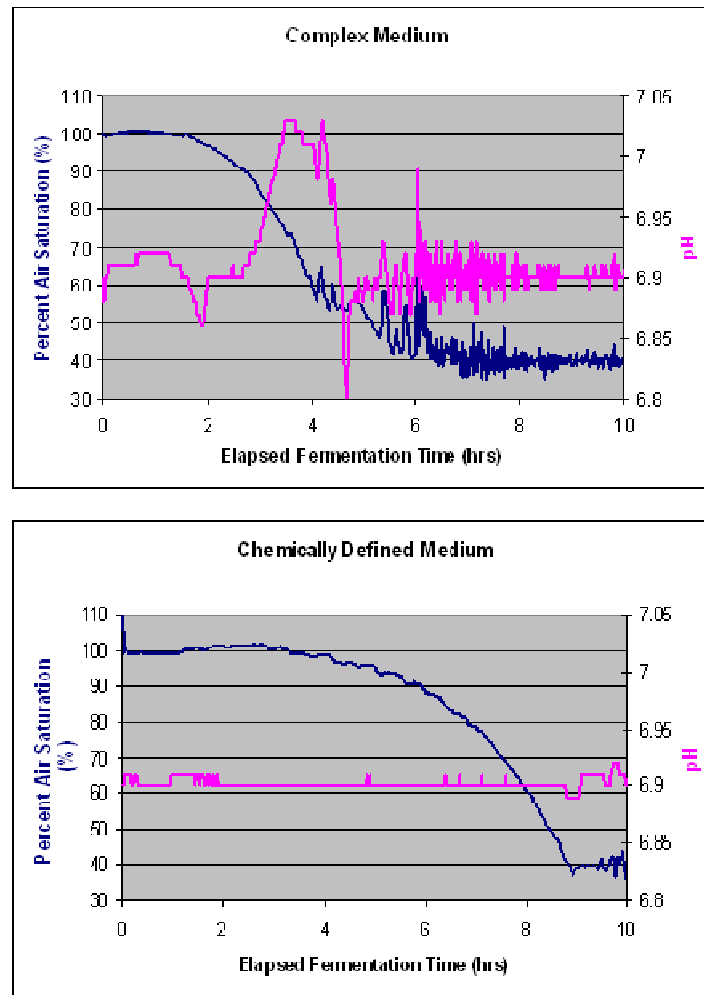


**Figure A2.3. Dissolved oxygen and pH profiles of fermentations in complex and chemically defined media.** C41 *E. coli* cells grown in complex medium generate a pH spike during early batch phase. This pH spike is not present in the early batch phase of the same cells grown in a chemically defined medium.

For constant feeding rate strategies, the feed medium addition was manually set in “Manual” mode at the culture’s pH spike. For linear feed rates, an automated program was used based on elapsed fermentation time (EFT). Feeding began at glucose depletion, which occurred after 12 hr EFT when chemically defined batch medium was used. The slope of the linear feed rate was changed by altering the constant value the EFT value was divided by. The actual feed rates that these setpoint values represent were determined in Section 2.5.1. An example of a linear feed program used in a chemically defined medium culture is shown in Figure A2.4.

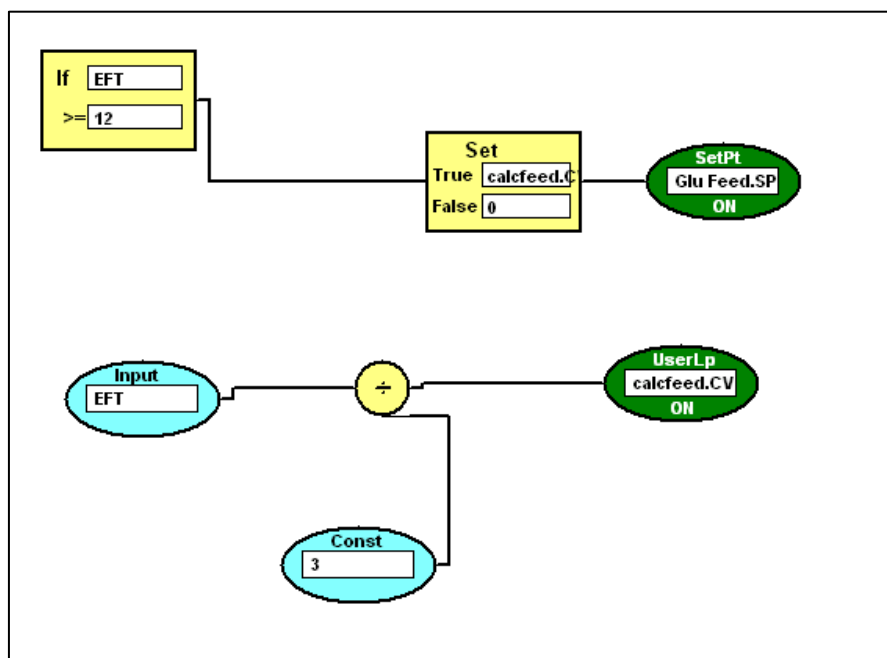


**Figure A2.4. Biocommand program for linear feed rate addition.** Feeding began when glucose was depleted in chemically defined medium fermentations at 12 hr elapsed fermentation time. The feeding rate could be increased by decreasing the value of the Const number.



#### ***A2.4. Chemically defined medium metals***

The trace metals in the feed medium added to the chemically defined medium cultures were prepared in sulfuric acid. This highly acidic solution made it impossible to implement the pH-stat feeding method. An attempt to reduce the acidity of the trace metals was attempted. The trace metals in sulfuric acid have a pH of 0.7 and will precipitate if the pH is increased above 2.5.

Copper, cobalt, zinc, borate, and calcium salts appeared to readily dissolve in water. Calcium chloride could be dissolved with the other metals, but it would then form a precipitate after an extended period of time. Sodium molybdate would precipitate in the presence of manganese chloride or ferrous sulfate. It was omitted because molybdate is primarily used for nitrate uptake, and there was no nitrate in the medium. Ferric sulfate  $[\text{Fe}_2(\text{SO}_4)_3 \cdot n\text{H}_2\text{O}]$  could not be dissolved in water, and ferrous sulfate  $[\text{FeSO}_4 \cdot 7\text{H}_2\text{O}]$  could stay in solution in water for only an appreciable amount of time, possibly because of the high concentration used. The trace metal solution without molybdate or iron had an innate pH of 4.6 in water. Adding all metals together in water created a pH 3.4 solution with heavy precipitation.

Since the metals require a low pH, the amount added to the feed medium was decreased to minimize the acidity in the chemically defined feed medium. Unfortunately, even with no metals in the feed medium, the glucose and magnesium solutions alone were able to sharply decrease the reactor pH and result in inadequate feeding with the pH-stat method. Ultimately, linear feed rates were used to ensure a successful high cell density culture with chemically defined medium.

### A2.5. Temperature shift programs

All cultures were run at 37°C in batch mode until a pH spike indicated glucose depletion. If temperatures were to be changed to a different set point for the production phase, this change was automatically initiated after feeding was initiated, as shown in Figure A2.5.

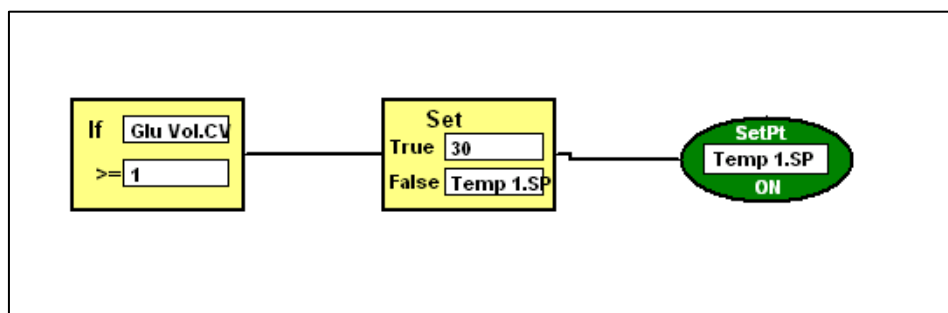


**Figure A2.5. Biocommand program for temperature shift.** When at least 1 ml of feed medium was added to the reactor, temperature could be shifted. The example program shown downshifted vessel temperature to 30°C during the production phase.

## APPENDIX 3

### SM14 PROCESS DEVELOPMENT

#### ***A3.1. Sm14 introduction***

Sm14-C62V antigen is a potential vaccine for schistosomiasis, a condition caused by the parasite *Schistosoma mansoni* that is found in unclean waters of undeveloped countries. The World Health Organization ranks schistosomiasis as the second most important infectious disease after malaria. An initial fermentation and purification process was developed by Dr. Leonardo Damasceno (now at Sanofi Pasteur, Swiftwater, PA). The purification process was based a procedure used to purify a single-chain antibody for A33 glycoprotein fragment [138].

#### ***A3.2. Supernatant processing***

The *Pichia pastoris* supernatant that contained Sm14 was washed using tangential flow filtration over a 3 kDa cassette (Pall) to remove the salts from the fermentation medium prior to an anion exchange column. On the manufacturing scale, most of the protein precipitated on the cassette (Figure A3.1a), and the final purification yield was 26.5 mg.

#### ***A3.3. Direct hydrophobic interaction chromatography***

Since hydrophobic interaction chromatography (HIC) is not affected by conductivity, the supernatant was loaded onto a Phenyl FF column at 1.00 and 1.25 M ammonium sulfate. At 1.25 M ammonium sulfate, no Sm14 protein was detected in the flowthrough fraction. This was not the case with the sample at 1.00 M ammonium sulfate, and the Sm14 was able to be partially purified over a 20 column volume (CV)

gradient from 1.25 to 0 M ammonium sulfate (Figure A3.1b). Silver-stained gels were loaded and run in the same way as SDS-PAGE, as described in Section 2.5.3, and then stained with a SilverQuest staining kit (Invitrogen).

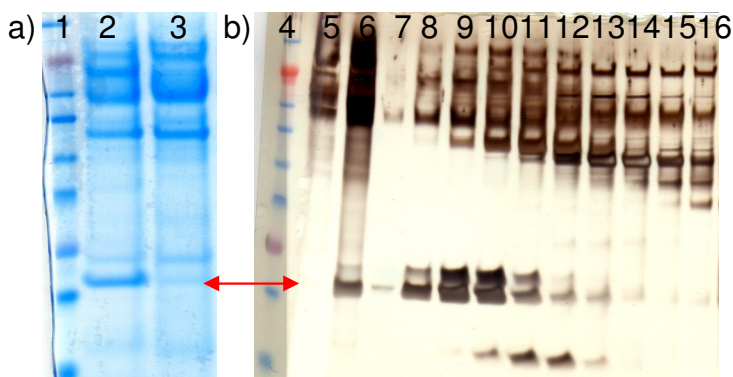


**Figure A3.1. SDS-PAGE of Sm14 after TFF or HIC purification.** Lane 1, 4: See Blue Plus 2 molecular weight standard (Invitrogen, Carlsbad, CA), Lane 2: Sm14 supernatant, Lane 3: Sm14 retentate, Lane 5: 1.25 M ammonium sulfate Sm14 flowthrough, Lane 6: 1.00 M ammonium sulfate SM14 flowthrough, Lane 7-16: Sm14 fractions off a Phenyl column at 1, 3, 5, 7, 9, 11, 13, 15, 17, and 19 CV. The Sm14 protein band is labeled with a red arrow.

#### ***A3.4. Direct anion exchange chromatography***

Sm14 supernatant could be purified on a Q XL anion exchange column (Invitrogen, Carlsbad, CA) if it was diluted three-fold in Loading Buffer [20 mM Tris, pH 8.0] prior to loading. Although purification could be achieved, it was not straightforward because the Sm14 would not tightly bind to the Q XL resin. For example, only 9 ml of diluted protein could be loaded per ml of resin. If the load volume was tripled, Sm14 would elute off of the column before the loading was completed. This was not a conductivity issue because the protein would elute off the column while it was still loading even if diluted 20-fold to the same conductivity as the Loading Buffer, 0.75 mS/cm. Even a 5 mM sodium chloride step gradient would immediately elute Sm14 off a column with many higher molecular weight contaminants. Increasing the pH of the load material up to 9.00 did not seem to

improve binding, but tight binding did occur if a pH 10.00 ethanolamine buffer was used.

Using pH 8.0 Tris buffers, the original anion exchange process used a gradient that went from 0 to 186 mM sodium chloride over 13 CV. It was found that many higher molecular weight contaminants could be removed without loss of Sm14 recovery if the gradient was kept at 100 mM sodium chloride. A final major contaminant could be removed by running a gradient from 0 to 8.4 mM sodium chloride over 35 CV and then increasing the gradient to 10m mM sodium chloride over the next 10 CV (Figure A3.2).

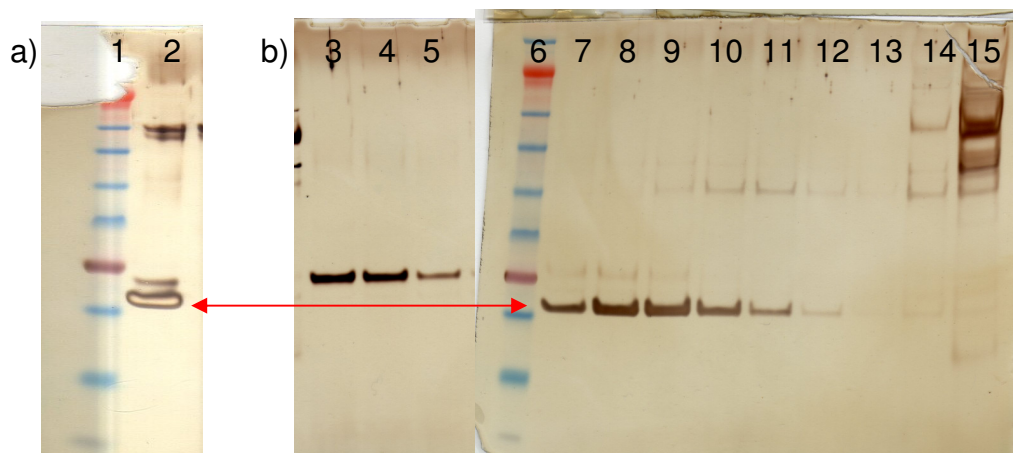


**Figure A3.2. Silver stain of Sm14 after anion exchange purification.** a) Sm14 recovered after original anion exchange process. b) Sm14 recovered after modified anion exchange process. A longer initial gradient removed a major contaminant (Lanes 3-5). Very pure Sm14 was separated (Lanes 7-12). High molecular weight contaminants were removed by decreasing the highest gradient concentrations (Lane 14-15). Marker is See Blue Plus 2 (Invitrogen). Sm14 protein is labeled with a red arrow.

These modifications were implemented during the third manufacturing run. The second manufacturing run increased total protein yields from 26.5 mg to 66.2 mg, but the product had more impurities. The third manufacturing run produced the purest material to date with a total protein yield of 138.5 mg (FigureA3.3).

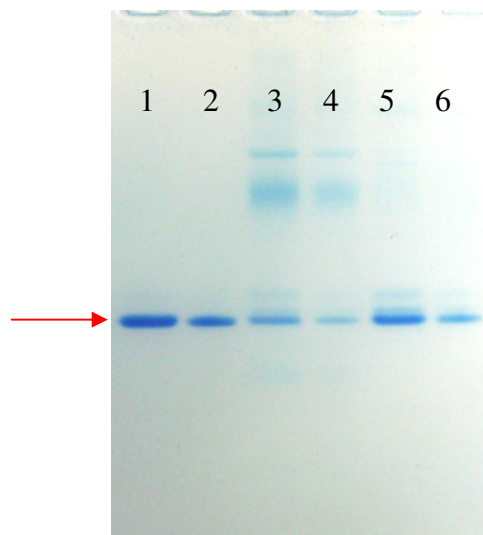


**Figure A3.3. SDS-PAGE of Sm14 produced at the manufacturing scale.** SDS-PAGE of Sm14 recovered after manufacturing runs #3 (Lanes 1, 2), #2 (Lanes 3, 4), and #1 (Lanes 5, 6). Odd lanes contain 10 mg of protein and even lanes contain 5 mg of protein. The Sm14 protein band is labeled with a red arrow.

## REFERENCES

- 138) L. Damasceno, I. Pla, H. Chang, L. Cohen, G. Ritter, L. Old, C. Batt, An optimized fermentation process for high-level production of a single-chain Fv antibody fragment in *Pichia pastoris*, Prot. Expr. Purif. 37 [2004] 18-26.

## APPENDIX 4

### NY-ESO-1 PROCESS DEVELOPMENT

#### ***A4.1. NY-ESO-1 process development introduction***

The original NY-ESO-1 fermentation and purification processes were developed by Dr. Todd Vannelli (now at Adnexus Therapeutics, Waltham, MA). This appendix describes contributions made to improve this process.

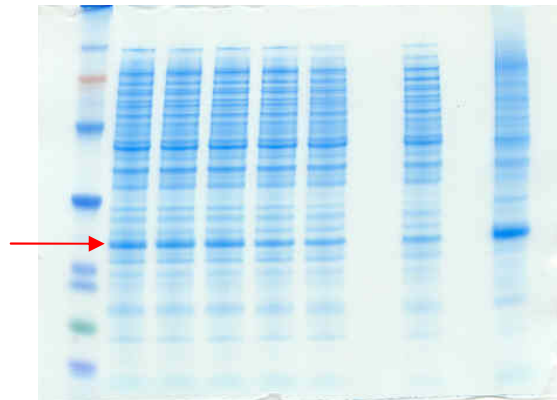
#### ***A4.2. NY-ESO-1 inclusion body wash***

After cell lysis, NY-ESO-1 inclusion bodies were originally washed by pelleting the insoluble protein and resuspending it in the wash solution described in Section 2.6. This process did not scale up well when 10 L of fermentation lysate was sent through a Carr Powerfuge Pilot Centrifuge (Pneumatic Scale Angelus, Cuyahoga Falls, OH). Although the Powerfuge is advertised to reach speeds of 20,000 rcf, it was not able to efficiently pellet the inclusion bodies that would pellet in a Sorvall RC-5B Superspeed Centrifuge (Thermo Fisher Scientific, Waltham, MA) under the same gravitational force (Figure A3.1).

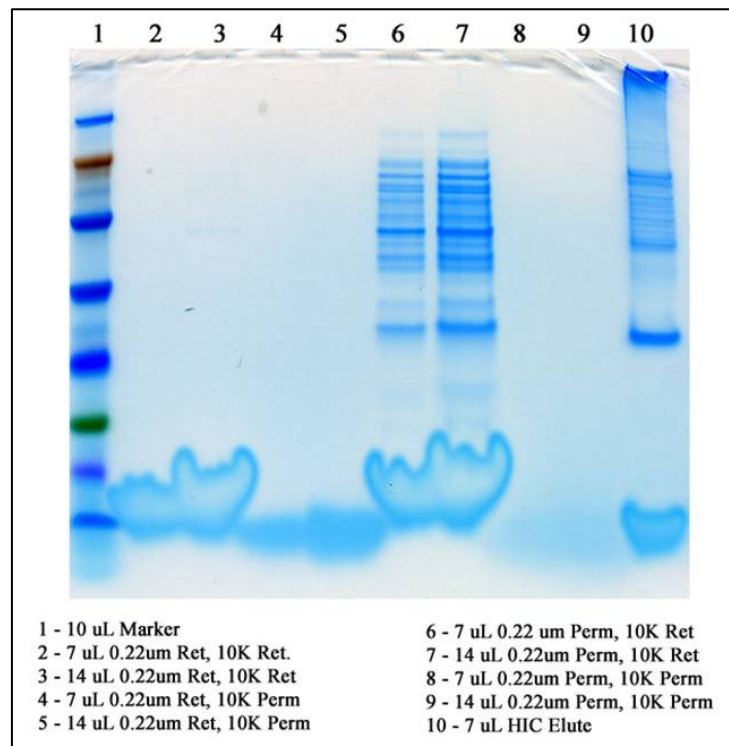
Instead of using the Powerfuge, a Millipore Proflux M-30 (Billerica, MA) was used to wash the inclusion bodies using tangential flow filtration (TFF). In the final process, the cell lysate was circulated parallel to a 0.2  $\mu\text{m}$  Centrasette II cassette (Pall Corporation, East Hills, NY). The diafiltration buffer (50 mM Tris, 1 mM ethylenediaminetetraacetic acid (EDTA), 200 mM sodium chloride, pH 8.0) of five-fold the initial lysate volume was used to wash the inclusion bodies. No Tween-20 was used in this wash buffer because it would create an artifact on SDS-PAGE (Figure



Figure A4.2).  $\beta$ -mercaptoethanol was also removed from the wash buffer because its absence had no detectable changes.



**Figure A4.1. SDS-PAGE of NY-ESO-1 lysate fractions through a continuous centrifuge.** Lane 1: Multimark molecular weight standard (Invitrogen), Lane 2-4: cell lysate, Lane 5, 6, 8: powerfuge flowthrough, Lane 10: powerfuge pellet. NY-ESO-1 is indicated by the red arrow.



**Figure A4.2. SDS-PAGE of tangential flow filtration fractions using a Tween-20 wash buffer.** NY-ESO-1 inclusion bodies were sent through a 0.22  $\mu$ m filter and retained using a 10 kDa filter. Tween-20 is visible as a blue shading below the 3 kDa marker and appears as a larger artifact in higher concentrations.

An immobilized metal affinity chromatography (IMAC) column was equilibrated with IMAC A buffer (4 M urea, 100 mM sodium phosphate, pH 7.5). The TFF retentate was diluted eight-fold in solubilization buffer (8.57 M urea, 100 mM sodium phosphate, pH 7.5) to a final urea concentration of 7.5 M. The solubilized inclusion bodies were loaded onto the IMAC column and chased off the column with IMAC A buffer. The protein was then washed and eluted with IMAC A buffer containing 75 and 500 mM imidazole, respectively. In comparison to the centrifugation-washed material, the material washed using tangential flow filtration showed a much larger absorbance peak during the 75 mM imidazole wash and a much smaller peak during 500 mM imidazole elution (Figure A4.3).

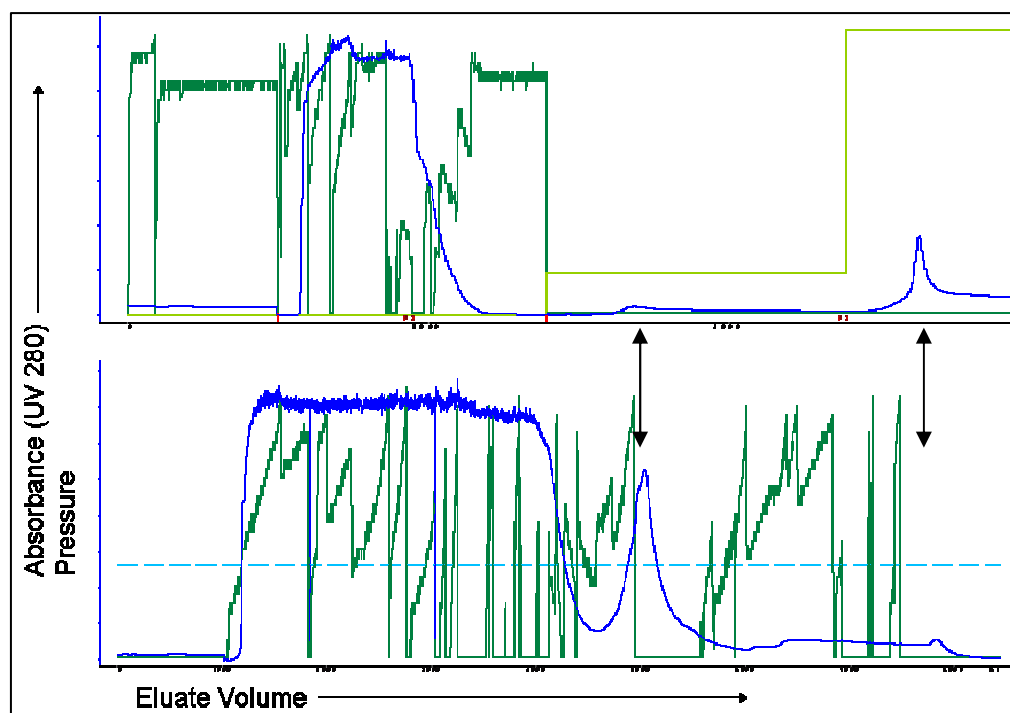


**Figure A4.3. IMAC chromatography profiles of NY-ESO-1.** Each profile contains a flowthrough, low imidazole wash, and elution peak. NY-ESO-1 washed using centrifugation resuspensions (top) had a sharper elution peak. The material washed using tangential flow filtration (bottom) had more material in the low imidazole wash. Blue lines are ultraviolet absorbance at 280 nm. Green lines are column pressure. The wash peaks are labeled with arrows.

#### ***A4.3. NY-ESO-1 protein precipitation during ion exchange chromatography***

NY-ESO-1 in the high imidazole fraction was buffer exchanged to [4 M urea, 50 mM Tris, pH 8.0] to remove salts. The original NY-ESO-1 purification process sent this material through a Q XL column without binding.

Upon scale-up, the NY-ESO-1 precipitated on the Q XL column and could not be removed with up to 1 M sodium chloride or 1% deoxycholate detergent. One of the changes made to the process upon scale-up was the change of urea manufacturer. The small scale process had used a granular urea (Mallinckrodt Baker, Phillipsburg, NJ), and the manufacturing process used bead urea (EMD Biosciences, San Diego, CA). Buffers using both types of urea were tested on a 5 ml HisTrap FF and a 5 ml HiTrap Q XL column (GE Healthcare). Both buffers produced 0.3 mg/ml IMAC elution fractions and 0.26 mg/ml Q XL loads. In both cases, there was also an undetectable level of protein in the Q XL flowthrough and subsequent 1 M sodium chloride wash. It was determined that the type of urea used did not affect the purification of NY-ESO-1, and there was another cause for its precipitation on the Q XL column.

NY-ESO-1 irreversibly bound to the Q XL column, which implied that it had precipitated. Several buffers were screened to determine which one would prevent the Q XL load from precipitating on the column. An aliquot of the NY-ESO-1 Q XL load was buffer exchanged to the respective buffer prior to loading on a 5 mL HiTrap Q XL column (GE Healthcare) in each of these cases. It was determined that a phosphate buffer instead of a Tris buffer at a lower pH solved this problem (Table A4.1). Changing the buffer base from Tris to sodium phosphate had the greatest influence. A buffer of [4 M urea, 50 mM Tris, pH 7.5] was also attempted, but the NY-ESO-1 solution became cloudy during the buffer exchange. It was concluded that NY-ESO-1 has a poor solubility in Tris buffer that caused protein loss through precipitation.

**Table A4.1. Recovery of NY-ESO-1 through a Q XL column using different buffers.** NY-ESO-1 was buffer exchanged into various buffers and flowed through a Q XL column. No protein was recovered when a Tris buffer was used.

Buffer	pH	urea	recovery
50 mM Tris	8.0	4 M	0.0%
100 mM Na Phos	8.0	4 M	62.1%
100 mM Na Phos	7.5	4 M	71.5%
100 mM Na Phos	7.5	8 M	91.3%

#### ***A4.4. NY-ESO-1 protein precipitation during hydrophobic interaction chromatography***

The Q XL flowthrough fraction was composed of NY-ESO-1 protein in [4 M urea, 100 mM sodium phosphate, pH 7.5]. Originally, this material was diluted 1:1 in [4 M urea, 100 mM sodium phosphate, 2 M ammonium sulfate, pH 7.5] to a final concentration of 1 M ammonium sulfate. This resulted in a cloudy precipitate of the NY-ESO-1 protein that would be lost in 0.5  $\mu$ m pre-column filtration or on the hydrophobic interaction chromatography (HIC) column itself.

The ammonium sulfate concentration was reduced to 0.95 M. Protein yields were increased from 0.340 to 0.415 mg of protein. Further studies are now determining the improved NY-ESO-1 yields achieved by lowering ammonium sulfate levels.

#### ***A4.5. NY-ESO-1 endotoxin removal***

##### ***A4.5.1. NY-ESO-1 endotoxin removal during ion exchange chromatography***

A scouting study was performed to determine if altering the pH in the anion exchange chromatography step could improve endotoxin removal. The protein was

buffer exchanged into and sent through the column without binding using a [4 M urea, 100 mM sodium phosphate] buffer. The tested pH's of this buffer were 6.5, 7.0, and 7.5. Q XL load retain from a manufacturing run was loaded in 7.5 ml aliquots on both equilibrated 1ml and 5 ml HiTrap Q XL column (GE Healthcare) and washed off with 5 ml of buffer. Protein recovered from each pH was identical. The load endotoxin concentration was 280 EU/ $\mu$ g. Endotoxin values were 84.5, 160, and 158 EU/ $\mu$ g off the 1 mL columns and 9.1, 7.0, and 4.9 EU/ $\mu$ g off the 5 ml columns for pH 6.5, 7.0, 7.5, respectively. So although the pH range tested did not have much influence on the endotoxin level, the use of additional Q XL resin helped significantly.

A more elaborate study [139] showed that up to 900,000 endotoxin units (EU) could be loaded onto 1 ml of Q XL resin. For future manufacturing runs, the amount of Q XL resin used was quintupled.

#### ***A4.5.2. NY-ESO-1 endotoxin removal during nickel chromatography***

A detergent-based endotoxin removal step was based off of a successful literature study [140]. NY-ESO-1 cell pellets were resuspended back to 1 L and washed on a 0.2  $\mu$ m TFF unit with 5 L of EDTA Buffer [100 mM sodium phosphate, 500 mM sodium chloride, 13.2 mM EDTA, pH 7.5]. The EDTA was removed by washing with 5 L of Phosphate Buffer [100 mM sodium phosphate, 200 mM sodium chloride, 100 mM potassium chloride, pH 7.5]. The retentate was concentrated to 500 mL and diluted to 4 L with Triton Buffer [100 mM sodium phosphate, 200 mM sodium chloride, 100 mM potassium chloride, 10 mM imidazole, 1.0% Triton X-114, 8 M urea, pH 7.5]. The solution was allowed to solubilize overnight.

An IMAC column was equilibrated with 5 CV of Triton Buffer and was loaded with the solubilized NY-ESO-1. Triton buffer was then used to wash off the endotoxin. It took 15 CV of a Urea Buffer [100 mM sodium phosphate, 4 M urea, pH

7.5] to wash out the triton, as detected with an online UV280 monitor. The column was then washed for 5 CV with [Urea Buffer + 75 mM imidazole] and eluted with 4 CV of [Urea Buffer + 500 mM imidazole].

Although the Reichelt study only used 0.1% Triton X-114, our studies found that 1.0% Triton X-114 would result in better endotoxin removal. Triton X-114 would typically form a cloudy solution at room temperature, but the Triton Buffer, which contained 8 M urea, was clear at room temperature. Temperature studies were performed to confirm that the Triton Buffer did not need to be kept at 4 °C, as was also done in the Reichelt study. The Triton Buffer would freeze if it was kept in ice, so the buffer could only be maintained at  $10 \pm 2$  °C during the course of a run that jacketed the IMAC column with ice. A 4 °C study was performed manually in a cold room with syringes. The Reichelt study also used a 50 CV wash of Triton Buffer. The triton concentration, buffer temperature, and wash volumes were evaluated using 5 mL HisTrap columns (GE Healthcare).

**Table A4.2. Endotoxin removal during IMAC under different triton concentrations, temperatures, and wash volumes.** Temperature was not important, but 1% triton-X114 and high wash volumes were necessary for endotoxin removal.

Run	Triton	Temp	Wash	EU/ $\mu$ g
1	0.0%	10°C	50CV	13.90
2	0.1%	10°C	50CV	1.32
3	0.1%	4°C	50CV	2.77
4	1.0%	10°C	50CV	0.14
5	1.0%	10°C	50CV	0.06
6	1.0%	10°C	10CV	0.73
7	1.0%	20.5°C	50CV	0.06
8	1.0%	20.5°C	5CV	1.64

After establishing the merits of using 1.0% triton-X114 and determining that temperature was not a significant factor, another study evaluated the use of different load volumes and wash volumes. The results are summarized in Figure A4.4. Increasing the wash volumes from 20 to 40 CV did slightly reduce the endotoxin concentration in the IMAC elution from 2.40 to 0.07 EU/ $\mu$ g. It also turned out that overloading the column did not result in increased protein yield and instead resulted in endotoxin levels as high as 29.8 EU/ $\mu$ g. It was later shown that by adding 1.0% deoxycholate buffer to the Triton Buffer, the endotoxin level could be reduced to 0.05 EU/ $\mu$ g with only a 5 CV wash after loading.

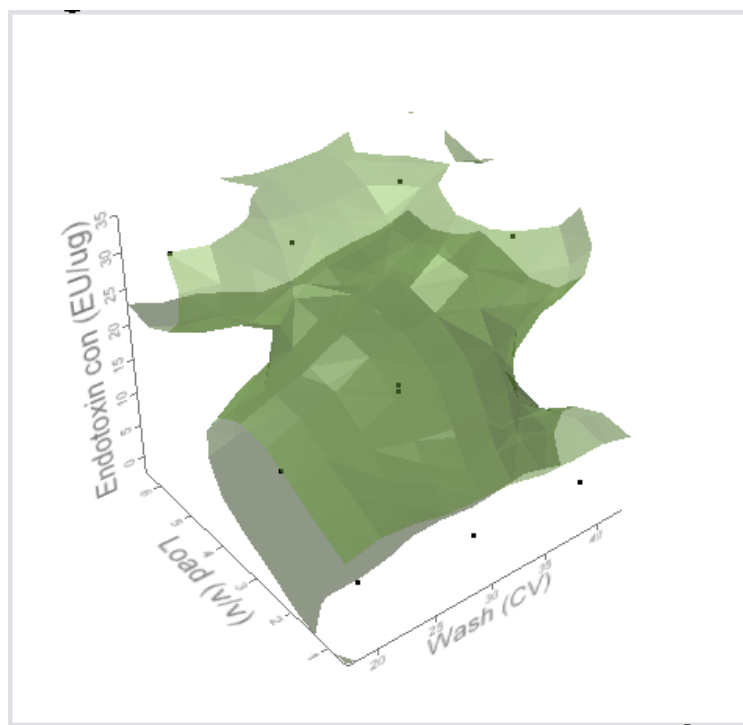


**Figure A4.4. Endotoxin removal during IMAC under different protein load volumes and wash volumes of triton buffer.** Overloading the nickel column resulted in an order of magnitude higher level of endotoxin in the IMAC elution. At the lowest load tested, wash volumes close to 50 CV were necessary to keep endotoxin levels below 1.0 EU/mg.

#### ***A4.5.3. Additional NY-ESO-1 endotoxin removal attempts***

Endotoxin removal was attempted using Endotrap Red (Cambrex, Charles City, IA) and Detoxigel (Thermo Fisher Scientific, Waltham, MA). Columns were drained of storage solution and flushed with Cambrex regeneration buffer and equilibration buffer. Q XL load retain from a manufacturing run was loaded and the protein concentration and endotoxin values of the flowthrough were compared with that of the load. The load sample had a protein concentration of 9.0 mg/ml and the flowthrough samples through the Endotrap Red and Detoxigel columns had protein concentrations of 0.7 and 0.5 mg/ml, respectively. Most of the protein was lost on these columns, and there was no improvement in endotoxin removal.

An increase of sodium chloride and EDTA was attempted to remove endotoxin during the tangential flow filtration (TFF) wash. A NY-ESO-1 cell pellet was resuspended to 1 L and washed with 5 L of [100 mM sodium phosphate, 770 mM sodium chloride, 120 mM EDTA, pH 7.5]. This process was unable to remove enough endotoxin to warrant its use.

Endotoxin removal was also attempted on the HIC column by changing the denaturant. A 2x dilution buffer was used to bring the ammonium sulfate concentration of the HIC load material to 1 M. As such, the most soluble dilution buffer used was [5 M guanidine hydrochloride, 2 M ammonium sulfate, 100 mM sodium phosphate, pH 7.5] resulting in a HIC load of concentrations [2.5 M guanidine hydrochloride, 4 M urea, 1 M ammonium sulfate, 100 mM sodium phosphate, pH 7.5]. This change had no effect on protein recovery or endotoxin removal.

#### ***A4.6. Purification of soluble NY-ESO-1***

There was very little NY-ESO-1 in the soluble fraction. The chloramphenicol acetyltransferase (CAT) protein was produced by the pRARE plasmid, and it showed



up at 26 kDa. Although NY-ESO-1 was 19 kDa, it ran at approximately the same size as CAT. Purification of the soluble fraction of NY-ESO-1 could only be evaluated with a western blot.

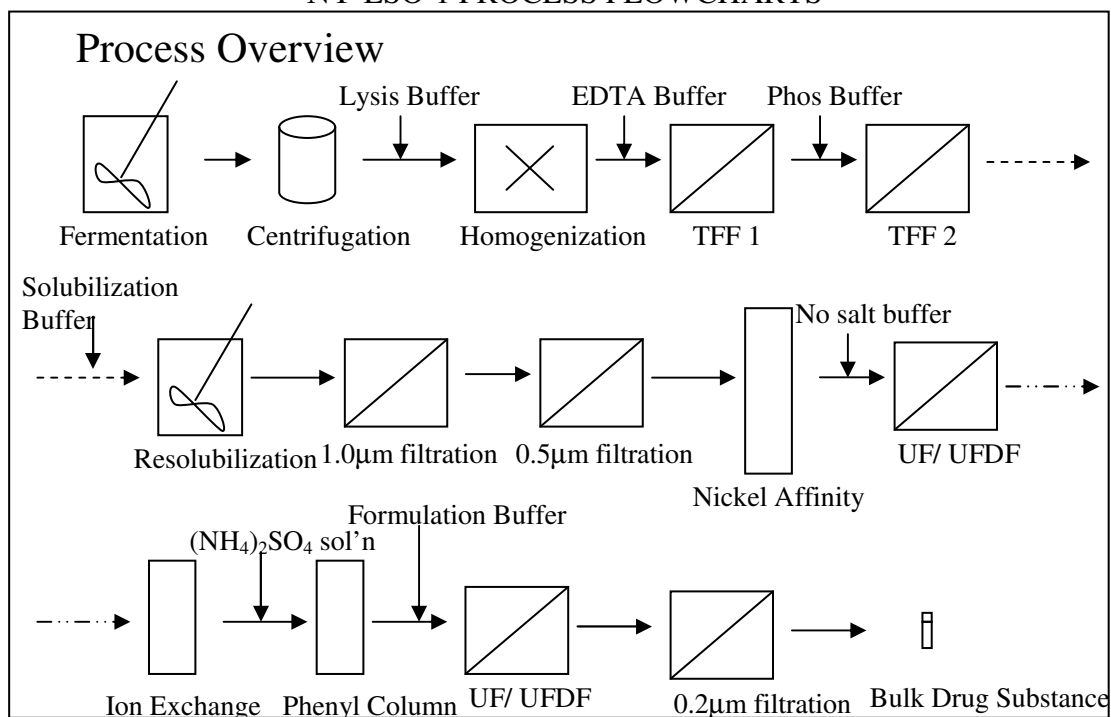
Using a [100 mM sodium phosphate, pH 7.5] buffer, soluble NY-ESO-1 could be found in the flowthrough and elution fractions of the IMAC column. Samples flowed through and did not bind to Q XL and Q FF anion exchange columns. Different ammonium sulfate concentrations were evaluated for the HIC column. Soluble NY-ESO-1 did not bind to a Phenyl column when 0.34 M ammonium sulfate was used. A little bound to the column at 0.63 M and most bound at 0.87 M.

## REFERENCES







- 139) R. Chen, C. Huang, B. Newton, G. Ritter, L. Old, C. Batt, Factors affecting endotoxin removal from recombinant therapeutic proteins by anion exchange chromatography, *Prot. Expr. Purif.* 64 [2009] 76-81.
- 140) P. Reichelt, C. Schwartz, M. Donzeau, Single step protocol to purify recombinant proteins with low endotoxin contents, *Prot. Expr. Purif.* 46 [2006] 483-488.



## APPENDIX 5

### NY-ESO-1 PROCESS FLOWCHARTS

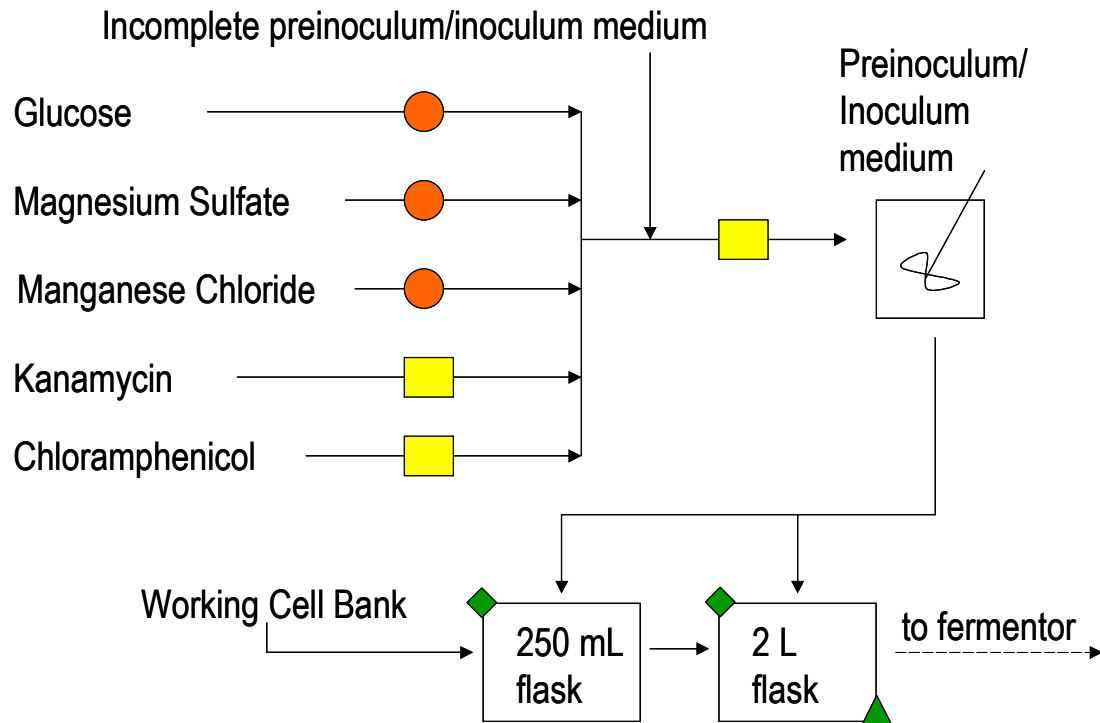


#### Legend:

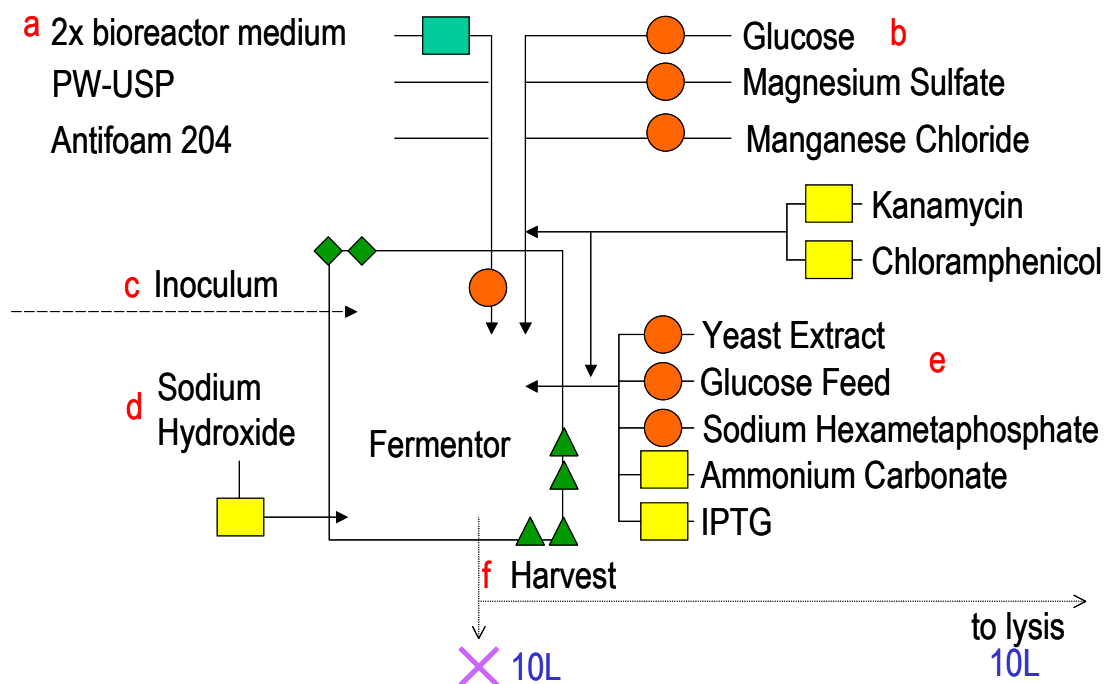
-  Heat sterilization
-  Filter sterilization, 0.22 µm, 0.5/0.2 µm, or 0.1 µm
-  Filtered, 1.2µm or 0.5 µm
-  Sterility sample
-  Retain sample
-  To waste
- 
- p     Permeate

r     Retentate
- 
-  Transfer Bag
- 
-  Mixing step

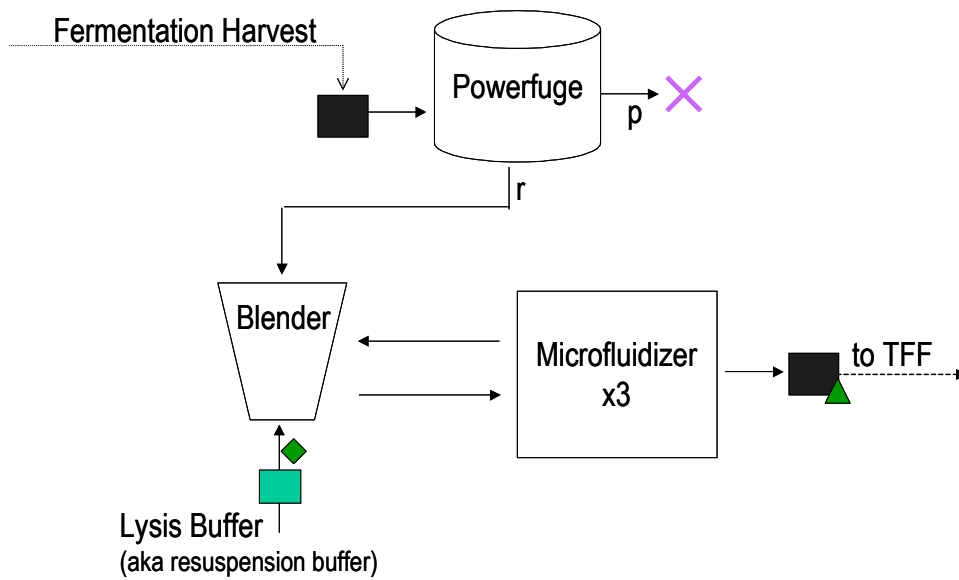
## 1. PREINOCULUM/INOCULUM



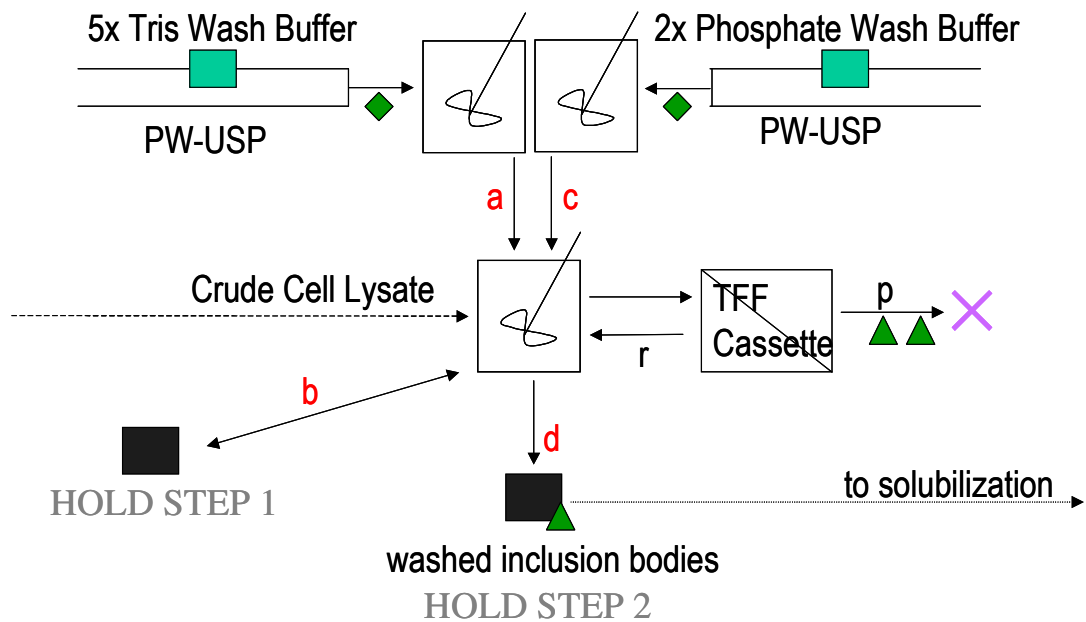
## 2. FERMENTATION



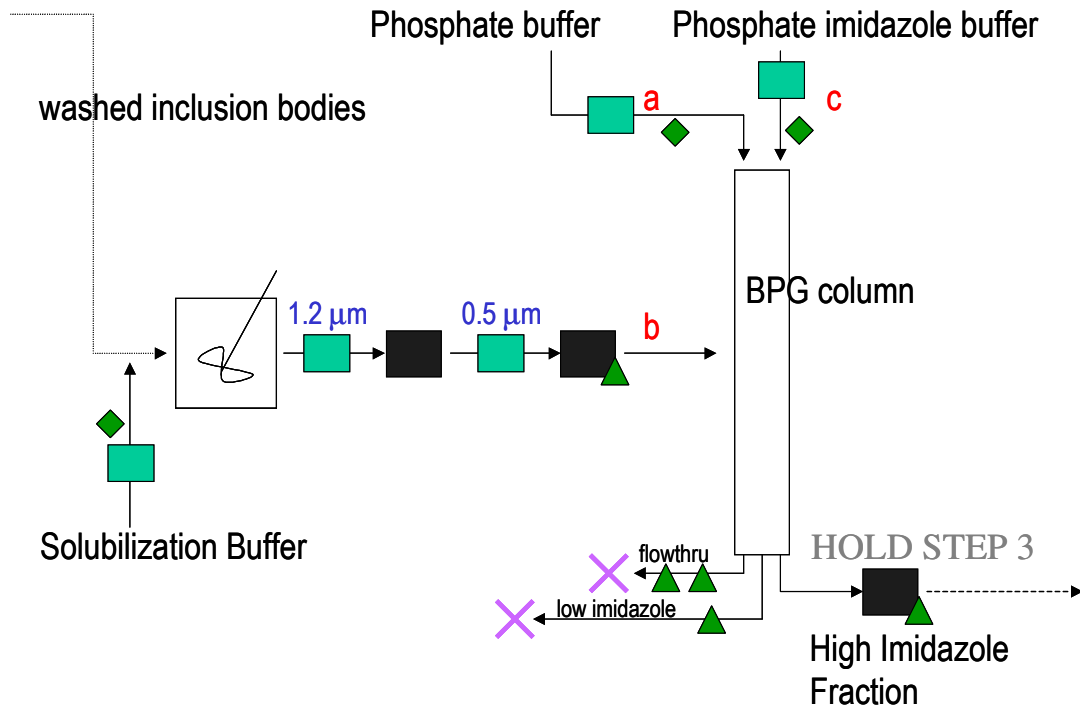
### 3. CELL LYSIS



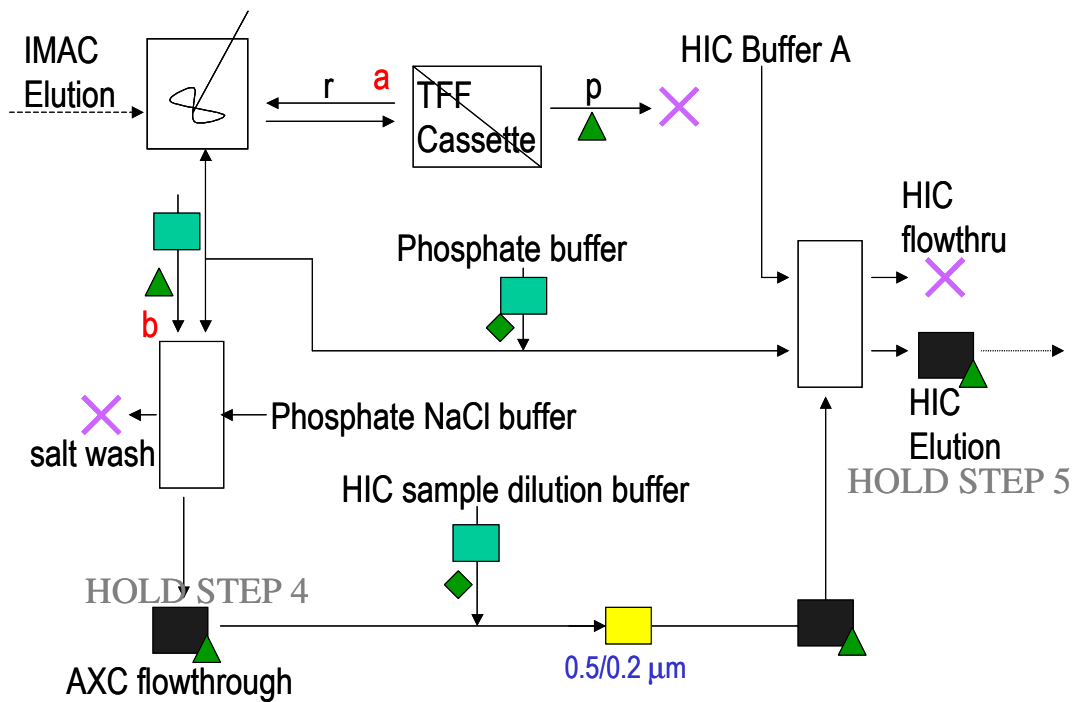
### 4. TANGENTIAL FLOW FILTRATION



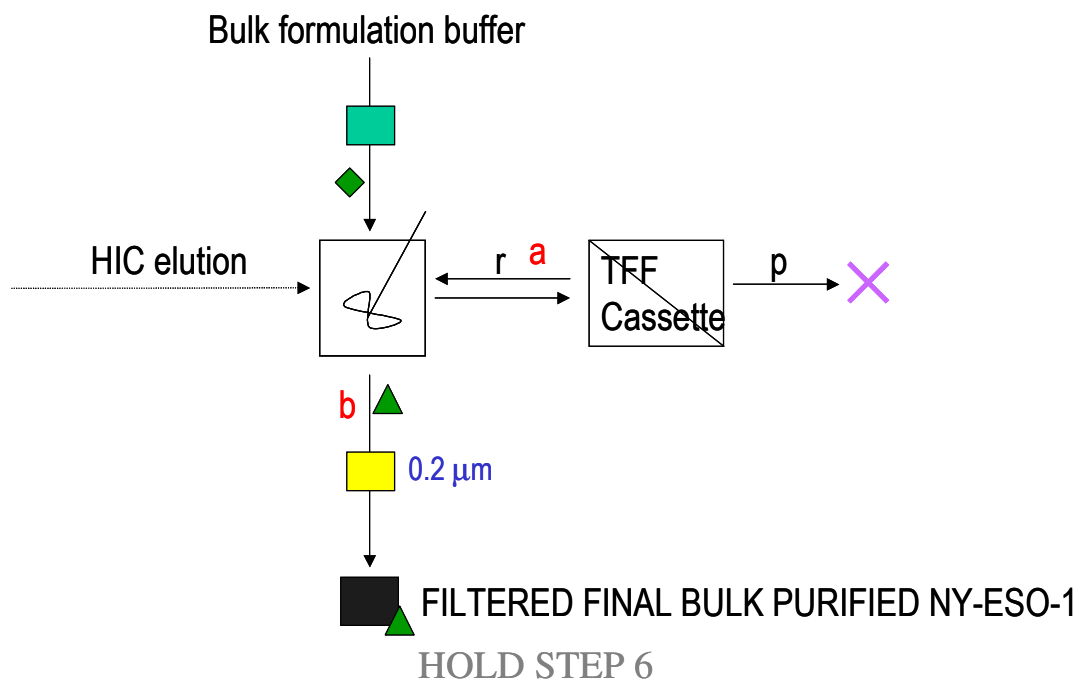
## 5. SOLUBILIZATION & CAPTURE



## 6. DOWNSTREAM PURIFICATION



## 7. POST-HIC PROCESSING



## APPENDIX 6

### MELAN-A EXPRESSION PROCESS DEVELOPMENT

#### ***A6.1. Melan-A research cell bank screening***

The initial Melan-A plasmid was constructed by Dr. Todd Vannelli. The Melan-A sequence was:

mgsshhhhhssglvprgshmpredahfiygypkkgghghsyttaeaaagigiltvilgvllligcwyrrrngyralm  
dkslhvgvtqcaltrrcpqegfdhrdskvslqekncepvvpnappayeklsaeqspppysp

The custom-made 9a24a plasmid containing the Melan-A sequence was transformed into competent C41 cells (see Section 2.3.4). The colonies were screened by suspending single colonies in 1 ml aliquots of complex batch medium (see Section 2.4.1). Eight different cultures were grown in 50 ml conical tubes. After agitation at room temperature overnight, the culture optical densities (OD<sub>600</sub>) were 15.1, 11.0, 9.8, 12.9, 6.0, 5.0, 3.3, and 9.5. Cultures were diluted to an optical density of 0.2 in 5 ml of complex batch medium and placed in a 37 °C shaker.

Induction was performed with the addition of 2 µl of 1 M IPTG to reach a final concentration of 0.4 mM IPTG when the culture OD<sub>600</sub> were 1.68, 1.18, 1.23, 1.50, 1.12, 0.98, 0.88, and 0.97. A preinduction sample was taken from culture #5 before IPTG was added. After four hr, the OD<sub>600</sub> were 4.16, 3.40, 3.80, 3.76, 4.02, 4.00, 3.84, and 3.64. Cell pellets were made from (1.3/OD) ml of broth. Protein was separated into soluble and insoluble fractions (see 2.5.3). A western blot of these samples (Figure A6.1) showed equal Melan-A production in all cultures. Culture #8 was selected to be made into the research cell bank (2.3.4).



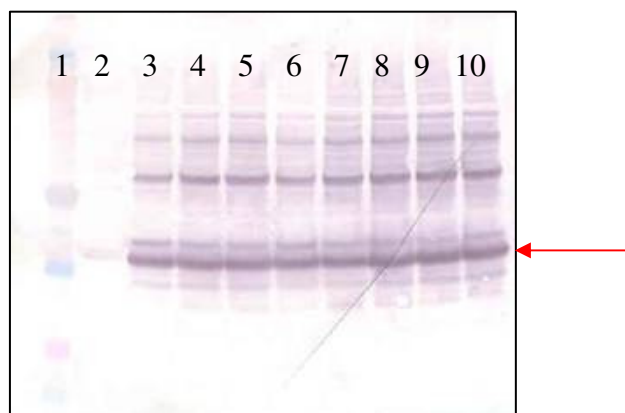


**Figure A6.1. Western blot of Melan-A production in transformed cells.** Lane 1 is a Multimark standard (Invitrogen, Carlsbad, CA). Lane 2 is a preinduction sample that shows negligible Melan-A production. Lanes 3-10 are Melan-A production in eight cultures after four hr of IPTG induction. A red arrow indicates the Melan-A monomer band.

#### ***A6.2. Melan-A genetic stability study***

A single 100-fold dilution was performed by mixing 10  $\mu$ l of culture into a 1 ml aliquot of phosphate buffer saline (PBS). The fermentation inoculum culture was diluted  $10^6$ -fold with three 100-fold dilutions in series. The harvest culture was diluted  $10^8$ -fold by conducting four 100-fold dilutions. Aliquots of 50  $\mu$ l of these dilutions were plated on plates with and without kanamycin and chloramphenicol. Plates were made using 20 g/L APS Luria broth and 15 g/L agar. The autoclaved solution was poured into petri dishes in 40 ml aliquots under sterile conditions. Colonies were allowed to form over a two day period at room temperature.

Performed in triplicate, the inoculum culture formed  $49 \pm 3$  and  $46 \pm 7$  colonies on plates with and without antibiotic, respectively. Also performed in triplicate, harvest cultures formed  $32 \pm 2$  and  $264 \pm 50$  colonies on plates with and without antibiotic, respectively. Even though kanamycin was included in the feed medium, this study shows that the culture had 100% antibiotic resistance in the inoculum stage, but it lost most of this resistance by the end of the fermentation. In TEM images of the harvest cells (Figure 2.12), very few cells also appear to be

producing inclusion bodies. This is possible because C41 cells are not RecA negative. Under stress, cells are able to lose their protein-producing plasmid. The cells that do not need to produce the protein and replicate the plasmid have a growth advantage and overtake the remaining the cells in the culture.

### ***A6.3. Melan-A production in BLR *E. coli****

BLR cells were transformed with the pET9a24a Melan-A plasmid using the same techniques in Section 2.3.4. A double transformation was performed to add a pRARE plasmid. From western blot analysis, it was determined that Melan-A expression in the BLR strain was improved compared to the C41 strain. It was also concluded that the pRARE plasmid was necessary for acceptable Melan-A expression (Figure A6.2).

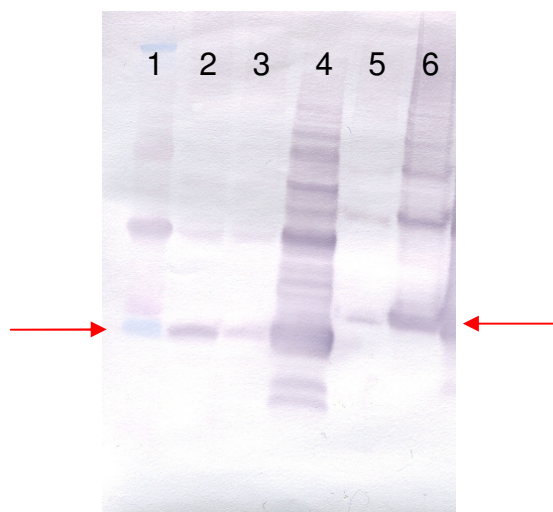


**Figure A6.2. Western blot of Melan-A produced from different strains of *E. coli*.** Lane 1: Multimark, Lane 2: BLR preinduction, Lane 3: BLR harvest, Lane 4: BLR pRARE harvest, Lane 5: C41 preinduction, Lane 6: C41 harvest. Red arrows indicate the Melan-A monomer bands.

It was recommended that the production cell line be change to BLR *E. coli* to possibly prevent genetic stability and improve process yields. The BLR strain is also

more commonly used for industrial production of recombinant proteins. It was not changed in the process because the NY-ESO-1 fermentation process had set precedence for using C41 *E. coli* in the Cornell University – Ludwig Institute for Cancer Research productions.

#### ***A6.4. Synthetic Melan-A production***

The Melan-A sequence was changed to:

mpredahfiygypkkghghsyttaceaaagiltvilgvllligcwycrrngyralmdkslhvgtqcaltrrcppegfdh  
rdsksvlqekncepvvpnappayeklsaeqspppysphhhhhh

Codons for the Melan-A sequence were changed so that the frequency of codon usage would match the codons naturally found in *E. coli* (Section 2.3.1). Compared to the original sequence (Section A6.1), the His-tag has been moved to the C-terminus and extraneous amino acids not part of the Melan-A protein were removed. This change created a smaller protein (Figure A6.3). Changing the position of the His-tag did not seem to alter any fermentation or purification yields.

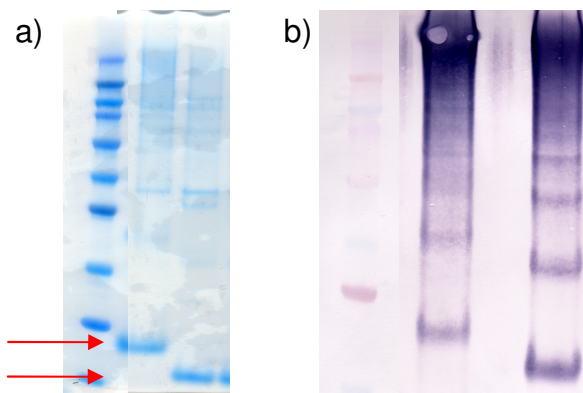


**Figure A6.3. SDS-PAGE and western blot of Melan-A and Syn-Melan-A.** a) SDS-PAGE and b) western blot of the previously produced Melan-A and the modified sequence. Syn-Melan-A is in the rightmost lanes. The former version had additional amino acids that were removed. See Blue Plus 2 molecular weight standard (Invitrogen) was used. Red arrows indicate the monomer bands.

#### ***A6.5. GroEL co-expression in Syn-Melan-A production***

A pGro7 plasmid (Takara, Madison, WI) was transformed into Syn-Melan-A C41 cells. These cells were cultured in 5 ml of complex fermentation batch medium in 50 ml conical tubes. Different cultures were supplemented with a 20% arabinose solution to a final concentration of 0.2%, 0.6%, 1.0%, 2.0%, and 4.0% (v/v).

Induction was performed with a final IPTG concentration of 2 mM. Although a western blot run with an anti-GroEL antibody (EMD Biosciences, San Diego, CA) confirmed the increased production of GroEL (Figure A6.4), no improvement in Melan-A expression or solubility was detected. Relative levels of GroEL and Melan-A produced were determined using ImageJ densitometry software.

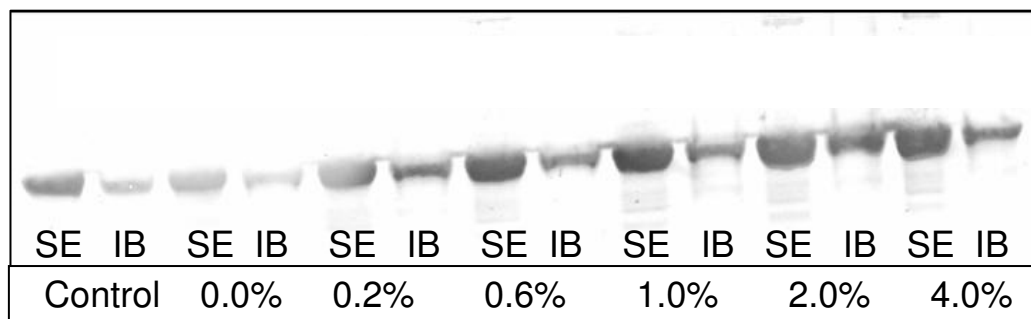


**Figure A6.4. Relative GroEL expression in Syn-Melan-A Gro7 cultures.** A Syn-Melan-A culture without the pGro7 plasmid was run as a control. Increasing arabinose up to 1% (v/v) more than tripled the expression of GroEL in the culture.

#### ***A6.6. Harvesting Conditions***

After high cell density *E. coli* fermentations of NY-ESO-1 and Syn-Melan-A, cells were harvested prior to centrifugation and lysis. Particularly on the manufacturing scale, the cells would be glucose-depleted and without pH, DO, and temperature control. A 2 L fermentation for each protein was evaluated in complex medium with and without the addition of 50 ml feed medium and with and without cooling the cells to 4 °C. Cells that did not receive cooling were removed from the

reactor and placed in a 37 °C incubator for 40 min. Cells that did receive cooling were brought down to 20 °C in the fermentor, which took 20 min, and placed in a 4 °C refrigerator for an additional 20 min. The two-step cooling procedure was used because cooling cells below the cloud point of Antifoam 204 would cause foaming in the reactor. In every combination of these harvest conditions, protein yields were identical as seen on SDS-PAGE (Figure A6.5).

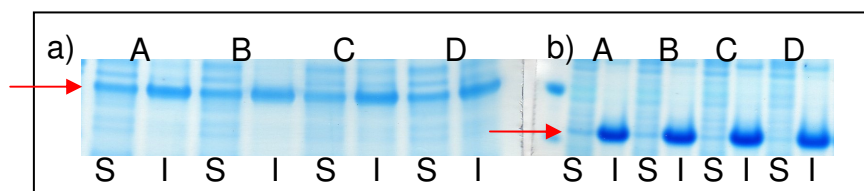


**Figure A6.5. SDS-PAGE of NY-ESO-1 and Syn-Melan-A under different harvesting conditions.** Soluble (S) and insoluble (I) fractions are indicated for a) NY-ESO-1 and b) Syn-Melan-A lysate samples. Condition A: feed added, no cooling, Condition B: no feeding, no cooling, Condition C: no feeding, 4 °C cooling, Condition D: feed added, 4 °C cooling. Red arrows indicate the respective bands.

#### A6.7. *Melan-A secretion in Pichia pastoris*

An attempt to produce Melan-A in *Pichia pastoris* was attempted. *P. pastoris* is a methylotrophic yeast that can reach high cell densities and secrete some proteins. If Melan-A could be secreted in *P. pastoris*, purification of the protein would be greatly simplified.

YPD (yeast extract peptone dextrose) plates were made using 1 M sorbitol and 15 g/L agar. Zeocin was added as the antibiotic to final concentrations of 100, 250, and 500 µg/ml. The pPICzαA plasmid was linearized by adding a 10 µl aliquot to 2 µl PmeI restriction enzyme, 0.5 µl 100x BSA, 5 µl Buffer 4, and 33 µl water. The DNA was precipitated with the addition of 5 µl 4 °C NaOAc and 100 µl of -20 °C ethanol. This mixture was divided into two aliquots and left at -20 °C overnight.

The precipitated DNA was centrifuged at 12,000 rcf for 15 min. Both pellets were each resuspended in 400  $\mu$ l of -20 °C 70% ethanol. After another centrifugation for 5 min, the supernatants were placed at 42 °C. X33 and Km71 *P. pastoris* cell banks were thawed, and 80  $\mu$ l aliquots were added to each washed DNA pellet. Each mixture was incubated in an electroporation cuvette for 5 min. Electroporation occurred using a BioRad Gene Pulser (Bio-Rad, Hercules, CA) at 1.50 kV, 200  $\Omega$ , and 25  $\mu$ FD. The mixture was then left at 30 °C for 2 hrs.

Plating was performed by adding a 50 ml drop of YPD and the transformed cell mixture onto sorbitol plates. For the Km71 cells, histidine was also added to the plate. BMM (buffered minimal methanol) plates were made by adding 50 ml 1 M potassium phosphate buffer pH 6.0, 50 ml 10x YNB (yeast nitrogen base), 1 ml 500x biotin, and 50 ml 10x (5%) methanol to a cooled, autoclaved solution of 345 ml water and 7 g agar. BMMH plates were BMM plates that also contained histidine. The BMM and BMMH plates were topped with a nitrocellulose membrane (Schleicher & Schuell, Keene, NH). Cells were lifted off of the YPD plates, imprinted on the BMM and BMMH plates, and incubated at 30 °C.

The nitrocellulose membranes were developed using western breeze reagents with an  $\alpha$ -Melan-A antibody. The Km71 cells did not secrete any Melan-A, and in future studies Km71H cells should be used instead for simplicity. The X33 cells did seem to produce some Melan-A (Figure A6.6a), so a select number of colonies were grown in liquid YPD medium. Methanol was added to induce protein production, and the cultures grew overnight at 16 °C. To analyze the intracellular fraction, glass beads in a breaking buffer were used. The secreted protein was precipitated with trichloroacetic acid (TCA) and ethanol ether and run on SDS-PAGE (Figure A6.6b,c). No Melan-A was found in either fraction.

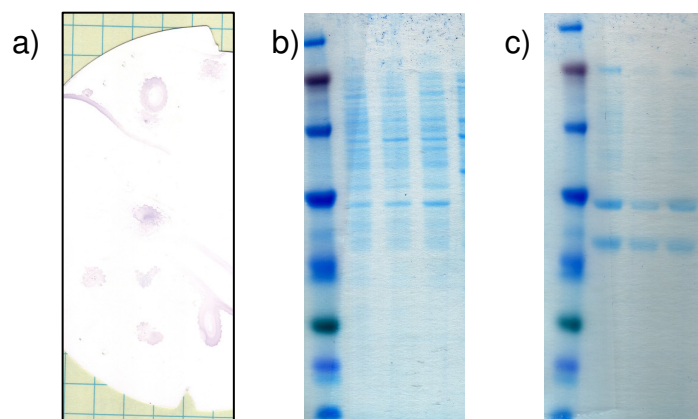


**Figure A6.6. Melan-A expression in *Pichia pastoris*.** a) Dot blot of Melan-A produced by X33 *Pichia* cells. Colonies were arranged in a matrix pattern on BMM plates. b) SDS-PAGE of intracellular Melan-A from *Pichia*. c) SDS-PAGE of extracellular Melan-A from *Pichia*.

## APPENDIX 7

### MELAN-A PURIFICATION PROCESS DEVELOPMENT

#### *A7.1. Melan-A clarification and solubilization*

##### *A7.1.1. Homogenization*

Cell pellets were resuspended to their original volume. The buffers used are described below. Pellets were thawed in a 37°C water bath for 10 min. If cell pellets were thawed in a 55°C water bath, they would become more viscous and difficult to resuspend. The cell pellets were then blended for several min at a speed low enough to prevent foaming. Lysate was created by sending the resuspended cell pellet through a homogenizer, as described in Section 2.6. The preparation of insoluble protein was evaluated for three different methods.

##### *A7.1.2. Insoluble protein preparation 1: pellet wash*

Cells pellets were resuspended in [50 mM Tris, 100 mM sodium chloride, pH 8.0]. The soluble protein fraction was separated from the insoluble protein fraction with a Sorvall centrifuge, described in Section 2.4.3. A GSA rotor was operated at 20,000 rcf. Insoluble protein pellets were resuspended and re-pelleted with [50 mM Tris base, 1% Tween-20, 0.5 M sodium chloride, 1 mM EDTA, pH 8.0] three times. It was assumed that the washed insoluble fraction consisted of only inclusion bodies (IBs). Unless otherwise specified, centrifugation-washed inclusion bodies were solubilized in [6 M guanidine hydrochloride, 4 M urea, 50 mM sodium phosphate, pH 7.5]. The solubilized inclusion bodies were centrifuged at 20,000 rcf once more to remove cell debris. The entire centrifugation-wash step could not be scaled-up, but



most of the Melan-A purification development work was performed with this starting material.

#### ***A7.1.3. Insoluble protein preparation 2: tangential flow filtration***

Cell pellets were resuspended in [50 mM sodium phosphate, 0.5 M sodium chloride, pH 7.5]. After lysis, the crude lysate was subject to a tangential flow filtration (TFF) wash, as performed with NY-ESO-1 (Section A4.2) with a 0.45  $\mu$ m membrane (Pall). The removal of Tween-20 from the wash buffer was being considered.

Melan-A inclusion bodies washed in [20 mM Tris, 300 mM sodium chloride, 1 mM EDTA] did not readily go through a 0.45  $\mu$ m membrane. If 1% Tween-20 was added to this buffer, inclusion bodies would still be retained. If 10 psi of back pressure was applied, however, a fraction of the inclusion bodies would cross the membrane. Additionally, if Tween-20 was added to the buffer while back pressure was being applied, additional Melan-A would pass through the filter (Figure A7.1).

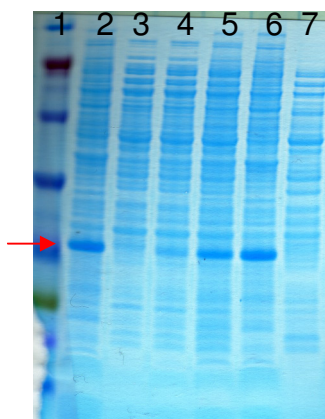


**Figure A7.1. SDS-PAGE of Melan-A fractions during tangential flow filtration.** Lane 1: Multimark, Lane 2: load, Lane 3: neutral permeate, Lane 4: permeate with back pressure, Lane 5: permeate with back pressure and Tween-20, Lane 6: retentate, Lane 7: permeate with Tween-20 only. A red arrow indicates the Melan-A band.

Unless otherwise specified, TFF-washed inclusion bodies were diluted in eight-fold in [8 M urea, 100 mM sodium phosphate, pH 7.5]. After an overnight solubilization, the protein was filtered through a 0.5  $\mu$ m Milligard Low Protein Binding (LPB) capsule filter (Millipore, Billerica, MA).

#### ***A7.1.4. Insoluble protein preparation 3: denaturant lysis***

Unless otherwise specified, denaturant lysis was performed by resuspending cell pellets in [7.5 M guanidine hydrochloride, 100 mM sodium chloride, pH 7.2]. Homogenization was conducted as normal. DNA and cell debris were pelleted using centrifugation at 4,000 rcf, in a SH-3000 rotor as described in Section 2.4.3. This low-force centrifugation could be scaled-up to the Powerfuge (Section A4.2). A gelatinous precipitate was removed, and the solubilized protein was filtered through a 0.5  $\mu$ m Milligard LPB capsule filter (Millipore).

#### ***A7.2. Melan-A immobilized metal affinity chromatography***

##### ***A7.2.1. Introduction***

The immobilized metal affinity chromatography (IMAC) column consisted of chelating sepharose FF resin (GE Healthcare, Piscataway, NJ) charged with a 2 M nickel sulfate solution. The two running buffers used for this column were IMAC A buffer [4 M urea, 50 mM sodium phosphate, 0.5 M sodium chloride, pH 7.5] and IMAC B buffer [4 M urea, 50 mM phosphoric acid, 0.5 M sodium chloride, 0.5 M imidazole, pH 7.5]. IMAC B buffer was diluted with IMAC A buffer in different proportions to gradually increase the imidazole concentration in the running buffer.

#### ***A7.2.2. Soluble Melan-A capture attempts***

Initial IMAC runs attempted to purify the soluble fraction of Melan-A protein. In these cases, no urea was added to either IMAC buffer. The column was equilibrated with 2 column volumes (CV) of urea-less IMAC A buffer and loaded with 2 ml of solubilized IBs per ml total column resin. A 1 ml prepacked HisTrap column (GE Healthcare, Piscataway, NJ) was used. The loaded column was flushed with 8 CV of urea-less IMAC buffer A and then washed with 2.5 CV each of 10%, 20%, 30%, and 100% urea-less IMAC B buffer. Based on Bradford, it was found the protein that flowed through the column during the loading stage had a concentration of 34.0 mg/ml. A 3.2 mg/ml protein solution left the column during the 10% B wash, a 0.7 mg/ml solution left during the 20% B wash, and no protein left the column in the 30% and 100% washes. A more refined step gradient washed the bound protein with 2.5 CV each of 1%, 2%, 3%, 4%, 5%, and 20% urea-less IMAC B buffer. The protein concentrations leaving the column during the 1%, 2%, and 3% washes were 0.7, 3.3, and 2.4 mg/ml, respectively. No protein was found in any of the latter buffer washes.

This inconsistency of the protein concentrations during the imidazole washes and the low concentrations of imidazole needed for these washes suggests that the eluted protein was only weakly attached with non-specific binding. As seen by SDS-PAGE, Melan-A did not bind to the IMAC column and was found only in the flowthrough fraction (FigureA7.2). The most possible explanation for this is that the folded Melan-A may bury its His tag. Changing the terminus where the His tag is located may prevent this phenomenon.

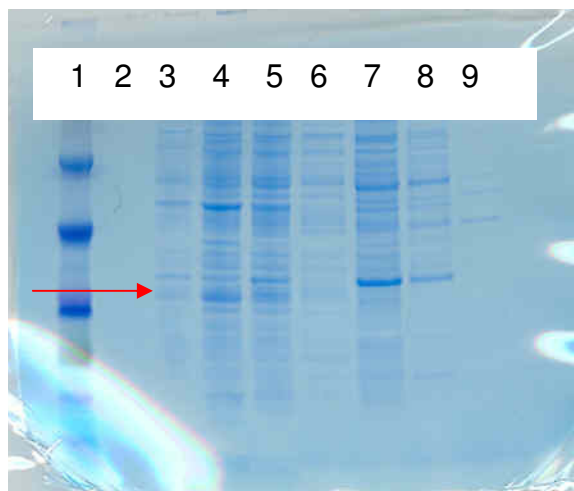


**Figure A7.2. SDS-PAGE of soluble Melan-A capture attempt on a nickel column.**

Lane 1: Multimark, Lane 3: load, Lane 4: flowthrough, Lane 5: chase, Lane 6: pre-elution, Lane 7: 50 mM imidazole wash, Lane 8: 100 mM imidazole wash, Lane 9: 150 mM imidazole wash. Melan-A is indicated by the red arrow.

#### ***A7.2.3. Insoluble Melan-A capture***

Using the same protocol as for the soluble Melan-A (Section A6.2.2) with the centrifugation-washed inclusion bodies (Section 6.1.2), total protein concentrations of the elution were 1.31, 0.64, 0.07 mg/ml during 33%, 66%, and 100% washes of IMAC B buffer with urea. A linear gradient was used to determine the optimal dilution of IMAC B buffer in IMAC A buffer to elute the Melan-A protein. It was estimated that Melan-A could be retained on the column using a 40% IMAC B buffer wash.

Using a 50 ml self-packed column, three separate runs were performed to determine the effectiveness of using a 30%, 40%, and 50% IMAC B buffer low imidazole wash. It was determined with SDS-PAGE that some Melan-A was lost in the 40% and 50% washes, but none was lost in the 30% wash (Figure A7.3). Total protein concentrations of the elutions from the 30%, 40%, and 50% runs were 1.11, 0.86, and 0.40 mg/ml, respectively. This indicated that a 30% wash was advantageous over higher washes in maintaining higher protein yields.

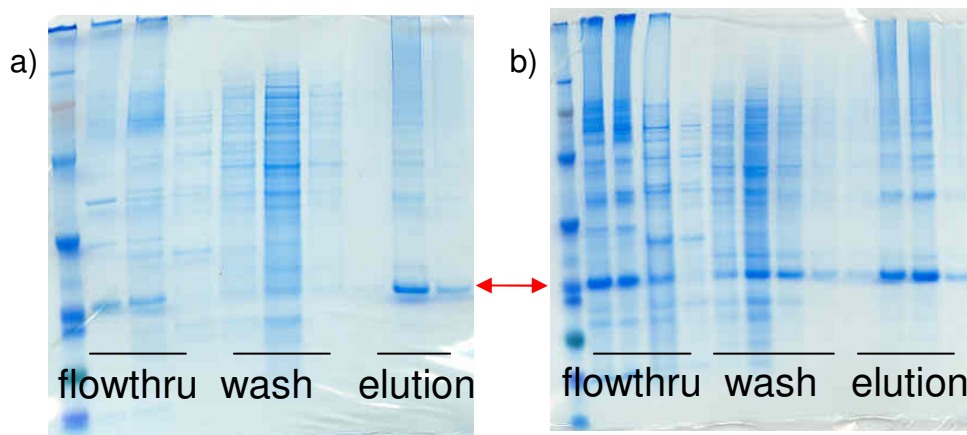


**Figure A7.3. SDS-PAGE of insoluble Melan-A capture on a nickel column.** Both gels are labeled with a Multimark (Invitrogen) standard and show flowthrough, low imidazole wash, and elution fractions. The a) 150 mM low imidazole wash run was able to lose less Melan-A than the b) 200 mM low imidazole wash run in the low imidazole wash fraction. Melan-A is indicated by the red arrow.

When further wash studies were performed and analyzed using a western blot, it was determined that a 15% IMAC B buffer low imidazole wash was needed in the low imidazole wash to prevent any detectable loss of Melan-A (Figure A7.4). A chromatogram with this final process change is shown in Figure A7.5.

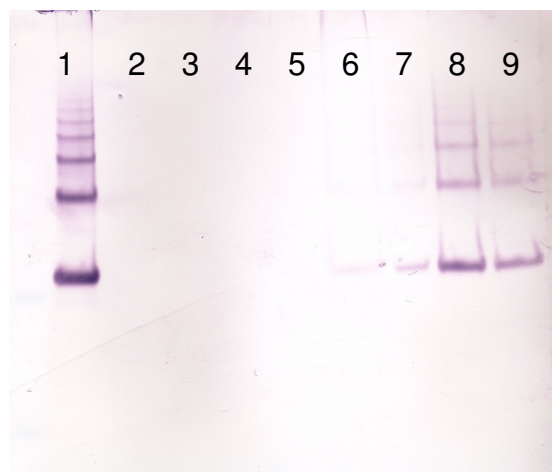


**Figure A7.4. Western blot of low imidazole washes of Melan-A on a nickel column.** Lane 1: load, Lane 2-9: eluates of increasing imidazole concentrations – 25, 50, 75, 100, 125, 150, 175, 200 mM. A faint band can be detected at 125 mM.

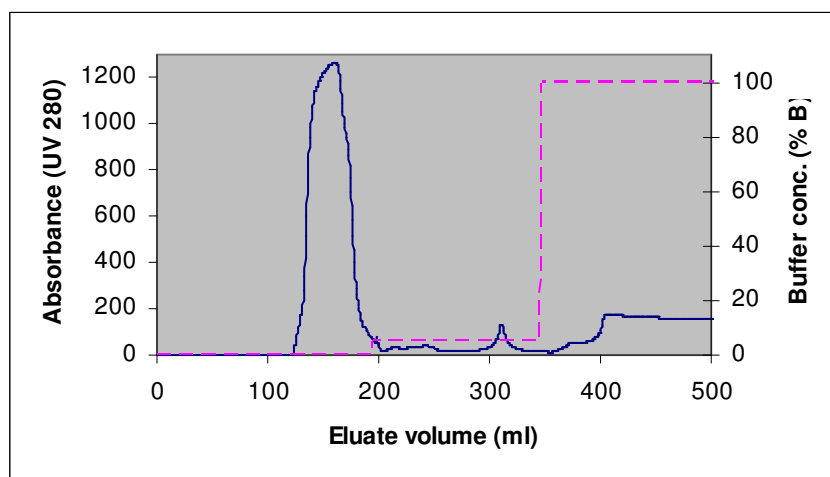


**Figure A7.5. Chromatogram of Melan-A on a nickel column.** The flowthrough, low imidazole, and imidazole peaks are shown at approximately 150, 310 and 375 ml, respectively. Solid blue line shows the ultraviolet absorbance measured at 280 nm. The dotted pink line is the percentage of IMAC buffer B in the inlet buffer. Baseline absorbance increases post-elution because of imidazole's innate UV absorbance.

Since the centrifugation step for this initial Melan-A development could not be scaled-up, a tangential flow filtration step was used (Section A7.1.3). Mimicking the NY-ESO-1 process (Section A4.2), a [8 M urea, 100 mM sodium phosphate buffer] was attempted used for Melan-A solubilization, and almost no Melan-A was recovered post-IMAC. It was found that Melan-A IMAC recovery was very dependent on high levels of strong denaturing agents. To maximize denaturing agent, the cell pellet was resuspended directly in solubilization buffer (Section A7.1.4). In general, protein yields could be maximized by using higher levels of guanidine and avoiding the inclusion body wash steps (Figure A7.6). Although some contaminating proteins were removed during the wash steps, the final purity of the IMAC elution was the same regardless of load preparation method.

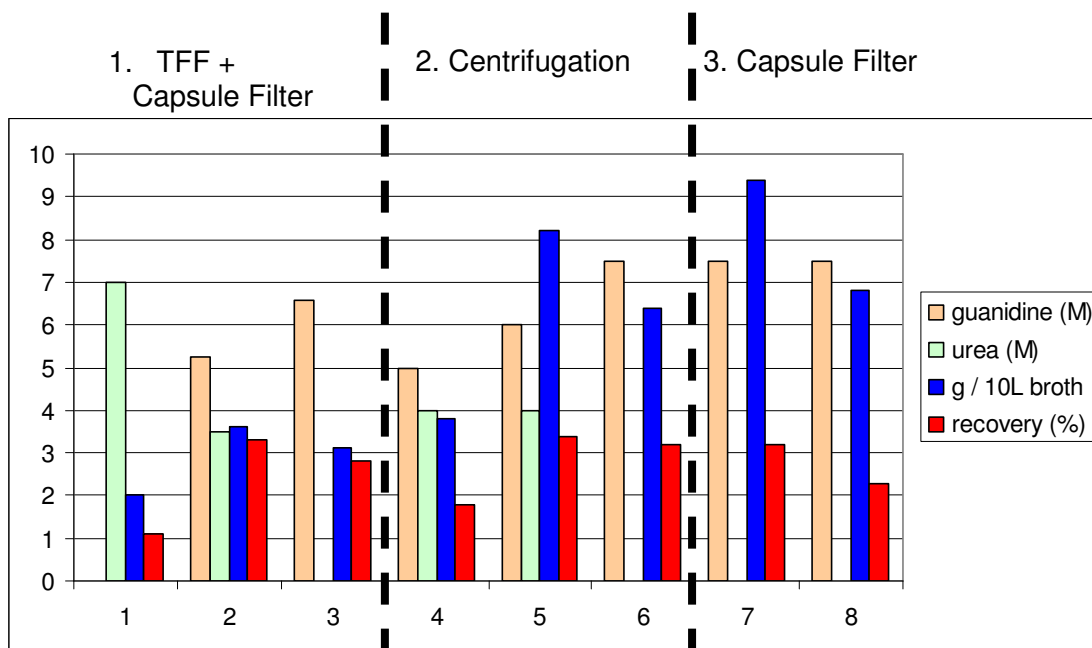


**Figure A7.6. Melan-A recovery on nickel column with different load preparations.** Load material was either washed using TFF and filtered, washed with centrifugation, or lysed in denaturant and filtered. Higher concentrations of denaturant were possible with the latter method and improved Melan-A recovery.

#### A7.2.4. Melan-A Refolding

Refolding was attempted in the IMAC column by loading the column and washing it with 2 CV of buffers containing 2.0, 1.0, and 0.5 M urea. As with previous runs, some of the protein flowed through the column during loading. Very little protein was found in the elution fractions. Bradford determined the total protein concentration of the elution fraction to be 0.10 mg/ml. It is possible that protein bled off of the column in undetectable concentrations while the protein was being refolded.

In a related study, Melan-A inclusion bodies were solubilized in [3 M urea, 100 mM sodium phosphate, 0.5 M sodium chloride, pH 7.5]. The total protein concentration of the load was 27.6 mg/ml. The flowthrough and wash concentrations were 11.9 and 2.5 mg/ml, respectively. The elution concentration was 0.1 mg/ml.

Most of the recovered Melan-A band was in the flowthrough fraction (Figure A7.7).

The implication is that Melan-A must be in high concentrations of chaotropic agents to bind and stay bound to the IMAC column.

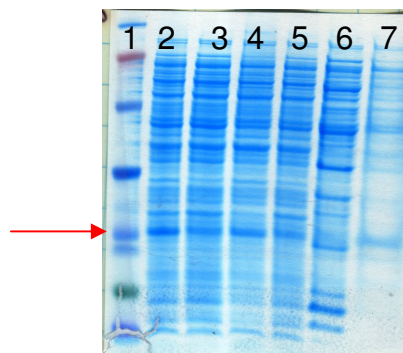


**Figure A7.7. SDS-PAGE of Melan-A capture on nickel column in 3 M urea.** Lane 1: Multimark (Invitrogen), Lane 2: load, Lane 3-4: flowthrough, Lane 5: wash, Lane 6: pre-elution, Lane 7: elution. Melan-A is indicated by the red arrow.

#### **A7.2.5. Cobalt column**

Instead of using nickel, the chelating sepharose FF resin could also be charged using cobalt. A 50 ml column was charged and purification was performed on solubilized Melan-A inclusion bodies. Melan-A did bind and elute off the cobalt column very similarly as it had done with the nickel column. Since there was no obvious advantage (Figure A7.8), this method was not investigated any further.

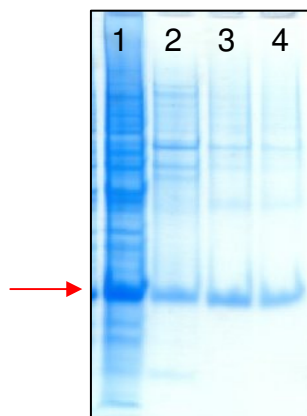


**Figure A7.8. SDS-PAGE of Melan-A purified on a cobalt column.** Lane 1: load, Lane 2: chase, Lane 3: pre-elution, Lane 4: elution. A red arrow indicates Melan-A.



### ***A7.3. Melan-A ion exchange chromatography***

Since the isoelectric point (pI) of Melan-A with a His-tag was calculated to be 8.65, it was decided to use a 10.5 carbonate buffer to bind the protein to an anion exchange (AXC) column and a 6.0 phosphate buffer to bind the protein to a cation exchange (CXC) column. The Ion Exchange (IEX) A buffer was [4 M urea, 20 mM carbonate, pH 10.5]; IEX B buffer was [4 M urea, 20 mM carbonate, 1 M sodium chloride, pH 10.5]; IEX C buffer was [4 M urea, 20 mM sodium phosphate, pH 6.3]; IEX D buffer was [4 M urea, 20 mM sodium phosphate, 1 M sodium chloride, pH 6.3]. A diafiltration step was performed using a 10 kDa Minimate cassette (Millipore, Billerica, MA) to buffer exchange the IMAC elution to IEX A or IEX C buffer.

Q HP and SP HP (GE Healthcare, Piscataway, NJ) columns were used for AXC and CXC, respectively. As expected, Melan-A in IEX A buffer bound to the Q HP column and Melan-A in the IEX C buffer bound to the SP HP column. Interestingly, the Melan-A in IEX C buffer at pH 6.3 also bound to the Q HP column. In all cases, some Melan-A was lost in the flowthrough fraction. The bound Melan-A could be eluted by changing the buffer pH, such as by increasing the IEX A to IEX C ratio on a SP HP column (Figure A7.9a). Bound Melan-A could also be eluted by increasing the salt concentration, such as increasing the IEX D to IEX C buffer ratio on a Q HP column (Figure A7.9b, Figure A7.10).

Q XL chromatography was later developed to be an endotoxin removal step for Melan-A [141]. A pH of 9.3 was necessary to dissociate the endotoxin from the positive charge of the Melan-A protein. The SP HP column could not be used for this process because the endotoxin would bind and elute off the column with the protein.

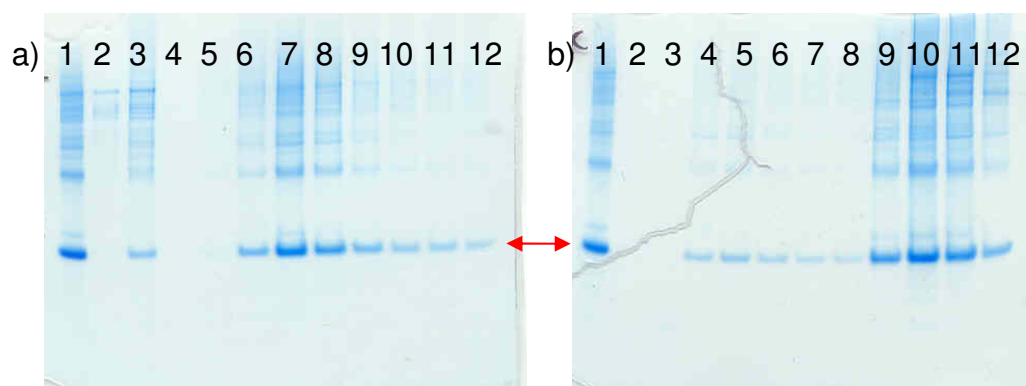


**Figure A7.9. SDS-PAGE of Melan-A purified on ion exchange columns.** a) Melan-A at pH 6.3 was eluted off a SP HP column with increasing pH. Lane 1: load, Lane 2-4: flowthrough, Lane 5-10: pH 6.85, 7.32, 7.86, 8.35, 8.79, 9.33, 10.37 washes. Lane 12: 1 M sodium chloride wash. b) Melan-A at pH 6.3 was eluted off a Q HP column with increasing salt at constant pH. Lane 1: load, Lane 2-7: flowthrough, Lane 8-12: 10, 15, 25, 30, 40 mM sodium chloride washes. The Melan-A band is indicated by a red arrow.

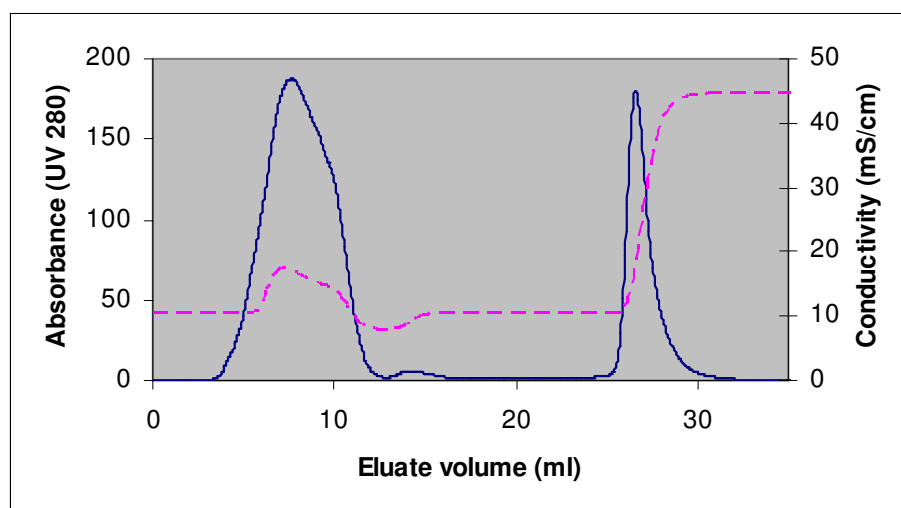


**Figure A7.10. Chromatogram of Melan-A on an ion exchange column.** Melan-A at pH 6.3 was eluted off of an ion exchange column with a single step gradient of salt. The solid blue line shows the eluate absorbance at 280 nm. The dotted pink line is the conductivity of the eluate. Protein is both lost in the flowthrough and eluted with the salt.

#### ***A7.4. Melan-A hydrophobic interaction chromatography***

Hydrophobic interaction chromatography (HIC) was investigated for use with Melan-A. A 500 g/L ammonium sulfate solution was made. This solution was added to the Melan-A IMAC elution to entice the exposure of hydrophobic groups while Melan-A was being loaded onto a Phenyl HP column (GE Healthcare). The protein was eluted using a gradient that removed the ammonium sulfate. All buffers contained [4 M urea, 100 mM sodium phosphate, 0 to 1 M ammonium sulfate, pH 7.5]. Even though loading with a 0.40 M ammonium sulfate concentration allowed Melan-A to bind to the Phenyl column and no protein was detected in the flowthrough on SDS-PAGE, increasingly better yields were obtained in the elution when 0.56, 0.63, and 0.76 M ammonium sulfate was used. At 0.87 M ammonium sulfate, there was visible cloudiness in the load material from precipitated protein, and protein yields were lower. Therefore the optimum ammonium sulfate concentration for Melan-A was estimated to be approximately 0.75 M (Figure A7.11). Unfortunately there was no improvement in Melan-A purity after binding and eluting to the Phenyl column.

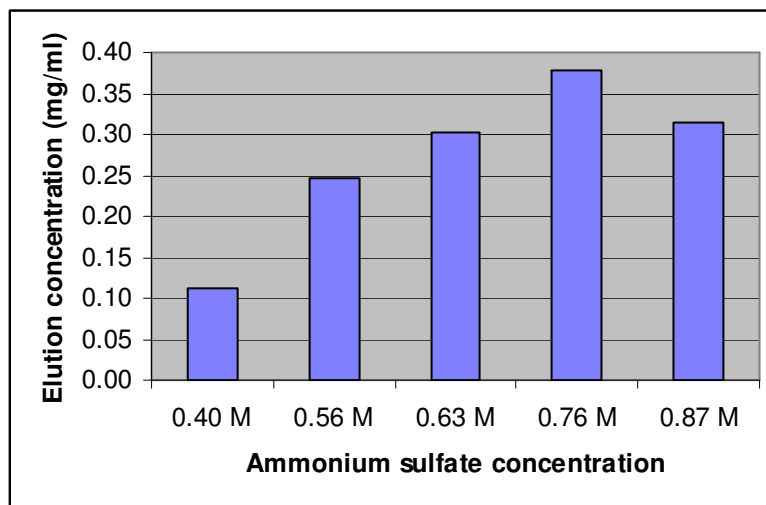


**Figure A7.11. Ammonium sulfate dependence of Melan-A binding on a Phenyl column.** Increasing concentrations of ammonium sulfate increased Melan-A recovery, but protein precipitation resulted in worse recovery at 0.87 M.

Sodium chloride was added to the Melan-A protein instead of ammonium sulfate in one case. A 5.17 M solution of sodium chloride was added to Melan-A until it precipitated. This occurred at 3.10 M sodium chloride. A successful HIC step was performed using a final concentration of 2.58 M sodium chloride. Again, the Melan-A protein could be bound and eluted off the Phenyl column, but it did not get separated from any of the contaminating proteins.

For purification of the cancer antigen SSX2, eluting with a 30 column volumes (CVs) gradient was able to separate the protein of interest from its impurities [142]. Melan-A was eluted using 30 CVs, but no purification advantage was gained (Figure A7.12).

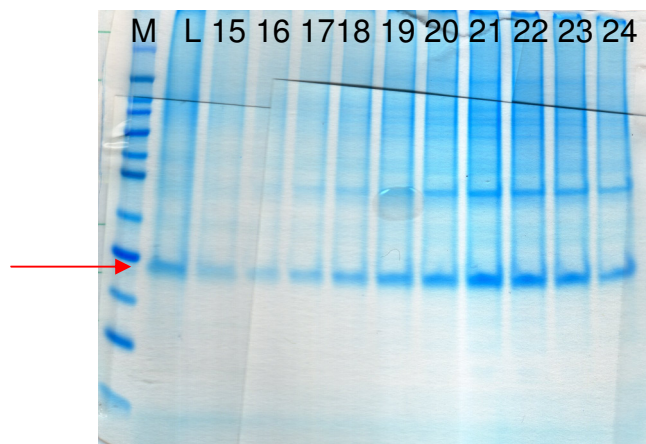


**Figure A7.12. SDS-PAGE of Melan-A purified on phenyl column.** M: Sharp molecular weight standard (Invitogen), L: load, Lane 15-24: fractions taken from 15-24 CV of the elution gradient. A red arrow indicates the Melan-A band.

#### ***A7.5. Melan-A size exclusion chromatography***

Size exclusion chromatography (SEC) was also attempted to purify Melan-A after IMAC capture. A Superdex 200 PG (GE Healthcare) column was used. The loading buffer was [4 M urea, 50 mM sodium phosphate, 0.15 M sodium chloride]. Sodium chloride was added upon the manufacturer's recommendation to prevent

nonspecific binding. Melan-A eluted early and did not gain any purity (Figure A7.13), suggesting that it was aggregated with the higher molecular weight contaminants. These results are consistent with results of HPLC analysis (Section A1.1).

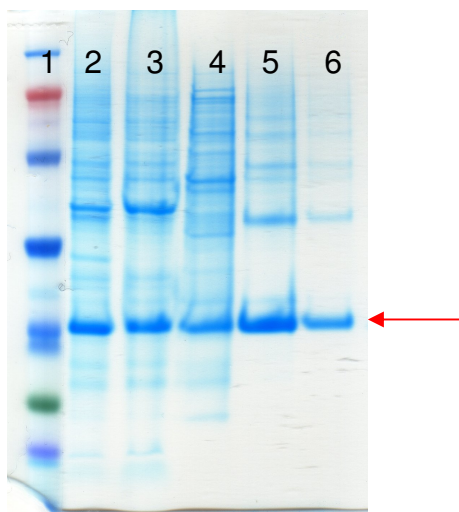


**Figure A7.13. SDS-PAGE of Melan-A fractions through IMAC and SEC.** Lane 1: Multimark, Lane 2-3: solubilized inclusion bodies, Lane 4: wash, Lane 5: IMAC elution, Lane 6: SEC eluate. The Melan-A band is indicated by a red arrow.

#### ***A7.6. Identification of contaminating proteins***

Some of the higher molecular weight protein contaminants of both Melan-A and NY-ESO-1 were isolated by SDS-PAGE and submitted to the Cornell Biotechnology Resource Center (BRC) for mass spectrometry identification. The contaminants included dimers of the respective proteins, elongation factor thermo unstable (EF-Tu), 50S ribosomal protein L2, glutamine synthetase,  $\beta$ -galactosidase, ClpB, and DnaK.

It was somewhat expected to find chaperone proteins associated with the proteins. DnaK, GroEL, and EF-Tu are the three most abundant proteins in *E. coli*. Chaperones bind to the protein while it is forming into inclusion bodies. DnaK and GroEL have been imaged on the peripheral and middle of inclusion bodies,

respectively [143]. EF-Tu is a DnaK substrate also very commonly found in inclusion bodies [144] and ClpB works with DnaK to disassemble these aggregates.  $\beta$ -galactosidase was also normal because its activity is induced by IPTG.

Western blotting was performed to confirm the presence of DnaK and GroEL in both purified Melan-A, NY-ESO-1, and SSX2. DnaK was detected in the final purified product of all three proteins. GroEL was only found in the final Melan-A and NY-ESO-1 products. According to western blotting, the GroEL in the SSX2 inclusion bodies was removed during the SSX2 HIC step [142]. Melan-A and NY-ESO-1 are hydrophobic proteins, so the chaperones are more likely to interact tightly with them.

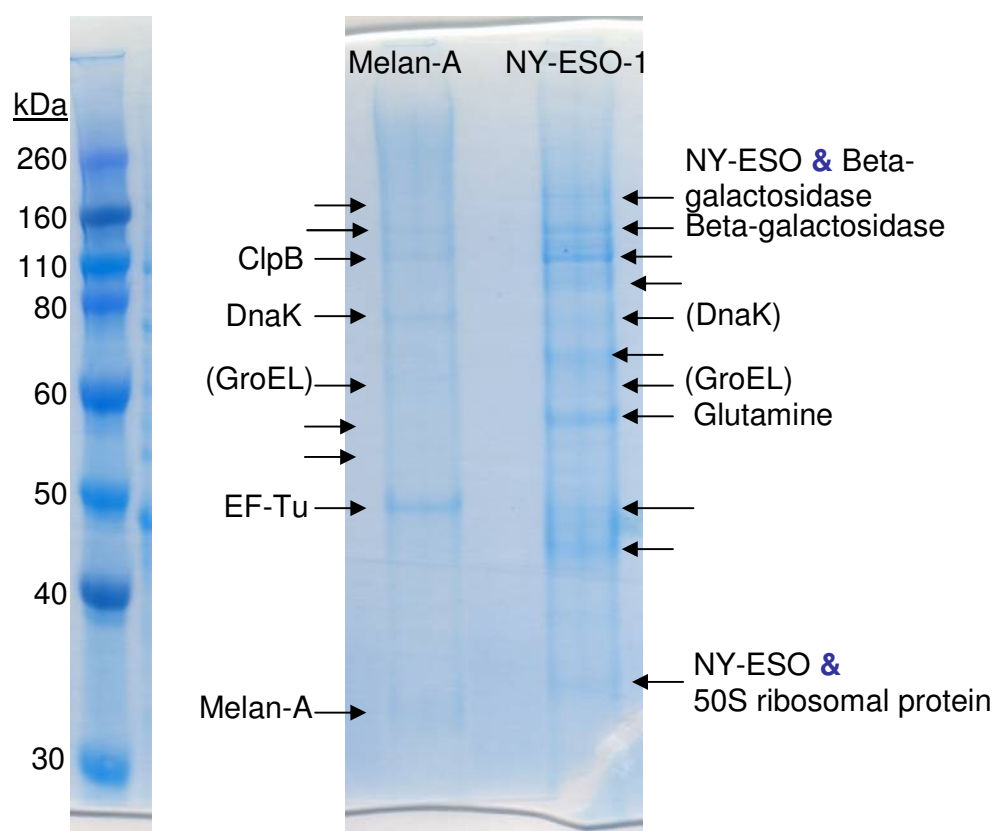


**Figure A7.14. SDS-PAGE of higher molecular contaminants in bulk Melan-A and NY-ESO-1 drug substance.** Most proteins were identified with mass spectroscopy. Proteins labeled within parenthesis were identified using a western blot.

### A7.7. Influence of reducing agent

Melan-A has five cysteine residues and thus is capable of forming disulfide bonds with itself and other proteins with free cysteine groups. Disulfide bonds cannot be formed in reducing conditions, such as in the presence of dithiothreitol (DTT) or  $\beta$ -mercaptoethanol. To make free cysteine groups inaccessible for bond formation, iodoacetamide can be used. Using an established protocol [145], a set of proteins including Melan-A were separately incubated in 20 mM DTT and 100 mM iodoacetamide. Samples were left at 65 °C for 1 hr. SDS-PAGE analysis shows that all of the proteins tested were far more aggregated in the presence of no reducing agent (Figure A7.15a). The presence of iodoacetamide, which is confirmed by a slight increase in molecular weight of conjugated samples, was not necessary. The level of reducing agent also did not seem to make a difference (Figure A7.15b).

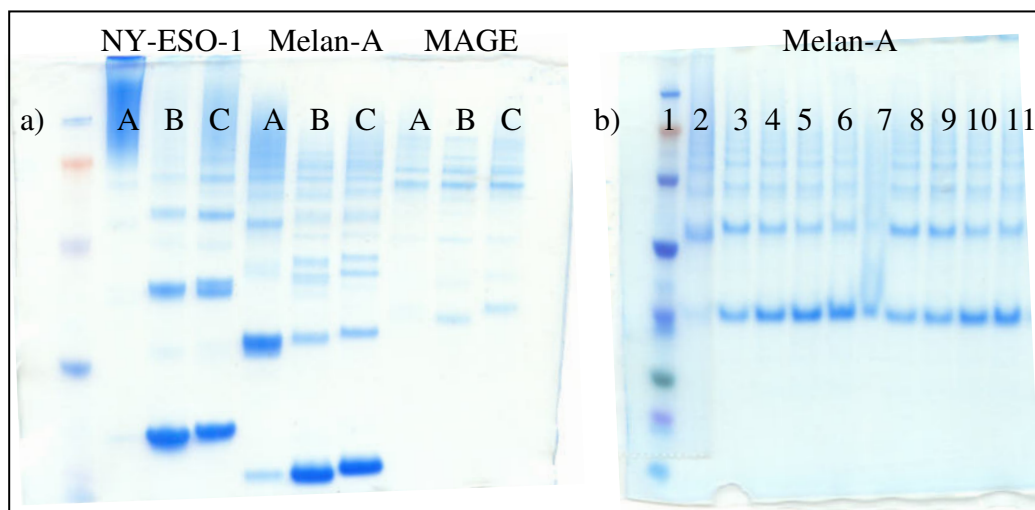


**Figure A7.15. SDS-PAGE of cancer antigens with and without reducing agent.** a) NY-ESO-1, Melan-A, and MAGE were run on an SDS-PAGE A) with no reducing agent, B) with 20 mM DTT, C) with 20 mM DTT and 100 mM iodoacetamide. b) Melan-A was loaded on a gel with increasing concentrations of  $\beta$ -mercaptoethanol and DTT. Lane 2: no reducing agent, Lane 3-7: 10 mM, 100 mM, 5%, 20%, 45%  $\beta$ -mercaptoethanol, Lanes 8-11: 1 mM, 10 mM, 100 mM, 45% DTT.

#### ***A7.8. Additives to improve Melan-A purification***

Detergents were used in an attempt to separate the hydrophobic interactions between Melan-A and its protein contaminants. In two separate cases, 1% Tween-20 or Triton-100 was added to the IMAC running buffers. The addition of 1% Tween-20 was also performed on an ion exchange column. In all cases, there was no noticeable difference compared to operating with the original buffers that did not contain detergent. This is consistent with the addition of SDS to the HPLC Melan-A load and running buffer (Section A1.1).

The use of reducing agents was also evaluated. The addition of 1 mM  $\beta$ -mercaptoethanol in all of the running buffers was ineffective in improving purity during the TFF wash or IMAC, IEX, or HIC columns. The  $\beta$ -mercaptoethanol concentration was increased to 10 mM in the HIC buffers, but this did not have any noticeable effect. Using 5 mM DTT was also ineffective in improving Melan-A purity during ion exchange. Using 5 mM DTT in the IMAC buffers was not possible because the reducing agent precipitated the nickel and turned the column black.

The addition of EDTA was also evaluated. During IEX, 40 mM EDTA was added to the load and running buffers. Likewise, the addition of 10 mM EDTA to the HIC buffers was not effective. Using 10 mM EDTA in the IMAC buffers was not possible because this low concentration of EDTA was enough to strip the nickel off of the column.

#### ***A7.9. Final Melan-A purification process***

In summary, Melan-A cell pellets were lysed in [7.5 M guanidine hydrochloride, 100 mM sodium phosphate, pH 7.2] and centrifuged to remove DNA and cell debris. The material was filtered through a 0.5  $\mu$ m filter (Millipore) and loaded onto an IMAC column with [4 M urea, 100 mM sodium phosphate, 0-500 mM



imidazole, pH 7.2]. Ammonium sulfate was added, and the protein was eluted off of a HIC column. The product was then buffer exchanged into [4 M urea, 100 mM sodium phosphate, pH 9.3] and sent through a Q XL column.

A 2 L fermentation was conducted for a prototype run. The packing flow rates of the columns were 650, 750, and 580 ml/min for a 10 cm column for chelating sepharose fast flow, Phenyl sepharose high performance, and Q sepharose fast flow resins. Packing rates were scaled down using constant linear flowrates. Total protein yields per liter of fermentation broth were 329, 167, and 156 mg after the IMAC, HIC, and Q XL columns, respectively. The protein fractions are visualized in Figure A7.16.

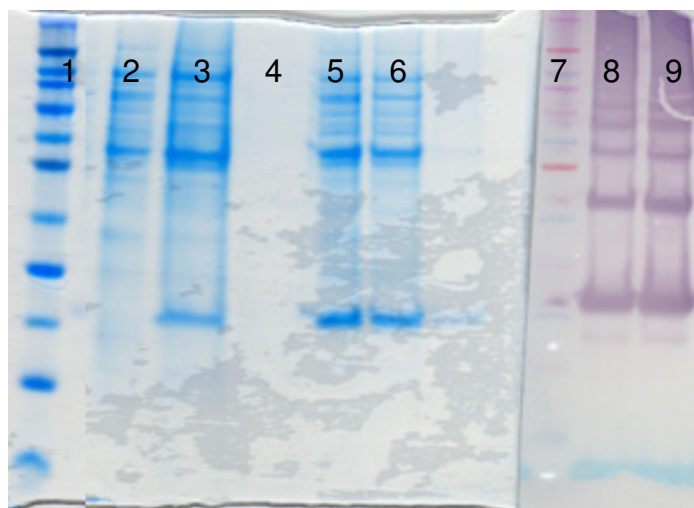


**Figure A7.16. SDS-PAGE and western blot of Syn-Melan-A during final purification process.** Lane 1, 7: See Blue Plus 2 Marker (Invitrogen), Lane 2: IMAC imidazole wash, Lane 3: IMAC elution, Lane 4: HIC flowthrough, Lane 5, 8: HIC elution, Lane 6, 9: Q XL flowthrough.

## REFERENCES

- 141) R. Chen, C. Huang, B. Newton, G. Ritter, L. Old, C. Batt, Factors affecting endotoxin removal from recombinant therapeutic proteins by anion exchange chromatography, *Prot. Expr. Purif.* 64 [2009] 76-81.
- 142) C. Huang, R. Chen, T. Vannelli, F. Lee, E. Ritter, G. Ritter, L. Old, C. Batt, Expression and purification of the cancer antigen SSX2: a potential cancer vaccine, *Prot. Expr. Purif.* 56 [2007] 212-219.
- 143) M. Carrió, A. Villaverde, Localization of chaperones DnaK and GroEL in bacterial inclusion bodies, *J. Bacteriol.* 187 [2005] 3599-3601.
- 144) A. Malki, T. Caldas, A. Parmeggiani, M. Kohiyama, G. Richarme, Specificity of elongation factor EF-TU for hydrophobic peptides, *Biochem. Biophys. Res. Commun.* 296 [2002] 749-754.
- 145) M. Crow, N. Karasawas, A. Sarris, Protein aggregation mediated by cysteine oxidation during the stacking phase of discontinuous buffer SDS-PAGE, *BioTechniques* 30 [2001] 311-316.

## APPENDIX 8

### MELAN-A SECONDARY STRUCTURE

#### *A8.1. Predicted secondary structure*

The Melan-A amino acid sequence was used to predict the protein's secondary structure using the Advanced Protein Secondary Structure Prediction Server (Chandigarh, India). Most of the protein was predicted to be a random coil, but the main hydrophobic region of the sequence was predicted to be an alpha helix. In the sequence shown, the highlighted, bold amino acid residues were predicted to be part of an alpha helix:

mpredahfiygyppkkghghsytt**aeccaagigiltvilgvliligcwycrr**ngyr**almdkslh**vg**h**gtqcaltrrcpgegfd  
hrdskvslqekncepvpnpappay**ek**lsaeqspppyspaa**aleh**hhhhh

#### *A8.2. Sample preparation*

Syn-Melan-A lysate was washed using tangential flow filtration. The retentate was kept as a representative sample of the inclusion bodies. The inclusion bodies were pelleted at 12,000 rcf and resuspended in Dialysis Buffer [20 mM sodium phosphate, pH 7.1]. This first sample was representative of Syn-Melan-A inclusion bodies.

After solubilization and purification through an IMAC column, the Syn-Melan-A in [4 M urea, 100 mM sodium phosphate, 0.5 M imidazole, pH 7.5] was subject to dialysis using a 20 kDa Slide-A-Lyzer® unit (Thermo Fisher Scientific, Waltham, MA) into Dialysis Buffer. Only 0.75 ml of IMAC elution sample was dialysed in 4 L of Dialysis Buffer that was gently mixed with a stir bar overnight. This second sample was representative of refolded Syn-Melan-A.

### A8.3. Circular Dichroism

Circular dichroism (CD) was performed on Syn-Melan-A samples using a CD spectrophotometer (Aviv Biomedical, Lakewood, NJ). CD-400 software was used to operate the system. Samples were diluted to 0.02-0.2 mg/ml to accommodate the system. The spectra of Syn-Melan-A inclusion bodies and refolded protein were measured.

The characteristic curve for an alpha helix has minima at approximately 208 and 225 nm during CD. The characteristic curve for a beta sheet has a minimum at 217 nm. Although the two minima for an alpha helix are not visible, the curve shown in Figure A8.1 does have an extended minimum which is not at 217 nm. It was suspected that both Syn-Melan-A inclusion bodies and refolded protein formed alpha helices.

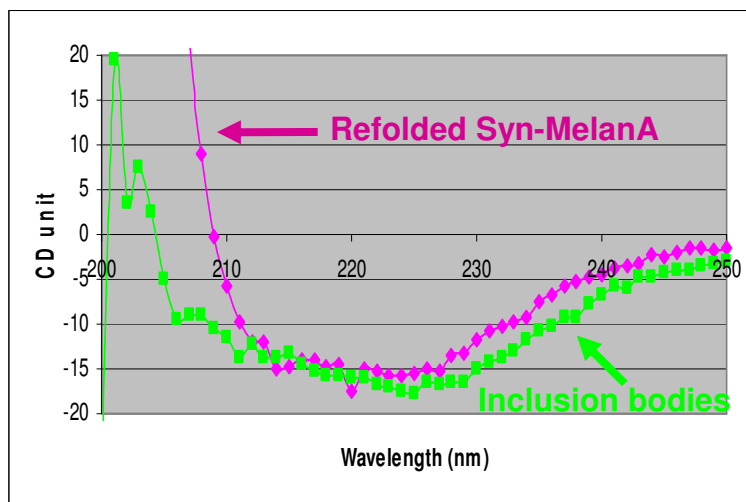


**Figure A8.1. Circular dichroism spectra of Syn-Melan-A inclusion bodies and refolded protein.** CD spectra were measured from 200 to 250 nm. The broad minima of the spectra suggest both Syn-Melan-A samples contained alpha helices.

### A8.4. Fourier transform infrared spectroscopy

Fourier transform infrared spectroscopy (FTIR) was also used to determine the secondary structure of Syn-MelanA. A Vertex80V FTIR spectrophotometer (Bruker

Optics, Billerica, MA) was used to measure the FTIR spectra of Syn-Melan-A inclusion bodies and refolded protein from 400 to 4,000 nm (Figure A8.2). A 1 ml aliquot of each sample was loaded into a liquid cell. The spectrum of water taken and subtracted from all measured spectra.

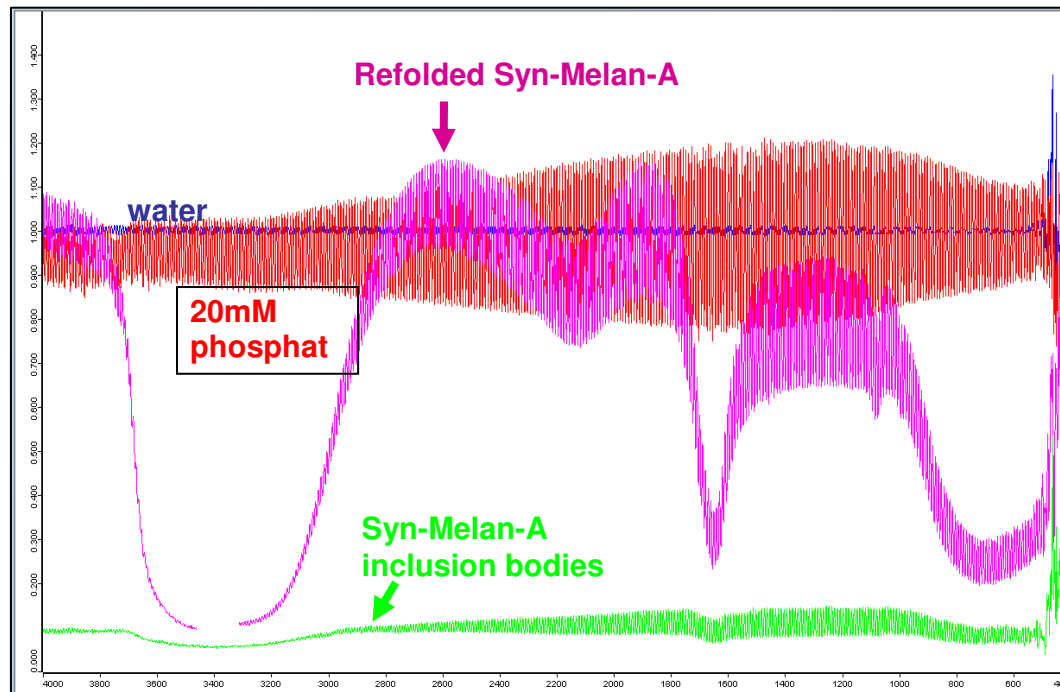


**Figure A8.2. FTIR spectra of Syn-Melan-A inclusion bodies and refolded protein.** FTIR spectra were determined from 400 to 4,000 nm. All samples were blanked with the spectrum from water.

As seen in Figure A8.3, both Syn-Melan-A samples have a minimum at 1650 nm. Minima from 1620 to 1640 nm typically suggest beta sheet structures, but minima from 1650 to 1658 nm suggest alpha helices. The FTIR data therefore also suggested that the secondary structure of Syn-Melan-A inclusion bodies and refolded protein were both alpha helices.

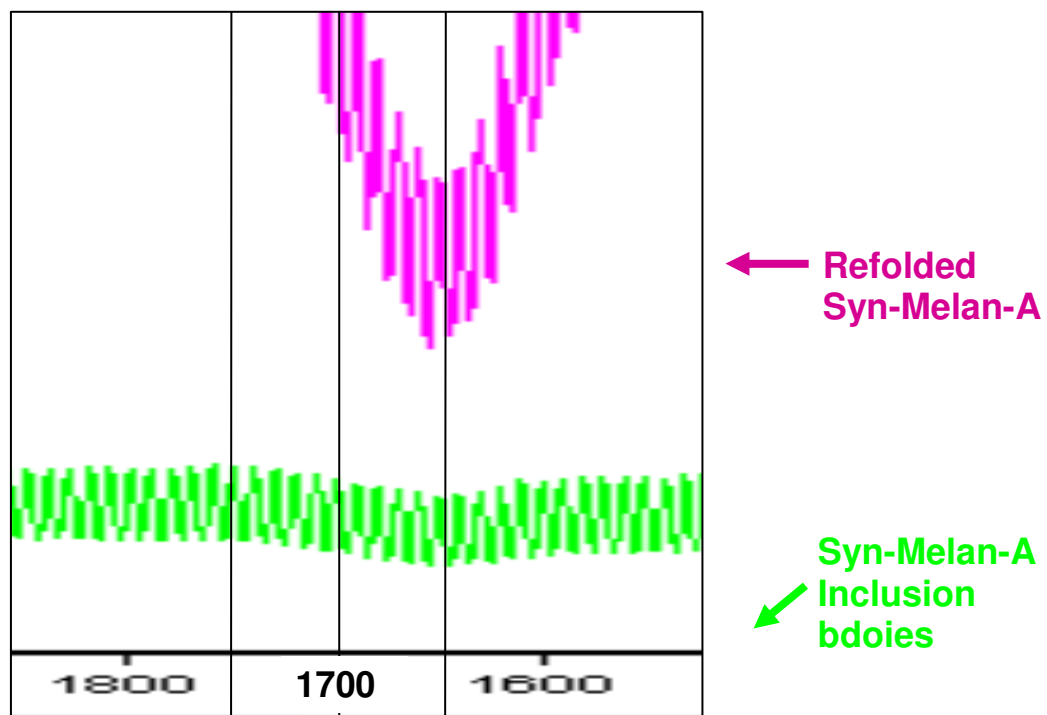


**Figure A8.3. FTIR spectra of Syn-Melan-A inclusion bodies and refolded protein, enlarged.** Both Syn-Melan-A samples had a minimum at 1650 nm, suggesting that they contained alpha helices.

## APPENDIX 9

### QUORUM SENSING STUDY

#### ***A9.1. Introduction to autoinducer 2***

Process development at the cellular level aims at increasing expression of the inserted plasmid. Cell-to-cell communication becomes an important factor because gene transcription is strongly regulated with intercellular signal molecules. The relevant bacterial phenomenon that occurs at high cell density is quorum sensing. Quorum sensing refers to the effect that the presence of an individual cell has on its neighbors. The chemical signals involved in quorum sensing have been named autoinducers. Since every cell regularly secretes these signals, the autoinducer concentration in growth medium has been described as the bacteria's biological measure of cell density. As with a number of bacterial species, *E. coli* has been found to use a furanoyl borate diester known as autoinducer 2 (AI-2) as a primary signal in quorum sensing [146].

After its discovery in *E. coli*, studies were performed to determine the factors that regulated AI-2 secretion. To uncouple effects of density from growth conditions, experiments were performed in a chemostat process. The results showed that AI-2 production was not density-dependent but instead shadowed changes in growth rate [147]. Another feature during fermentations is that AI-2 levels rapidly decrease and remain at minimum detection once the cells have been induced and enter stationary phase [148].

The drop of AI-2 levels at slower rates of metabolism is not fully understood. There is insufficient data about degradation or catabolism of the compound. The most recent data suggest that the drop may largely be an issue of AI-2 uptake into the cell.

A study has shown that the drop upon induction is not the result of production ceasing because LuxS, the synthase for AI-2, continues to be active during these phases [149]. *Salmonella enterica* serovar Typhimurium uptakes AI-2 by a Lsr (*luxS* regulated) transport system. *E. coli* has a homolog of this transport system, designated as the b1513 operon, which is induced by AI-2. These transporters have been found to be susceptible to catabolite repression [150]. This means that in a glucose-rich environment, such as fresh growth medium, the transporters are not transcribed so that external levels of AI-2 can accumulate. Then in glucose-limited situations, common in HCDC, the transporter quickly intakes this accumulated AI-2.

AI-2 serves as a signal of the growth potential in a cell's environment. Adverse conditions therefore result lower concentrations. When a heat shock stress is induced, for example, AI-2 production ceases. Similar results have been obtained through ethanol and oxidative stresses, and all poststress AI-2 levels decrease at a faster rate than controls. An induced stringent response, caused by serine hydroxamate addition, also results in lower AI-2 production [147]. A stringent response, which is the lack of cellular resources to produce protein [151], is also caused by expression of foreign protein upon induction [152]. Induction itself, already stated to cause an AI-2 depletion, first triggers a global stress response [153]. All these stresses would be expected to lead to AI-2 depletion simply by the fact that they also slow down the metabolic processes of the cell [147].

There is evidence to show that AI-2 has a direct effect on a cell's ability to produce protein. Conditioned medium is cell-free medium that cells have already grown in, which will include standard levels of AI-2. *LacZ* fusions have been used to show that conditioned medium activates a  $\sigma^{38}$  alternative sigma factor [154]. Microarray analysis has shown that conditioned medium also triggers a  $\sigma^{54}$  homolog



of LuxO activation in *V. harveyi* [155]. Stress responses similarly activate specific sigma factors and will typically result in lower protein production levels [156].

Initial work on the addition of AI-2 to cultures has shown that the presence of AI-2 alone was able to increase production levels of foreign protein. Earlier studies have shown that the addition of conditioned medium, which is assumed to contain autoinducers, can increase a culture's ability to produce particular proteins of interest [157, 158]. More recently, an *E. coli* mutant without the ability to synthesize AI-2 specifically was used. These cells were shown to produce 3-4 fold less target protein than a second mutant that corrected for the AI-2 removal [159].

Previous studies regarding the effect of AI-2 have almost all relied on the addition of conditioned medium. Conditioned medium has been deemed nonideal for such experiments because contaminating by-products of cellular metabolism affect cell growth and behavior [160]. The AI-2 synthase LuxS has also been co-expressed in *E. coli* cells. It would be preferred, however, to instead add pure AI-2 to a culture since this does not place an extra burden on the cells and provides more flexibility in experiments. Conversely, studies have been performed with *LuxS* deletion mutants, but LuxS is an important part of the activated methyl cycle in bacteria [160].

If the presence of AI-2 does cause changes improvements in recombinant protein expression, it can added to the fermentation during a culture. There are now methods to synthesize and purify AI-2 *in vitro* using a method based on biosynthetically-produced enzymes [161, 162] and additional organic chemical synthesis methods [163, 164, 165].

If the presence of AI-2 is deleterious to protein expression, then it can be destroyed or blocked. Acyl-homoserine lactonase has been used *in vivo* to cleave and eliminate the effects of AI-1 in a virulent strain of bacteria [166]. Although a similar substance to cleave AI-2 has yet to be discovered, there exists a furanose additive that

has been shown to inhibit AI-2 activity in *E. coli* by 26,600 fold without any effects of toxicity [167]. This creates a preferred method of effective AI-2 decrease instead of using a *luxS* mutant because AI-2 levels can be stoichiometrically reduced and not completely eliminated.

#### ***A9.2. Chemical synthesis attempt of autoinducer 2***

The Semmelhack chemical synthesis was attempted because its publication included nuclear magnetic resonance (NMR) spectra of five chemical intermediates and the final product in the article supplement. Its synthesis was attempted by Dr. Aaron Strickland.

All reagents were obtained from Sigma-Aldrich (St. Louis, MO). L-gulonic acid g-lactone (20.02 g) and p-toluene sulfonic acid monohydrate (0.203 g) were mixed in 100 ml N,N-dimethylformamide. An addition of 1,1-dimethoxycyclohexane (28.1 g) was made, and the solution was left mixing for 48 hr. Triethylamine (100 ml) was added and mixing was continued for another hr. The reaction was then concentrated at 60°C under a vacuum. Toluene (500 ml) was added and the solution was left at -20°C for 24 hr. The precipitate was collected, washed in toluene, and dried under vacuum for 24 hr at room temperature, resulting in 10 g of material. A portion of this first intermediate product (5.05 g) was then added to a mixture of potassium periodate (100 g) and potassium bicarbonate (100 g) in 28 ml water. Dichloromethane (50 ml) was added and the reaction was left to mix for 18 hr. More dichloromethane (50 ml) was added and a saturated sodium chloride solution was gradually added to a final addition volume of 30 ml over 3 hr. Some gelatinous precipitation gradually formed and was removed. The aqueous layer was mixed with water and the second intermediate product was extracted with dichloromethane.

NMR was performed using a Varian (Palo Alto, CA) instrument to confirm the accuracy of the intermediates. The spectra of the first intermediate made matched the spectra from the Semmelhack supplement. The second intermediate contained impurities. This is suspected because the volume of and mixing time after sodium chloride addition were not precise and the precipitation in the reaction never formed an expected gel layer. More information or trial work was necessary to complete the second step of the chemical synthesis.

### ***A9.3. The *Vibrio harveyi* organism***

Comprehensive work involving AI-2 has been performed in *Vibrio harveyi*. Its two autoinducers, AI-1 and AI-2, cause measurable self-bioluminescence to occur [168]. Since one of these autoinducers is the same AI-2 produced from multiple bacterial species, *V. harveyi* can be used to quantify AI-2 concentrations in conditioned media from *E. coli* fermentations. The BB170 strain developed for this assay [169] cannot detect AI-1 and was acquired from Dr. Anthony Hay (Cornell) with the permission of Dr. Bonnie Bassler (Princeton). Cells were transferred on a plate of commercial marine broth.

The identity of *V. harveyi* was confirmed by sequencing 16s rRNA and matching this with the AM183755 locus publically available from the National Center for Biotechnology Information (NCBI). Genomic DNA was isolated using a kit (Qiagen, Germantown, MD) and the desired gene fragment was amplified using a polymerase chain reaction (PCR). Briefly, cells were grown up in a shake flask to an optical density of 4.0. A 0.5 ml aliquot was removed, pelleted, and resuspended in tissue lysis buffer (ATL buffer). A 3 hr incubation was performed at 55°C after 20 µl of proteinase K was added. After a 200 µl addition of AL buffer, the mixture was incubated at 70°C for 10 min, and then 200 µl of cold ethanol was added. Genomic

DNA was bound, washed, and eluted off of a DNeasy spin column at a volume of 100  $\mu$ l and a concentration of 96 ng/ $\mu$ l. The primers used in the PCR were 5' – GAA AGC CAC GGC TCA AGG CCA – 3' and 5' – TTA ACA CAT GCA AGT CGA GCG G – 3'. Each primer was added in 2.5  $\mu$ l aliquots to 0.5  $\mu$ g DNA, 25  $\mu$ l 2x biomix (Bioline, Taunton, MA), and 15  $\mu$ l of water. The Biomix contained the Taq polymerase necessary for PCR. A 1% agarose gel in TAE (tris acetate EDTA) buffer was used to confirm a successful PCR of the 456 ng/ $\mu$ l 821 base pair region (Figure A9.1a). The amplified product was purified using Wizard DNA purification kit (Promega, Madison, WI). Briefly, the product was captured on a column and washed with 80% isopropanol. Diluting the concentration below 100 ng/ml, 0.4 ml of PCR product, 0.8 ml of primer were mixed in 16.8 ml of water and sent to Cornell Biotechnology Resource Center (BRC) for sequencing. The extracted sequence matched NCBI sequence (Figure A9.1b), compared using Vector NTI software (Invitrogen).

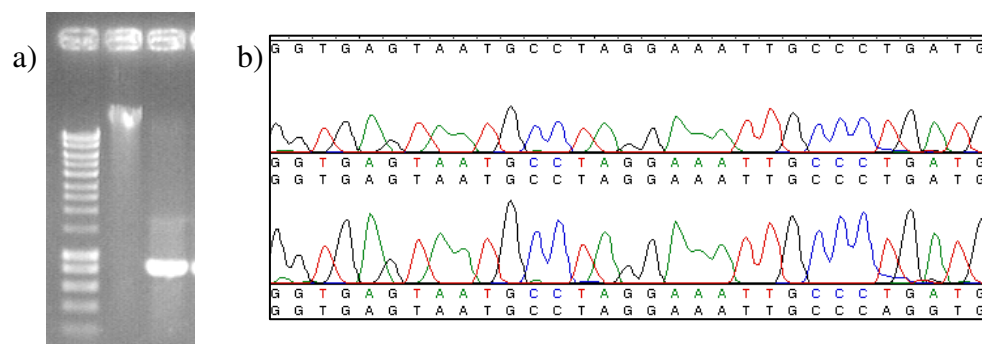


**Figure A9.1. Agarose gel and sequence evaluation of *V. harveyi* 16s rRNA.** a) Lane 1: Hyperladder marker (Bioline), Lane 2: *V. harveyi* genomic DNA, Lane 3: Amplified *V. harveyi* 16s rRNA. b) Partial comparison of amplified 16s rRNA sequence with database sequence.

#### ***A9.4. Autoinducer 2 detection assay***

The AI-2 detection assay is a bioassay that measures the relative luminescence of a *V. harveyi* culture that is exposed to the AI-2 molecule. Experimental samples are compared to a control group since the sensor strain does have the ability to produce AI-2 by itself.

The autoinducer bioassay medium was [0.3 M sodium chloride, 0.05 M magnesium sulfate, 0.2% casamino acids, 10 mM potassium phosphate, 1 mM L-arginine, 20 ml/L glycerol, 4 µg/ml riboflavin, 40 µg/ml thiamine, pH 7.5]. When 10 µl of cell bank was grown in 125 ml of autoinducer bioassay medium at 30°C, it took 17 hr to reach an optical density of 0.8. At this density, the cells were bioluminescent.

The assay requires that the cells are diluted to stop the bioluminescence and the addition of 10% (v/v) conditioned medium. To make conditioned medium, a bacterial culture sample was centrifuged, and the supernatant was filtered through a 0.2 µm filter. If this filtration was not performed, trace cells in the supernatant would interfere with the sensitive assay. A 10 µl aliquot of conditioned medium was added to 100 µl of *V. harveyi* culture in autoinducer bioassay medium at an optical density of 0.8. Samples were loaded in 96-well plates, white with clear bottom (Corning Inc., Corning, NY). Measurements were performed in a Lumicount luminescence microplate reader (Packard, United Kingdom) with a PMT value of 600. The emission spectra of the *V. harveyi* was measured by Dr. Byung-Ryool Hyun (Figure A8.2).

Initial measurements were performed with the addition of conditioned medium of undiluted *V. harveyi* cultures at O.D. 0.8. Responses to the conditioned medium were detected in various dilutions of the *V. harveyi* culture. Higher dilutions of the cells delayed luminescence peaks, and the addition of 10% (v/v) conditioned medium activated luminescence earlier (Figure A9.3a). If only 5% (v/v) conditioned medium was added, luminescence would occur sooner than when 10% (v/v) conditioned

medium was added. The addition of 20% (v/v) conditioned medium as only slightly better than the 10% (v/v) addition (Figure A9.3b).

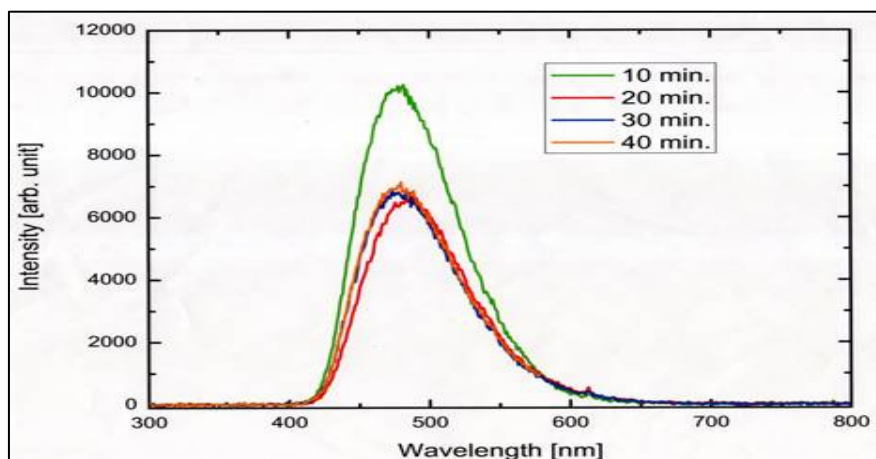


**Figure A9.2. Emission spectra of *V. harveyi* luminescence.** Measurement of the emission of a *V. harveyi* culture over time was conducted by Dr. Byung-Ryool Hyun. Intensity dropped over time, but the peak intensity was constantly detected at approximately 490 nm.

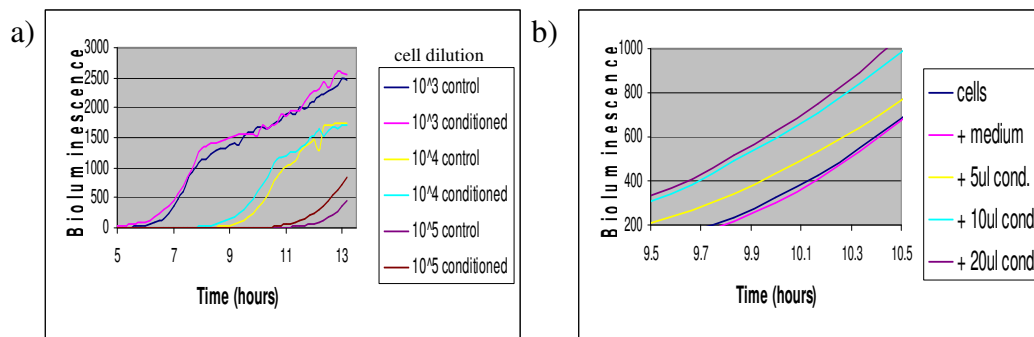


**Figure A9.3. Luminescence of *V. harveyi* culture with conditioned medium.** a) *V. harveyi* culture with and without 10% conditioned medium at different cell dilutions. b) Different amounts of conditioned medium were added to a diluted culture of *V. harveyi*. Blank medium was added as a negative control.

#### A9.5. Autoinducer 2 detection assay with glucose

If blank complex *E. coli* fermentation medium was added, the luminescence would rise and fall, creating a luminescence peak. This peak occurred earlier if conditioned medium from an early stage *E. coli* culture was added (Figure A8.4). The

percentage of luminescence increased was measured at the 8 hr timepoint for consistency. For example, in Figure A9.4, the culture with conditioned medium was at 486 luminescence units at 8 hr, the culture with blank medium was at 69 luminescence units at this same time, and the conditioned medium therefore created a 7.04-fold increase in luminescence. Modifications needed to be made to the assay for fermentation samples in late-stage growth when glucose was at undetectable levels.

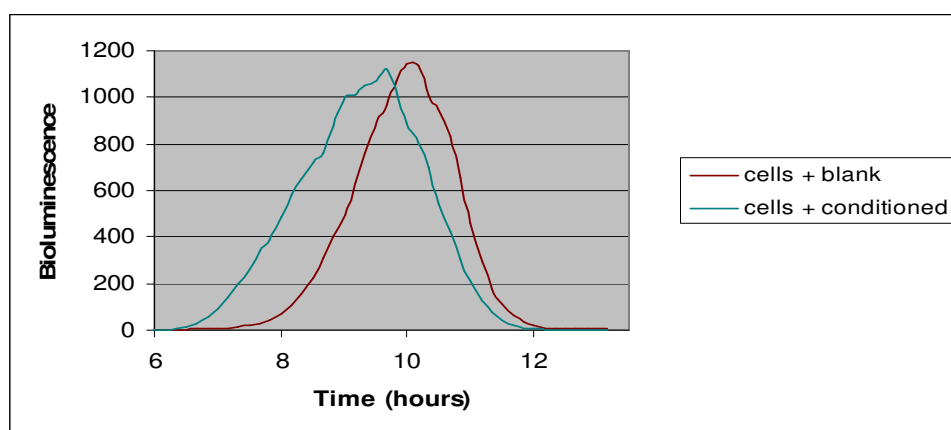


**Figure A9.4. Luminescence curves from diluted *V. harveyi* cultures with fermentation samples.** Blank fermentation medium created a luminescence peak. Conditioned medium caused this luminescence to occur earlier. The percentage of increased luminescence was measured at 8 hr.

A very important detail about the AI-2 detection assay is that the luminescence of the *V. harveyi* culture is greatly influenced by the presence of glucose, which is very commonly used in *E. coli* fermentation media recipes. The *V. harveyi* bioassay is influenced by pH, DNA damaging reagents, arginine, salt, glucose, oxygen tension, borate, and possibly iron. The original autoinducer bioassay medium consisted of potassium phosphate, arginine, salt, and glycerol [170]. It is logical that while the phosphate salt control the pH, arginine and salt were added to saturate any inhibitory effects. Meanwhile, glucose was replaced with glycerol, and this assay cannot be used

with any media that contains glucose. Literature regarding this effect of glucose is inconsistent (Table A9.1).

**Table A9.1. Summary of glucose effects on AI-2 bioassay from literature.** Conflicting observations have been made on the influence of small concentrations of glucose on the autoinducer 2 bioassay.

Group	Observed luminescence	Glucose concentration
Nealson, 1972	inhibited	> 28 mM
DeLisa, 2001	2.5x increase	5 mM
	6.3x increase	50 mM
De Keersmaecker, 2003	“complete” inhibition	> 2 mM
Turovskiy, 2006	20x increase	0.44 mM

The effect of adding only glucose and glucose plus a glucose-rich conditioned medium sample to the *V. harveyi* detector culture was determined. While low concentrations of glucose promote initial luminescence, high concentrations of glucose are inhibitory during later phases of luminescence (Figure A9.5). These results perhaps help to explain the inconsistent observations in the literature. It is important to note that the initial luminescence of the same conditioned medium sample does not change when extra glucose is added (Figure A9.5b). Since only the early luminescence of the cultures is used in the detection assay, a surplus of glucose normalizes luminescence (Figure A9.6). This modification permitted the use of fermentation samples in the AI-2 bioassay. The quantitative results agree with



previous studies that show high levels of AI-2 during exponential growth phase and depleted levels during stationary phase (Figure A9.7).

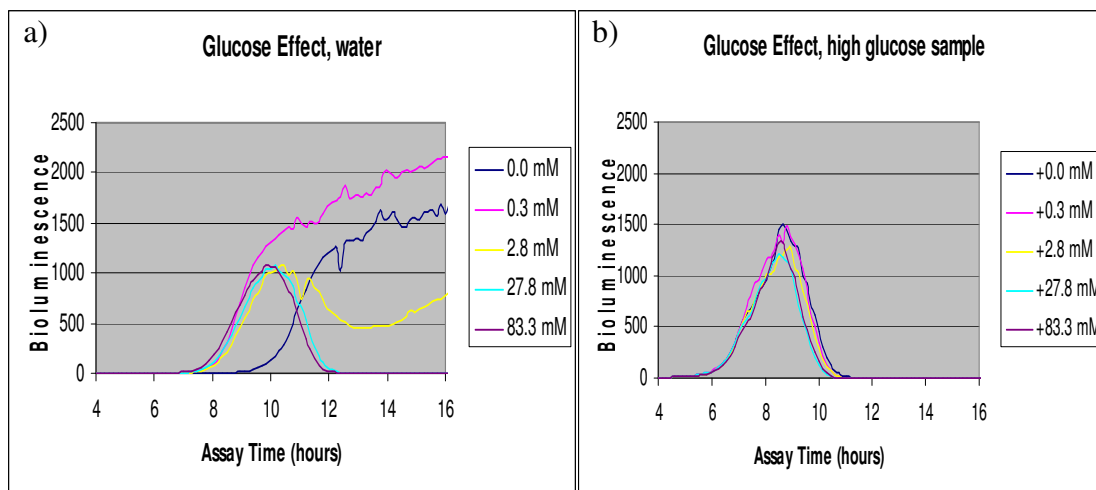


**Figure A9.5. Influence of glucose addition to autoinducer 2 bioassay.** a) Increasing concentrations of glucose were added to the *V. harveyi* culture. Any addition of glucose increased the start time of luminescence. Higher levels of glucose decreased late levels of luminescence. b) For a glucose-rich conditioned medium sample, the addition of glucose had no effect.

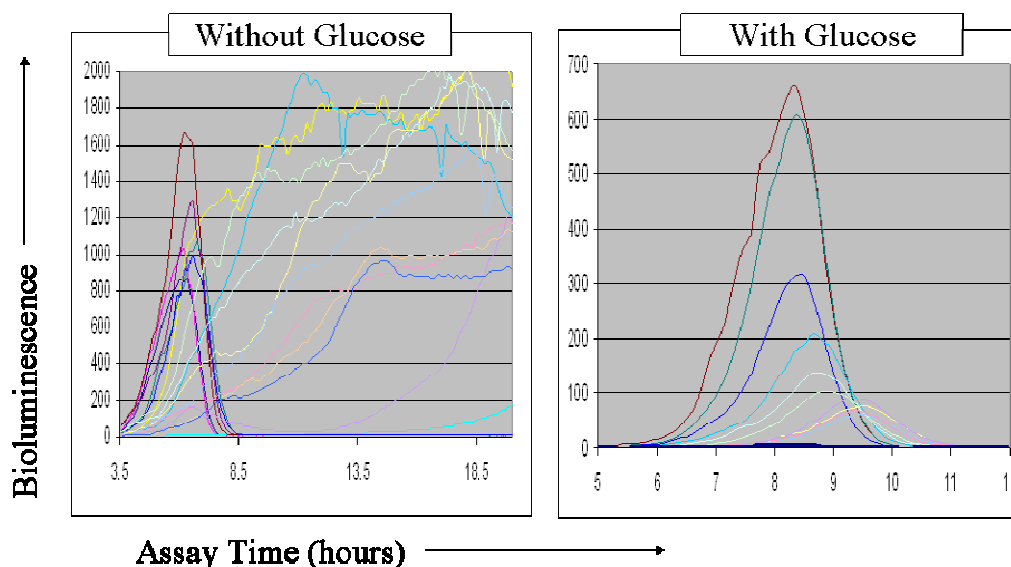


**Figure A9.6. Effect of glucose on *V. harveyi* luminescence from conditioned medium.** Without the addition of glucose, early fermentation samples created luminescence peaks and later fermentation samples did not settle. With the addition of glucose, luminescence peaks were well-behaved.

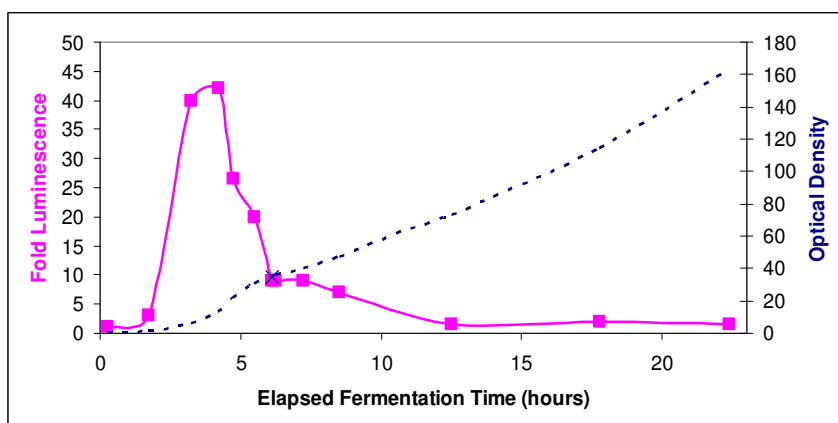


**Figure A9.7. Autoinducer 2 levels during a high cell density fermentation.** Conditioned medium samples were acquired for various time points during a high cell density *E. coli* fermentation. Their relative level of AI-2 was determined using a *V. harveyi* bioassay. The dotted blue line is the optical density, and the solid pink line is the relative AI-2 intensity.

#### ***A9.6. Intracellular autoinducer 2 measurements***

AI-2 levels drop in an *E. coli* culture as the cells enter stationary phase [171]. It is hypothesized that the cells consume the autoinducer to create this drop. The internal AI-2 levels within an *E. coli* culture were then measured to determine if the molecule accumulated within the cells.

Samples of 40 ml were taken from a high cell density culture at regular time points. The OD<sub>600</sub> of the samples was measured (Section 2.5.2), and the cells were pelleted at 8,000 rcf in a SLA-600TC rotor in the ultracentrifuge described in Section A4.2. The cells were then washed and resuspended in water before being lysed in a high pressure homogenizer, as described in Section 2.6. The lysate samples were assayed with a *V. harveyi* culture (Section A9.5) and their luminescence-stimulation was compared to that of water. Values were normalized for cell density to determine specific levels of AI-2 per cell. There was no accumulation of the AI-2 molecule in the cells found (Table A9.2).

**Table A9.2. Intracellular autoinducer 2 levels of a high cell density *E. coli* fermentation.** Samples from a high cell density fermentation were sampled, and the AI-2 of the lysate was measured. AI-2 levels were normalized by the cell density in the first sample to determine any trends in specific internal AI-2 levels.

EFT (hrs)	Luminescence	
	raw	by mass
1	135%	135%
1.5	139%	96%
3	160%	77%
4.5	170%	68%
5.45	191%	61%
5.45	178%	47%
6.7	190%	41%
10.45	206%	35%
12.75	185%	32%
15.22	195%	30%
18	190%	26%
20.2	192%	25%
22.36	200%	24%
24.71	186%	22%

#### ***A9.7. LuxS deletion mutants***

The *ygaG* gene is a 516 base pair sequence that codes for LuxS, the synthase of AI-2. Its removal was performed by Chung-Jr Huang in C41 *E. coli* cells to create a negative control for the AI-2 experiments. To do this, FY and RY fragments were created. These fragments were 500 base pairs on the bacterial chromosome upstream and downstream of the *ygaG* gene. They were created using PCR with a set of primers for each fragment. The fragments were ligated together to form a FYRY sequence, and this ligation product was PCR-amplified using the primers from the non-ligated ends. The goal was to delete the *ygaG* sequence by replacing the FY-*ygaG*-RY sequence with FYRY.

FYRY was purified and extracted from an agarose gel and ligated into a pKNG1-FY vector. The plasmid was transformed into SRM cells, and successful transformants were screened using streptomycin resistance. SRM and C41 cells were individually grown to optical densities of 0.5 without any antibiotics. The cells were then combined, pelleted, and resuspended in 100  $\mu$ l of 0.9% sodium chloride. The

mixture was left unmixed on a plate overnight to promote conjugation. Cells were then grown on a chloramphenicol plate with 10% sucrose to induce recombination.

The genome of the *LuxS* mutant and of a control C41 organism were individually PCR amplified using the FYRY primers for the unligated ends. An agarose gel stained with ethidium bromide shows that the control organism has, as expected, a 1,500 base pair fragment, and the *LuxS* mutant has a 1,000 base pair fragment (Figure A9.8). The mutant, unfortunately, did not fail to stimulate luminescence in the AI-2 detection assay. The mutants were grown in the complex fermentation batch medium to an OD<sub>600</sub> of 4.5 and LB medium, and the conditioned media's luminescence stimulation was compared to the respective blank media. It should be noted that no AI-2 signal should be detected when LB medium is used without glucose supplementation [146].

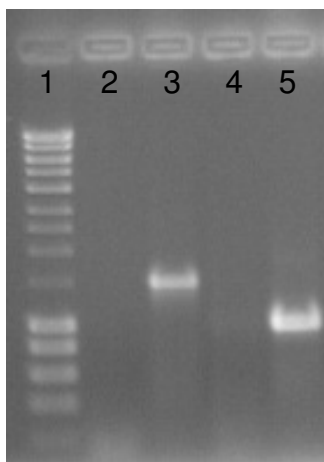


**Figure A9.8. Agarose gel of FY-ygaG-RY and FYRY fragments.** The *LuxS* mutant lacked the ygaG gene. When amplified with FY and RY primers, its fragment (Lane 5) was smaller than the control organism (Lane 3).

#### ***A9.8. Lag phase studies***

Cells typically repeat a lag in their growth phase when they are inoculated into fresh medium, even if the medium composition and operating conditions are identical.

It was therefore hypothesized that the cells operate under the control of a quorum sensing factor. Both *E. coli* and *V. harveyi* cells would enter exponential growth phase faster when supplemented with their respective conditioned medium. Studies were conducted with 5 ml cultures in 50 ml conical tubes. After exponential growth was initiated, the cells grew at the same specific growth rate. The results of using various concentrations of conditioned medium for *E. coli* are shown in Figure A9.9. Cells would not grow in 100% conditioned medium. When conditioned medium was added from different growth phases of fermentation, it was found that the conditioned medium with the highest level of AI-2 increased lag phase and conditioned medium with almost no AI-2 decreased the lag phase (Figure A9.10). These results suggested that AI-2 was not responsible for conditioned medium's ability to decrease lag phase. The reason increasing blank medium addition from 5% to 10% was able to decrease lag phase is unknown.

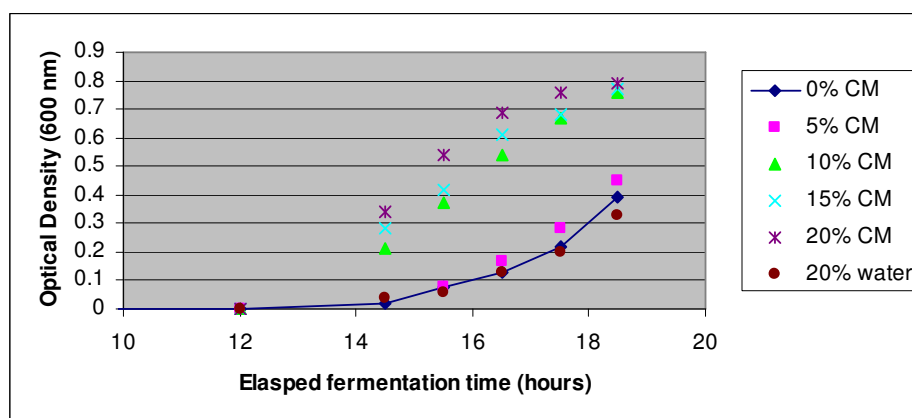


**Figure A9.9. Growth curves of *E. coli* fermentations supplemented with conditioned medium.** Although the addition of water was not able to change the growth pattern of *E. coli*, the addition of conditioned medium decreased lag phase proportionately.

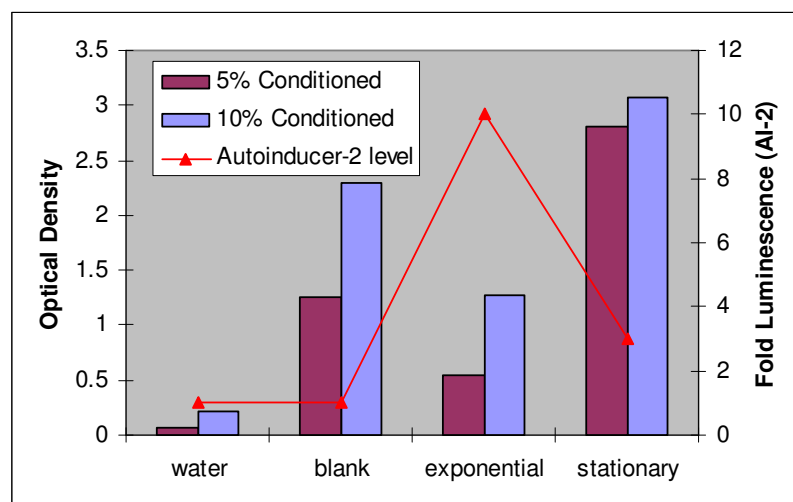


**Figure A9.10. Autoinducer 2 levels in conditioned medium and their effect to decrease lag phase.** Water, blank medium, conditioned medium from exponential growth phase, and conditioned medium from stationary growth phase were added in 5% and 10% (v/v) to *E. coli* cultures. The conditioned medium with the greatest AI-2 level did not result in the shortest lag time.

The results of this study are supported by another study that showed conditioned medium from *E. coli* with high AI-2 levels could not reduce the lag phase in growth for *Listeria innocua* [172]. Yet another group was able to decrease lag phase using conditioned medium from stationary growth phase. Their classification of the growth-stimulating substance suggest it is a small, non-proteinaceous, non-ionic organic molecule [173]. In other work, it was determined that the transition from exponential phase to stationary phase is through cell signaling and not a nutrient limitation [174].

### **A9.9. Discussion**

AI-2's inability to reduce the lag phase in bacterial growth is not the only example where AI-2 could not explain quorum sensing phenomenon. One study showed that pure AI-2 was responsible for increased biofilm formation [175], but

multiple studies that also used pure AI-2 did not support this conclusion [176]. Although it had been suspected that AI-2 was responsible for virulence in Enterohemorrhagic *E. coli* O157:H7 pathogenicity [177], repeated experiments with pure AI-2 [178] disproved this theory. Similar to the growth-stimulating substance, the pathogenicity-stimulating substance has not been identified.

AI-2 was originally suspected to be a quorum sensing molecule because it was able to activate luminescence in *V. harveyi*. In order for this to happen, the AI-2 produced from interspecies bacteria, such as *E. coli*, actually had to undergo a conformational change that included the incorporation of a borate group [179]. Considering this molecular change, the AI-2 produced by *E. coli* and the AI-2 used as a quorum sensing signal in *V. harveyi* are quite different.

During a high cell density *E. coli* fermentation, AI-2 is produced when glucose is plentiful and consumed when glucose has been depleted, much like acetate and other metabolites. It has been suspected that AI-2 is nothing more than an unpreferential carbon source for *E. coli* [160, 176]. Most experiments that suggested AI-2 was a quorum sensing factor for *E. coli* were conducted with conditioned medium. Among the experiments that use pure AI-2, many show that the molecule does not have any quorum sensing effect on *E. coli*. If AI-2 is to be considered as a quorum sensing molecule for *E. coli*, more evidence is now needed to support this theory.

## REFERENCES

- 138) M. Surette, B. Bassler, Quorum Sensing in *Escherichia coli* and *Samonella typhimurium*, Proc. Natl. Acad. Sci. USA 95 [1998] 7046-7050.
- 139) M. DeLisa, J. Valdes, W. Bentley, Mapping stress-induced changed in autoinducer AI-2 production in chemostat-cultivated *Escherichia coli* K-12, J. Bacteriol. 183 [2001] 2918-2928.
- 140) M. DeLisa, J. Valdes, W. Bentley, Quorum signaling via AI-2 communicates the 'metabolic burden' associated with heterologous protein production in *Escherichia coli*, Biotechnol. Bioeng. 75 [2001] 439-450.
- 141) K. Xavier, B. Bassler, Regulation of uptake and processing of the quorum-sensing autoinducer AI-2 in *Escherichia coli*, J. Bacteriol. 187 [2005] 238-248.
- 142) L. Wang, Y. Hashimoto, C. Tsao, J. Valdes, W. Bentley, Cyclic AMP (cAMP) and cAMP receptor protein influence both synthesis and uptake of extracellular autoinducer 2 in *Escherichia coli*, J. Bacteriol. 187 [2005] 2066-2076.
- 143) A. Panda, R. Khan, S. Mishra, R. Appa, S. Totey, Influences of yeast extract on the specific cellular yield of ovine growth hormone in *E. coli*, Bioprocess Eng. 22 [2000] 379-383.
- 144) M. Yamagishi, J. Cole, M. Nomura, F. Studier, J. Dunn, Stringent control in *Escherichia coli* also applies to transcription by T7 RNA polymerase, J. Biol. Chem. 9 [1987] 3940-3943.
- 145) R. Gill, J. Valdes, W. Bentley, A comparative study of global stress gene regulation in response to overexpression of recombinant proteins in *Escherichia coli*, Metabol. Eng. 2 [2000] 178-189.



- 146) R. Baca-DeLancey, M. South, X. Ding, P. Rather, *Escherichia coli* genes regulated by cell-to-cell signaling, Proc. Natl. Acad. Sci. USA 96 [1999] 4610-4614.
- 147) M. DeLisa, C. Wu, L. Wang, J. Valdes, W. Bentley, DNA microarray-based identification of genes controlled by autoinducer 2-stimulated quorum sensing in *Escherichia coli*, J. Bacteriol. 183 [2001] 5239-5247.
- 148) W. Ryan, P. Collier, L. Lored, J. Pope, R. Sachdev, Growth kinetics of *Escherichia coli* and expression of a recombinant protein and its isoforms under heat shock conditions, Biotechnol. Prog. 12 [1996] 596-601.
- 149) C. Lee, M. Shuler, The effect of inoculum density and conditioned medium on the production of ajmalicine and catharanthine from immobilized *Catharanthus roseus* cells, Biotechnol. Bioeng. 67 [2000] 61-71.
- 150) R. Nozawa, R. Sekiguchi, T. Yokota, Stimulation by conditioned medium of L-929 fibroblasts, *E. coli* lipopolysaccharide, and muramyl dipeptide of candidacidal activity of mouse macrophages, Cell Immunol. 53 [1980] 116-124.
- 151) M. DeLisa, W. Bentley, Bacterial autoinduction: looking outside the cell for new metabolic engineering targets, Microbial Cell Factories 1 [2002] 1-9.
- 152) K. Winzer, K. Hardie, P. Williams, Bacterial cell-to-cell communication: sorry, can't talk now – gone to lunch! Curr. Opin. Microbiol. 5 [2002] 216-222.
- 153) S. Schauder, K. Shokat, M. Surette, B. Bassler, The LuxS family of bacterial autoinducers: biosynthesis of a novel quorum-sensing signal molecule, Mol. Microbiol. 41 [2001] 463-476.

- 154) R. Fernandes, W. Bentley, AI-2 biosynthesis module in a magnetic nanofactory alters bacterial response via localized synthesis and delivery, *Biotechnol. Bioeng.* 102 [2009] 390-399.
- 155) M. Semmelhack, S. Campagna, M. Federle, B. Bassler, An expeditious synthesis of DPD and boron binding studies, *Org. Lett.* 7 [2005] 567-572.
- 156) S. De Keersmaecker, C. Varszegi, N. Boxel, L. Habel, K. Metzger, R. Daniels, K. Marchal, D. Vos, J. Vanderleyden, Chemical synthesis of (S)-4,5-dihydroxy-2,3-pentanedione, a bacterial signal molecule precursor, and validation of its activity in *Salmonella typhimurium*, *J. Biol. Chem.* 280 [2005] 19563-19568.
- 157) M. Meijler, L. Hom, G. Kaufmann, K. McKenzie, C. Sun, J. Moss, M. Matsushita, K. Janda, Synthesis and biological validation of a ubiquitous quorum-sensing molecule, *Angew. Chem. Int. Ed.* 43 [2004] 2106-2108.
- 158) Y. Dong, L. Wang, J. Xu, H. Zhang, X. Zhang, L. Zhang, Quenching quorum-sensing-dependent bacterial infection by an N-acyl-homoserine lactonase, *Nature* 411 [2001] 813-817.
- 159) D. Ren, J. Sims, T. Wood, Inhibition of biofilm formation and swarming of *Escherichia coli* by (5Z)-4-bromo-5-(bromomethylene)-3-butyl-2(5H)-furanone, *Environ. Microbiol.* 3 [2001] 731-736.
- 160) B. Bassler, M. Wright, R. Showalter, M. Silverman, Multiple signaling systems controlling expression of luminescence in *Vibrio harveyi*: sequence and function of genes encoding a second sensory pathway, *Mol. Microbiol.* 13 [1994] 273-286.
- 161) B. Bassler, E. Greenberg, A. Stevens, Cross-species induction of luminescence in the quorum-sensing bacterium *Vibrio harveyi*, *J. Bacteriol.* 179 [1997] 4043-4045.

- 162) E. Greenberg, J. Hastings, S. Ulitzer, Induction of luciferase synthesis in *Beneckea harveyi* by other marine bacteria, Arch. Microbiol. 120 [1979] 87-91.
- 163) B. Lazazzera, Quorum sensing and starvation: signals for entry into stationary phase, Curr. Opin. Microbiol. 3 [2000] 177-182.
- 164) L. Yang, F. Portugal, W. Bentley, Conditioned medium from *Listeria innocua* stimulates emergence from a resting state: not a response to *E. coli* quorum sensing autoinducer AI-2, Biotechnol. Prog. 22 [2006] 387-393.
- 165) D. Weichart, D. Kell, Characterization of an autostimulatory substance produced by *Escherichia coli*, Microbiology 147 [2001] 1875-1885.
- 166) X. Carbonell, J. Corchero, R. Cubarsí, P. Vila, A. Villaverde, Control of *Escherichia coli* growth rate through cell density, Microbiol. Res. 157 [2002] 257-265.
- 167) A. González-Barrios, R. Zuo, Y. Hashimoto, L. Yang, W. Bentley, T. Wood, Autoinducer 2 controls biofilm formation in *Escherichia coli* through a novel motility quorum-sensing regulator (MqsR, B3022), J. Bacteriol. 188 [2006] 305-316.
- 168) Y. Turovskiy, D. Kashtanov, B. Paskhover, M. Chikindas, Quorum sensing: fact, fiction, and everything in between, Adv. Appl. Microbiol. 62 [2007] 191-234.
- 169) V. Sperandio, J. Mellies, W. Nguyen, S. Shin, J. Kaper, Quorum sensing controls expression of the type III secretion gene transcription and protein secretion in enterohemorrhagic and enteropathogenic *Escherichia coli*, Proc. Natl. Acad. Sci. USA 96 [1999] 15196-15201.
- 170) M. Walters, M. Sircili, V. Sperandio, AI-3 synthesis is not dependent on *luxS* in *Escherichia coli*, J. Bacteriol. 188 [2006] 5668-5681.

- 171) S. Miller, K. Xavier, S. Campagna, M. Taga, M. Semmelhack, B. Bassler, F. Hughson, *Salmonella typhimurium* recognizes a chemically distinct form of the bacterial quorum-sensing signal AI-2, Mol. Cell 15 [2004] 677-687.
- 172) K. Nealson, J. Hastings, A. Eberhard, Catabolite repression of bacterial bioluminescence – functional implications, Proc. Natl. Acad. Sci. USA 69 [1972] 1073-1076.
- 173) Y. Turovskiy, M. Chikindas, Autoinducer-2 bioassay is a qualitative, not quantitative method influenced by glucose, J. Microbiol. Methods, 66 [2006] 497-503.